THE GEOMETRY OF QUADRATIC POLYNOMIAL DIFFERENTIAL SYSTEMS WITH A FINITE AND AN INFINITE SADDLE–NODE (C)

JOAN C. ARTÉS
Departament de Matemàtiques, Universitat Autònoma de Barcelona, 08193 Bellaterra, Barcelona, Spain
E–mail: artes@mat.uab.cat

ALEX C. REZENDE[1] AND REGILENE D. S. OLIVEIRA[2]
Departamento de Matemática, Universidade de São Paulo, 13566–590, São Carlos, São Paulo, Brazil,
E–mail: [1] arezende@icmc.usp.br, [2] regilene@icmc.usp.br

Planar quadratic differential systems occur in many areas of applied mathematics. Although more than one thousand papers have been written on these systems, a complete understanding of this family is still missing. Classical problems, and in particular, Hilbert's 16th problem [Hilbert, 1900, Hilbert, 1902], are still open for this family. Our goal is to make a global study of the family **QsnSN** of all real quadratic polynomial differential systems which have a finite semi–elemental saddle–node and an infinite saddle–node formed by the collision of two infinite singular points. This family can be divided into three different subfamilies, all of them with the finite saddle–node in the origin of the plane with the eigenvectors on the axes and with the eigenvector associated with the zero eigenvalue on the horizontal axis and (A) with the infinite saddle–node in the horizontal axis, (B) with the infinite saddle–node in the vertical axis and (C) with the infinite saddle–node in the bisector of the first and third quadrants. These three subfamilies modulo the action of the affine group and time homotheties are three–dimensional and we give the bifurcation diagram of their closure with respect to specific normal forms, in the three–dimensional real projective space. The subfamilies (A) and (B) have already been studied [Artés *et al.*, 2013b] and in this paper we provide the complete study of the geometry of the last family (C). The bifurcation diagram for the subfamily (C) yields 371 topologically distinct phase portraits with and without limit cycles for systems in the closure $\overline{\mathbf{QsnSN}(\mathbf{C})}$ within the representatives of $\mathbf{QsnSN}(\mathbf{C})$ given by a chosen normal form. Algebraic invariants are used to construct the bifurcation set. The phase portraits are represented on the Poincaré disk. The bifurcation set of $\overline{\mathbf{QsnSN}(\mathbf{C})}$ is not only algebraic due to the presence of some surfaces found numerically. All points in these surfaces correspond to either connections of separatrices, or the presence of a double limit cycle. *Keywords:* Quadratic differential systems; finite saddle–node; infinite saddle–node; phase portraits; bifurcation diagram; algebraic invariants. *AMS Subject classification: Primary*: 34C40, 51F14; *Secondary*: 14D05, 14D25.

1. Introduction, brief review of the literature and statement of results

Here we call *quadratic differential systems*, or simply *quadratic systems*, differential systems of the form

$$\begin{aligned} \dot{x} &= p(x,y), \\ \dot{y} &= q(x,y), \end{aligned} \tag{1}$$

where p and q are polynomials over $\mathbb{R}$ in x and y such that the $\max(\deg(p),\deg(q)) = 2$. To such a system one can always associate the quadratic vector field

$$\xi = p\frac{\partial}{\partial x} + q\frac{\partial}{\partial y}, \tag{2}$$

as well as the differential equation

$$q\,dx - p\,dy = 0. \tag{3}$$

The class of all quadratic differential systems (or quadratic vector fields) will be denoted by **QS**.

We can also write system (1) as

$$\begin{aligned} \dot{x} &= p_0 + p_1(x,y) + p_2(x,y) = p(x,y), \\ \dot{y} &= q_0 + q_1(x,y) + q_2(x,y) = q(x,y), \end{aligned} \tag{4}$$

where p_i and q_i are homogeneous polynomials of degree i in the variables x and y with real coefficients and $p_2^2 + q_2^2 \neq 0$.

Even after hundreds of studies on the topology of real planar quadratic vector fields, it is kind of impossible to outline a complete characterization of their phase portraits, and attempting to topologically classify them, which occur rather often in applications, is quite a complex task. This family of systems depends on twelve parameters, but due to the action of the group $\mathrm{Aff}(2,\mathbb{R})$ of real affine transformations and time homotheties, the class ultimately depends on five parameters, but this is still a large number.

The main goal of this paper is to complete the study of the class **QsnSN** of all quadratic systems possessing a finite saddle–node $\overline{sn}_{(2)}$ and an infinite saddle–node of type $\binom{\overline{0}}{2}SN$. We recall that a finite saddle–node is a semi–elemental singular point whose neighborhood is formed by the union of two hyperbolic sectors and one parabolic sector. By a semi–elemental point we mean a point with zero determinant of its Jacobian with only one eigenvalue equal to zero. These points are known in classical literature as semi–elementary, but we use the term *semi–elemental* introduced in [Artés *et al.*, 2013a] as part of a set of new definitions more deeply related to singularities, their multiplicities and, especially, their Jacobian matrices. In addition, an infinite saddle–node of type $\binom{\overline{0}}{2}SN$ is obtained by the collision of an infinite saddle with an infinite node. There are two types of infinite saddle–nodes and the second one is denoted by $\binom{\overline{1}}{1}SN$ which is obtained by the collision of a finite node (respectively, finite saddle) with an infinite saddle (respectively, infinite node) and which will appear in some of the phase portraits.

If we have a finite saddle–node $\overline{sn}_{(2)}$, the possibility of having two other finite singular points is present. Indeed, in case the remaining singularities did not go to infinity, then there are two other singularities in the finite plane, either real, or complex, or the origin may have higher multiplicity.

The class **QsnSN** is divided into three subfamilies according to the position of the infinite saddle–node, namely **QsnSN**(**A**), **QsnSN**(**B**) and **QsnSN**(**C**). In [Artés *et al.*, 2014] the authors gave a partition of the closure of the first two subfamilies and this paper presents a continuation in the study of this subclass **QsnSN** presenting the analysis of the closure of the last subfamily **QsnSN**(**C**).

For this analysis we follow the pattern set out in [Artés *et al.*, 2006] and, in order to avoid repeating technical sections which are the same for both papers, we refer to the paper mentioned for more complete information.

We now give the notion of *graphics*, which play an important role in obtaining limit cycles when they are due to connection of separatrices, for example.

A *(non-degenerate) graphic* as defined in [Dumortier *et al.*, 1994] is formed by a finite sequence of singular points $r_1, r_2, \ldots, r_n$ (with possible repetitions) and non–trivial connecting orbits γ_i for $i = 1, \ldots, n$ such that γ_i has r_i as α–limit set and r_{i+1} as ω–limit set for $i < n$ and γ_n has r_n as α–limit set and r_1 as ω–limit set. Also normal orientations n_j of the non–trivial orbits must be coherent in the sense that if γ_{j-1} has left–hand orientation then so does γ_j. A *polycycle* is a graphic which has a Poincaré return map.

A *degenerate graphic* is formed by a finite sequence of singular points $r_1, r_2, \ldots, r_n$ (with pos-

sible repetitions) and non–trivial connecting orbits and/or segments of curves of singular points γ_i for $i = 1, \ldots, n$ such that γ_i has r_i as α–limit set and r_{i+1} as ω–limit set for $i < n$ and γ_n has r_n as α–limit set and r_1 as ω–limit set. Also normal orientations n_j of the non–trivial orbits must be coherent in the sense that if γ_{j-1} has left–hand orientation then so does γ_j. For more details, see [Dumortier *et al.*, 1994].

In [Artés *et al.*, 1998] the authors proved the existence of 44 topologically different phase portraits for the structurally stable quadratic planar systems modulo limit cycles, also known as the codimension–zero quadratic systems. Roughly speaking, these systems are characterized by having all singularities, finite and infinite, simple, no separatrix connection, and where any nest of limit cycles is considered as a single point with the stability of the outer limit cycle. The next step is the classification of the structurally unstable quadratic systems of codimension–one which have one and only one of the simplest structurally unstable objects: a saddle–node of multiplicity two (finite or infinite), a separatrix from one saddle point to another, and a separatrix forming a loop for a saddle point with its divergence nonzero. All the phase portraits of codimension one are split into four groups according to the possession of a structurally unstable element: (A) possessing a finite semi–elemental saddle–node, (B) possessing an infinite semi–elemental saddle–node $\overline{\binom{0}{2}}SN$, (C) possessing an infinite semi–elemental saddle–node $\overline{\binom{1}{1}}SN$, and (D) possessing saddle connection.

The study of the codimension–one systems is already in progress [Artés & Llibre, 2014], all topological possibilities have already been found, some of them have already been proved impossible and many representatives have been found, but some cases without candidate still remain. One of the ways to obtain codimension–one phase portraits is considering a perturbation of known phase portraits of quadratic systems of higher codimension. This perturbation would decrease the codimension of the system and a representative for a topological equivalence class in the family of the codimension–one systems may be found and added to the existing classification.

In order to contribute to this classification, some families of quadratic systems of codimension greater than one have been studied, e.g. systems with a weak focus of second order (see [Artés *et al.*, 2006]), with a finite semi–elemental triple node (see [Artés *et al.*, 2013b]) and the two first subfamilies possessing saddle–nodes (see [Artés *et al.*, 2014]). It is worth mentioning that in [Artés *et al.*, 2013b], the authors show that, after a quadratic perturbation of one of the phase portraits of that family, a new phase portrait of codimension one is proved being realizable.

The present study is part of this attempt of classifying all the codimension–one quadratic systems. Although the phase portraits from subfamilies $\overline{\mathbf{QsnSN(A)}}$ and $\overline{\mathbf{QsnSN(B)}}$ could not contribute in this goal, subfamily $\overline{\mathbf{QsnSN(C)}}$ yields *all* of the phase portraits of group (A), and some of group (B), of codimension–one quadratic systems, including missing cases, as stated in Corollary 1.4.

In the normal form (5), the class $\overline{\mathbf{QsnSN(C)}}$ is partitioned into 1034 parts: 199 three–dimensional ones, 448 two–dimensional ones, 319 one–dimensional ones and 68 points. This partition is obtained by considering all the bifurcation surfaces of singularities, one related to the presence of invariant straight lines, one related to connections of separatrices, one related to the presence of invariant parabola and one related to the presence of a double limit cycle, modulo "islands".

Theorem 1.1. *There exist* 371 *topologically distinct phase portraits for the closure of the family of quadratic vector fields having a finite saddle–node* $\overline{sn}_{(2)}$ *and an infinite saddle–node of type* $\overline{\binom{0}{2}}\,SN$ *located in the bisector of the first and third quadrants and given by the normal form* (5) *(class* $\overline{\mathbf{QsnSN(C)}}$*). The bifurcation diagram for this class is the projective tridimensional space* $\mathbb{RP}^3$*. All these phase portraits are shown in Figs. 1 to 11. Moreover, the following statements hold:*

(a) There exist 259 *topologically distinct phase portraits in* $\mathbf{QsnSN(C)}$*;*

(b) There exist 49 *phase portraits possessing at least one simple limit cycle (or an odd number of them taking into account their multiplicity), and they are in the parts* V_5*,* V_{17}*,* V_{27}*,* V_{33}*,* V_{54}*,* V_{80}*,* V_{89}*,* V_{90}*,* V_{94}*,* V_{99}*,* V_{100}*,* V_{117}*,* V_{118}*,* V_{134}*,* V_{137}*,* V_{168}*,* V_{176}*,* V_{178}*,* V_{179}*,* V_{180}*,* V_{183}*,* V_{194}*,* $1S_4$*,* $1S_{12}$*,* $1S_{13}$*,* $1S_{16}$*,* $1S_{20}$*,* $1S_{58}$*,* $1S_{59}$*,* $1S_{60}$*,*

$1S_{72}$, $2S_{49}$, $2S_{54}$, $2S_{61}$, $4S_{25}$, $4S_{26}$, $5S_5$, $5S_{22}$, $7S_{27}$, $7S_{28}$, $7S_{53}$, $7S_{56}$, $7S_{74}$, $7S_{81}$, $7S_{83}$, $1.4L_3$, $1.5L_6$, $1.7L_4$ *and* $2.5L_{13}$*;*

(c) There exists one phase portrait with at least one double limit cycle (or an odd number of them taking into account their multiplicity), and it is in the part $10S_1$*;*

(d) There exist two phase portraits with at least two limit cycles (or an even number of them taking into account their multiplicity), and they are in the parts V_{88} *and* V_{182}*;*

(e) There exist 107 *phase portraits with nondegenerate graphics (located in only one place in the phase portrait), and they are in the parts* V_6, V_{53}, V_{102}, V_{107}, V_{113}, V_{138}, V_{166}, V_{168}, V_{172}, V_{173}, V_{174}, V_{176}, V_{183}, V_{189}, $1S_5$, $1S_6$, $1S_{14}$, $1S_{15}$, $1S_{21}$, $1S_{25}$, $1S_{26}$, $1S_{28}$, $1S_{30}$, $1S_{33}$, $1S_{36}$, $1S_{37}$, $1S_{40}$, $1S_{43}$, $1S_{44}$, $1S_{45}$, $1S_{55}$, $1S_{59}$, $1S_{60}$, $1S_{65}$, $1S_{66}$, $1S_{71}$, $2S_{62}$, $4S_{13}$, $4S_{36}$, $4S_{51}$, $5S_{23}$, $5S_{33}$, $7S_1$, $7S_2$, $7S_7$, $7S_{10}$, $7S_{17}$, $7S_{22}$, $7S_{27}$, $7S_{29}$, $7S_{31}$, $7S_{32}$, $7S_{33}$, $7S_{41}$, $7S_{42}$, $7S_{52}$, $7S_{57}$, $7S_{58}$, $7S_{70}$, $7S_{71}$, $7S_{72}$, $7S_{74}$, $7S_{77}$, $7S_{78}$, $7S_{79}$, $7S_{81}$, $7S_{83}$, $7S_{85}$, $1.1L_2$, $1.1L_3$, $1.1L_4$, $1.4L_4$, $1.4L_5$, $1.4L_7$, $1.4L_8$, $1.4L_{12}$, $1.4L_{13}$, $1.5L_4$, $1.5L_5$, $1.7L_1$, $1.7L_2$, $1.7L_3$, $1.7L_5$, $1.7L_6$, $1.7L_{18}$, $1.7L_{21}$, $1.7L_{28}$, $1.7L_{29}$, $1.7L_{32}$, $1.7L_{33}$, $2.7L_{18}$, $2.7L_{19}$, $2.7L_{20}$, $2.8L_1$, $2.8L_2$, $4.7L_1$, $5.7L_1$, $5.7L_9$, $5.7L_{14}$, $7.7L_4$, $7.7L_5$, P_{31}, P_{43}, P_{50}, P_{52}, P_{60} *and* P_{65}*;*

(f) There exist 14 *phase portraits with two disjoint graphics, and they are in the parts* V_{169}, V_{177}, $1S_{53}$, $1S_{56}$, $1S_{57}$, $7S_{67}$, $7S_{75}$, $7S_{76}$, $7S_{82}$, $1.7L_{27}$, $1.7L_{30}$, $1.7L_{31}$, $7.7L_6$ *and* $7.7L_7$*;*

(g) There exist 7 *phase portraits with degenerate graphics, and they are in the parts* $1.2L_8$, $1.3L_2$, P_{23}, P_{57}, P_{58}, P_{64} *and* P_{65}.

In Table 2 we compare the number of phase portraits possessing some geometrical features such as for instance limit cycles or graphics between the class $\mathbf{QsnSN(C)}$ and its border.

Corollary 1.2. *There exist* 14 *topologically distinct phase portraits which appear simultaneously in at least two of the three families* $\overline{\mathbf{QsnSN(A)}}$, $\overline{\mathbf{QsnSN(B)}}$ *and* $\overline{\mathbf{QsnSN(C)}}$. *The correspondences are indicated in Table 1 and the phase portraits in each row are topologically equivalent.*

Table 1. Topological equivalence among phase portraits from families $\overline{\mathbf{QsnSN(A)}}$, $\overline{\mathbf{QsnSN(B)}}$ and $\overline{\mathbf{QsnSN(C)}}$

$\overline{\mathbf{QsnSN(A)}}$	$\overline{\mathbf{QsnSN(B)}}$	$\overline{\mathbf{QsnSN(C)}}$
V_{15}		$4S_{13}$
$3S_1$		$2.4L_9$
$3S_2$		$2.4L_1$
$3S_3$		$2.4L_3$
$3S_4$		$2.4L_5$
$3.4L_1$		P_{22}
$5S_2$	$5S_3$	
	V_6	$4S_{15}$
	V_7	$4S_{44}$
	$9S_1$	$2S_{41}$
	$5.9L_1$	$2.5L_{10}$
$1.2L_2$	$1.4L_1$	$1.3L_2$
P_1	P_1	P_{23}
P_3	P_2	P_{57}

Corollary 1.3. *There exist* 417 *topologically distinct phase portraits in* $\overline{\mathbf{QsnSN}}$.

Corollary 1.4. *After applying a perturbation, some chosen phase portraits in Figs. 1 to 11 yield all the topologically possible phase portrait of codimension–one from group* (A) *expected to exist. So, the seven codimension–one phase portraits from group* (A) *whose realizability was missing can be constructed after perturbations of some chosen phase portraits from* $\overline{\mathbf{QsnSN(C)}}$*; and three codimension–one phase portraits from group* (B) *whose realizability was missing can be constructed after perturbations of some chosen phase portraits from* $\overline{\mathbf{QsnSN(C)}}$.

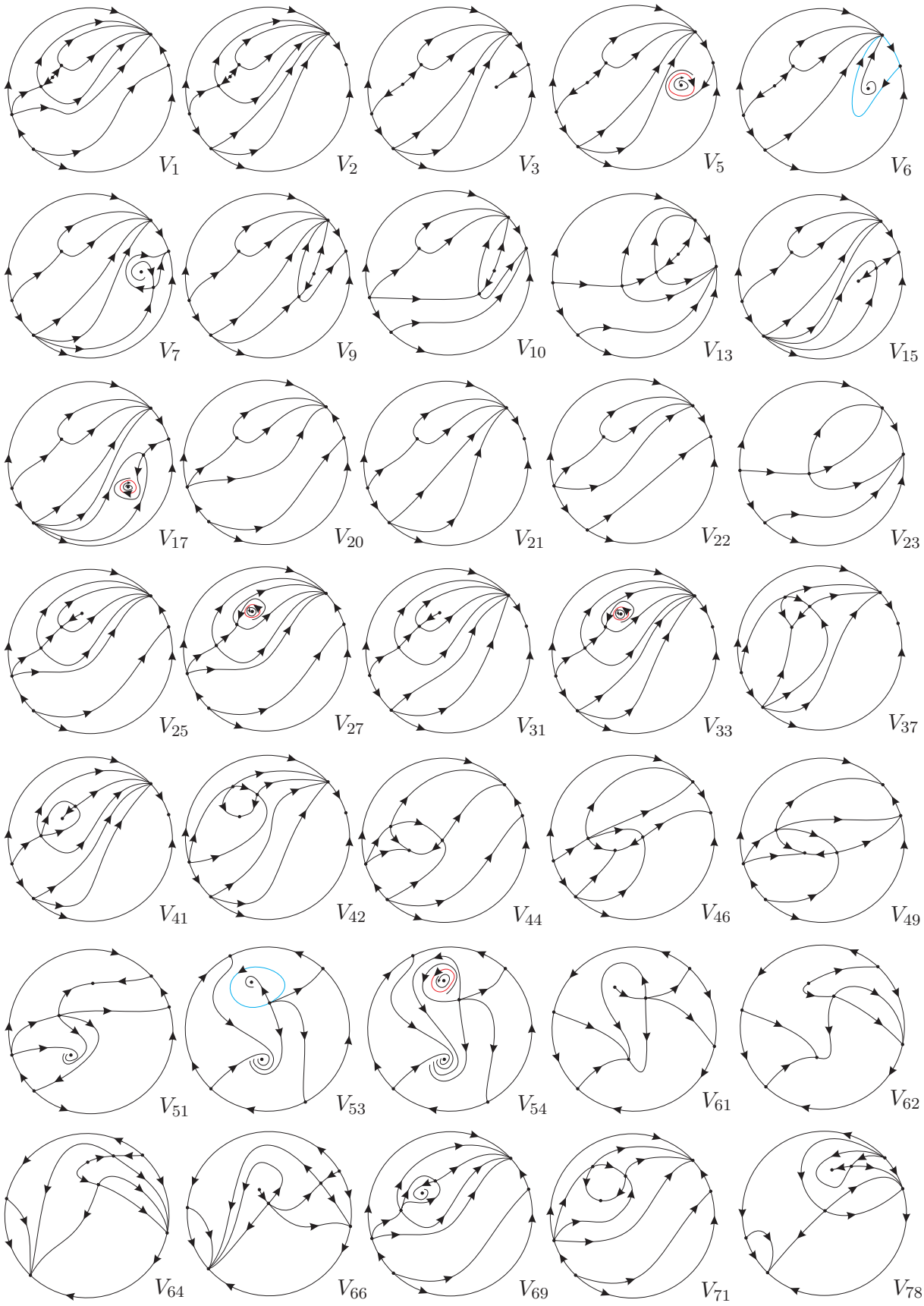

Fig. 1. Phase portraits for quadratic vector fields with a finite saddle–node $\overline{sn}_{(2)}$ and an infinite saddle–node of type $\overline{\binom{0}{2}}SN$ in the bisector of first and third quadrants

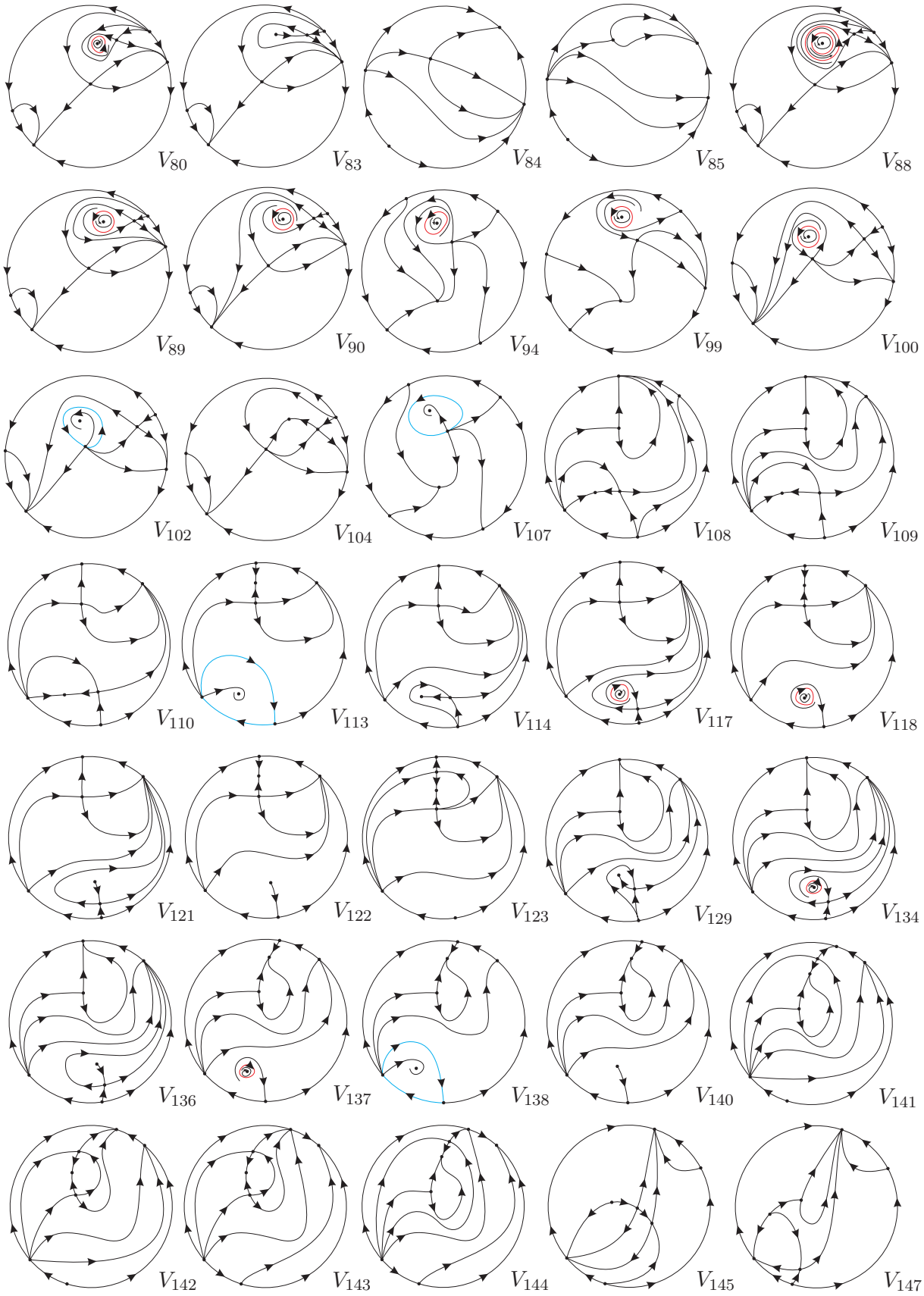

Fig. 2. Continuation of Fig. 1

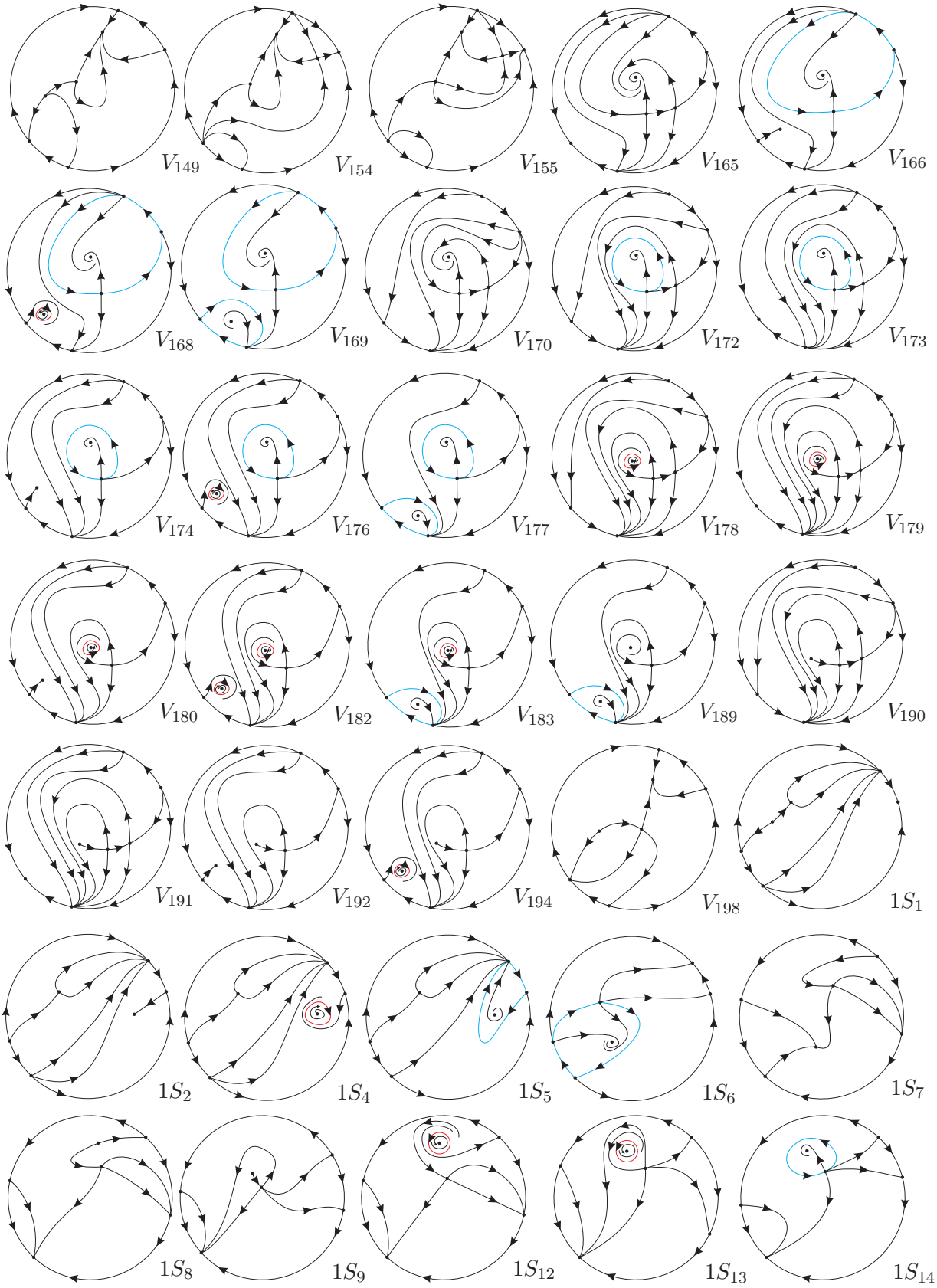

Fig. 3. Continuation of Fig. 2

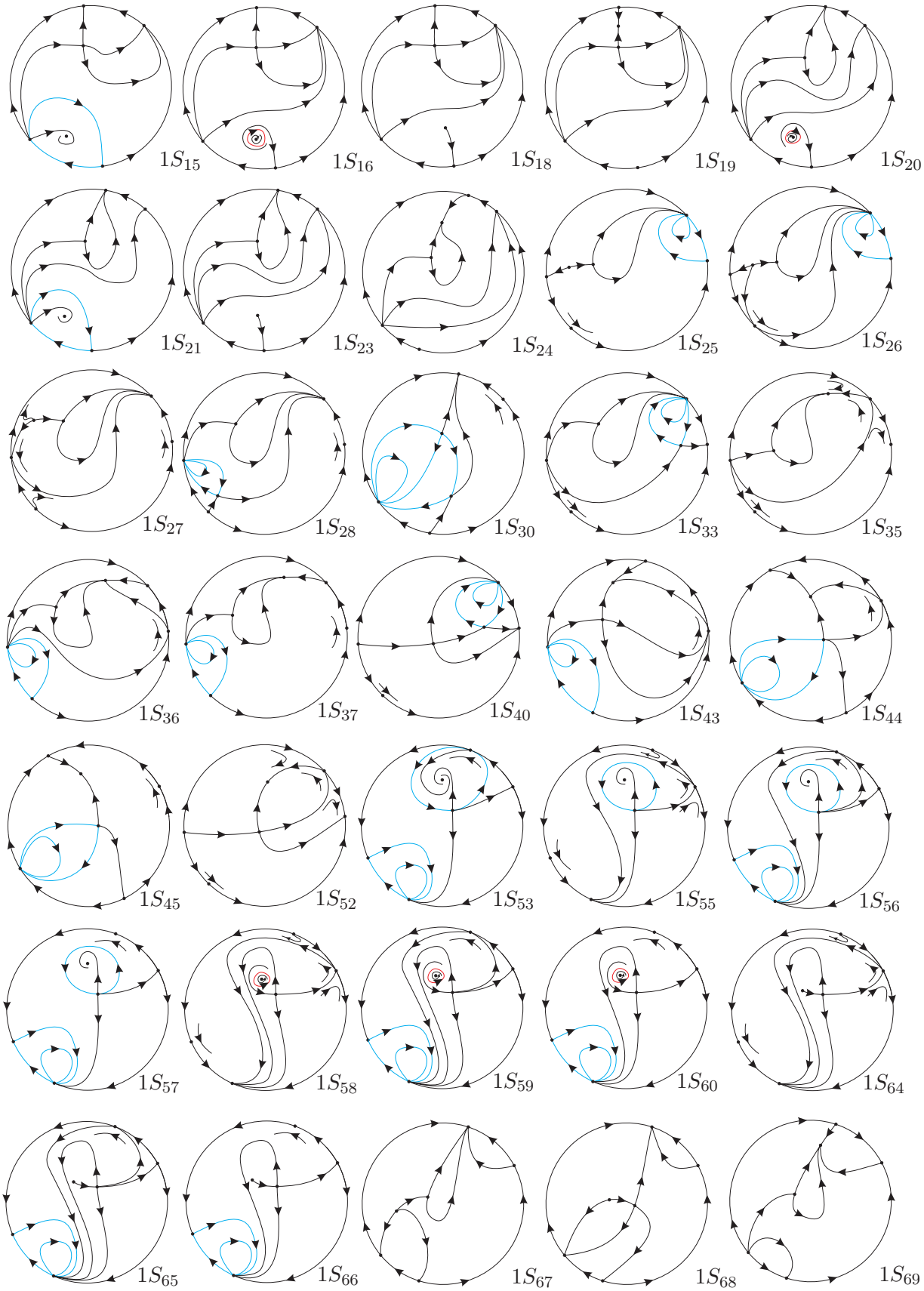

Fig. 4. Continuation of Fig. 3

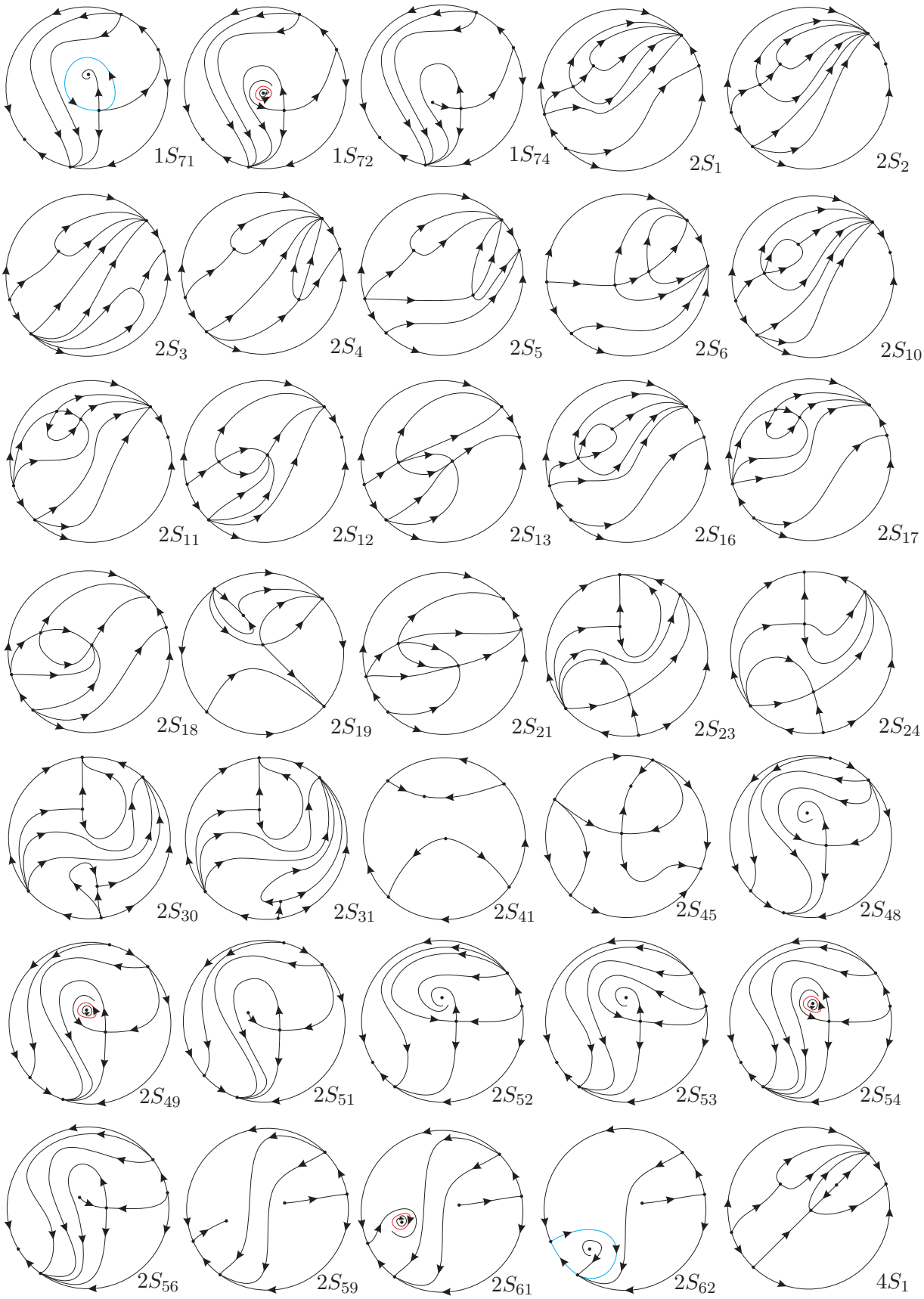

Fig. 5. Continuation of Fig. 4

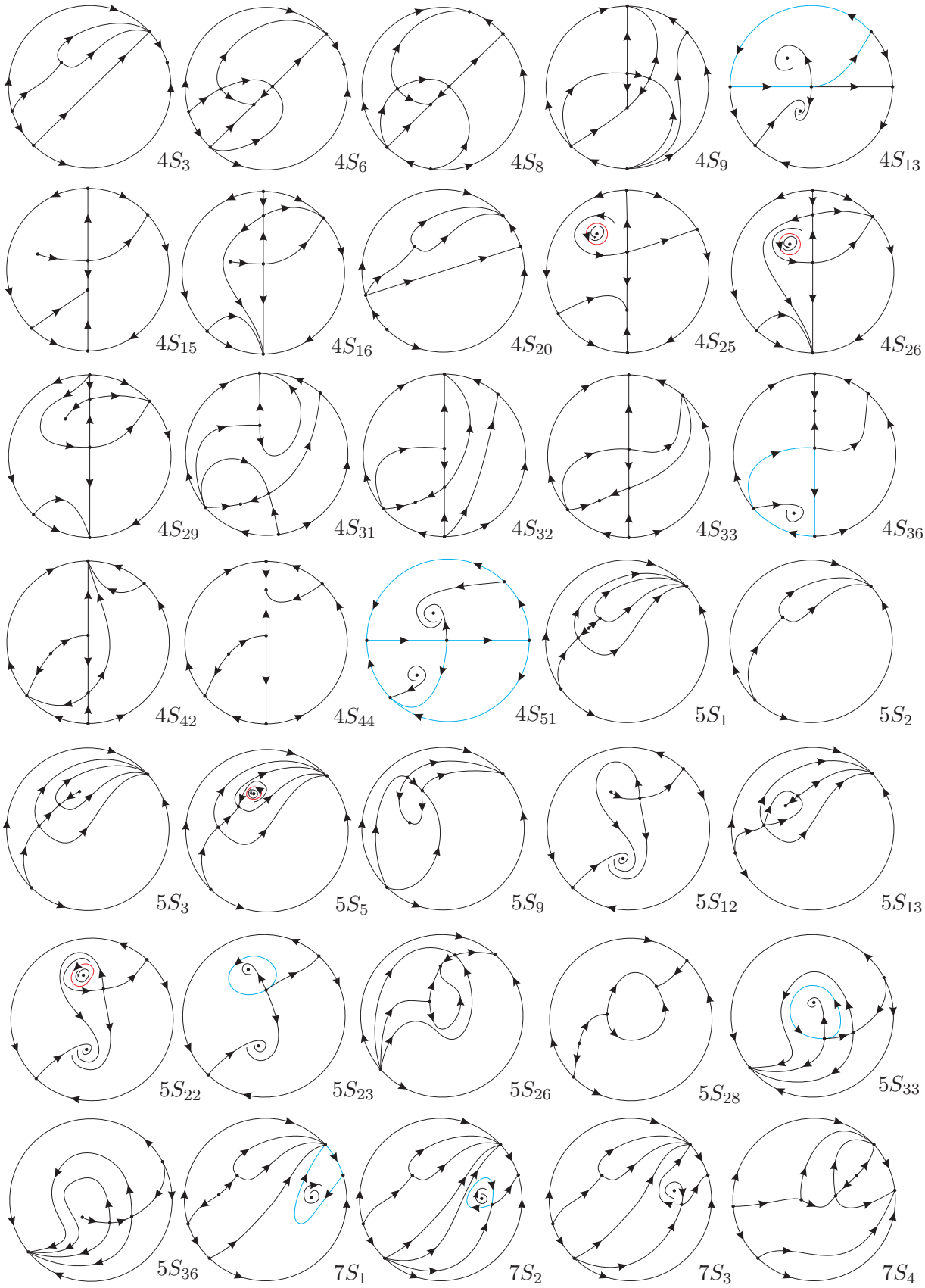

Fig. 6. Continuation of Fig. 5

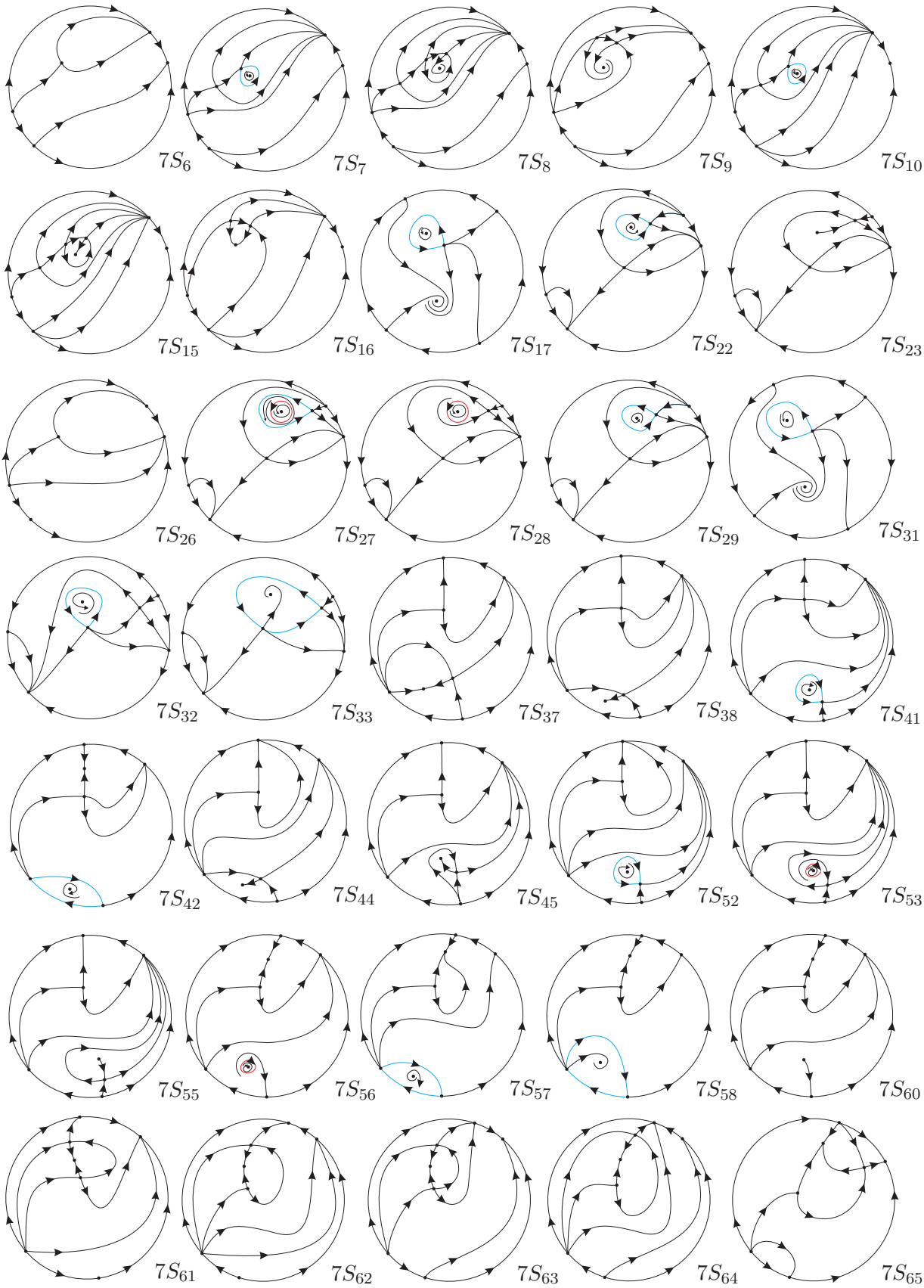

Fig. 7. Continuation of Fig. 6

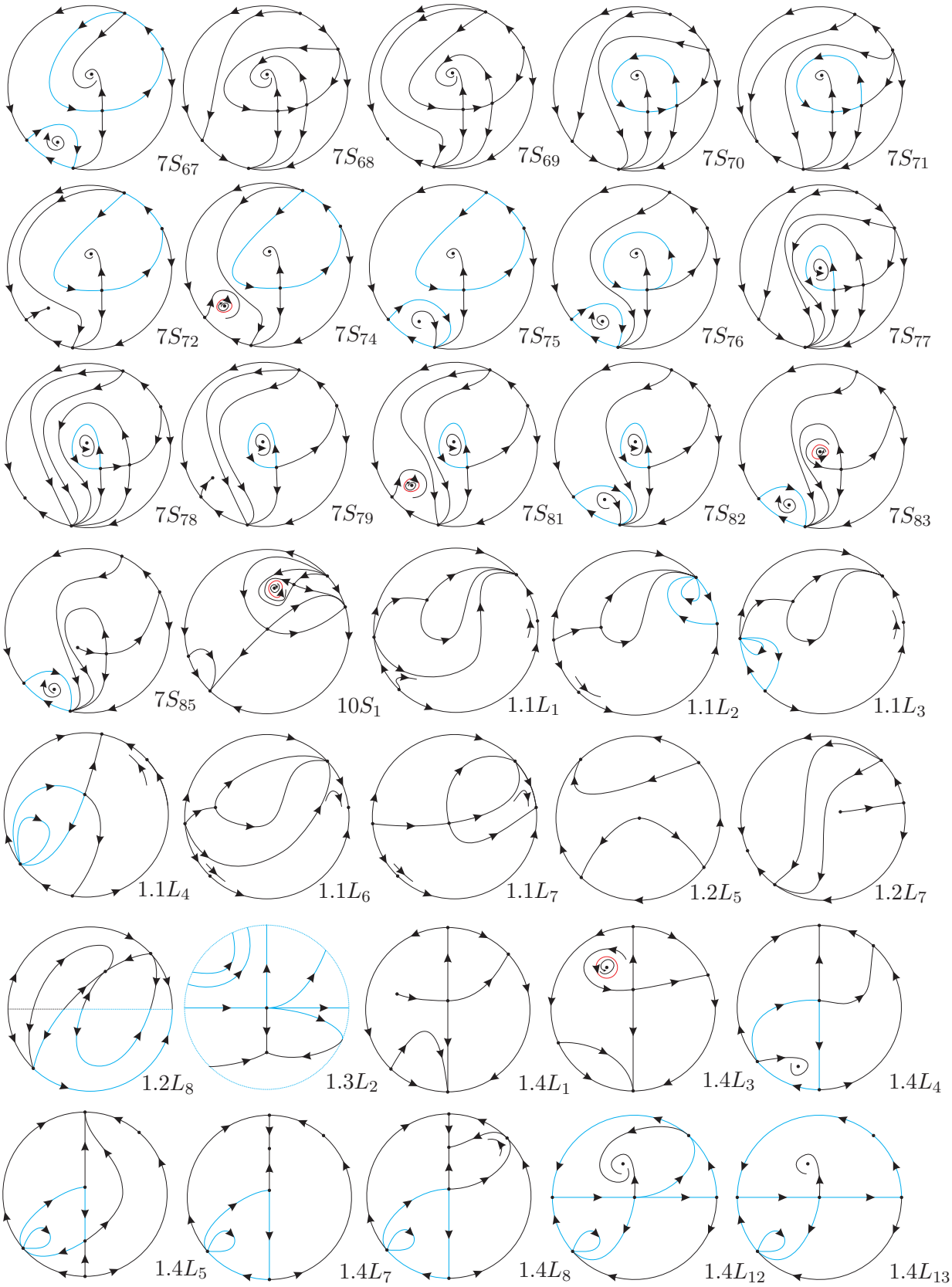

Fig. 8. Continuation of Fig. 7

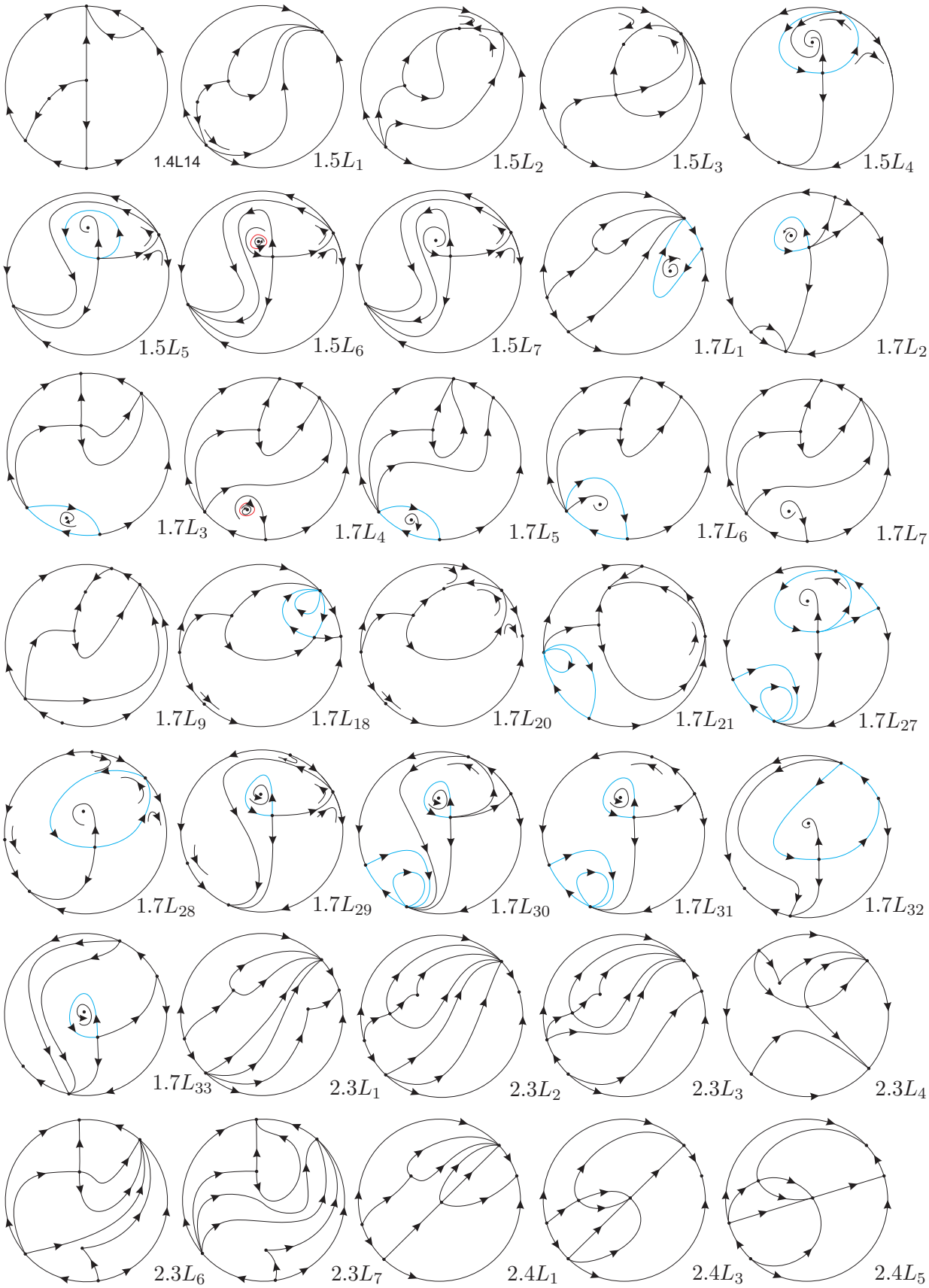

Fig. 9. Continuation of Fig. 8

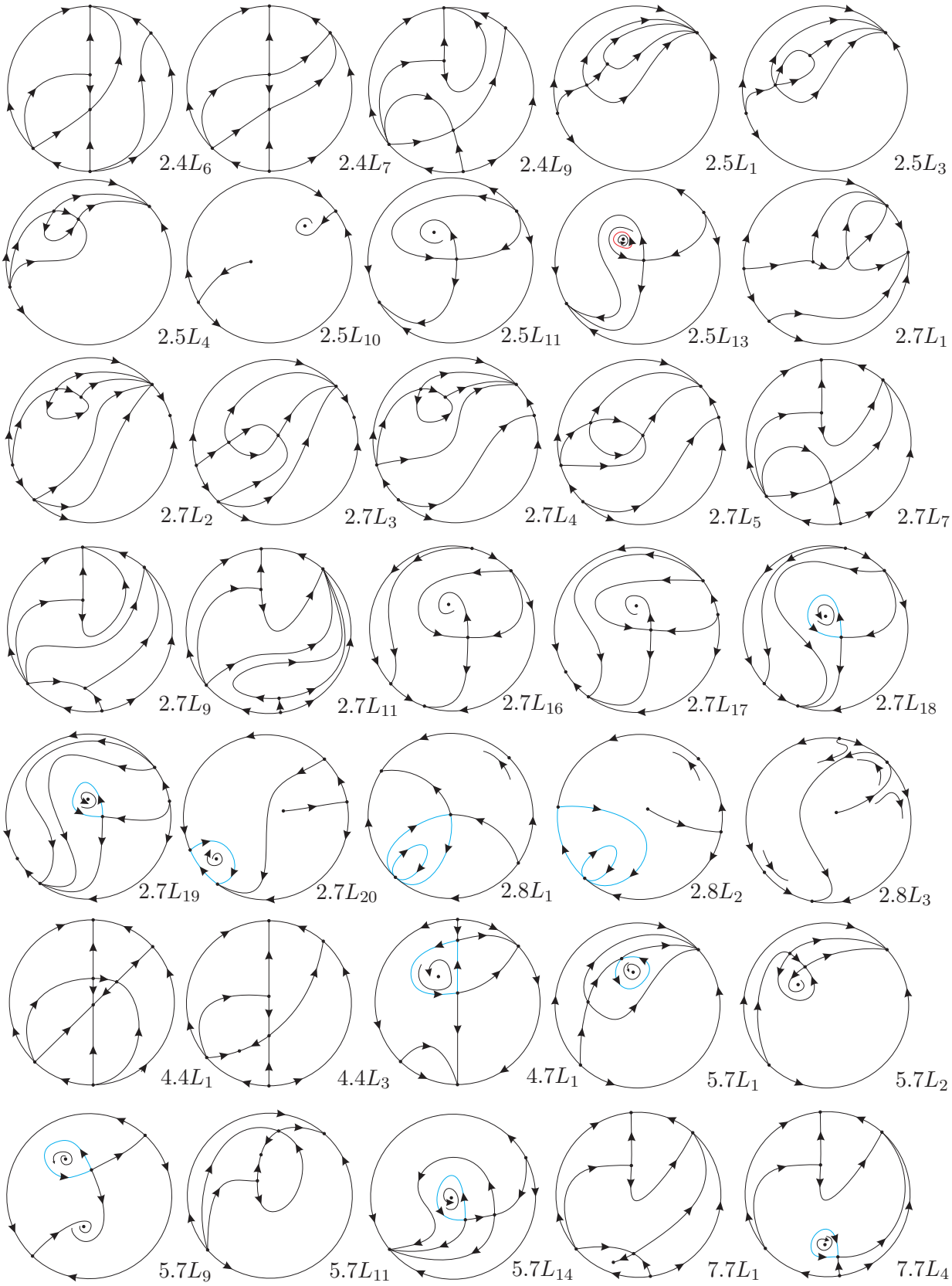

Fig. 10. Continuation of Fig. 9

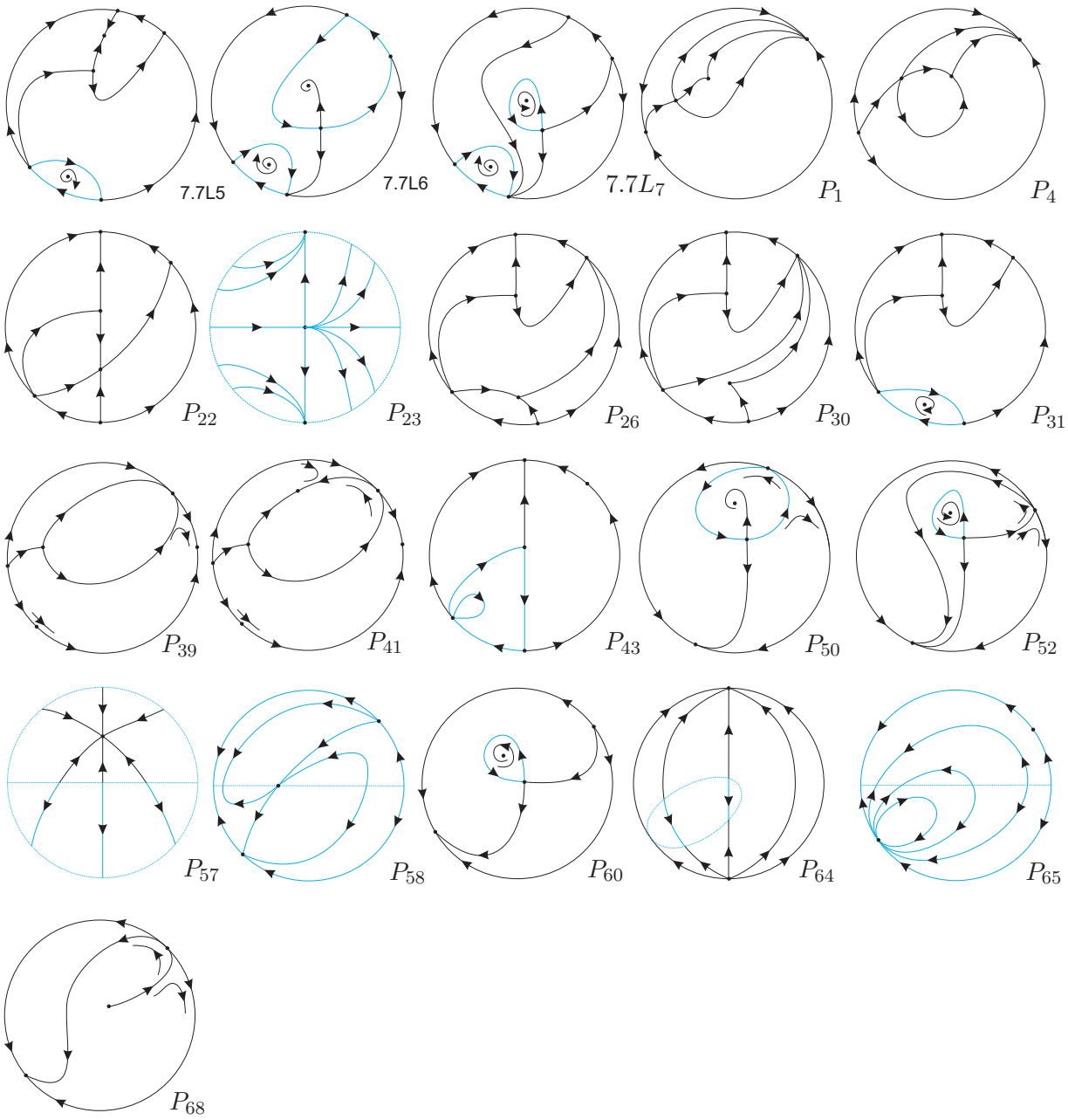

Fig. 11. Continuation of Fig. 10

Table 2. Comparison between the set **QsnSN**(**C**) and its border

	QsnSN(**C**)	border of **QsnSN**(**C**)
Distinct phase portraits	259	112
Phase portraits with exactly one limit cycle	39	10
Phase portraits with two/double limit cycles	2/1	0
Phase portraits with a finite number of nondegenerate graphics	72	14
Phase portraits with an infinite number of nondegenerate graphics	0	35
Phase portraits with degenerate graphics	0	7

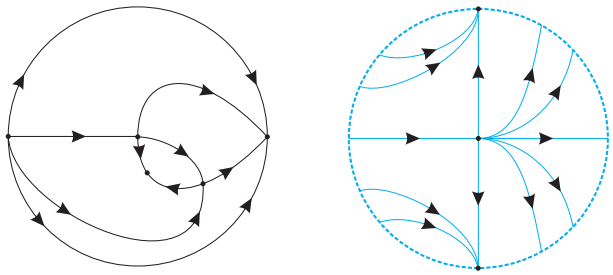

(a) (b)

Fig. 12. (a) This phase portrait is topologically equivalent to $5S_2$ from $\overline{\mathbf{QsnSN}(\mathbf{A})}$ and $5S_3$ from $\overline{\mathbf{QsnSN}(\mathbf{B})}$. (b) This phase portrait is topologically equivalent to P_1 from $\overline{\mathbf{QsnSN}(\mathbf{A})}$ and $5S_3$ from $\overline{\mathbf{QsnSN}(\mathbf{B})}$

Remark 1.5. Phase portrait P_{65} belongs to two different categories in Theorem 1.1 since some of its graphics are nondegenerate.

Remark 1.6 ***(Corrigendum)***. (1) In [Artés *et al.*, 2014] the phase portraits $5S_2$ from $\overline{\mathbf{QsnSN}(\mathbf{A})}$ and $5S_3$ from $\overline{\mathbf{QsnSN}(\mathbf{B})}$ are wrong. The correct picture is given in Fig. 12(a). Moreover, they are equivalent which was not noticed then.

(2) In [Artés *et al.*, 2014] the phase portraits P_1 from $\overline{\mathbf{QsnSN}(\mathbf{A})}$ and P_1 from $\overline{\mathbf{QsnSN}(\mathbf{B})}$ are wrong. The correct picture is given in Fig. 12(b).

For the class $\mathbf{QsnSN}(\mathbf{C})$, from its 259 topologically different phase portraits, 94 occur in three–dimensional parts, 119 in two–dimensional parts, 42 in one–dimensional parts and 4 occur in a single zero–dimensional part.

In Figs. 1 to 11 we have denoted all the singular points with a small disk. We have plotted with wide curves the separatrices and we have added some orbits drawn on the picture with thinner lines to avoid confusion in some required cases.

Remark 1.7. We label the phase portraits according to the parts of the bifurcation diagram where they occur. These labels could be different for two topologically equivalent phase portraits occurring in distinct parts. Some of the phase portraits in 3–dimensional parts also occur in some lower dimensional parts bordering these 3–dimensional parts. An example occurs when a node turns into a focus. An analogous situation happens for phase portraits in 2–dimensional or 1–dimensional parts, coinciding with a phase portrait situated on their border.

The work is organized as follows. In Sec. 2 we describe the normal form for the subfamily of systems having a finite saddle–node and an infinite saddle–node of type $\overline{\binom{0}{2}}SN$ in the bisector of the first and the third quadrant.

For the study of real planar polynomial vector fields two compactifications are used. In Sec. 3 we describe very briefly the Poincaré compactification on the 2–dimensional sphere.

In Sec. 4 we list some very basic properties of general quadratic systems needed in this study.

In Sec. 5 we mention some algebraic and geometric concepts that were introduced in [Schlomiuk *et al.*, 2001, Llibre *et al.*, 2004] involving intersection numbers, zero–cycles, divisors, and T–comitants and invariants for quadratic systems as used by the Sibirskii school. We refer the reader directly to [Artés *et al.*, 2006] where these concepts are widely explained.

In Sec. 6, using algebraic invariants and T–comitants, we construct the bifurcation surfaces for the class $\overline{\mathbf{QsnSN}(\mathbf{C})}$ and in Sec. 7 we comment about the possible existence of "islands" in the bifurcation diagram.

In Sec. 8 we introduce a global invariant denoted by $\mathcal{I}$, which classifies completely, up to topological equivalence, the phase portraits we have obtained for the systems in the class $\overline{\mathbf{QsnSN}(\mathbf{C})}$. Theorem 8.21 shows clearly that they are uniquely determined (up to topological equivalence) by the values of the invariant $\mathcal{I}$.

2. Quadratic vector fields with a finite saddle–node $\overline{sn}_{(2)}$ and an infinite saddle–node of type $\overline{\binom{0}{2}}SN$

In [Artés *et al.*, 2014] we have constructed the normal forms for the subfamilies $\overline{\mathbf{QsnSN}(\mathbf{A})}$ and $\overline{\mathbf{QsnSN}(\mathbf{B})}$ from the normal form for semi–elemental singularity using [Andronov *et al.*, 1973]. It remains to construct the normal form for subfamily $\overline{\mathbf{QsnSN}(\mathbf{C})}$. Its construction will follow the same steps of the previous two subfamilies and it is given in the next result.

Proposition 2.1. *Every system with a finite semi–elemental double saddle–node* $\overline{sn}_{(2)}$ *with its eigenvectors in the direction of the axes, with the eigenvector associated with the zero eigenvalue on the horizontal axis, and an infinite saddle–node of type* $\binom{0}{2}SN$ *located in the endpoints of the bisector of the first and third quadrants can be brought via affine transformations and time rescaling to the following normal form*

$$\begin{aligned}\dot{x} &= gx^2 + 2hxy + (n-g-2h)y^2,\\ \dot{y} &= y + \ell x^2 + (2g+2h-2\ell-n)xy\\ &\quad + (2h+\ell+2(n-g-2h))y^2,\end{aligned} \tag{5}$$

where g, h, ℓ *and* n *are real parameters and* $g \neq 0$.

Proof. By Andronov *et al.* [Andronov *et al.*, 1973], if a quadratic system has a semi–elemental singular point at the origin, it can always be written into the form

$$\begin{aligned}\dot{x} &= gx^2 + 2hxy + ky^2,\\ \dot{y} &= y + \ell x^2 + 2mxy + ny^2.\end{aligned} \tag{6}$$

Moreover, if $g \neq 0$, then we have a double saddle–node $\overline{sn}_{(2)}$ with its eigenvectors in the direction of the axes. The next step is to place the point $\binom{0}{2}SN$ at $[1:1:0]$ of the local chart U_1 with coordinates (w,z). For that, we must guarantee that the point $[1:1:0]$ is a singularity of the flow in U_1,

$$\begin{aligned}\dot{w} &= \ell + (-g+2m)w + (-2h+n)w^2 - kw^3 + wz,\\ \dot{z} &= (-g-2hw-kw^2)z.\end{aligned}$$

Then, we set $n = g+2h+k-\ell-2m$ and, by analyzing the Jacobian of the former system after the substitution in n, we set $m = (g-k-2\ell)/2$ in order to have the eigenvalue associated to the eigenvector on $z=0$ being null. Finally, we apply the rotation $k = n-g-2h$ in the parameter space and obtain the normal form (5). We note that this rotation is just to simplify the bifurcation diagram. ∎

To study the closure of the family $\mathbf{QsnSN}(\mathbf{C})$ within the set of representatives of $\mathbf{QsnSN}(\mathbf{C})$ in the parameter space of the normal form (5) it is necessary to consider the case $g=0$.

The next result assures the existence of invariant straight lines under certain conditions for systems (5).

Lemma 2.2. *For all* $g \in \mathbb{R}$, *systems* (5) *possess the following invariant straight lines under the specific condition:*

(i) $\{x=0\}$, *if* $h=(n-g)/2$;

(ii) $\{y=0\}$, *if* $\ell=0$;

(iii) $\{y=x-1/n\}$, *if* $\ell=g$ *and* $n\neq 0$.

Proof. We consider the algebraic curves

$$\begin{aligned}f_1(x,y) &\equiv x=0,\\ f_2(x,y) &\equiv y=0,\\ f_3(x,y) &\equiv ny-nx+1=0,\end{aligned}$$

and we show that the polynomials

$$\begin{aligned}K_1(x,y) &= gx+(n-g)y,\\ K_2(x,y) &= 1+(2g+2h-n)x-2(g+h-n)y,\\ K_3(x,y) &= ny,\end{aligned}$$

are the cofactors of $f_1=0$, $f_2=0$ and $f_3=0$, respectively, after restricting systems (5) to the respective conditions. ∎

Systems (5) depend on the parameter $\lambda = (g,h,\ell,n) \in \mathbb{R}^4$. We consider systems (5) which are nonlinear, i.e. $\lambda=(g,h,\ell,n)\neq 0$. Applying the affine transformation $X=\alpha x$, $Y=\alpha y$, with $\alpha\neq 0$, we obtain

$$\begin{aligned}\dot{X} &= \alpha' gX^2 + 2\alpha' hXY + \alpha'(n-g-2h)Y^2,\\ \dot{Y} &= y + \alpha'\ell x^2 + \alpha'(2g+2h-2\ell-n)XY\\ &\quad + \alpha'(2h+\ell+2(n-g-2h))Y^2,\end{aligned}$$

for $\alpha' = 1/\alpha$, $\alpha\neq 0$.

Then, this transformation takes the system with parameters (g,h,ℓ,n) to a system with parameters $(\alpha' g, \alpha' h, \alpha'\ell, \alpha' n)$. Hence, instead of considering as parameter space $\mathbb{R}^4$, we may consider $\mathbb{RP}^3$.

But, since for $\alpha'=-1$ all the signs change, we may consider $g\geq 0$ in $[g:h:k:n]$. Since $g^2+h^2+k^2+n^2=1$, then $g=\sqrt{1-(h^2+k^2+n^2)}$, where $0\leq h^2+k^2+n^2\leq 1$.

We can therefore view the parameter space as a ball $\overline{\mathcal{B}} = \{(h,\ell,n)\in\mathbb{R}^3;\ h^2+\ell^2+n^2\leq 1\}$, where on the equator two opposite points are identified. When $n=0$, we identify the point $[g:h:\ell:0]\in\mathbb{RP}^3$ with $[g:h:\ell]\in\mathbb{RP}^2$. So, this subset $\{n=0\}\subset\overline{\mathcal{B}}$ can be identified with $\mathbb{RP}^2$, which can be viewed as a disk with two opposite points on the circumference (the equator) identified (see Fig. 13).

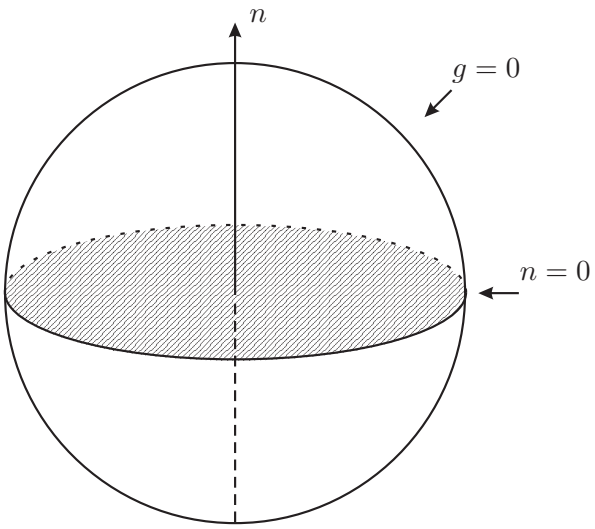

Fig. 13. The parameter space

For $g \neq 0$, we get the affine chart:

$$\mathbb{RP}^3 \setminus \{g = 0\} \leftrightarrow \mathbb{R}^3$$
$$[g : h : \ell : n] \mapsto \left(\frac{h}{g}, \frac{\ell}{g}, \frac{n}{g}\right) = (\overline{h}, \overline{\ell}, \overline{n})$$
$$[1 : \overline{h} : \overline{\ell} : \overline{n}] \mapsto (\overline{h}, \overline{\ell}, \overline{n}).$$

The plane $g = 0$ in $\mathbb{RP}^3$ corresponds to the equation $h^2+\ell^2+n^2 = 1$ (the full sphere $\mathbb{S}^2$) and the line $g = n = 0$ in $\mathbb{RP}^3$ corresponds to the equation $h^2 + \ell^2 = 1$ (the equator $n = 0$ of $\mathbb{S}^2$).

We now consider planes in $\mathbb{R}^3$ of the form $\overline{n} = n_0$, where n_0 is a constant. The projective completion of such a plane in $\mathbb{RP}^3$ has the equation $n - n_0 g = 0$. So, we see how the slices $\overline{n} = n_0$ need to be completed in the ball (see Fig. 14). We note that when $g = 0$ necessarily we must have $n = 0$ on such a slice, and thus the completion of the image of the plane $\overline{n} = n_0$, when visualized in $\mathbb{S}^3$, must include the equator.

The specific equations of the correspondence of the points in the plane $\overline{n} = n_0$ of $\mathbb{R}^3$ (n_0 a constant) onto points in the interior of $\mathbb{S}^2$ ($\mathcal{B} = \{(h, \ell, n) \in \mathbb{R}^3;\ h^2 + \ell^2 + n^2 < 1\}$) follows from the bijection:

$$\mathbb{R}^3 \leftrightarrow \mathcal{B}$$
$$(\overline{h}, \overline{\ell}, \overline{n}) \leftrightarrow \left(\frac{\overline{h}}{c}, \frac{\overline{\ell}}{c}, \frac{\overline{n}}{c}\right)$$

with $c = \sqrt{\overline{h}^2 + \overline{\ell}^2 + \overline{n}^2 + 1}$. That is, for each plane $\overline{n} =$ constant in $\mathbb{R}^3$, there corresponds a half ellipsoid $h^2 + \ell^2 + n^2(1 + n_0^2)/n_0^2 = 1,\ n \geq 0$ (see Fig. 14).

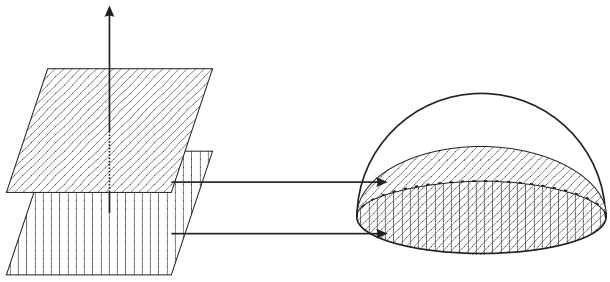

Fig. 14. Correspondence between planes and ellipsoides

3. The Poincaré compactification and the complex (real) foliation with singularities on $\mathbb{CP}^2$ ($\mathbb{RP}^2$)

A real planar polynomial vector field ξ can be compactified on the sphere as follows. We identify the $xy-$plane with the plane $Z = 1$ in the space $\mathbb{R}^3$ with coordinates X, Y, Z. The central projection of the vector field ξ on the sphere of radius one yields a diffeomorphic vector field on the upper hemisphere and also another vector field on the lower hemisphere. There exists (for a proof see [Gonzales, 1969]) an analytic extension $cp(\xi)$ of the vector field ξ on the whole sphere having the same phase curves as the one constructed above from the polynomial vector field. The projection of the closed northern hemisphere H^+ of $\mathbb{S}^2$ on $Z = 0$ under $(X, Y, Z) \to (X, Y)$ is called *the Poincaré disc*. A singular point r of $cp(\xi)$ is called an *infinite* (respectively, *finite*) singular point if $r \in \mathbb{S}^1$, the equator (respectively, $r \in \mathbb{S}^2 \setminus \mathbb{S}^1$). The vector field $cp(\xi)$ restricted to the upper hemisphere completed with the equator is called the *Poincaré compactification of a polynomial vector field* ξ.

For every vector field

$$p\frac{\partial}{\partial x} + q\frac{\partial}{\partial y}, \tag{7}$$

where $p(x, y)$ and $q(x, y)$ are polynomials with real coefficients, or equivalently for every differential system

$$\dot{x} = p(x, y), \qquad \dot{y} = q(x, y), \tag{8}$$

we consider the associated differential $1-$form $\omega_1 =$

$q(x,y)dx - p(x,y)dy$, and the differential equation

$$\omega_1 = 0, \tag{9}$$

which defines a foliation with singularities on $\mathbb{C}^2$. The affine plane $\mathbb{C}^2$ is compactified on the complex projective space $\mathbb{CP}^2 = (\mathbb{C}^3 \setminus \{0\})/\sim$, where $(X,Y,Z) \sim (X',Y',Z')$ if, and only if, $(X,Y,Z) = \lambda(X',Y',Z')$ for some complex $\lambda \neq 0$. The equivalence class of (X,Y,Z) will be denoted by $[X:Y:Z]$.

The foliation with singularities defined by equation (9) on $\mathbb{C}^2$ can be extended to a foliation with singularities on $\mathbb{CP}^2$ and the 1−form ω_1 can be extended to a meromorphic 1−form ω on $\mathbb{CP}^2$ which yields an equation $\omega = 0$, i.e.

$$\begin{aligned} A(X,Y,Z)dX + B(X,Y,Z)dY \\ + C(X,Y,Z)dZ = 0, \end{aligned} \tag{10}$$

whose coefficients A, B, C are homogeneous polynomials of the same degree and satisfy the relation:

$$\begin{aligned} A(X,Y,Z)X + B(X,Y,Z)Y \\ + C(X,Y,Z)Z = 0, \end{aligned} \tag{11}$$

Indeed, consider the map $i : \mathbb{C}^3 \setminus \{Z=0\} \to \mathbb{C}^2$, given by $i(X,Y,Z) = (X/Z, Y/Z) = (x,y)$ and suppose that $\max\{\deg(p), \deg(q)\} = m > 0$. Since $x = X/Z$ and $y = Y/Z$ we have:

$$dx = \frac{ZdX - XdZ}{Z^2}, \quad dy = \frac{ZdY - YdZ}{Z^2},$$

the pull–back form $i^*(\omega_1)$ has poles at $Z = 0$ and yields the equation

$$\begin{aligned} i^*(\omega_1) = q\left(\frac{X}{Z}, \frac{Y}{Z}\right)\frac{ZdX - XdZ}{Z^2} \\ - p\left(\frac{X}{Z}, \frac{Y}{Z}\right)\frac{ZdY - YdZ}{Z^2} = 0. \end{aligned}$$

Then, the 1−form $\omega = Z^{m+2} i^*(\omega_1)$ in $\mathbb{C}^3 \setminus \{Z \neq 0\}$ has homogeneous polynomial coefficients of degree $m+1$, and for $Z = 0$ the equations $\omega = 0$ and $i^*(\omega_1) = 0$ have the same solutions. Therefore, the differential equation $\omega = 0$ can be written as (10), where

$$\begin{aligned} A(X,Y,Z) &= ZQ(X,Y,Z) \\ &= Z^{m+1} q\left(\frac{X}{Z}, \frac{Y}{Z}\right), \\ B(X,Y,Z) &= -ZP(X,Y,Z) \\ &= -Z^{m+1} p\left(\frac{X}{Z}, \frac{Y}{Z}\right), \\ C(X,Y,Z) &= YP(X,Y,Z) \\ &\quad - XQ(X,Y,Z). \end{aligned} \tag{12}$$

Clearly A, B and C are homogeneous polynomials of degree $m+1$ satisfying (11).

In particular, for our quadratic systems (5), A, B and C take the following forms:

$$\begin{aligned} A(X,Y,Z) =& (\ell X^2 + (2g + 2h - 2\ell - n)XY \\ &+ (2n - 2g - 2h + \ell)Y^2 + YZ)Z \\ B(X,Y,Z) =& -(gX^2 + 2hXY + (n - g - 2h)Y^2)Z, \\ C(X,Y,Z) =& -\ell X^3 + (n - g - 2h + 2\ell)X^2 Y \\ &+ (2g + 4h - \ell - 2n)XY^2 \\ &- (g + 2h - n)Y^3 - XYZ. \end{aligned} \tag{13}$$

We note that the straight line $Z = 0$ is always an algebraic invariant curve of this foliation and that its singular points are the solutions of the system: $A(X,Y,Z) = B(X,Y,Z) = C(X,Y,Z) = 0$. We note also that $C(X,Y,Z)$ does not depend on b.

To study the foliation with singularities defined by the differential equation (10) subject to (11) with A, B, C satisfying the above conditions in the neighborhood of the line $Z = 0$, we consider the two charts of $\mathbb{CP}^2$: $(u,z) = (Y/X, Z/X)$, $X \neq 0$, and $(v,w) = (X/Y, Z/Y)$, $Y \neq 0$, covering this line. We note that in the intersection of the charts $(x,y) = (X/Z, Y/Z)$ and (u,z) (respectively, (v,w)) we have the change of coordinates $x = 1/z$, $y = u/z$ (respectively, $x = v/w$, $y = 1/w$). Except for the point $[0:1:0]$ or the point $[1:0:0]$, the foliation defined by equations (10),(11) with A, B, C as in (12) yields in the neighborhood of the line $Z = 0$ the foliations associated with the systems

$$\begin{aligned} \dot{u} =& uP(1,u,z) - Q(1,u,z) = C(1,u,z), \\ \dot{z} =& zP(1,u,z), \end{aligned} \tag{14}$$

or

$$\begin{aligned} \dot{v} =& vQ(v,1,w) - P(v,1,w) = -C(v,1,w), \\ \dot{w} =& wP(v,1,w). \end{aligned} \tag{15}$$

In a similar way we can associate a real foliation with singularities on $\mathbb{RP}^2$ to a real planar polynomial vector field.

4. A few basic properties of quadratic systems relevant for this study

The following results hold for any quadratic system:

(i) A straight line either has at most two (finite) contact points with a quadratic system (which include the singular points), or it is formed by trajectories of the system; see Lemma 11.1 of [Ye *et al.*, 1986]. We recall that by definition a *contact point* of a straight line L is a point of L where the vector field has the same direction as L, or it is zero.

(ii) If a straight line passing through two real finite singular points r_1 and r_2 of a quadratic system is not formed by trajectories, then it is divided by these two singular points in three segments $\overline{\infty r_1}$, $\overline{r_1 r_2}$ and $\overline{r_2 \infty}$ such that the trajectories cross $\overline{\infty r_1}$ and $\overline{r_2 \infty}$ in one direction, and they cross $\overline{r_1 r_2}$ in the opposite direction; see Lemma 11.4 of [Ye *et al.*, 1986].

(iii) If a quadratic system has a limit cycle, then it surrounds a unique singular point, and this point is a focus; see [Coppel, 1966].

(iv) A quadratic system with an invariant straight line has at most one limit cycle; see [Coll & Llibre, 1988].

(v) A quadratic system with more than one invariant straight line has no limit cycle; see [Bautin, 1954].

The proof of the next result can be found in [Artés *et al.*, 1998].

Proposition 4.1. *Any graphic or degenerate graphic in a real planar polynomial differential system must either*

1) surround a singular point of index greater than or equal to +1, or

2) contain a singular point having an elliptic sector situated in the region delimited by the graphic, or

3) contain an infinite number of singular points.

5. Some algebraic and geometric concepts

In this article we use the concept of intersection number for curves (see [Fulton, 1969]). For a quick summary see Sec. 5 of [Artés *et al.*, 2006].

We shall also use the concepts of zero–cycle and divisor (see [Hartshorne, 1977]) as specified for quadratic vector fields in [Schlomiuk *et al.*, 2001]. For a quick summary see Sec. 6 of [Artés *et al.*, 2006].

We shall also use the concepts of algebraic invariant and T–comitant as used by the Sibirskii school for differential equations. For a quick summary see Sec. 7 of [Artés *et al.*, 2006].

In the next section we describe the algebraic invariants and T–comitants which are relevant in the study of family (5), see Sec. 6.

6. The bifurcation diagram of the systems in $\overline{\mathbf{QsnSN(C)}}$

6.1. Bifurcation surfaces due to the changes in the nature of singularities

From Sec. 7 of [Artés *et al.*, 2008] and [Vulpe, 2011] we get the formulas which give the bifurcation surfaces of singularities in $\mathbb{R}^{12}$, produced by changes that may occur in the local nature of finite singularities. From [Schlomiuk *et al.*, 2005] we get equivalent formulas for the infinite singular points. These bifurcation surfaces are all algebraic and they are the following:

Bifurcation surfaces in $\mathbb{RP}^3$ due to multiplicities of singularities

($\mathcal{S}_1$) This is the bifurcation surface due to multiplicity of infinite singularities involved with finite singular points. This occurs when at least one finite singular point collides with at least one infinite singular point. This is a quartic whose equation is

$$\mu = n^2(-g^2 - 2gh + 2h\ell + \ell^2 + gn) = 0.$$

($\mathcal{S}_2$) Since this family already has a saddle–node at the origin, the invariant $\mathbb{D}$ is always zero. The next $T-$comitant related to finite singularities is $\mathbb{T}$. If this $T-$comitant vanishes, it may mean either the existence of another finite semi–elemental singular point, or the origin being a singular point of higher

multiplicity, or the system being degenerate. The equation of this surface is

$$\mathbb{T} = -12g^2\,(g^2 + 2gh + h^2 - gn) = 0.$$

($\mathcal{S}_5$) Since this family already has a saddle–node at infinity formed by the collision of two infinite singularities, the invariant η is always zero. In this sense, we have to consider a bifurcation related to the existence of either the double infinite singularity $\binom{0}{2}SN$ plus a simple one, or a triple one. This phenomenon is ruled by the $T-$comitant $\widetilde{M}$. The equation of this surface is

$$\widetilde{M} = (g + 2h + \ell - n)^2 = 0.$$

The surface of C^∞ bifurcation points due to a strong saddle or a strong focus changing the sign of their traces (weak saddle or weak focus)

($\mathcal{S}_3$) This is the bifurcation surface due to weak finite singularities, which occurs when the trace of a finite singular point is zero. The equation of this surface is given by

$$\begin{aligned}\mathcal{T}_4 = n(&-4g^3 - 8g^2h - 4g^2\ell - 4gh\ell - 8h^2\ell\\ &- 4h\ell^2 + 4g^2n + 4g\ell n + \ell^2 n) = 0.\end{aligned}$$

We note that this bifurcation surface can either produce a topological change, if the weak point is a focus, or just a C^∞ change, if it is a saddle. However, in the case this bifurcation coincides with a loop bifurcation associated with the same saddle, the change is also topological, as we can see later in the analysis of systems (5) (see page 55).

The surface of C^∞ bifurcation due to a node becoming a focus

($\mathcal{S}_6$) This surface will contain the points of the parameter space where a finite node of the system turns into a focus. This surface is a C^∞ but not a topological bifurcation surface. In fact, when we only cross the surface ($\mathcal{S}_6$) in the bifurcation diagram, the phase portraits do not change topologically. However, this surface is relevant for isolating the parts where a limit cycle surrounding an anti-saddle cannot exist. The equation of this surface is given by $W_4 = 0$, where

$$\begin{aligned}W_4 = n^2(&16g^6 + 64g^5h + 64g^4h^2 - 32g^5\ell\\ &- 160g^4h\ell - 192g^3h^2\ell - 16g^4\ell^2 + 32g^3h\ell^2\\ &+ 112g^2h^2\ell^2 - 32gh^3\ell^2 + 32g^3\ell^3 + 64g^2h\ell^3\\ &+ 32h^3\ell^3 + 16h^2\ell^4 - 32g^5n - 64g^4hn\\ &+ 64g^4\ell n + 160g^3h\ell n + 8g^3\ell^2 n - 80g^2h\ell^2 n\\ &+ 16gh^2\ell^2 n - 40g^2\ell^3 n - 8gh\ell^3 n - 16h^2\ell^3 n\\ &- 8h\ell^4 n + 16g^4n^2 - 32g^3\ell n^2 + 8g^2\ell^2 n^2\\ &+ 8g\ell^3 n^2 + \ell^4 n^2).\end{aligned}$$

Bifurcation surface in $\mathbb{RP}^3$ due to the presence of invariant straight lines

($\mathcal{S}_4$) This surface will contain the points of the parameter space where an invariant straight line appears (see Lemma 2.2). This surface is split in some parts. Depending on these parts, the straight line may contain connections of separatrices from different points or not. So, in some cases, it may imply a topological bifurcation and, in others, just a C^∞ bifurcation. The equation of this surface is given by

$$\text{Inv} = \ell(\ell - g)\,(g + 2h - n) = 0.$$

These bifurcation surfaces are all algebraic and they, except ($\mathcal{S}_4$), are the bifurcation surfaces of singularities of systems (5) in the parameter space. We shall discover other two bifurcation surfaces not necessarily algebraic. On one of them the systems have global connection of separatrices different from that given by ($\mathcal{S}_4$) and on the other the systems possess double limit cycle. The equations of these bifurcation surfaces can only be determined approximately by means of numerical tools. Using arguments of continuity in the phase portraits we can prove the existence of these components not necessarily algebraic in the part where they appear, and we can check them numerically. We shall name them surfaces ($\mathcal{S}_7$) (connection of separatrices) and ($\mathcal{S}_{10}$) (double limit cycles).

Remark 6.1. On surface ($\mathcal{S}_{10}$), the respective systems have at least one double limit cycle. Although this surface is obtained numerically, we can predict in which portion of the bifurcation diagram it can be placed. It must be in the neighborhood of the points of the bifurcation diagram corresponding to

a weak focus $f^{(2)}$ or a weak saddle $s^{(1)}$ which forms a loop. So, according to [Vulpe, 2011; Main Theorem, item (b_2)], the necessary condition for the existence of weak points of order two or higher is governed by $\mathcal{T}_4 = \mathcal{F}_1 = 0$. The expression of $\mathcal{F}_1$ is given by $\mathcal{F}_1 = -2g^2 - 4gh + 4g\ell + 6h\ell + 2gn - 3\ell n$.

We shall foliate the 3−dimensional bifurcation diagram in $\mathbb{RP}^3$ by the planes $n = n_0$, n_0 constant, plus the open half sphere $g = 0$ and we shall give pictures of the resulting bifurcation diagram on these planar sections on a disk or in an affine chart of $\mathbb{R}^2$.

In what follows we work in the chart of $\mathbb{RP}^3$ corresponding to $g \neq 0$, and we take $g = 1$. To do the study, we shall use pictures which are drawn on planes $n = n_0$ of $\mathbb{RP}^3$, having coordinates $[1 : h : \ell : n_0]$. In these planes the coordinates are (h, ℓ) where the horizontal line is the h−axis.

As the final bifurcation diagram is quite complex, it is useful to introduce colors for each one of the bifurcation surfaces. They are:

(a) the curve obtained from the surface $(\mathcal{S}_1)$ is drawn in blue (a finite singular point collides with an infinite one);

(b) the curve obtained from the surface $(\mathcal{S}_2)$ is drawn in green (two finite singular points different from the saddle–node collide);

(c) the curve obtained from the surface $(\mathcal{S}_3)$ is drawn in yellow (when the trace of a singular point becomes zero);

(d) the curve obtained from the surface $(\mathcal{S}_4)$ is drawn in purple (the presence of invariant straight lines);

(e) the curve obtained from the surface $(\mathcal{S}_5)$ is drawn in red (three infinite singular points collide);

(f) the curve obtained from the surface $(\mathcal{S}_6)$ is drawn in black (an antisaddle is on the edge of turning from a node to a focus or vice versa);

(g) the curve obtained from the surface $(\mathcal{S}_7)$ is drawn in purple (the connection of separatrices); and

(h) the curve obtained from the surface $(\mathcal{S}_{10})$ is drawn in gray (presence of a double limit cycle).

The following lemmas of this section study the geometrical behavior of the surfaces for $g \neq 0$ (the case $g = 0$ will be considered separately), that is, their singularities, their intersection points and their extrema (maxima and minima) with respect to the coordinate n. We will not provide the complete proof of all the following lemmas since many of them are similar one of the other. Their complete proofs can be found in [Rezende, 2014].

Lemma 6.2. *For $gn \neq 0$, surface $(\mathcal{S}_1)$ has no singularities and, for $g \neq 0$ and $n = 0$, it has two straight lines of singularities given by $[1 : h : 1 : 0]$ and $[1 : h : -1 - 2h : 0]$.*

Proof. As surface $(\mathcal{S}_1)$ is the union of a double plane and a conic with no singularities, its singularities will be the intersection between these two components. In this sense, we set $n = 0$ and, solving the expression of the conic with respect to ℓ, we find the straight lines $[1 : h : 1 : 0]$ and $[1 : h : -1-2h, 0]$. ■

Lemma 6.3. *For $g \neq 0$, surface $(\mathcal{S}_2)$ has no singularities. Moreover, this surface assumes its minimum (with respect to the coordinate n) at $h = -1$.*

Proof. Setting $g \neq 0$, it follows straightforwardly from the expression of $\mathbb{T} = -12(1 + 2h + h^2 - n)$ and parameterizing this surface, we obtain $[1 : h : \ell : (1+h)^2]$ which clearly has a minimum at $h = -1$, which corresponds to $n = 0$. ■

Lemma 6.4. *For $gn \neq 0$, surface $(\mathcal{S}_3)$ has a straight line of singularities given by $[1 : 1/2 : -2 : n]$. Moreover, in this surface there exist two distinguished points: $[1 : 1/2 : -2 : 2]$ and $[1 : 1/2 : -2 : 9/4]$. For $g \neq 0$ and $n = 0$, surface $(\mathcal{S}_3)$ has two curves of singularities: the straight line $[1 : h : -1 - 2h : 0]$ and the hyperbola $[1 : h : -1/h : 0]$, and they intersect at the points $[1 : -1 : 1 : 0]$ and $[1 : 1/2 : -2 : 0]$.*

Proof. For $gn \neq 0$, surface $(\mathcal{S}_3)$ is the union of the plane $\{n = 0\}$ and the cubic $C = 4n-8h-4+(4n-4h-8h^2-4)\ell+(n-4h)\ell^2 = 0$. Computing the derivatives of C and solving them (for $g \neq 0$) we get

the straight line $[1 : 1/2 : -2 : n]$ of singularities. We verify that the determinant of the Hessian of C restricted to this straight line is identically zero. In addition, calculating the discriminant of C with respect to h and ℓ, we obtain, respectively,

$$\begin{aligned}\mathrm{Discrim}_h(C) =& 16(2+\ell)^2(1-2\ell+\ell^2+2\ell n),\\ \mathrm{Discrim}_\ell(C) =& 16(2h-1)^2(1+2h+h^2-n).\end{aligned}$$

So, the resultant of both discriminants with respect to h vanishes if, and only if, $\ell = -2$ or $n = (-1+2\ell-\ell^2)/(2\ell)$, implying that $n = 9/4$ (which is obtained by evaluating the resultant on the line of singularities) is a distinguished point.

Now, we want to investigate the existence of a value of the parameter $n = n_0$ at which the cubic C factorizes, i.e. we want to rewrite C as one of the following forms:

$$\begin{aligned}C(h,\ell,n_0) =& (h-h_0)\,D_2(h,\ell) \quad \text{or}\\ C(h,\ell,n_0) =& (\ell-\ell_0)\,D_2(h,\ell),\end{aligned}$$

where $D_2(h,\ell)$ is a polynomial of degree 2 in the variables h and ℓ. For this, we rewrite the cubic C in the forms:

$$\begin{aligned}C_1(h,\ell,n_0) =& (n_0-4h)\ell^2 - 4(1+h+2h^2-n_0)\ell\\ &- 4(1+2h-n_0),\\ C_2(h,\ell,n_0) =& -8\ell h^2 - 4(2+\ell+\ell^2)h\\ &- 4 - 4\ell + 4n_0 + 4\ell n_0 + \ell^2 n_0.\end{aligned}$$

As we are interested in the set of zeroes of C, we equalize to zero the coefficients of C_1 and C_2 in the variables ℓ and h, respectively, and we conclude that only possible solution comes from the zeroes of C_1 which is $h = 1/2, n_0 = 2$. Thus, we can factorize the cubic C as $C(h,\ell,2) = -2(2h-1)(2+2\ell+2h\ell+\ell^2)$, implying that $n = 2$ is also a distinguished value of the parameter n.

In the case $g \neq 0$ and $n = 0$, we have $\mathcal{T}_4 \equiv 0$. Denoting by F the derivative of $\mathcal{T}_4$ with respect to n, we obtain $F = -4(1+2h+\ell)(1+h\ell)$, implying that $1+2h+\ell = 0$ and $1+h\ell = 0$ are the singular curves of $(\mathcal{S}_3)$ with $n = 0$, which correspond to the projective curves $[1 : h : -1-2h : 0]$ and $[1 : h : -1/h : 0]$. In addition, it is easy to see that both curves intersect at the points $[1 : -1 : 1 : 0]$ and $[1 : 1/2 : -2 : 0]$. ■

Lemma 6.5. *For $g \neq 0$, surface $(\mathcal{S}_4)$ has two straight lines of singularities given by $[1 : (n-1)/2 : 0 : n]$ and $[1 : (n-1)/2 : 1 : n]$.*

Lemma 6.6. *For $g \neq 0$, surface $(\mathcal{S}_5)$ has no singularities.*

Lemma 6.7. *For $gn \neq 0$, surface $(\mathcal{S}_6)$ has two curves of singularities: $[1 : (n-1)/2 : 0 : n]$ (a straight line) and $[1 : (\ell-2)/\ell : \ell : 4(4-7\ell+2\ell^2+\ell^3)/(\ell(-4+4\ell+\ell^2))]$. Moreover, the curve $[1 : (\ell-2)/\ell : \ell : 4(4-7\ell+2\ell^2+\ell^3)/(\ell(-4+4\ell+\ell^2))]$ assumes its extrema (with relation to the coordinate n) in the values $\ell = -4$, $\ell = 1$, $\ell = (-3 \pm \sqrt{41})/4$ and $\ell = f^{-1}(n_0)$, where $f = 4(4-7\ell+2\ell^2+\ell^3)/(\ell(-4+4\ell+\ell^2))$ and $n_0 = (3 - (1548 - 83\sqrt{249})^{1/3}/3^{2/3} - 61/(3(1548 - 83\sqrt{249}))^{1/3})/2$. For $g \neq 0$ and $n = 0$, its singularities lie on the two straight lines $[1 : h : 1 : 0]$ and $[1 : h : -1-2h : 0]$ and on the two curves $[1 : (1-2\ell \pm \sqrt{1-4\ell+5\ell^2-2\ell^3})/\ell^2 : \ell : 0]$.*

Proof. For the computation of the singular curves of $(\mathcal{S}_6)$ we refer to [Rezende, 2014]. To compute the extrema of the curve $[1 : (\ell-2)/\ell : \ell : 4(4-7\ell+2\ell^2+\ell^3)/(\ell(-4+4\ell+\ell^2))]$, we equalize the last coordinate to n and obtain the polynomial $p = -4(\ell-1)^2(4+\ell)+\ell(-4+4\ell+\ell^2)n$. Computing its discriminant with respect to ℓ, we have:

$$\mathrm{Discrim}_\ell(p) = 256n(125-17n-9n^2+2n^3),$$

whose solutions are $n = 0$ and $n = (3 - (1548 - 83\sqrt{249})^{1/3}/3^{2/3} - 61/(3(1548 - 83\sqrt{249}))^{1/3})/2 \approx -3.40133804\ldots$. Besides, we consider the leading coefficient of p in ℓ and solve it with respect to n, obtaining $n = 4$. This proves that p has degree 3 for every n, except when $n = 4$. Finally, solving the equation $p = 0$ by substituting n by the singular values of n, we obtain $\ell = -4$, $\ell = 1$, $\ell = (-3 \pm \sqrt{41})/4$ and $\ell = f^{-1}(n_0)$, where $f = 4(4-7\ell+2\ell^2+\ell^3)/(\ell(-4+4\ell+\ell^2))$ and $n_0 = (3 - (1548 - 83\sqrt{249})^{1/3}/3^{2/3} - 61/(3(1548 - 83\sqrt{249}))^{1/3})/2$, which are the critical values of the curve with respect to n. ■

Lemma 6.8. *For $g \neq 0$, the invariant $\mathcal{F}_1$ defined in Remark 6.1 has a straight line of singularities given by $[1 : (3n-4)/6 : 2/3 : n]$.*

Lemma 6.9. *For $g \neq 0$, surfaces $(\mathcal{S}_1)$ and $(\mathcal{S}_2)$ intersect along the straight line $[1 : -1 : \ell : 0]$ and the parabola $[1 : h : -h : (1+h)^2]$. Moreover, the curve $[1 : h : -h : (1+h)^2]$ assumes its extremum*

(with relation to the coordinate n) in the value $h = -1$ and, in addition, the contact along this curve is even.

Proof. Solving the system of equations

$$(\mathcal{S}_1) : n^2(-1-2h+2h\ell+\ell^2+n) = 0,$$
$$(\mathcal{S}_2) : -12(1+2h+h^2-n) = 0,$$

we obtain the two solutions $h = -1, n = 0$ and $\ell = -h, n = (1+h)^2$, which correspond to the curves $[1 : -1 : \ell : 0]$ and $[1 : h : -h : (1+h)^2]$, respectively.

It is easy to see that the extremum of the coordinate n of the curve $[1 : h : -h : (1+h)^2]$ is reached at $h = -1$ and its minimum value is $n = 0$.

To prove the contact between both surfaces along the curve $\gamma = [1 : h : -h : (1+h)^2]$, we apply the affine change of coordinates given by $n = 1 + 2h + h^2 - v$, $v \in \mathbb{R}$. Under this transformation, the gradient vector of $(\mathcal{S}_2)$ along the curve γ is $\nabla\mathbb{T}(\gamma) = [1 : 0 : 0 : -12]$, whereas the gradient vector of $(\mathcal{S}_1)$ along the curve γ is $\nabla\mu(\gamma) = [1 : 0 : 0 : -1]$, whose last coordinate is always negative. As $\nabla\mu(\gamma)$ does not change its sign, this vector will always point to the same direction in relation to $(\mathcal{S}_2)$ restricted to the previous change of coordinates. Then, the surface $(\mathcal{S}_1)$ remains only on one of the two topological subspaces delimited by the surface $(\mathcal{S}_2)$. ■

Lemma 6.10. *For $g \neq 0$, surfaces $(\mathcal{S}_1)$ and $(\mathcal{S}_3)$ has the plane $\{n = 0\}$ as a common component. Besides, the surfaces intersect along the straight lines $[1 : h : 1 : 0]$, $[1 : h : -1-2h : 0]$ and $[1 : h : 0 : 1+2h]$, the hyperbola $[1 : h : -1/h : 0]$ and the curve $[1 : -\ell(\ell+3)/4 : \ell : (2-3\ell+\ell^3)/2]$. Moreover, this last curve assumes its extrema (with relation to the coordinate n) in the values $\ell = \pm 1$ and $\ell = \pm 2$.*

Lemma 6.11. *For $g \neq 0$, surfaces $(\mathcal{S}_1)$ and $(\mathcal{S}_4)$ intersect along the straight lines $[1 : -1/2 : \ell : 0]$, $[1 : h : 0 : 0]$, $[1 : h : 1 : 0]$, $[1 : h : 0 : 1+2h]$ and $[1 : -\ell/2 : \ell : 1-\ell]$.*

Lemma 6.12. *For $g \neq 0$, surfaces $(\mathcal{S}_1)$ and $(\mathcal{S}_5)$ intersect along the straight lines $[1 : h : -1-2h : 0]$ and $[1 : (n-1)/2 : 0 : n]$.*

Lemma 6.13. *For $g \neq 0$, surfaces $(\mathcal{S}_1)$ and $(\mathcal{S}_6)$ has the plane $\{n = 0\}$ as a common component. Besides, the surfaces intersect along the straight lines $[1 : h : 1 : 0]$, $[1 : h : -1-2h : 0]$ and $[1 : -(\ell+1)/2 : \ell : 0]$ and the curves $[1 : h : -(1+2h \pm (1+h)\sqrt{(1+2h)})/h^2 : 0]$ and $[1 : -\ell(\ell+7)/8 : \ell : (\ell-1)^2(\ell+4)/4]$. Moreover, this last curve assumes its extrema (with relation to the coordinate n) in the values $\ell = -4$, $\ell = -7/3$, $\ell = 1$ and $\ell = 8/3$.*

Lemma 6.14. *For $g \neq 0$, surfaces $(\mathcal{S}_2)$ and $(\mathcal{S}_3)$ intersect along the straight line $[1 : -1 : \ell : 0]$ and the curve $[1 : h : 2h/(h-1) : (1+h)^2]$. Moreover, they have a contact of order two along the curve $[1 : h : 2h/(h-1) : (1+h)^2]$, and this curve has the straight line $\{h = 1\}$ as an asymptote.*

Lemma 6.15. *For $g \neq 0$, surfaces $(\mathcal{S}_2)$ and $(\mathcal{S}_4)$ intersect along the parabolas $[1 : h : 0 : (1+h)^2]$ and $[1 : h : 1 : (1+h)^2]$ and the straight line $[1 : 0 : \ell : 1]$. Moreover, the curves $[1 : h : 0 : (1+h)^2]$ and $[1 : h : 1 : (1+h)^2]$ assume their extremum (with relation to the coordinate n) in the value $h = -1$.*

Lemma 6.16. *For $g \neq 0$, surfaces $(\mathcal{S}_2)$ and $(\mathcal{S}_5)$ intersect along the curve $[1 : h : h^2 : (1+h)^2]$. Moreover, the curve $[1 : h : h^2 : (1+h)^2]$ assumes its extrema (with relation to the coordinate n) in the value $h = -1$.*

Lemma 6.17. *For $g \neq 0$, surfaces $(\mathcal{S}_2)$ and $(\mathcal{S}_6)$ intersect along the straight line $[1 : -1 : \ell : 0]$ and the curve $[1 : h : 2h/(h-1) : (1+h)^2]$. Moreover, they have a contact of order two along the curve $[1 : h : 2h/(h-1) : (1+h)^2]$ and this curve has the straight line $\{h = 1\}$ as an asymptote.*

Lemma 6.18. *For $g \neq 0$, surfaces $(\mathcal{S}_3)$ and $(\mathcal{S}_4)$ intersect along the straight lines $[1 : -1/2 : \ell : 0]$, $[1 : h : 0 : 0]$, $[1 : h : 1 : 0]$, $[1 : 1/2 : \ell : 2]$, $[1 : h : 0 : 1+2h]$ and $[1 : -\ell/4 : \ell : (2-\ell)/2]$ and the parabola $[1 : h : 1 : 8(1+h)^2/9]$. Moreover, this parabola assumes its extremum (with relation to the coordinate n) in the value $h = -1$.*

Lemma 6.19. *For $g \neq 0$, surfaces $(\mathcal{S}_3)$ and $(\mathcal{S}_5)$ intersect along the straight lines $[1 : h : -1-2h : 0]$, $[1 : (n-1)/2 : 0 : n]$ and $[1 : (3+n)/6 : 2(n-3)/3 : n]$.*

Lemma 6.20. *For $g \neq 0$, surfaces $(\mathcal{S}_3)$ and $(\mathcal{S}_6)$ has the plane $\{n = 0\}$ as a common component. Besides, the surfaces intersect along the curves $[1 : h : -1-2h : 0]$, $[1 : -1/\ell : \ell : 0]$, $[1 : h : 1 : 0]$, $[1 : h : -(1+2h \pm (1+h)\sqrt{1+2h})/h^2 : 0]$, $[1 : h : 0 : 1+2h]$, $[1 : \ell/(\ell-2) : \ell : 4(\ell-1)^2/(\ell-2)^2]$ and $[1 : (-2+2\ell+\ell^2)/(-4+2\ell+\ell^2) : \ell : 4(\ell-1)^2(2+\ell)(4+\ell)/(-4+2\ell+\ell^2)^2]$. Moreover, the curve $[1 : \ell/(\ell-2) : \ell : 4(\ell-1)^2/(\ell-2)^2]$ has the straight line $\{\ell = 2\}$ as an asymptote and corresponds to a even contact between the surfaces, and the curve $[1 : (-2+2\ell+\ell^2)/(-4+2\ell+\ell^2) : \ell : 4(\ell-1)^2(2+\ell)(4+\ell)/(-4+2\ell+\ell^2)^2]$ assumes its extrema (with relation to the coordinate n) in the values $\ell = -4$, $\ell = -2$, $\ell = 1$, $\ell = -3 \pm \sqrt{17}$, $\ell = -5 \pm \sqrt{21}$ and $\ell = 3 - \sqrt{21} \pm 4\sqrt{2(13 - 2\sqrt{21})/17}$.*

Lemma 6.21. *For $g \neq 0$, surface $(\mathcal{S}_3)$ and surface $(\mathcal{S}_{\mathcal{F}_1})$ given by $\{\mathcal{F}_1 = 0\}$ intersect along the curves $[1 : (1-2\ell)/(3\ell-2) : \ell : 0]$, $[1 : h : 0 : 1+2h]$ and $[1 : (4-8\ell+3\ell^2 \pm \sqrt{3}\sqrt{(2+\ell)^3(3\ell-2)})/(16-24\ell) : \ell : (12-24\ell+3\ell^2 \pm \sqrt{3}\sqrt{(2+\ell)^3(3\ell-2)})/(8-12\ell)]$. Moreover, this last curves assume their extrema (with relation to the coordinate n) in the values $\ell = -2$, $\ell = 7/10$, $\ell = 1$ and $\ell = (-7 \pm 5\sqrt{5})/6$.*

Lemma 6.22. *For $g \neq 0$, surfaces $(\mathcal{S}_4)$ and $(\mathcal{S}_5)$ intersect along the curves $[1 : (n-1)/2 : 0 : n]$ and $[1 : n/2 - 1 : 1 : n]$.*

Lemma 6.23. *For $g \neq 0$, surfaces $(\mathcal{S}_4)$ and $(\mathcal{S}_6)$ intersect along the curves $[1 : -1/2 : \ell : 0]$, $[1 : h : 1 : 0]$, $[1 : (n-1)/2 : 0 : n]$ and $[1 : (n-1)/2 : -4(n-1)/(n-2)^2 : n]$. Moreover, the curve $[1 : (n-1)/2 : -4(n-1)/(n-2)^2 : n]$ assumes its extrema (with relation to the coordinate n) in the value $\ell = 1$.*

Lemma 6.24. *For $g \neq 0$, surfaces $(\mathcal{S}_5)$ and $(\mathcal{S}_6)$ intersect along the curves $[1 : h : -1-2h : 0]$, $[1 : -(\ell+1)/2 : \ell : 0]$ and $[1 : -(16-24\ell+9\ell^2+\ell^3)/(8\ell-6\ell^2) : \ell : 4(\ell-1)^2(4+\ell)/(\ell(3\ell-4))]$. Moreover, the curve $[1 : -(16-24\ell+9\ell^2+\ell^3)/(8\ell-6\ell^2) : \ell : 4(\ell-1)^2(4+\ell)/(\ell(3\ell-4))]$ assumes its extrema (with relation to the coordinate n) in the values $\ell = -4$, $\ell = 1$ and $\ell = f^{-1}(n_0)$, where $f(\ell) = 4(\ell-1)^2(4+\ell)/(\ell(3\ell-4))$ and $n_0 = (130 - 4511/(208855 + 16956\sqrt{471})^{1/3} + (208855 + 16956\sqrt{471})^{1/3})/27$.*

The purpose now is to find the slices in which the intersection among at least three surfaces or other equivalent phenomena happen. Since there exist 25 distinct curves of intersections or contacts between two any surfaces, we need to study 325 different possible intersections of these surfaces. As the relation is very long, we will reproduce only a few of them deploying the different algebraic techniques used to solve them. The full set of proves can be found on the web page http://mat.uab.es/∼artes/articles/qvfsn2SN02/qvfsn2SN02.html.

Remark 6.25. In the next four lemmas we use the following notation. A curve of intersection or contact between two surfaces will be denoted by $solAByC$, where $A < B$ are the numbers of the surfaces involved in the intersection or contact and C is a cardinal. Moreover, these four lemmas illustrate the different techniques we use to solve the intersection among at least three surfaces or other equivalent phenomena.

Lemma 6.26. *Surfaces $(\mathcal{S}_1)$, $(\mathcal{S}_2)$ and $(\mathcal{S}_3)$ intersect in slices when $n = 0$ and $n = 1$.*

Proof. By Lemmas 6.9 and 6.10, we have the curves $\text{sol12y1} = \left[1 : h : -h : (1+h)^2\right]$ and $\text{sol13y2} = \left[1 : -\ell(3+\ell)/4 : \ell : (2 - 3\ell + \ell^3/2\right]$. By equalizing each corresponding coordinate and solving the obtained system, we have the solutions $h = -1, \ell = 1$ and $h = \ell = 0$. Since the curves are parametrized by h and ℓ, we must substitute the solutions of the system in the expressions of the curves and consider the value of the coordinate n. Then, the values of n where the three surfaces intersect are $n = 0$ and $n = 1$. ■

Lemma 6.27. *Surfaces $(\mathcal{S}_3)$, $(\mathcal{S}_5)$ and $(\mathcal{S}_6)$ intersect in slices when $n = 6$ and $n = 9$.*

Proof. By Lemmas 6.19 and 6.24, we have the curves $\text{sol35y2} = [1 : (3+n)/6 : 2(n-3)/3 : n]$ and

$$\text{sol56y1} = \left[1 : (16 - 24\ell + 9\ell^2 + \ell^3)/2\ell(3\ell - 4) : \ell : 4(\ell-1)^2(4+\ell)/\ell(3\ell-4)\right].$$

By equalizing each corresponding coordinate and solving the obtained system, we get the solutions $\ell = 2, n = 6$ and $\ell = 4, n = 9$. Then, the values of

n where the three surfaces intersect are $n = 6$ and $n = 9$. ■

Lemma 6.28. *Surfaces* $(\mathcal{S}_1)$, $(\mathcal{S}_3)$ *and* $(\mathcal{S}_5)$ *intersect in slice when* $n = 3$.

Proof. By Lemmas 6.10 and 6.19, we have the curves sol13y1 $= [1 : h : 0 : 1 + 2h]$ and sol35y2 $= [1 : (3 + n)/6 : 2(n - 3)/3 : n]$. By equalizing each corresponding coordinate and solving the obtained system, we have the solution $h = 1, n = 3$. Then, the value of n where the three surfaces intersect is $n = 3$. ■

Lemma 6.29. *Surfaces* $(\mathcal{S}_1)$, $(\mathcal{S}_4)$, $(\mathcal{S}_5)$ *and* $(\mathcal{S}_6)$ *intersect in slice when* $n = 1$.

Proof. By Lemmas 6.12 and 6.23, we have the curves sol15y1 $= [1 : (n - 1)/2 : 0 : n]$ and sol46y2 $= \big[1 : (n - 1)/2 : -4(n - 1)/(n - 2)^2 : n\big]$. By equalizing each corresponding coordinate and solving the obtained system, we get the solution $n = 1$, which is the value of n where the four surfaces intersect is $n = 1$. ■

The next result presents all the algebraic values of n corresponding to singular slices in the bifurcation diagram. Its proof follows from Lemmas 6.26 to 6.29 and by computing all the remaining 321 different possible intersections or contacts among three or more surfaces.

Lemma 6.30. *The full set of needed algebraic singular slices in the bifurcation diagram of family* $\overline{\mathbf{QsnSN(C)}}$ *is formed by* 20 *elements which correspond to the values of* n *in* (16).

The numeration in (16) is not consecutive since we reserve numbers for other slices not algebraically determined and for generic slices.

Now we sum up the content of the previous lemmas. In (16) we list all the algebraic values of n where significant phenomena occur for the bifurcation diagram generated by singularities. We first have the two extreme values for n, i.e. $n = -\infty$ (corresponding to $g = 0$) and $n = 9$. We remark that to perform the bifurcation diagram of all singularities for $n = -\infty$ we set $g = 0$ and, in the remaining three variables (h, ℓ, n), yielding the point $[h : \ell : n]$ in $\mathbb{RP}^2$, we take the chart $n \neq 0$ in which we may assume $n = -1$.

$$
\begin{aligned}
&n_1 = 9, \quad n_{15} = 6,\\
&n_{17} = \frac{1}{27}\left(130 - \frac{4511}{\sqrt[3]{\alpha}} + \sqrt[3]{\alpha}\right),\ \alpha = 208855 + 16956\sqrt{471},\\
&n_{25} = 4,\ n_{19} = 125/27,\ n_{21} = 9/2,\ n_{23} = \frac{3}{100}(102 + 7\sqrt{21}),\\
&n_{27} = \tfrac{(\beta-8)(\beta-2)(\beta+7)^2}{\left(\sqrt[3]{2\delta^2}+98\sqrt[3]{\frac{4}{\delta^2}}+\beta+6\right)^2},\ \beta = 14\sqrt[3]{\tfrac{2}{\delta}} + \sqrt[3]{4\delta},\ \delta = 61 - 9\sqrt{29},\\
&n_{29} = 2 + \sqrt{2},\ n_{31} = 3,\ n_{33} = 8/3,\ n_{37} = 9/4,\\
&n_{41} = \frac{3}{100}(102 - 7\sqrt{21}), \quad n_{45} = 2, \quad n_{55} = 1,\\
&n_{57} = 2 - \sqrt{2}, \quad n_{59} = 1/2, \quad n_{83} = 0,\\
&n_{85} = \frac{1}{2}\left(\frac{3 - \sqrt[3]{\rho}}{3^{2/3}} - \frac{61}{\sqrt[3]{3\rho}}\right),\ \rho = 1548 - 83\sqrt{249}\\
&n_{87} = -\infty.
\end{aligned}
\tag{16}
$$

In order to determine all the parts generated by the bifurcation surfaces from $(\mathcal{S}_1)$ to $(\mathcal{S}_{10})$, we first draw the horizontal slices of the three–dimensional parameter space which correspond to the explicit values of n obtained in Lemma 6.30. However, as it will be discussed later, the presence of nonalgebraic bifurcation surfaces will be detected and the singular slices corresponding to their singular behavior as we move from slice to slice will be approximately determined. We add to each interval of singular values of n an intermediate value for which we represent the bifurcation diagram of singularities. The diagram will remain essentially unchanged in these open intervals except the parts affected by the bifurcation. All the sufficient values of n are shown in (17).

The values indexed by positive odd indices in (17) correspond to explicit values of n for which there exists a bifurcation in the behavior of the systems on the slices. Those indexed by even values are just intermediate points which are necessary to the coherence of the bifurcation diagram.

Due to the presence of many branches of nonalgebraic bifurcation surfaces, we cannot point out exactly neither predict the concrete value of n where the changes in the parameter space happen. Thus, with the purpose to set an order for these changes in the parameter space, we introduce the following notation. If the bifurcation happens between two concrete values of n, then we add or subtract a sufficiently small positive value ε_i or ε_j^* to/from a concrete value of n; this concrete value of n (which is a reference value) can be any of the

two values that define the range where the non–concrete values of n are inserted. The representation ε_i means that the n_i refers to a generic slice, whereas ε_j^* means that the n_j refers to a singular slice. Moreover, considering the values ε_i, ε_i^*, ε_{i+1} and ε_{i+1}^*, it means that $\varepsilon_i < \varepsilon_i^* < \varepsilon_{i+1} < \varepsilon_{i+1}^*$ meanwhile they belong to the same interval determined by algebraic bifurcations.

We now begin the analysis of the bifurcation diagram by studying completely one generic slice and after by moving from slice to slice and explaining all the changes that occur. As an exact drawing of the curves produced by intersecting the surfaces with the slices gives us very small parts which are difficult to distinguish, and points of tangency are almost impossible to recognize, we have produced topologically equivalent figures where parts are enlarged and tangencies are easy to observe.

The reader may find the exact pictures as well as most of the proves of this chapter in the web page http://mat.uab.es/∼artes/articles/qvfsn2SN02/qvfsn2SN02.html.

Notation. We now describe the labels used for each part of the bifurcation space. The subsets of dimensions 3, 2, 1 and 0, of the partition of the parameter space will be denoted respectively by V, S, L and P for Volume, Surface, Line and Point, respectively. The surfaces are named using a number which corresponds to each bifurcation surface which is placed on the left side of the letter S. To describe the portion of the surface we place an index. The curves that are intersection of surfaces are named by using their corresponding numbers on the left side of the letter L, separated by a point. To describe the segment of the curve we place an index. Volumes and Points are simply indexed (since three or more surfaces may be involved in such an intersection).

We consider an example: the surface $(\mathcal{S}_1)$ splits into 5 different two–dimensional parts labeled from $1S_1$ to $1S_5$, plus some one–dimensional arcs labeled as $1.iL_j$ (where i denotes the other surface intersected by $(\mathcal{S}_1)$ and j is a number), and some zero–dimensional parts. In order to simplify the labels in all figures we see **V1** which stands for the TEX notation V_1. Analogously, **1S1** (respectively, **1.2L1**) stands for $1S_1$ (respectively, $1.2L_1$). And the same happens with many other pictures.

$$
\begin{array}{ll}
n_0 = 10 & n_{44} = 2 + \varepsilon_{12} \\
n_1 = 9 & n_{45} = 2 \\
n_2 = 9 - \varepsilon_1 & n_{46} = 19/10 \\
n_3 = 9 - \varepsilon_1^* & n_{47} = 19/10 - \varepsilon_{13}^* \\
n_4 = 9 - \varepsilon_2 & n_{48} = 17/10 \\
n_5 = 9 - \varepsilon_2^* & n_{49} = 17/10 - \varepsilon_{14}^* \\
n_6 = 9 - \varepsilon_3 & n_{50} = 17/10 - \varepsilon_{14} \\
n_7 = 9 - \varepsilon_3^* & n_{51} = 41/25 + \varepsilon_{15}^* \\
n_8 = 9 - \varepsilon_4 & n_{52} = 41/25 \\
n_9 = 9 - \varepsilon_4^* & n_{53} = 8/5 + \varepsilon_{16}^* \\
n_{10} = 9 - \varepsilon_5 & n_{54} = 8/5 \\
n_{11} = 9 - \varepsilon_5^* & n_{55} = 1 \\
n_{12} = 9 - \varepsilon_6 & n_{56} = 81/100 \\
n_{13} = 9 - \varepsilon_6^* & n_{57} = 2 - \sqrt{2} \\
n_{14} = 9 - \varepsilon_7 & n_{58} = 9/16 \\
n_{15} = 6 & n_{59} = 1/2 \\
n_{16} = 119/20 & n_{60} = 9/25 \\
n_{17} \approx 5.89088\ldots & n_{61} = 9/25 - \varepsilon_{17*} \\
n_{18} = 21/4 & n_{62} = 81/40 \\
n_{19} = 125/27 & n_{63} = 81/40 - \varepsilon_{18}^* \\
n_{20} = 114/25 & n_{64} = 81/40 - \varepsilon_{18} \\
n_{21} = 9/2 & n_{65} = 81/40 - \varepsilon_{19}^* \\
n_{22} = 108/25 & n_{66} = 81/40 - \varepsilon_{19} \\
n_{23} = \frac{3}{100}(102 + 7\sqrt{21}) & n_{67} = 81/40 - \varepsilon_{20}^* \\
n_{24} = 401/100 & n_{68} = 81/40 - \varepsilon_{20} \\
n_{25} = 4 & n_{69} = 81/40 - \varepsilon_{21}^* \\
n_{26} = 2304/625 & n_{70} = 4/25 \\
n_{27} \approx 3.63495\ldots & n_{71} = 4/25 - \varepsilon_{22}^* \\
n_{28} = 7/2 & n_{72} = 4/25 - \varepsilon_{22} \\
n_{29} = 2 + \sqrt{2} & n_{73} = 4/25 - \varepsilon_{23}^* \\
n_{30} = 16/5 & n_{74} = 4/25 - \varepsilon_{23} \\
n_{31} = 3 & n_{75} = 4/25 - \varepsilon_{24}^* \\
n_{32} = 14/5 & n_{76} = 4/25 - \varepsilon_{24} \\
n_{33} = 8/3 & n_{77} = 4/25 - \varepsilon_{25}^* \\
n_{34} = 8/3 - \varepsilon_8 & n_{78} = 9/100 \\
n_{35} = 8/3 - \varepsilon_8^* & n_{79} = 9/100 - \varepsilon_{26}^* \\
n_{36} = 8/3 - \varepsilon_9 & n_{80} = 9/100 - \varepsilon_{26} \\
n_{37} = 9/4 & n_{81} = 9/100 - \varepsilon_{27}^* \\
n_{38} = 11/5 & n_{82} = 1/25 \\
n_{39} = 11/5 - \varepsilon_9^* & n_{83} = 0 \\
n_{40} = 11/5 - \varepsilon_{10} & n_{84} = -1 \\
n_{41} = \frac{3}{100}(102 - 7\sqrt{21}) & n_{85} \approx -3.40133\ldots \\
n_{42} = \frac{3}{100}(102 - 7\sqrt{21}) - \varepsilon_{11} & n_{86} = -4 \\
n_{43} = 2 + \varepsilon_{12}^* & n_{87} = -\infty
\end{array}
\tag{17}
$$

In Fig. 15 we represent the generic slice of the parameter space when $n = n_0 = 10$, showing only the algebraic surfaces. We note that there are some dashed branches of surface $(\mathcal{S}_3)$ (in yellow) and $(\mathcal{S}_4)$ (in purple). This means the existence of a weak saddle, in the case of surface $(\mathcal{S}_3)$, and the existence of an invariant straight line without connecting sep-

aratrices, in the case of surface ($\mathcal{S}_4$); they do not mean a topological change in the phase portraits but a C^∞ change. In the next figures we will use the same representation for these characteristics of these two surfaces.

With the purpose to explain all the changes in the bifurcation diagram, we would have to present two versions of the picture of each slice: one of them without labels and the other with labels in each new part (as we have done in [Artés *et al.*, 2013b] and [Artés *et al.*, 2014]).

However, as the number of slices is considerably large (see equation (17) – 88 slices to be more precise) we would have to present about 176 pictures, which would occupy a large number of pages. Then, we will present only the labeled drawings (just the "important part" in each slice) containing the algebraic and nonalgebraic bifurcation surfaces. In the next section, we prove the existence of such nonalgebraic surfaces and their necessity for the coherence of the bifurcation diagram.

Remark 6.31. Wherever two parts of equal dimension d are separated only by a part of dimension $d-1$ of the black bifurcation surface ($\mathcal{S}_6$), their respective phase portraits are topologically equivalent since the only difference between them is that a finite antisaddle has turned into a focus without change of stability and without appearance of limit cycles. We denote such parts with different labels, but we do not give specific phase portraits in pictures attached to Theorem 1.1 for the parts with the focus. We only give portraits for the parts with nodes, except in the case of existence of a limit cycle or a graphic where the singular point inside them is portrayed as a focus. Neither do we give specific invariant description in Sec. 8 distinguishing between these nodes and foci.

6.2. Bifurcation surfaces due to connections

We start this section explaining the generic slice when $n = 10$. In this slice we will make a complete study of all its parts, whereas in the next slices we will only describe the changes. Some singular slices will produce only few changes which are easy to describe, but others can produce simultaneously many changes, even a complete change of all parts and these will need a more detailed description.

As said in last section, in Fig. 15 we present the slice when $n = 10$ with only the algebraic surfaces. We now place for each set of the partition on this slice the local behavior of the flow around all the singular points. For a specific value of the parameters of each one of the sets in this partition we compute the global phase portrait with the numerical program P4 [Artés *et al.*, 2005, Dumortier *et al.*, 2006]. In fact, all the phase portraits in this study can be obtained not only numerically but also by means of perturbations of the systems of codimension one.

In this slice we have a partition in 2−dimensional parts bordered by curved polygons, some of them bounded, others bordered by infinity. From now on, we use lower–case letters provisionally to describe the sets found algebraically so not to interfere with the final partition described with capital letters.

For each 2−dimensional part we obtain a phase portrait which is coherent with those of all their borders. Except eight parts, which are shown in Fig. 15 and named as follows:

- v_5: the curved triangle bordered by yellow and blue curves and infinity;
- v_8: the curved quadrilateral bordered by blue, yellow and black curves and infinity;
- v_{10}: the curved triangle bordered by purple and yellow curves and infinity;
- v_{12}: the pentagon bordered by yellow, purple, green and purple curves and infinity;
- v_{22}: the quadrilateral bordered by two parallel purple and two parallel green curves;
- v_{27}: the curved quadrilateral bordered by yellow, red and black curves and infinity;
- v_{33}: the curved triangle bordered by yellow, red and black curves;
- v_{54}: the curved triangle bordered by purple and yellow curves and infinity;

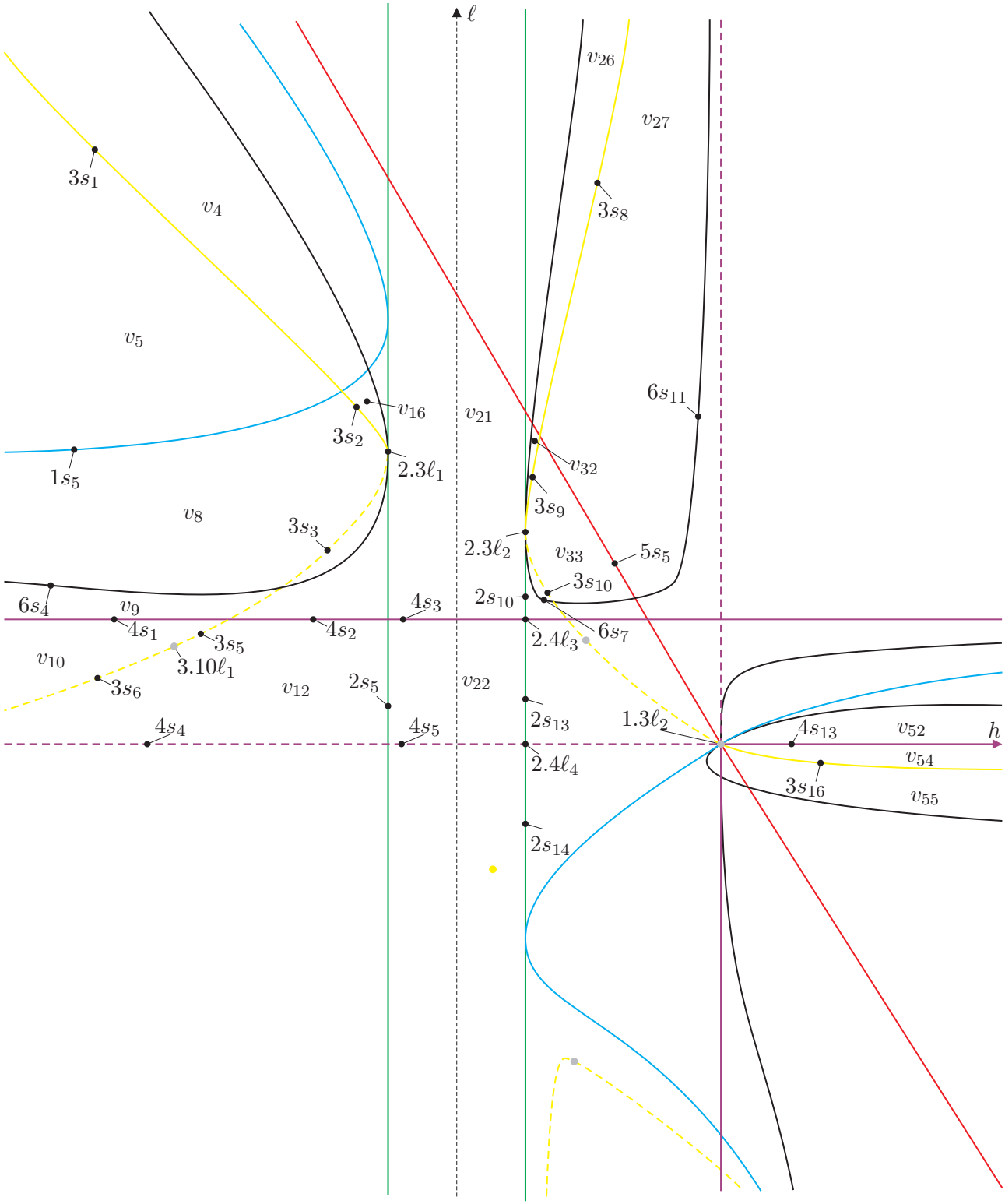

Fig. 15. Slice of parameter space when $n = 10$ (only algebraic surfaces)

We consider the segment $3s_1$ in Fig. 15, which is one of the borders of part v_5. On this segment, the corresponding phase portrait possesses a weak focus (of order one) and, consequently, this branch of surface $(\mathcal{S}_3)$ corresponds to a Hopf bifurcation. This means that either in v_4 or in v_5 we must have a limit cycle; in fact it is in v_5. The same happens on $3s_2$, one of the borders of part v_8, implying the existence of a limit cycle either in v_8 or in v_{16}; and in fact it is in v_8.

However, in case of part v_5, when approaching $1s_5$ and with the help of the program P4, the limit cycle has already been lost; and in case of part v_8, when approaching $3s_3$ and/or $6s_4$, the limit cycle has also disappeared. After these remarks, each one of the parts v_5 and v_8 must be split into two parts separated by a new surface $(\mathcal{S}_7)$ having at least two elements (curves $7S_1$ and $7S_3$ in Fig. 23) such that one part has limit cycle and the other does not, and the borders $7S_1$ and $7S_3$ correspond to a connection between separatrices. In spite of the necessity of these two branches of surface $(\mathcal{S}_7)$, there must exist at least one more element of this surface to make this part of the diagram space coherent. We talk about the element $7S_2$ (see Fig. 23) which also corresponds to connection of separatrices but different from that happening on $7S_1$ and $7S_3$.

Numerically, it can be checked that part v_5 splits into V_5 with one limit cycle and V_6 without limit cycles, and part v_8 splits into V_7 and V_8 without limit cycles and V_{17} with one limit cycle. Even though parts V_7 and V_8 have no limit cycles, they provide topologically distinct phase portraits since the connection of separatrices on $7S_3$ (respectively, on $7S_1$) is due to the saddle–node $\overline{\binom{0}{2}}SN$ and the finite saddle (respectively, is due to the saddle–node $\overline{\binom{0}{2}}\,SN$ and an infinite saddle), i.e. connection of separatrices from different points, whereas the connection on $7S_2$ is due to a saddle itself (i.e. a loop–type connection). We plot the complete bifurcation diagram for these two parts in Fig. 23. We also show the sequence of phase portraits along these subsets in Fig. 16.

Now, we carry out the analysis of parts v_{10}, v_{12} and v_{22}. We consider part v_9. The respective phase portrait is topologically equivalent to the one in V_8 with the focus turned into a node. On $4s_1$, the separatrix of the infinite saddle–node connects with a separatrix of the finite saddle producing an invariant straight line linking the pair of infinite saddle–nodes. When entering part v_{10}, this connection is broken and the position of the separatrices of the infinite saddle–node and the finite saddle is changed in relation to the position represented in V_9. However, when we approach $4s_4$, the phase portrait in a neighborhood of this segment is topologically different from the one we described just after entering part v_{10}. Indeed, the phase portrait in v_{10} near $4s_1$ possesses a "basin" passing through the saddle–node, i.e. two separatrices of the saddle–node end at the same infinite singular point, whereas the phase portrait in v_{10} near $4s_4$ does not possess the "basin" and each one of the same two separatrices of the saddle–node ends in different infinite singular points.

As a result, there must exist at least one element $7S_4$ of surface $(\mathcal{S}_7)$ dividing part v_{10} in two "new" parts, V_{10} and V_{11}, which represents a bifurcation due to the connection between a separatrix of a finite saddle–node with a separatrix of a finite saddle. It is worth mentioning that the segments $3s_5$ and $3s_6$ and the point $3.10\ell_1$ refer to the presence of weak saddle (of order one and two, respectively) which implies that part v_{12} is topologically equivalent to v_{10}. Then, part v_{12} must also be divided in V_{12} and V_{13} by an element $7S_5$ of surface $(\mathcal{S}_7)$ with the same bifurcation as $7S_4$. Coupled with this idea, we have parametrized the yellow surface, "walked" on it and found that there exist a topological change in the phase portraits obtained.

In addition, we have done the same with the green surface (i.e. we have parametrized it) and found that segment $2s_5$ also presents two distinct phase portraits and they are topologically equivalent to the ones described above. This suggests that an element $7S_6$ of surface $(\mathcal{S}_7)$ divides part v_{22} in two "new" ones, V_{22} and V_{23}, where $7S_6$ corresponds to a bifurcation due to the connection between two separatrices from a finite and an infinite saddle–nodes. Therefore, we know that $7S_6$ has one of its endpoints on $2s_5$ (dividing it in $2S_5$ and $2S_6$) and Lemma 6.32 assures that the other endpoint is $2.4\ell_3$.

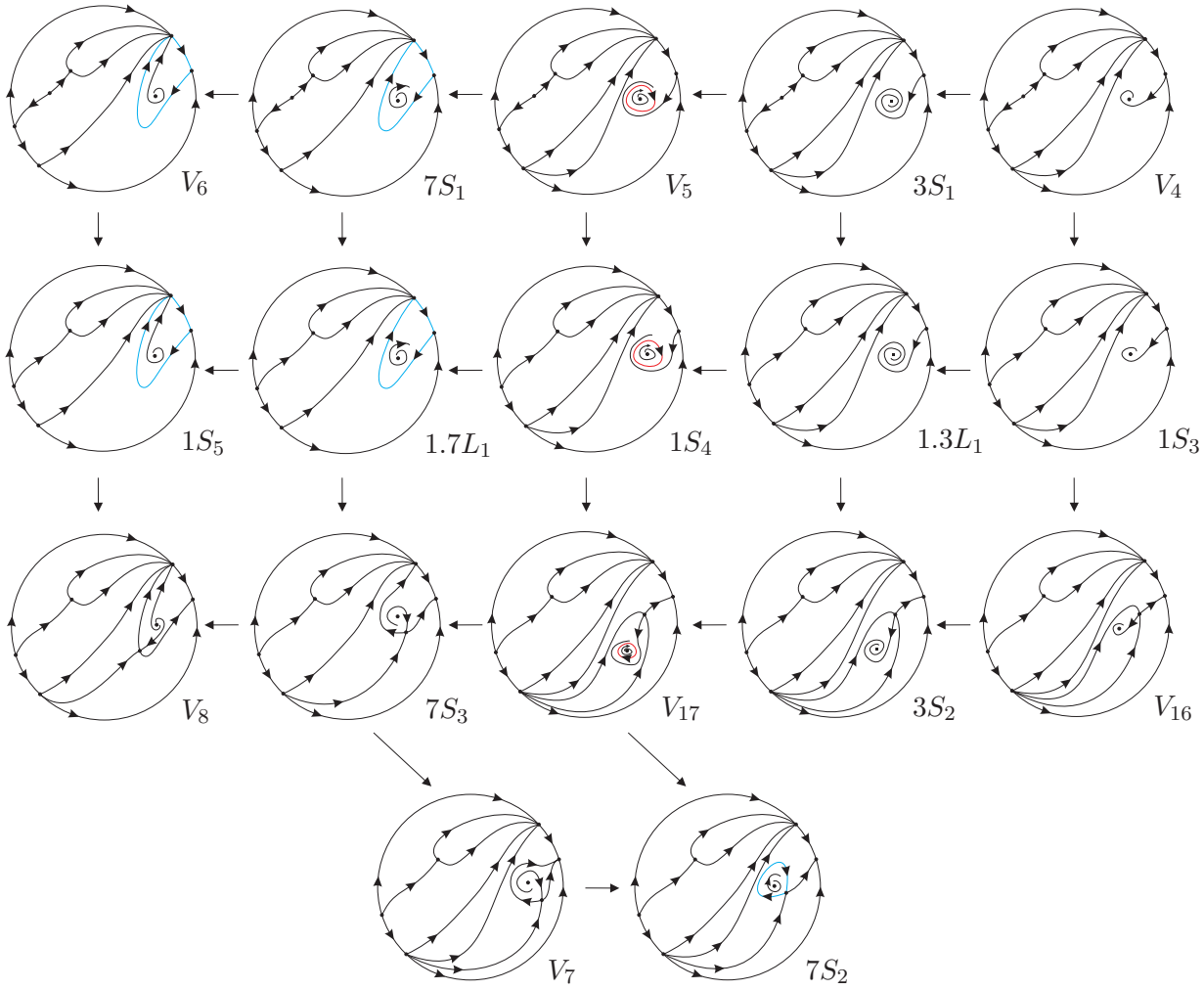

Fig. 16. Sequence of phase portraits in parts v_5 and v_8 of slice $n = 10$. We start from v_4. We recall that the phase portrait $3S_1$ is equivalent to the phase portrait V_4 up to a weak focus (represented by a little black square) instead of the focus. When crossing $3s_1$, we shall obtain the phase portrait V_5 in subset v_5. From this point we may choose three different ways to reach the subset v_8 by crossing the blue curve: (1) from the phase portrait $1.3L_1$ to the V_{17}; (2) from the phase portrait $1S_4$ to the V_{17}; and (3) from the phase portrait $1.7L_1$ to the V_7, V_8, V_{17}, $1S_4$, $7S_2$ and $7S_3$

Lemma 6.32. *The endpoint of* $7S_6$ *(rather than the one which is on* $2s_5$*) is* $2.4\ell_3$.

Proof. Numerical tools evidence that the endpoint of $7S_6$, rather than the one which is on $2s_5$, is $2.4\ell_3$. In what follows, we prove that this endpoint cannot be on segments $4s_3$ and $2s_{13}$.

If this endpoint were located on $4s_3$, there must exist an invariant straight line linking the pair of infinite saddle–nodes producing a connection between their separatrices. On the other hand, we would have two options. The first one would be that this endpoint of $7S_6$ should correspond to a phase portrait in which the separatrices of the finite saddle–node connects with the invariant straight line, which is itself a connection of two separatrices (see Fig. 17(a) to visualize the probable movement of the separatrices in $4S_3$), producing a triple connection of separatrices; in addition, the invariant straight line should remain, what would be a contradiction since we would have three non–collinear infinite singular points involved in the "final" connection. And the second option would be the birth of another finite singular point on this straight line which would make the "new" connection possible, but in v_{22} there exists only one finite singular point.

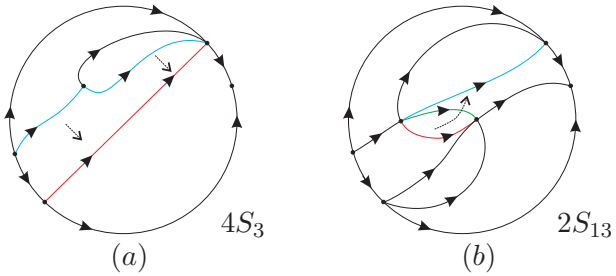

Fig. 17. (a) The probable movement of the separatrices to form another connection in phase portrait $4S_3$. The straight line in red is produced by the connection of the separatrices of the infinite saddle–nodes (the characteristic of $4S_3$) and the separatrices in blue of the finite saddle–node would tend to the straight line and provoke a triple connection of separatrices having the invariant straight line remained; (b) The probable movement of the separatrices to form a connection in phase portrait $2S_{13}$. In order to have a phase portrait with characteristics of curve $7S_6$, it would be necessary that the separatrix in red of a finite saddle–node connects with the separatrix of the infinite saddle–node in blue, but before it is necessary that either the red or the blue separatrix connects with the green one

Now, if the endpoint of $7S_6$ were located on $2s_{13}$, then another saddle–node should appear in the finite part and it would send its separatrix associated to the null eigenvalue to an infinite node and one of the other two separatrices would be received by the nodal sector of the other finite saddle–node and the other separatrix would be received by the nodal part of an infinite saddle–node. If there would exist an intersection between $7S_6$ and $2s_{13}$, then a separatrix of a finite saddle–node would have to connect with the separatrix of an infinite saddle–node as sketched in Fig. 17(b). However, there exists a separatrix in the middle of these two that prevents this connection before the connection between some of these two with the one from the middle. Then, it is impossible to have an intersection between $7S_6$ and $2s_{13}$.

As shown above, the endpoint of $7S_6$ is not on $4s_3$ nor in $2s_{13}$ and this confirms the evidence pointed out by the numerical calculations that $7S_6$ ends at $2.4\ell_3$. ■

We plot the complete bifurcation diagram for these two parts in Fig. 23. We also show the sequence of phase portraits along these subsets in Fig. 18.

We now perform the study of parts v_{27} and v_{33}. We consider the segment $3s_8$ in Fig. 15, which is one of the borders of part v_{27}. Analogously, on this segment, the corresponding phase portrait possesses a weak focus (of order one) and, consequently, this branch of surface ($\mathcal{S}_3$) corresponds to a Hopf bifurcation. This means that either in v_{26} or in v_{27} we must have a limit cycle; in fact it is in v_{27}. The same happens on $3s_9$, one of the borders of part v_{33}, implying the existence of a limit cycle either in v_{32} or in v_{33}; and in fact it is in v_{33}.

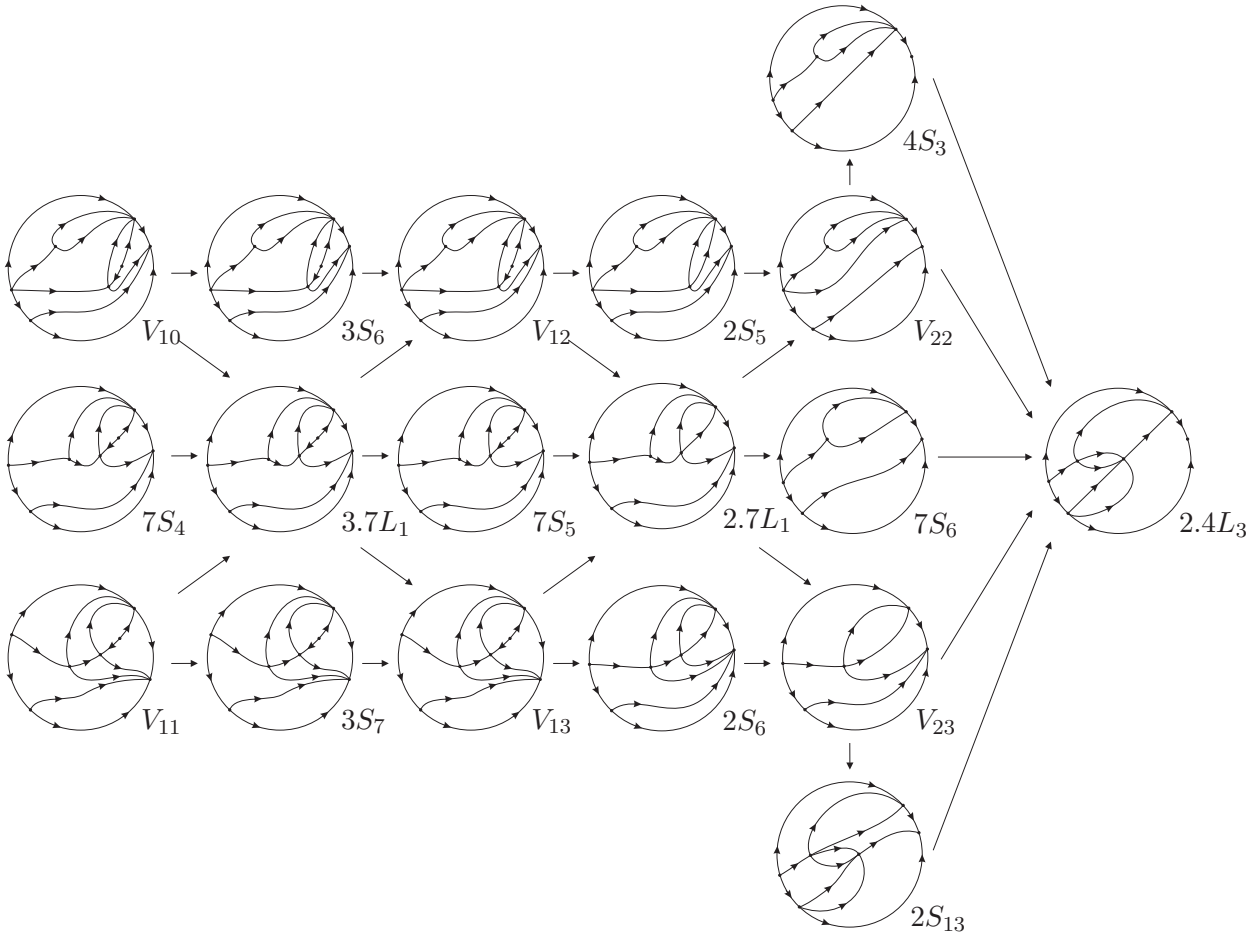

Fig. 18. Sequence of phase portraits in parts v_{10}, v_{12} and v_{22} of slice $n = 10$. We start from v_{10}. We recall that the phase portraits V_{10}, $3S_6$ and V_{12} are topologically equivalent due to a weak saddle. The same happens to $7S_4$, $3.7L_1$ and $7S_5$, and to V_{11}, $3S_7$ and V_{13}. From V_{12}, $7S_5$ and V_{13}, we cross the segment $2s_5$, where the finite saddle and finte node collide giving birth to a saddle–node, and we have three possibilites: $2S_5$, $2.7L_1$ and $2S_{16}$. Entering part v_{22}, this just–born saddle–node disappears; this part was divided in three and the respective phase portraits V_{22}, $7S_6$ and V_{23} are topologically distinct among them, and they tend to the phase portrait $2.4L_3$ either directly or passing through $4S_3$ and $2S_{13}$

However, approaching $6s_{11}$, the limit cycle has been lost, which implies the existence of at least one more element of surface $(\mathcal{S}_7)$ (curve $7S_7$ in Fig. 24); furthermore, the phase portrait in a small neighborhood of $6s_{11}$ is not coherent to that obtained just after making disappear the limit cycle. If we fix a value of the parameter ℓ in order to be in this part and we make the parameter h increase from $3s_8$ towards $6s_{11}$, then we obtain four topologically distinct phase portraits with no separatrix connection inside part v_{27}, which implies the existence of not only one but at least three elements of surface $(\mathcal{S}_7)$, the curves $7S_7$, $7S_8$ and $7S_9$ in Fig. 24; such new phase portraits are V_{27}, with limit cycle, and V_{28}, V_{29} and V_{30}, without limit cycles (see Fig. 19 for a sequence of phase portraits in these parts). As the segment $5s_5$ corresponds to changes in the infinite singular points, the finite part of the phase portraits remain unchanged and these elements of surface $(\mathcal{S}_7)$ intersect $5s_5$. Consequently, v_{33} is also split into four parts having the same behavior in the finite part with relation to the corresponding "new" parts in v_{27}; such new phase portraits are V_{33}, with limit cycle, and V_{34}, V_{35} and V_{36}, without limit cycles, and the branches of surface $(\mathcal{S}_7)$ which are the continuation of the segments $7S_7$, $7S_8$ and $7S_9$ are, respectively, $7S_{10}$, $7S_{11}$ and $7S_{12}$.

Remark 6.33. One of the separatrices in the connection on the curves $7S_7$, $7S_8$, $7S_9$, $7S_{10}$, $7S_{11}$ and $7S_{12}$ is always from a finite saddle.

Lemma 6.34. *The curve $7S_7$ has one of its ends at the point $2.3\ell_2$.*

Proof. Numerical analysis suggests that the curve $7S_7$, which corresponds to a loop–type bifurcation, has one of its ends at the point $2.3\ell_2$. Indeed, if the starting point of $7S_7$ were any point of segments $3s_9$ or $3s_{10}$, we would have the following incoherences. Firstly, if this starting point were on $3s_9$, then a portion of this subset must not refer to a Hopf bifurcation, which contradicts the fact that on $3s_9$ we have a weak focus of order one. Secondly, if the starting point were on $3s_{10}$, then a portion of this segment must also refer to a Hopf bifurcation since we a limit cycle in V_{33}, which is also a contradiction. ■

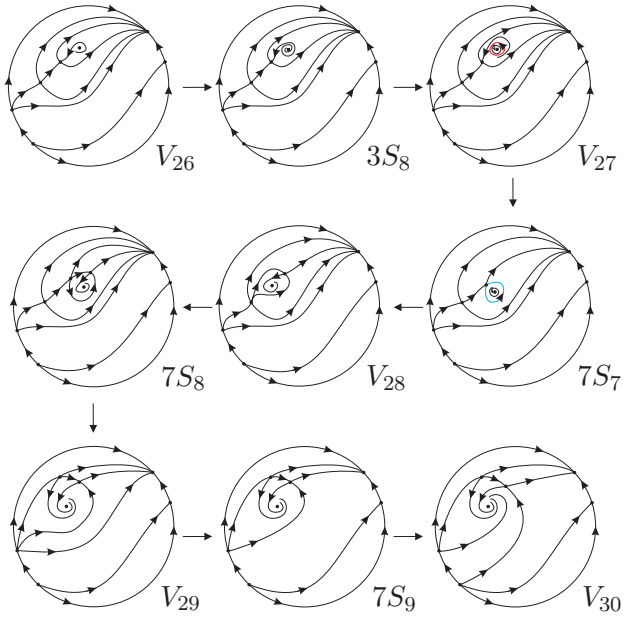

Fig. 19. Sequence of phase portraits in part v_{27} of slice $n = 10$. We start from v_{26}. We recall that the phase portrait $3S_8$ is equivalent to the phase portrait V_{26} up to a weak focus (represented by a little black square) in place of the focus. When crossing $3s_8$, we shall obtain the phase portrait V_{27} in subset v_{27} possessing a limit cycle. Then, on $7S_7$ two separatrices of the finite saddle connect themselves producing a loop; this loop is broken and one of the separatrices of the saddle goes towards the focus and the other comes from the nodal part of the saddle–node in V_{28}; thus, that separatrix of the saddle coming from the nodal sector of the saddle–node connects with one of the separatrices of the saddle–node producing another separatrices connection on $7S_8$; after this connection is broken, the separatrix of the saddle–node goes towards the focus and the separatrix of the saddle comes from the infinite saddle–node, characterizing part V_{29}; then, on $7S_9$ one more connection of separatrices is produced between the same separatrix of the saddle and the separatrix of the infinite saddle–node; and, finally, on V_{30} this separatrices connection is broken and the separatrix of the infinite saddle–node goes towards the focus and the separatrix of the saddle comes from the infinite node

Since the subsets $3s_{10}$ and $6s_7$ correspond respectively to the presence of a weak saddle and the node–focus bifurcation, they do not imply a topological change in the phase portrait. Under these circumstances, the segments $7S_{11}$ and $7S_{12}$ intersect both subsets $3s_{10}$ and $6s_7$ causing only C^∞ changes in the phase portraits and they will end on segment $2s_{10}$ dividing it in three new parts: $2S_{10}$, $2S_{11}$ and

$2S_{12}$. The reason why they do not cross $2s_{10}$ is that, if they did so, the connection of the separatrices would have to remain. However, in part v_{21} there exists only one finite singular point (namely, $\overline{sn}_{(2)}$), i.e. the finite saddle and node that existed on the right side of $2s_{10}$ have collapsed on this segment and become a complex point after crossing it. Following this idea, Remark 6.33 has no sense in part v_{21}. In Fig. 20 we show the sequence of phase portraits from part $2.3L_2$ to $2S_{12}$.

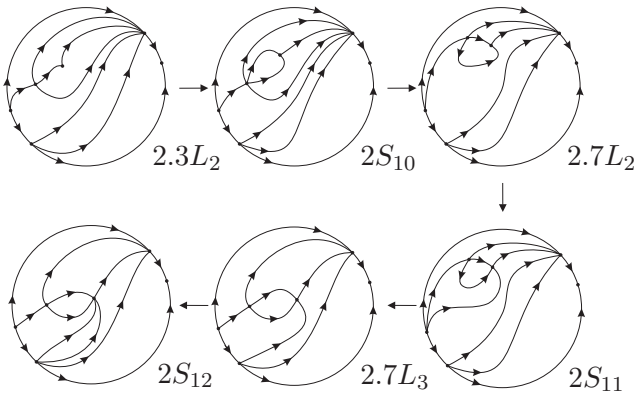

Fig. 20. Sequence of phase portraits in part $2s_{10}$ of slice $n = 10$. We start from $2.3\ell_2$. This part produces only one phase portrait $2.3L_2$ which possesses finite saddle–node and a cusp (we remark that this point is the intersection of many surfaces, inducing a degeneracy — the cusp point). On $2S_{10}$ the cusp turns into a saddle–node having two of its separatrices sent from the nodal part of the remaining saddle–node. At $2.7L_2$, one separatrix of one saddle–node connects with one separatrix of the other saddle–node and, on $2S_{11}$, this connection is broken and we have the creation of two "basins" which intersect at the two saddle–nodes. Then, on $2.7L_3$ a connection of separatrices is produced between the separatrix of the infinite saddle–node and one separatrix of one of the finite saddle–nodes and, finally, on $2S_{12}$ this connection is broken and we obtain the portrait above

Finally, we analyze part v_{54}. We start in part v_{52}. In this portion of the parameter space, the corresponding phase portrait possesses the saddle–node and two foci in the finite part and saddle–nodes and saddles at infinity. When we cross the curve $4s_{13}$, its phase portrait possesses $\{(x, 0);\ x \in \mathbb{R}\}$ as an invariant straight line linking the infinite saddles. The presence of this invariant straight line produces a connection of separatrices between one from a saddle and the other from the finite saddle–node (the one associated to the null eigenvalue). Entering part v_{54}, this invariant line disappears and the separatrices in question change position, which forces the separatrix of the saddle–node start from its own nodal sector, forming a graphic.

On the other hand, we start from part v_{55}. There, the corresponding phase portrait also possesses the saddle–node and two foci in the finite part and saddle–nodes and saddles at infinity. On $3s_{16}$, which is a common border of parts v_{54} and v_{55}, the corresponding phase portrait possesses a weak focus (of order one) and, consequently, this branch of surface $(\mathcal{S}_3)$ corresponds to a Hopf bifurcation. This means that either in v_{54} or in v_{55} we must have a limit cycle; in fact it is in v_{54}.

After these remarks, we conclude that part v_{54} must be split into two parts separated by a new surface $(\mathcal{S}_7)$ having at least one element $7S_{17}$ (see Fig. 24) such that one part has limit cycle and the other does not, and the border $7S_{17}$ corresponds to a connection of two separatrices of the same saddle–node in a loop, because the limit cycle disappears and one of the phase portraits in v_{54} possesses a graphic attached to the saddle–node.

Lemma 6.35 assures that the segment $7S_{17}$ starts from (or ends at) $1.3\ell_2$ and is not bounded.

Lemma 6.35. *The segment $7S_{17}$ starts from (or ends at) $1.3\ell_2$ and is not bounded.*

Proof. If $7S_{17}$ started on $3s_{16}$, there would exist a portion of this segment without limit cycles, which is a contradiction since it corresponds to a Hopf bifurcation. On the other hand, if $7S_{17}$ started on $4s_{13}$, two types of connection of separatrices should happen: the connection between the separatrix of the infinite saddle with the separatrix of the finite saddle–node associated to the null eigenvalue (creating an invariant straight line) and the loop–type connection in the finite saddle–node. If both connections happen, there must exist a degenerate portion of $4s_{13}$ in which this segment would start. Using numerical tools, we verify that $7S_{17}$ starts from $1.3\ell_2$. Moreover, using the same arguments, the segment $7S_{17}$ can end neither on $3s_{16}$ nor on $4s_{13}$, implying that it is unbounded. ∎

We can check numerically that part v_{54} splits into V_{53}, without limit cycles, and V_{54}, with limit cycle. We plot the complete bifurcation diagram for these two parts in Fig. 24. We also show the

sequence of phase portraits along these subsets in Fig. 22.

Having analyzed all the parts pointed out on page 29 and explained the existence of all possible nonalgebraic surfaces in there (modulo islands), we have finished the study of the generic slice $n = 10$ for the family $\overline{\mathbf{QsnSN(C)}}$. However, we cannot be sure that these are all the additional bifurcation curves in this slice. There could exist others which are closed curves small enough to escape our numerical research. For all other two–dimensional parts of the partition of this slice, whenever we join two points which are close to different borders of the part, the two phase portraits are topologically equivalent. So, we do not encounter more situations than the ones mentioned above. In short, it is expected that the complete bifurcation diagram for $n = 10$ is the one shown in Figs. 23 and 24. In these and the next figures, we have colored in light yellow the parts with one limit cycle, in light green the parts with two limit cycles, in black the labels referring to new parts which are created in a slice and in red the labels corresponding to parts which has already appeared in previous slices.

The next step is to decrease the values of n, according to equation (17), and make an analogous study for each one of the slices that we need to consider and also look for changes when going from one slice to the next one.

For all values of n greater than zero, the second and third quadrants of the bifurcation diagram remain unchanged (i.e., for all $n > 0$, there exist no topological bifurcations in the second and third quadrants in the parameter space). So, as we move from $n > 9$ towards infinity, all the slices are topologically equivalent to slice $n = 10$ and, at the limit to infinity, the bifurcation diagram tends to be the one shown in Fig. 25.

We now start decreasing the values of n in order to explain as much as we can the bifurcations in the parameter space.

We consider the curved triangles in the first quadrant of slice $n = 10$: V_{31}, V_{32} and V_{33}, all having $2.3\ell_2$ as a common vertex. As we move down from $n = 10$ to $n = 9$ (a singular slice), these three triangles collapse in a single point ($2.5L_2$) and, for values of $n < 9$, but very close to it, two triangles V_{68} and V_{69} appear in the upper part limited by the red curve. In addition, as we have already proved,

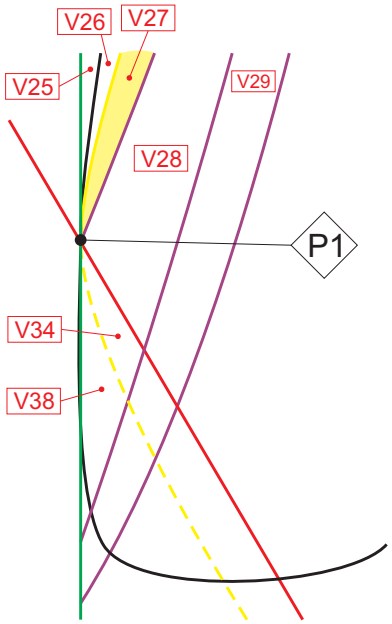

Fig. 21. Slice of parameter space when $n = 9$ (see Fig. 24)

there exist some elements of surface ($\mathcal{S}_7$) near these triangles and we either have the purple bifurcations persisting next to the triangles, or not. The first possibility is true, because after numerical analysis for values of n less than 9, but very close to it, we still verify the same changes in the phase portraits as shown in the sequence in Fig. 19. As the endpoint of the curve $7S_7$ is $2.3\ell_2$ (see Lemma 6.34) and this point collapses and reappears in the part over the red curve, it is natural that $7S_7$ follows the same movement. However, the other elements of surface ($\mathcal{S}_7$) in this part remain starting from the segment $2s_{10}$. These facts are illustrated in Figs. 21 to 38. For the transition of the slices drawn in these figures, it is clear that we need at least 13 values of n (apart from $n = 9$) to have coherence in the bifurcation diagram. Those values of n cannot be concretely determined, but we know they lie on the open interval between $n = 6$ and $n = 9$.

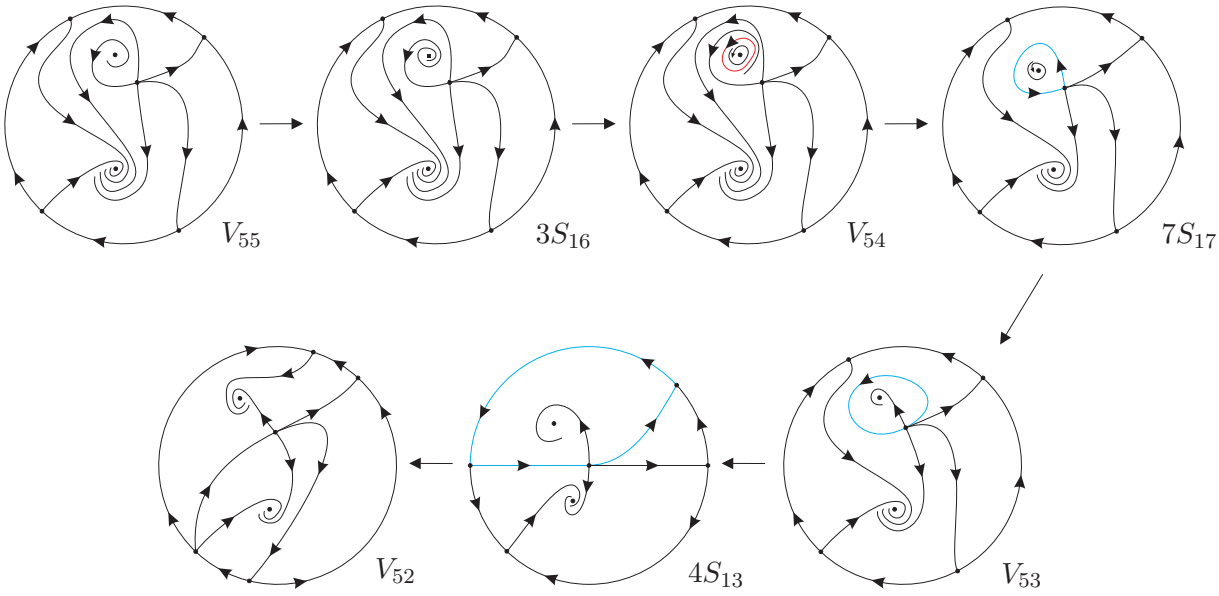

Fig. 22. Sequence of phase portraits in part v_{54} of slice $n = 10$. We start in v_{55}, whose corresponding phase portrait is V_{55}. On $3s_{16}$, one of the foci becomes weak (represented as a small square in $3S_{16}$) and it gives birth to a limit cycle when we enter part v_{54}; see phase portrait V_{54}. Then, on $7S_{17}$, two separatrices of the saddle–node connect forming a loop, which "kills" the limit cycle. After that, we obtain the portrait V_{53} in which there exists no connection of separatrices but only a graphic. A graphic remains when we lie on $4s_{13}$, but the corresponding phase portrait $4S_{13}$ possesses an invariant straight line and connection of separatrices. Finally, in v_{52} the graphic disappears and we obtain the phase portrait V_{52}

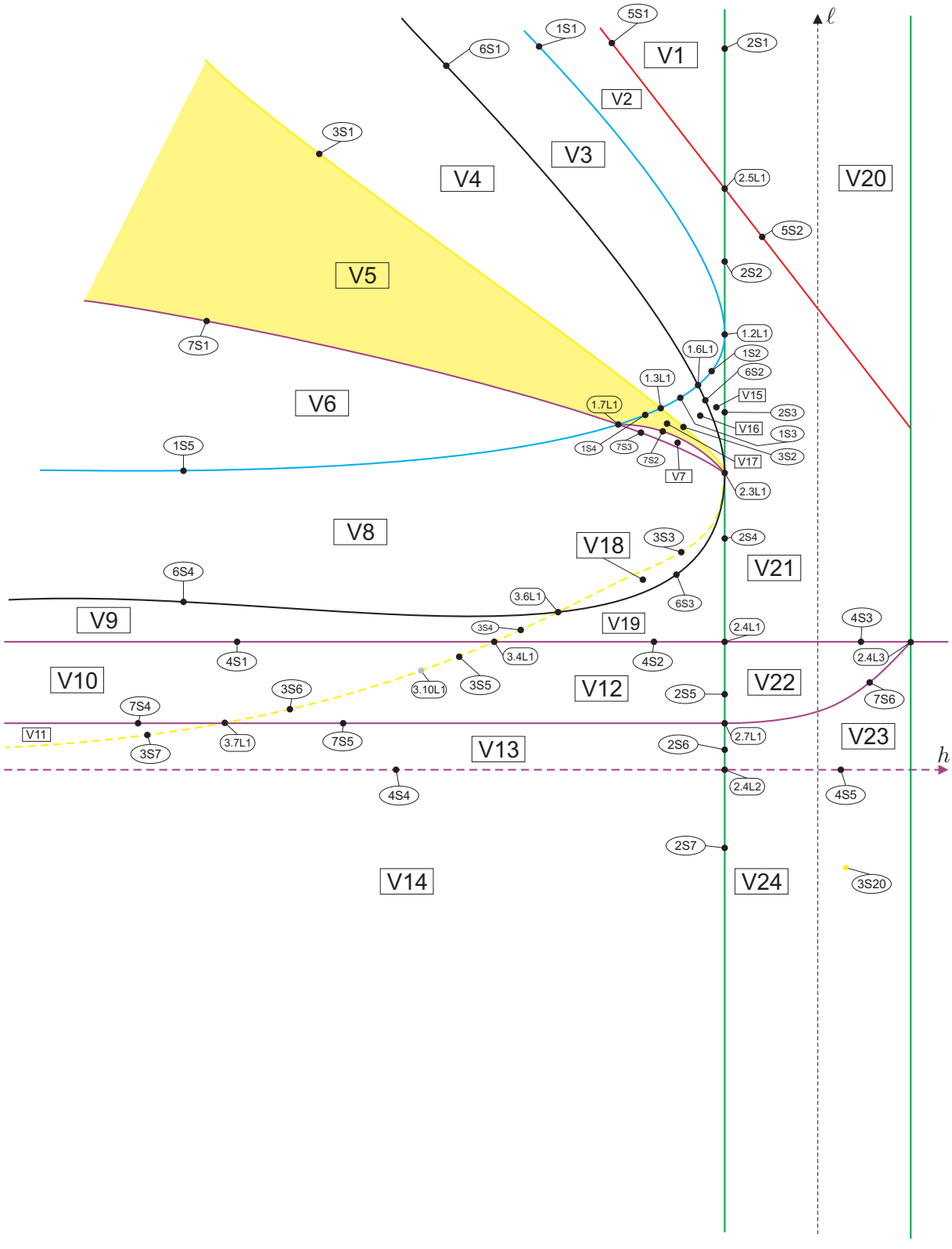

Fig. 23. Complete bifurcation diagram for slice $n = 10$ (second and third quadrants)

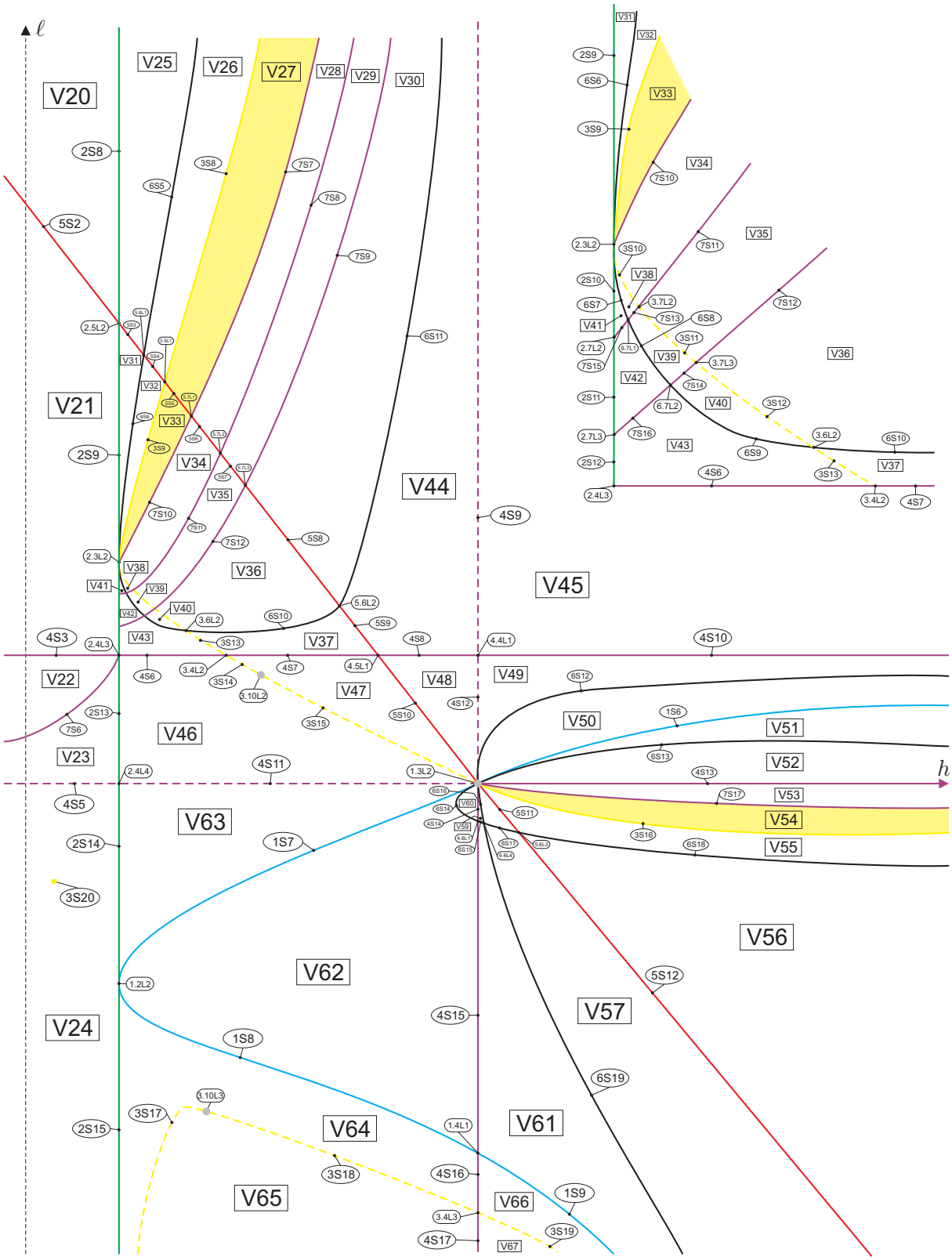

Fig. 24. Complete bifurcation diagram for slice $n = 10$ (first and fourth quadrants)

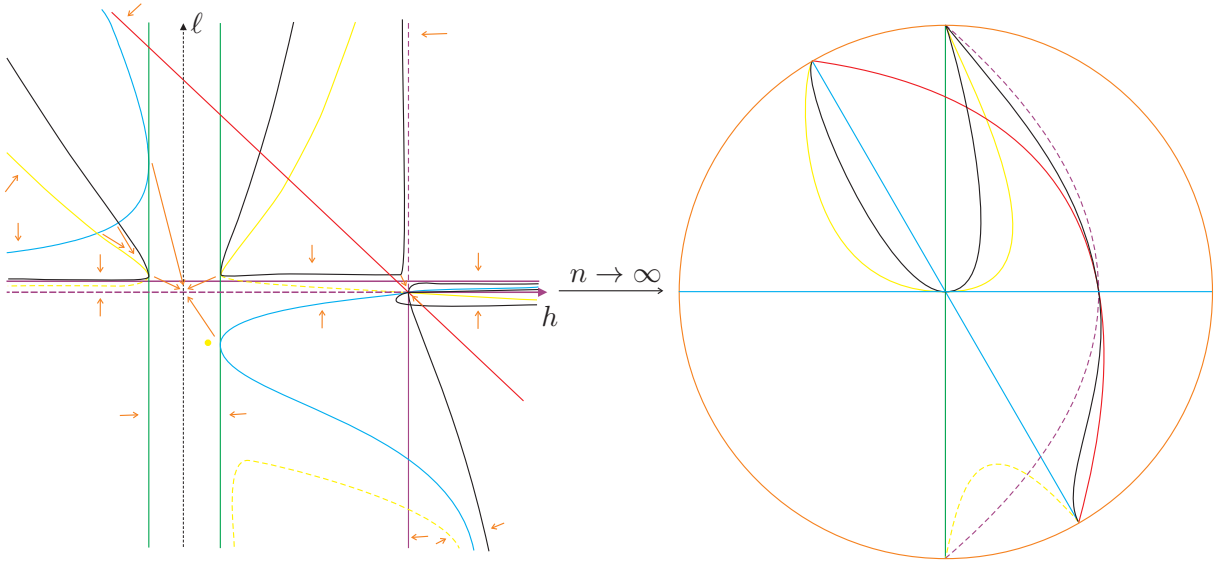

Fig. 25. The transition from $n > 9$ to infinity. The orange arrows show the movement the curves must do as $n \to \infty$

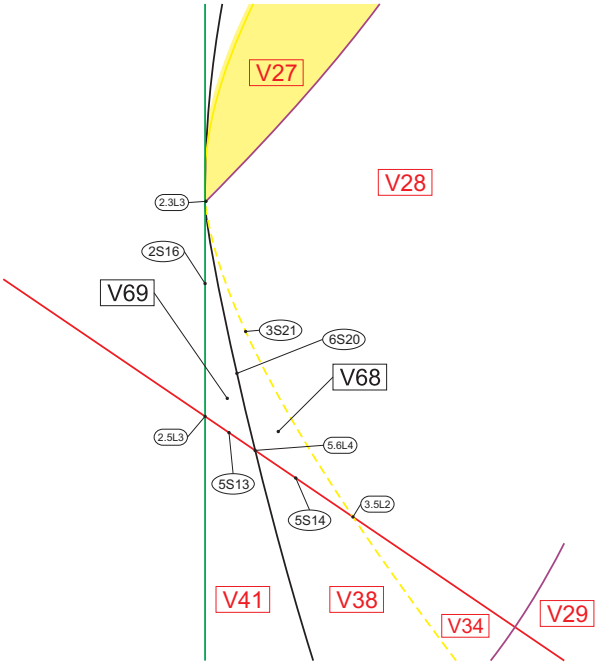

Fig. 26. Slice of parameter space when $n = 9 - \varepsilon_1$ (see Fig. 21)

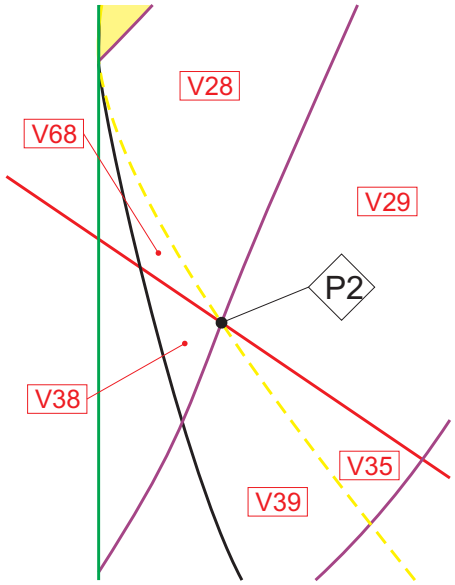

Fig. 27. Slice of parameter space when $n = 9 - \varepsilon_1^*$ (see Fig. 26)

Figs. 29 to 38 illustrate needed slices for the coherence of the bifurcation diagram. The intersection points between the purple curves with the green curve will "go up" in the sense of increasing ℓ and cross the intersection point between the red and green curves (this intersection is renamed as different slices succeed). Consequently, the same will happen to the entire purple segments. However, there exist other bifurcation curves intersecting these purple curves. Then, the slices within these figures show step by step the movement of these purple curves until they are all in the upper part limited by the red curve. Each one of Tables 3 to 9 presents the "dead" and the "born" parts (of higher dimension in that slice) in the transition from one generic slice to another passing through a singular slice in the middle of them from $n = 10$ to $n = 9 - \varepsilon_7$.

Table 3. Transition from slice $n = 10$ to $n = 9 - \varepsilon_1$

Dead parts	Parts in sing. slice	Born parts
V_{31}, V_{32}, V_{33}	P_1	V_{68}, V_{69}

In Figs. 39 to 42 we still remain in the first

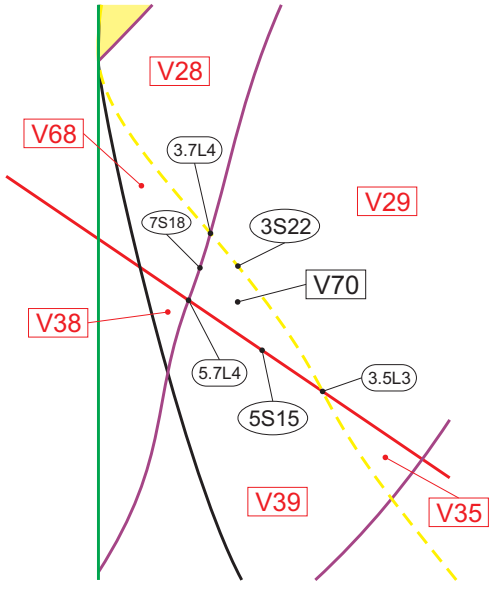

Fig. 28. Slice of parameter space when $n = 9 - \varepsilon_2$ (see Fig. 27)

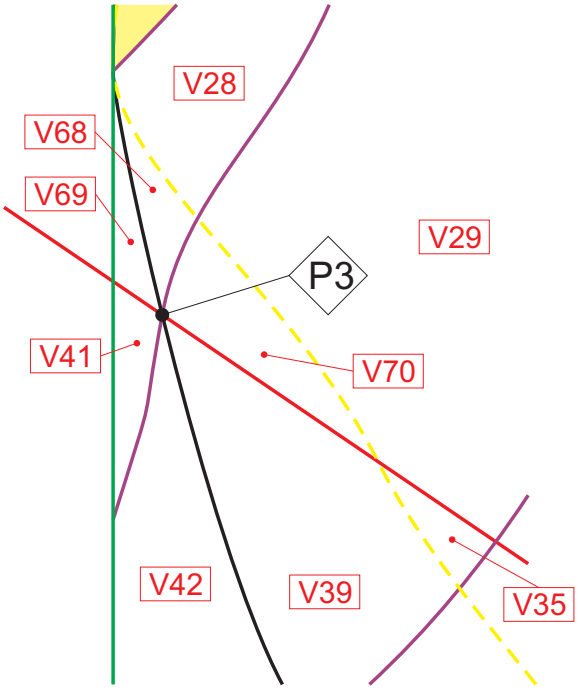

Fig. 29. Slice of parameter space when $n = 9 - \varepsilon_2^*$ (see Fig. 28)

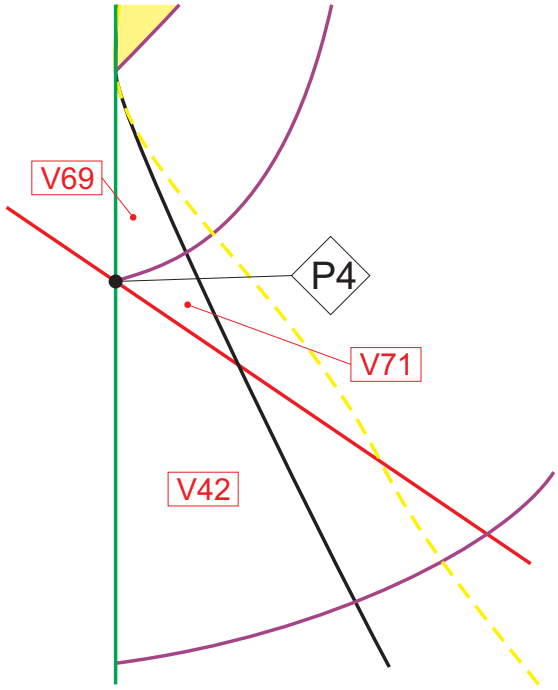

Fig. 31. Slice of parameter space when $n = 9 - \varepsilon_3^*$ (see Fig. 30)

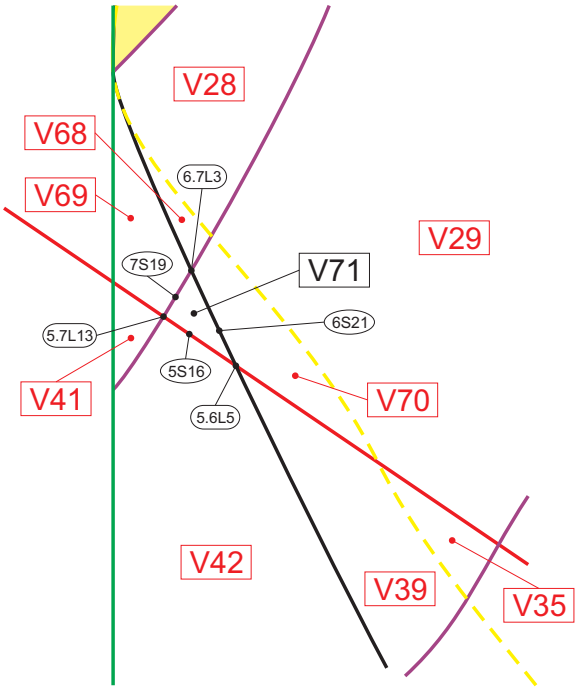

Fig. 30. Slice of parameter space when $n = 9 - \varepsilon_3$ (see Fig. 29)

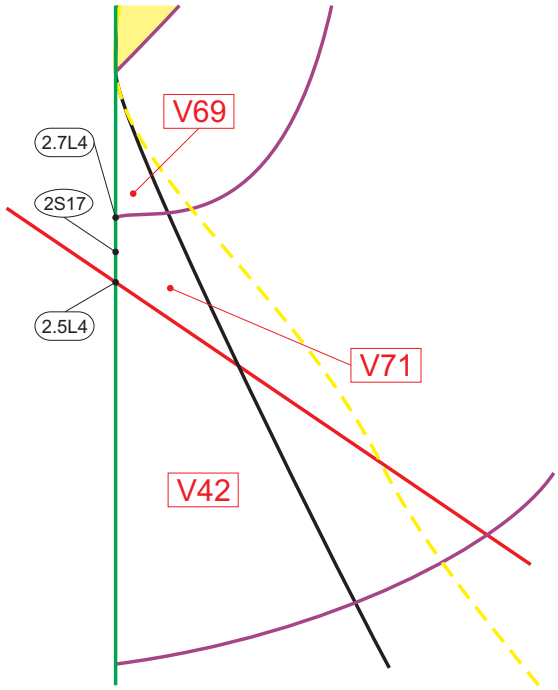

Fig. 32. Slice of parameter space when $n = 9 - \varepsilon_4$ (see Fig. 31)

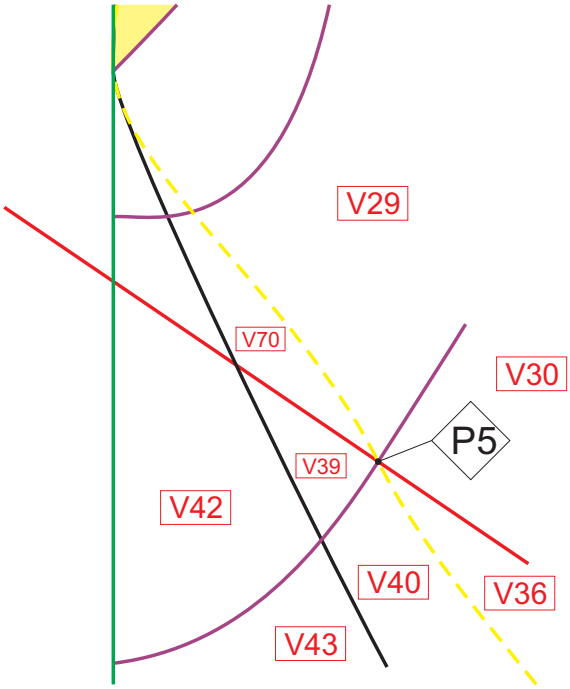

Fig. 33. Slice of parameter space when $n = 9 - \varepsilon_4^*$ (see Fig. 32)

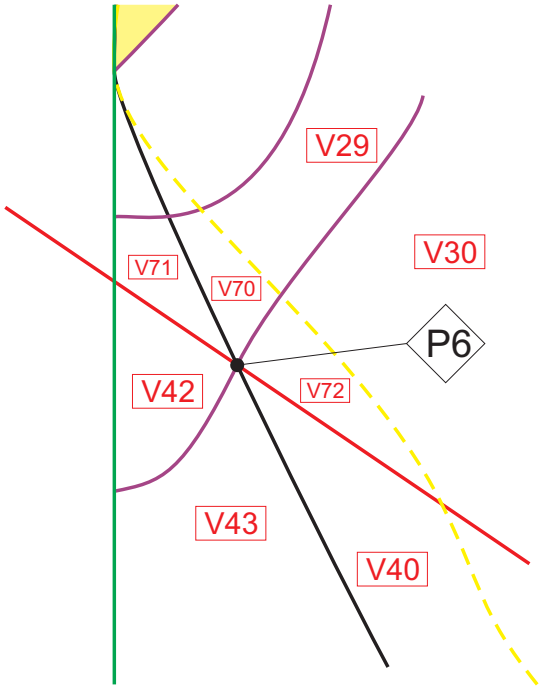

Fig. 35. Slice of parameter space when $n = 9 - \varepsilon_5^*$ (see Fig. 34)

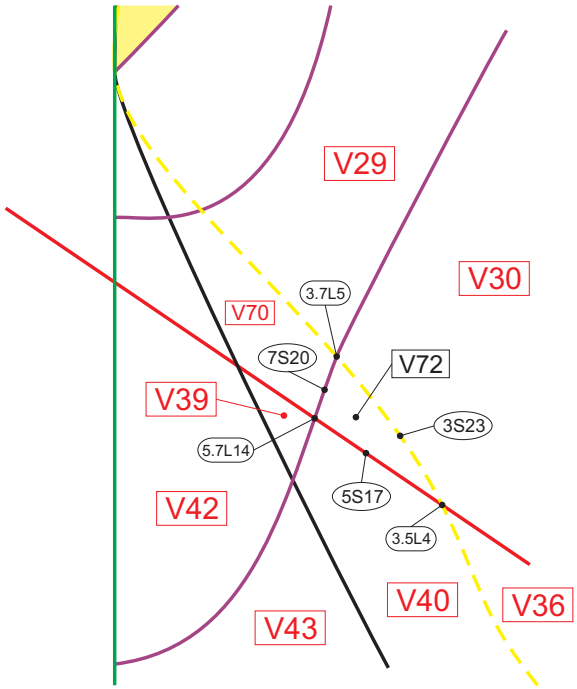

Fig. 34. Slice of parameter space when $n = 9 - \varepsilon_5$ (see Fig. 33)

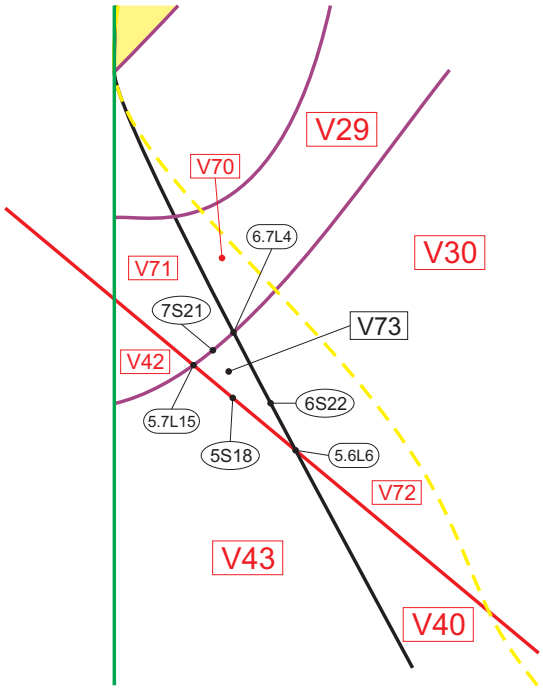

Fig. 36. Slice of parameter space when $n = 9 - \varepsilon_6$ (see Fig. 35)

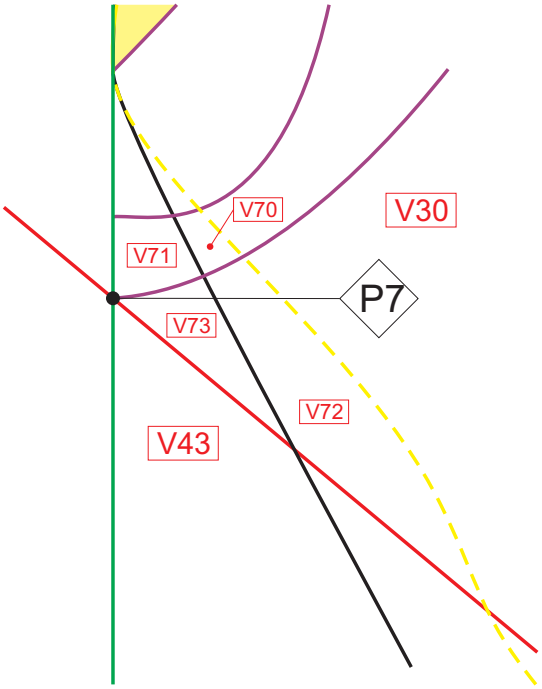

Fig. 37. Slice of parameter space when $n = 9 - \varepsilon_6^*$ (see Fig. 36)

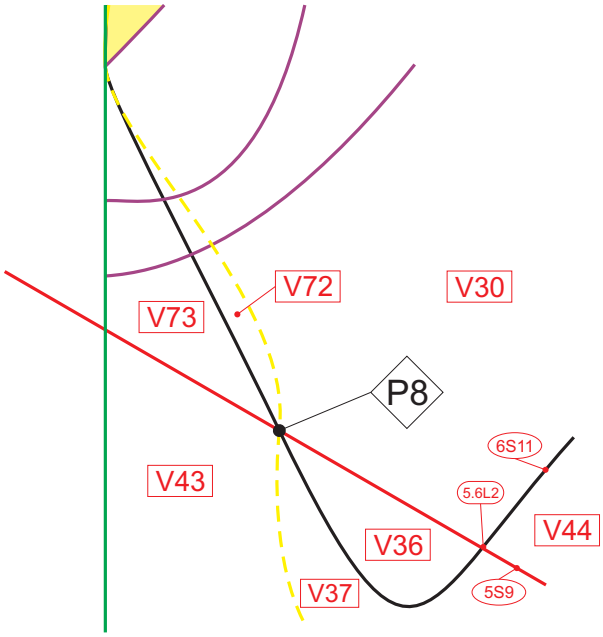

Fig. 39. Slice of parameter space when $n = 6$ (see Fig. 38)

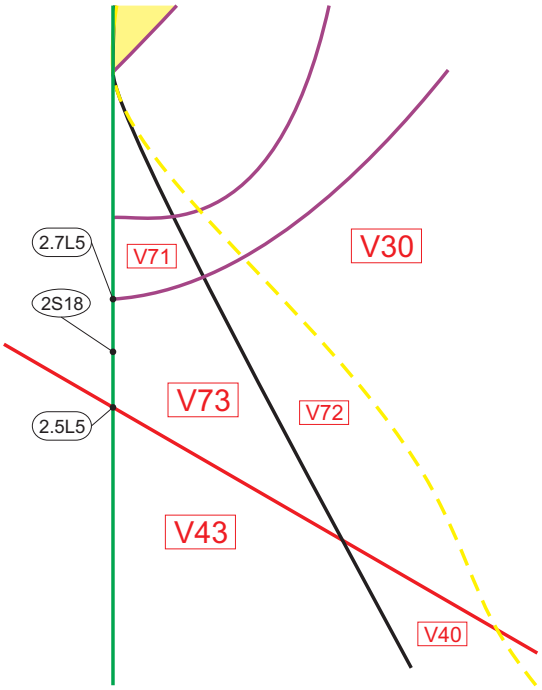

Fig. 38. Slice of parameter space when $n = 9 - \varepsilon_7$ (see Fig. 37)

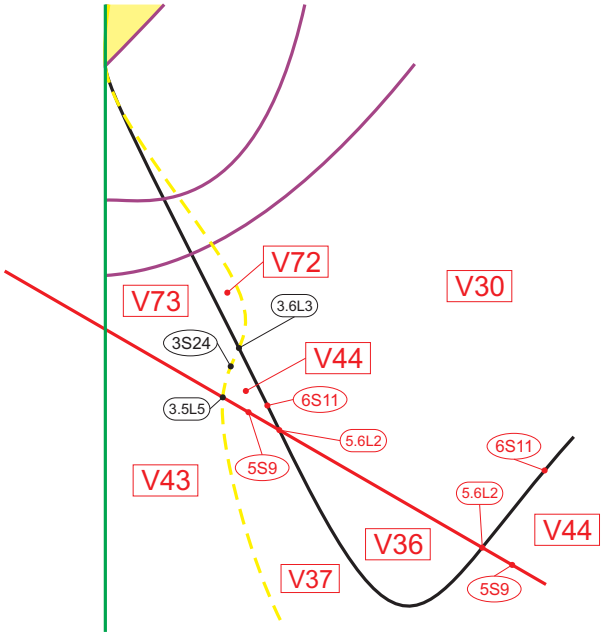

Fig. 40. Slice of parameter space when $n = 119/20$ (see Fig. 39)

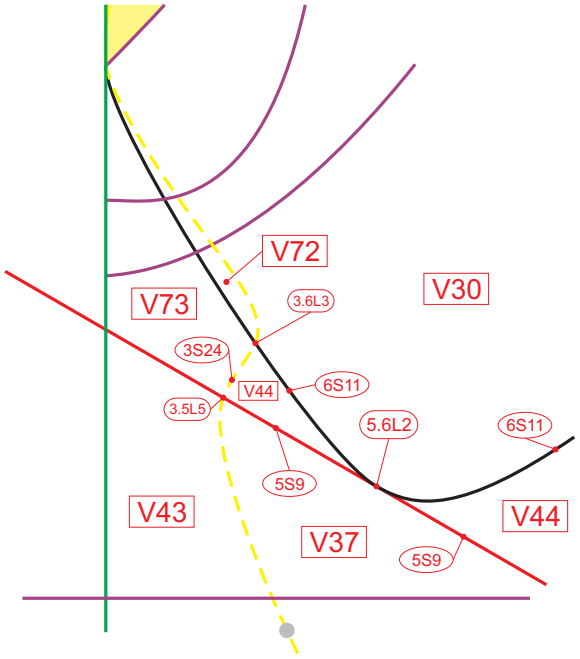

Fig. 41. Slice of parameter space when $n = n_{17} \approx 5.8908\ldots$ (see Fig. 40)

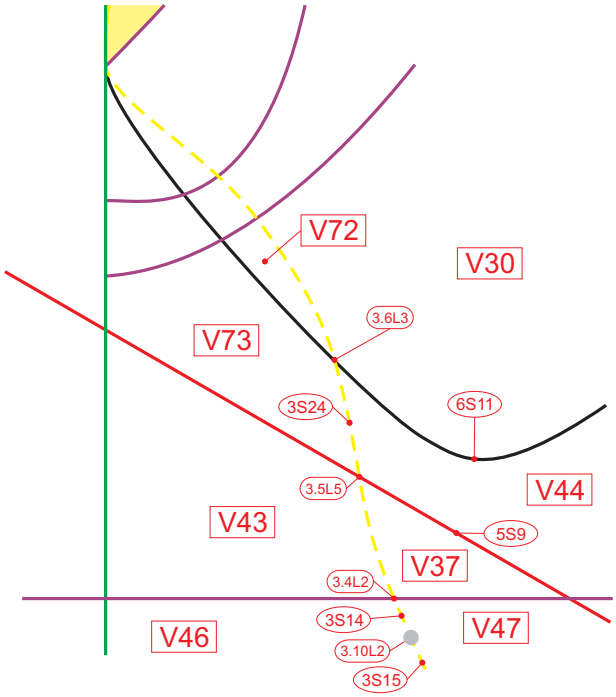

Fig. 42. Slice of parameter space when $n = 21/4$ (see Fig. 41)

Table 4. Transition from slice $n = 9 - \varepsilon_1$ to $n = 9 - \varepsilon_2$

Dead parts	Parts in sing. slice	Born parts
V_{34}	P_2	V_{70}

Table 5. Transition from slice $n = 9 - \varepsilon_2$ to $n = 9 - \varepsilon_3$

Dead parts	Parts in sing. slice	Born parts
V_{38}	P_3	V_{71}

Table 6. Transition from slice $n = 9 - \varepsilon_3$ to $n = 9 - \varepsilon_4$

Dead parts	Parts in sing. slice	Born parts
V_{41}	P_4	$2S_{17}$

Table 7. Transition from slice $n = 9 - \varepsilon_4$ to $n = 9 - \varepsilon_5$

Dead parts	Parts in sing. slice	Born parts
V_{35}	P_5	V_{72}

Table 8. Transition from slice $n = 9 - \varepsilon_5$ to $n = 9 - \varepsilon_6$

Dead parts	Parts in sing. slice	Born parts
V_{39}	P_6	V_{73}

Table 9. Transition from slice $n = 9 - \varepsilon_6$ to $n = 9 - \varepsilon_7$

Dead parts	Parts in sing. slice	Born parts
V_{42}	P_7	$2S_{18}$

quadrant and they show the interaction among the algebraic surfaces $(\mathcal{S}_3)$, $(\mathcal{S}_5)$ and $(\mathcal{S}_6)$, and it is not necessary to consider nonalgebraic bifurcation surfaces to keep the coherence. Neither their existence is needed in the fourth quadrant shown in Figs. 43 and 44. We observe that, even if $n = 125/27$ is a critical value corresponding to a singular slice, the intersection produced here is not labeled as a point but a line due to the fact that it is a contact point and, when we pass to the next (generic) slice, this contact point becomes two transversal ones but its

characteristic remains; so, there exists no sense in changing its label. There will exist more situations like this in what follows. Tables 10 to 12 show the death and birth of parts from slice $n = 9 - \varepsilon_7$ to $n = 114/25$.

Table 10. Transition from slice $n = 9 - \varepsilon_7$ to $n = 119/20$. The "born" part V_{44}^* is not new since it will join later with V_{44} (see Fig. 42)

Dead parts	Parts in sing. slice	Born parts
V_{40}	P_8	V_{44}^*

Table 11. Transition from slice $n = 119/20$ to $n = 21/4$. The symbol '$\emptyset$' means that no new part was "born"

Dead parts	Parts in sing. slice	Born parts
V_{36}	$5.6L_2$	$\emptyset$

Table 12. Transition from slice $n = 21/4$ to $n = 114/25$. The symbol '$\emptyset$' means that no part was "dead"

Dead parts	Parts in sing. slice	Born parts
$\emptyset$	$1.6L_2$	V_{36}

Returning back to the first quadrant, the point in gray corresponds to a weak saddle of second order (see the point $3.10L_2$ in Fig. 24). When $n = 9/2$, the curved triangle bordered by yellow (plus the gray point), purple and red curves bordering V_{37} ($3S_{13}$, $4S_7$, $5S_9$ and $3.10L_2$) collapses and reappears creating new parts, as seen in Figs. 45 and 46. Table 13 shows the "dead" and "born" parts after this bifurcation.

Moving back to the forth quadrant to the continuation of the movement shown in Figs. 43 and 44, the black curve produces the same movement as before but now contacting the yellow curve, according to Figs. 47 and 48, and Table 14 presents the new parts.

In Fig. 49 we represent fourth quadrant of the slice of the parameter space when $n = 4$. When $n > 4$, there exists a point of intersection among surfaces $(\mathcal{S}_2)$, $(\mathcal{S}_3)$ and $(\mathcal{S}_6)$; more precisely, the point $2.3L_3$ in Fig. 26. According to Lemmas 6.14,

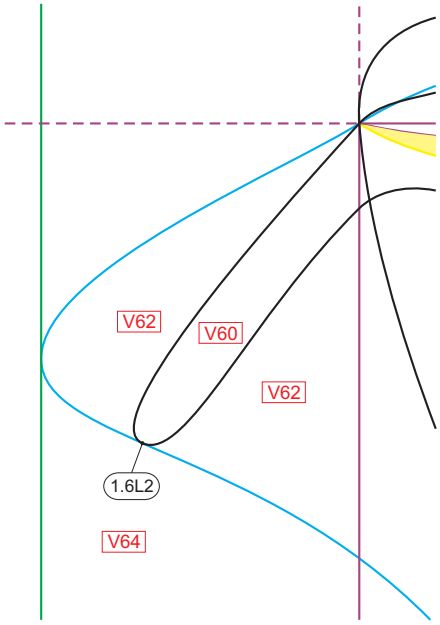

Fig. 43. Slice of parameter space when $n = 125/27$ (see Fig. 24)

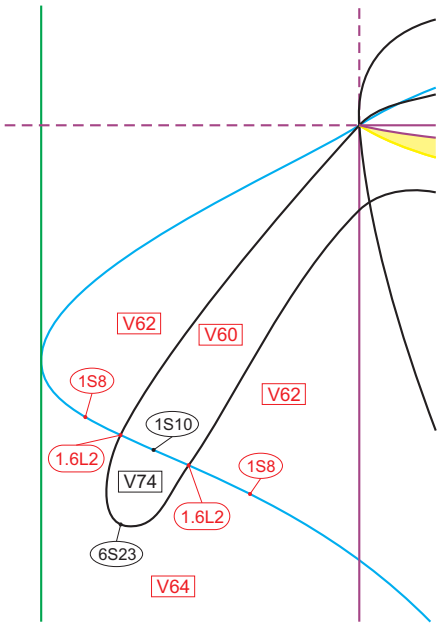

Fig. 44. Slice of parameter space when $n = 114/25$ (see Fig. 43)

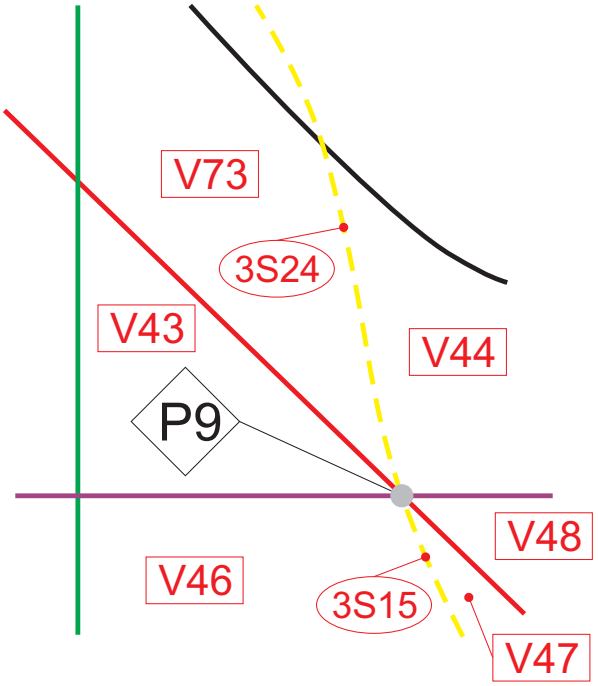

Fig. 45. Slice of parameter space when $n = 9/2$ (see Fig. 42)

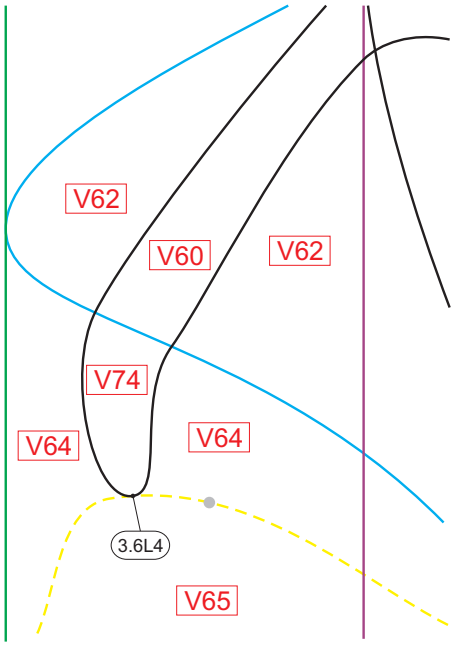

Fig. 47. Slice of parameter space when $n = 3(102 + 7\sqrt{21})/100$ (see Fig. 44)

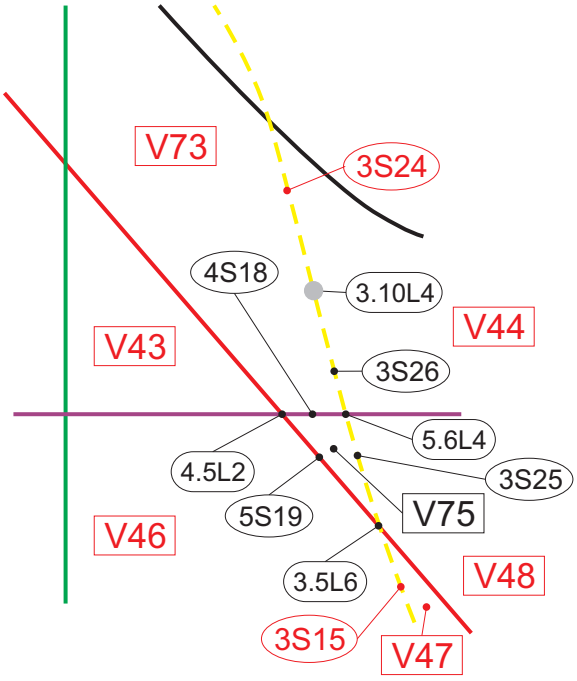

Fig. 46. Slice of parameter space when $n = 108/25$ (see Fig. 45)

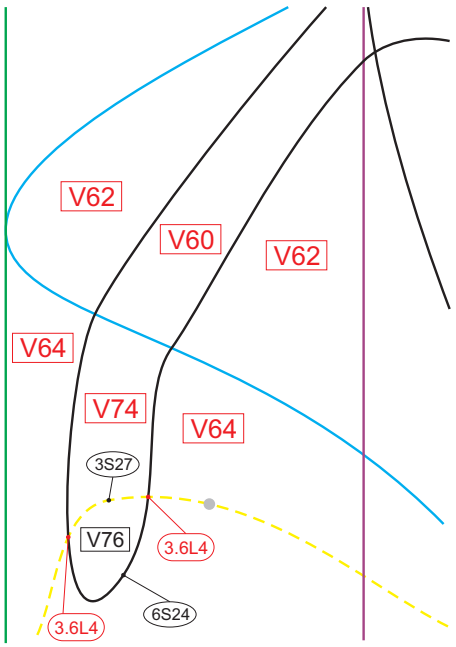

Fig. 48. Slice of parameter space when $n = 401/100$ (see Fig. 47)

Table 13. Transition from slice $n = 21/4$ to $n = 108/25$

Dead parts	Parts in sing. slice	Born parts
V_{37}	P_9	V_{75}

Table 14. Transition from slice $n = 114/25$ to $n = 401/100$. The symbol '$\emptyset$' means that no part was "dead"

Dead parts	Parts in sing. slice	Born parts
$\emptyset$	$3.6L_4$	V_{76}

6.17 and 6.20, the expression of this point (or, seen in the projective space, this curve) is $[1 : h : 2h/(h-1) : (1+h)^2]$. As $h \to 1^+$, we have $n \to 4^+$ and $2.3L_3$ goes to $+\infty$ (since the coordinate ℓ goes to $+\infty$). An analogous argument is applied to the point $3.6L_4$ in Fig. 48 (the one in the left side) and we conclude it also goes to $-\infty$. Thus, we conclude that the segment $6S_{24}$ in Fig. 48 breaks apart, obtaining the configuration shown in Fig. 49. Moreover, there exist two portions of collapsing of curves, forming the points P_{10} and P_{11}. Considering the next slice when $n = 2304/625$, the collapsed curves separate and form three curved triangles: V_{77}, V_{84} and V_{85}. Furthermore, the expressions for the points $2.3L_3$ and $3.6L_4$ now make sense and the points coincide at infinity and appear as $2.3L_4$ in the lower part of the slice. Together with them, four more elements of surface $(\mathcal{S}_7)$ must exist in order to keep the coherence of the bifurcation diagram. We plot a portion of the slice when $n = 2304/625$ in Fig. 50. See in Table 15 the parts which disappeared and were created when we pass through slice $n = 4$.

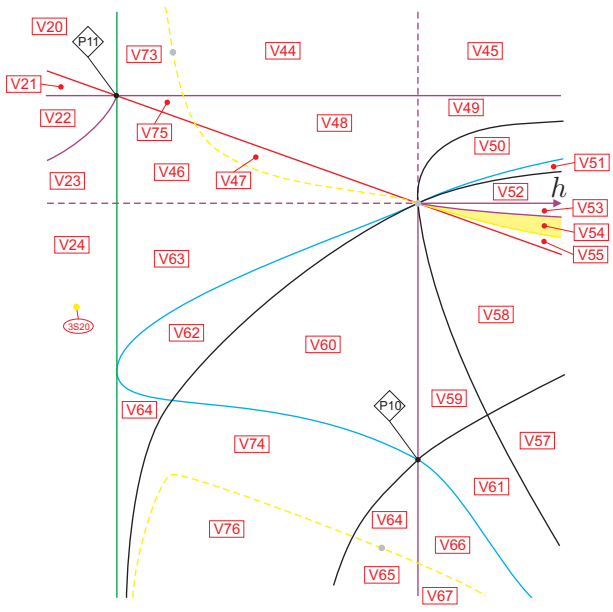

Fig. 49. Slice of parameter space when $n = 4$ (see Figs. 24, 45 and 48)

Table 15. Transition from slice $n > 4$ to $n = 2304/645$. The notation V_{62}^* means that only one of the two apparently disconnected parts of V_{62} in Fig. 48 has died. Moreover, the point $2.7L_5$ in Fig. 38 tends to P_{64} as $n \to \infty$ "killing" all the above volumes (and respective borders) and $2.7L_6$ comes from P_{64} (when $n = -\infty$) "bringing" a new set of volumes and borders

Dead parts	Parts in sing. slice	Born parts
V_{62}^*	P_{10}	V_{77}
V_{26}, V_{27}, V_{28}, V_{29}, V_{30}, V_{68}, V_{69}, V_{70}, V_{71}, V_{72}	P_{64}	V_{78}, V_{79}, V_{80}, V_{81}, V_{82}, V_{83}
$2.7L_5$	P_{64}	$2.7L_6$
V_{43}	P_{11}	V_{84}, V_{85}

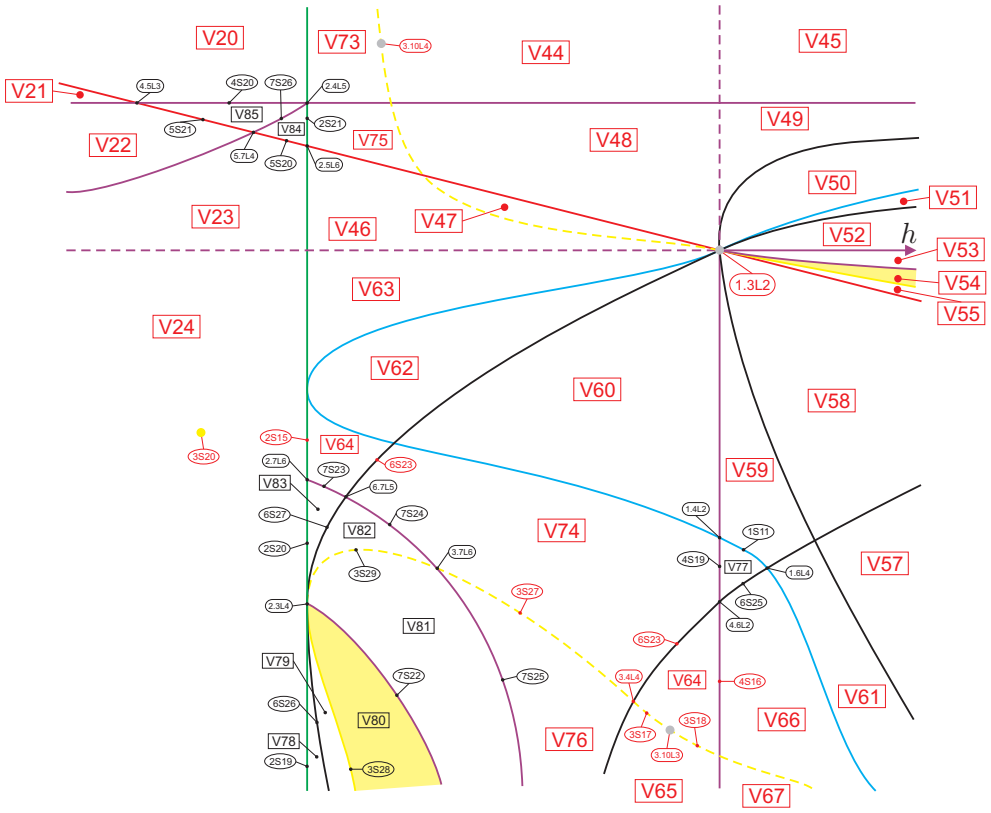

Fig. 50. Slice of parameter space when $n = 2304/625$ (see Fig. 49)

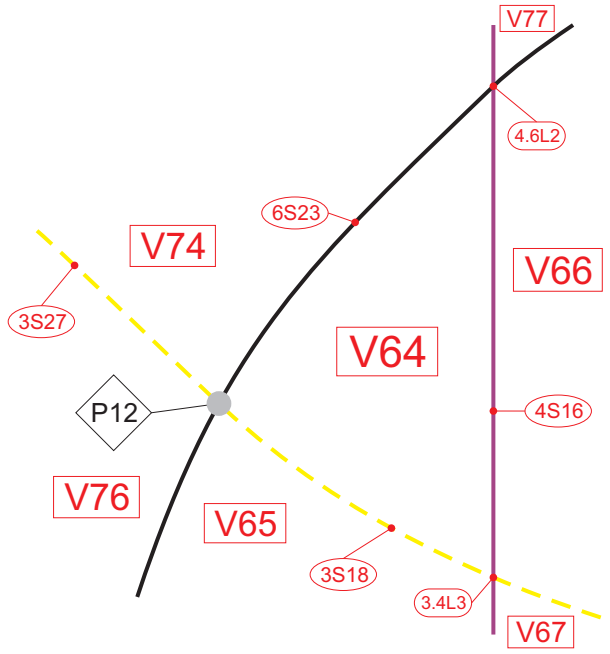

Fig. 51. Slice of parameter space when $n = n_{27} \approx 3.6349\ldots$ (see Fig. 50)

In Figs. 51 to 54 we show the movement of the gray point $3.10L_3$ and the purple straight line containing segment $4S_{16}$, when n moves down from $n = n_{27} \approx 3.6349\ldots$ to $n = n_{31} = 3$. Tables 16 and 17 presents the death and birth of parts in this transition.

Table 16. Transition from slice $n = 2304/625$ to $n = 7/2$

Dead parts	Parts in sing. slice	Born parts
$3S_{12}$	P_{12}	$3S_{30}$

Table 17. Transition from slice $n = 7/2$ to $n = 16/5$. The notation V_{64}^* means that only one of the two apparently disconnected parts of V_{64} in Fig. 52 has died

Dead parts	Parts in sing. slice	Born parts
V_{64}^*	P_{13}	V_{86}

When $n = 3$, surfaces $(\mathcal{S}_3)$ and $(\mathcal{S}_5)$ do not intersect transversally, possessing a point of contact, as we can see in Fig. 55 and in Table 18. We note that in the next slice when $n = 14/5$ there exists an-

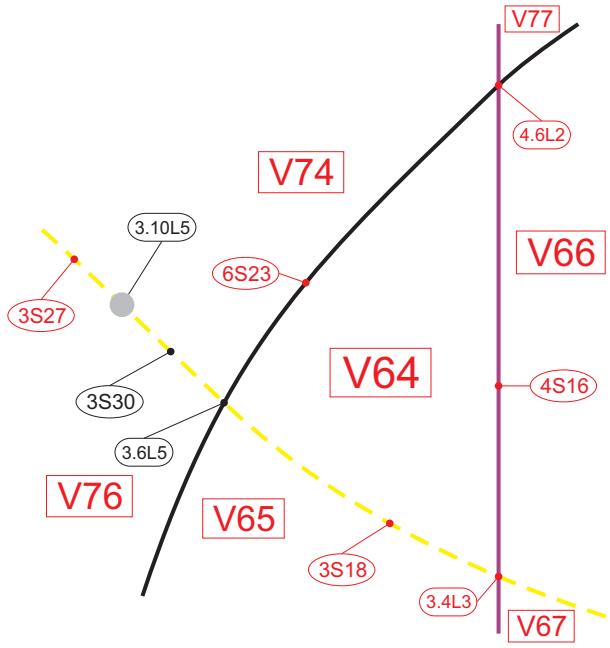

Fig. 52. Slice of parameter space when $n = 7/2$ (see Fig. 51)

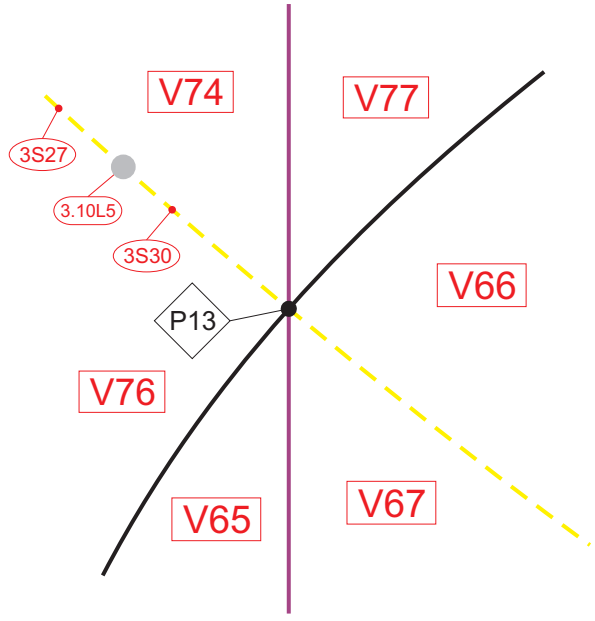

Fig. 53. Slice of parameter space when $n = 2 + \sqrt{2}$ (see Fig. 52)

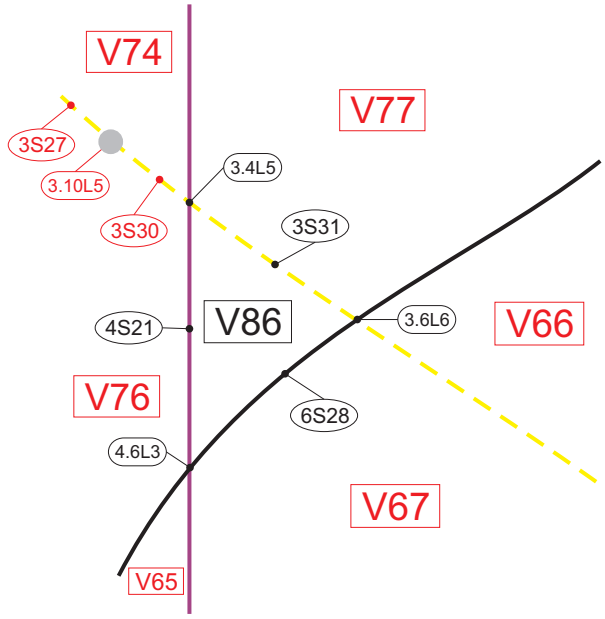

Fig. 54. Slice of parameter space when $n = 16/5$ (see Fig. 53)

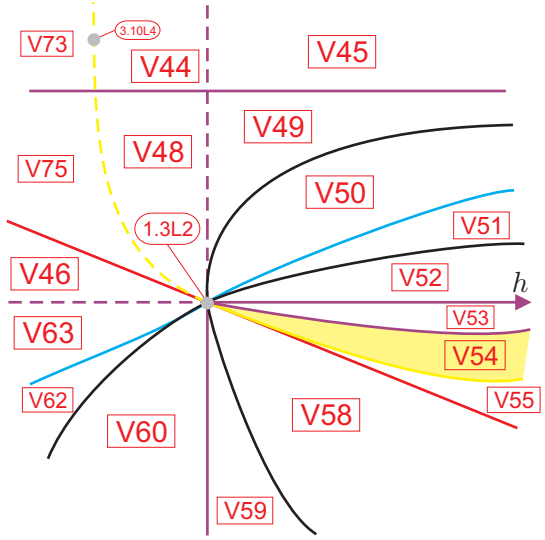

Fig. 55. Slice of parameter space when $n = 3$ (see Fig. 50)

other part with limit cycles (V_{87}) as represented in Fig. 56. In the sequence, we claim that at $n = 8/3$ the point $3.10L_4$ goes to infinity (more precisely, to the point P_{64}). Indeed, according to Lemma 6.21, the last coordinate of the expression of this point is

$$n = \frac{12 - 24\ell + 3\ell^2 - \sqrt{3(2+\ell)^3(3\ell-2)}}{8 - 12\ell},$$

and solving it with respect to n, we obtain three solutions. Now, if we substitute the value $n = 8/3$ in these solutions, they are not defined, since $3n-8$ is a factor in the three denominators, proving our claim. The parameter space at this level is shown in Fig. 57.

Table 18. Transition from slice $n > 3$ to $n = 14/5$

Dead parts	Parts in sing. slice	Born parts
V_{47}	$1.3L_2$	V_{87}

However, when we move down the value of n, the expression above makes sense again and the point reappears as $3.6L_6$ in the parameter space, but in the lower part (in the fourth quadrant), according to Fig. 58 (this figure is an ampliation of a portion of Fig. 50). When this point reappears,

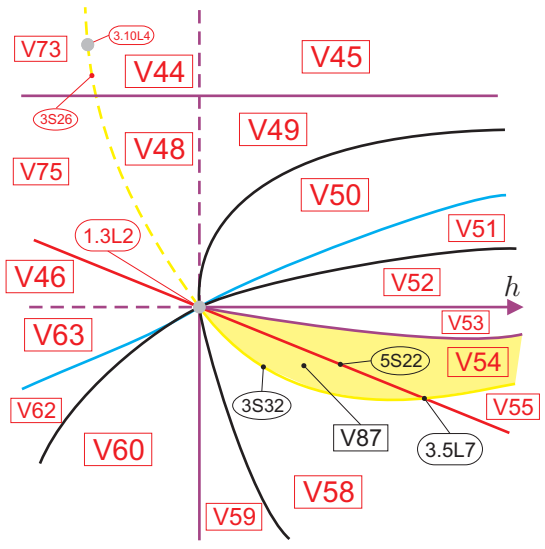

Fig. 56. Slice of parameter space when $n = 14/5$ (see Fig. 55)

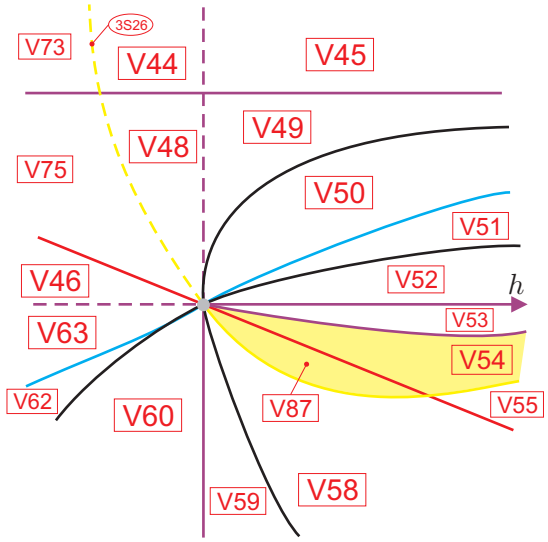

Fig. 57. Slice of parameter space when $n = 8/3$ (see Fig. 56)

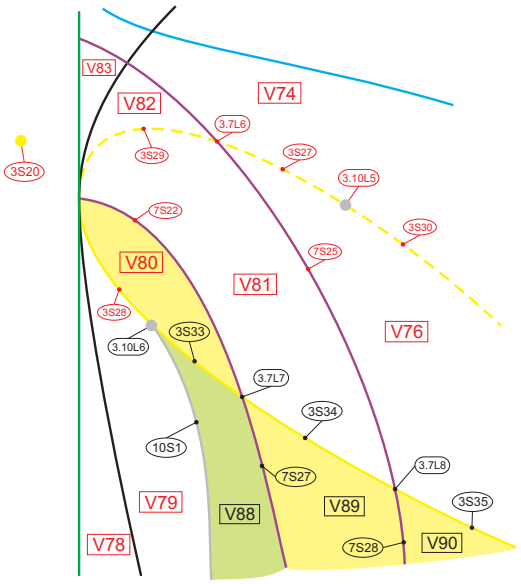

Fig. 58. Slice of parameter space when $n = 8/3 - \varepsilon_8$ (see Fig. 50)

it "brings" the curves $7S_{22}$ (loop–type connection) and $7S_{25}$ (heteroclinic connection between the finite saddle–node and the finite saddle), making them intersect $3S_{28}$. This phenomenon can be verified by fixing $n < 8/3$, but sufficiently close to this value, and parameterizing the segment $3S_{28}$ in the coordinate ℓ, for example, and for each value of h, we construct the phase portrait with the program P4 and verify that the connections of separatrices which correspond to the curves $7S_{22}$ and $7S_{25}$ occur on this segment. In addition, we must have an element of surface $(\mathcal{S}_{10})$ which corresponds to a bifurcation of double limit cycle in order to keep the coherence in the bifurcation diagram. Lemma 6.36 assures the existence of such surface.

Lemma 6.36. *Segment $10S_1$ corresponds to a bifurcation of double limit cycle and its borders are $3.10L_6$ and P_{64} (this last one from slice $n = -\infty$).*

Proof. We consider Fig. 58. Part V_{80} first appeared in slice when $n = 2304/625$ and its corresponding phase portrait possesses a limit cycle. We note that on the segments $3S_{28}$, $3S_{33}$, $3S_{34}$, $3S_{35}$ and on their linking points the phase portraits possess a weak focus of order at least one and, consequently, they refer to a Hopf bifurcation. If we are in part V_{80} and cross the segment $3S_{28}$, we enter part V_{79} and the limit cycle is lost. Following this idea, the same should happen if we cross the segment $3S_{33}$, but that is not what happens. After crossing this segment, the limit cycle persisted when entering part V_{88}. In fact the Hopf bifurcation creates a second limit cycle.

We can confirm this by moving along a different path. There exist no limit cycles in the phase portraits of parts V_{81} and V_{76} and, after crossing the segments $3S_{34}$ and $3S_{35}$, respectively, we enter in parts V_{89} and V_{90}, whose corresponding phase portraits have a limit cycle. As the segment $7S_{28}$ is the continuation of $7S_{25}$, it refers to a heteroclinic connection of separatrices between the finite saddle–node and the finite saddle, and it also possesses a limit cycle, since the separatrix which enrolls in the limit cycle is not involved in the connection. Now, considering the segment $7S_{27}$, we know it is the continuation of $7S_{22}$ and, hence, a loop–type bifurcation happens on it. So, we have two possibilities after crossing it and entering in part V_{88}: either

the limit cycle dies, or another one is created. In fact the second possibility is which happens, since there already exist at least one limit cycle in V_{88}, confirming that there exist two limit cycles in the representatives of part V_{88}.

We note that these two limit cycles are around the same focus, because there exists only one focus in this portion of the parameter space. Then, as in part V_{79} we do not have limit cycles and in V_{88} we have two of them (around the same focus), there must exist at least one element $10S_1$ of surface $(\mathcal{S}_{10})$ dividing these two parts and corresponding to the presence of a double limit cycle.

Now, it remains to prove where $10S_1$ starts from. As we have already discussed, the point $3.10L_4$ (corresponding to the presence of a weak saddle of order two) went to infinity and returned back in the lower part of the forth quadrant, being labeled as $3.10L_6$ and corresponding to the presence of a weak focus of order two. With this in mind, it is more comprehensible that leaving part V_{80} and crossing the yellow curves, we enter in two topologically distinct parts, one with limit cycles and the other without them. The linking point $3.10L_6$ of the segments $3S_{28}$ and $3S_{33}$ is responsible for this, i.e. if we "walk" along the segment $3S_{28}$, which does not possess limit cycle, and cross $3.10L_6$, the focus becomes weaker and a Hopf bifurcation happens, implying the birth of a limit cycle in the representatives of $3S_{33}$. Then, by this argument and by numerical evidences, the segment $10S_1$ starts from $3.10L_6$. Since surface $(\mathcal{S}_{10})$ has been born at P_{64} in slice $n = 8/3$, this point is still a border of $10S_1$. ■

We show in Fig. 59 an ampliation of the neighborhood in the parameter space of the point $3.10L_6$ with the corresponding phase portraits. Table 19 presents the "dead" and "born" parts when we go from slice $n = 14/5$ to $n = 8/3 - \varepsilon_8$.

Table 19. Transition from slice $n = 14/5$ to $n = 8/3-\varepsilon_8$

Dead parts	Parts in sing. slice	Born parts
$3.10L_4$	P_{64}	V_{88}, V_{89}, V_{90}

We now continue moving down the values of n and the next important value to be considered is $n = n_{35} = 8/3 - \varepsilon_8^*$. At this level, the point $3.10L_5$ (see Fig. 58) moves towards the intersection

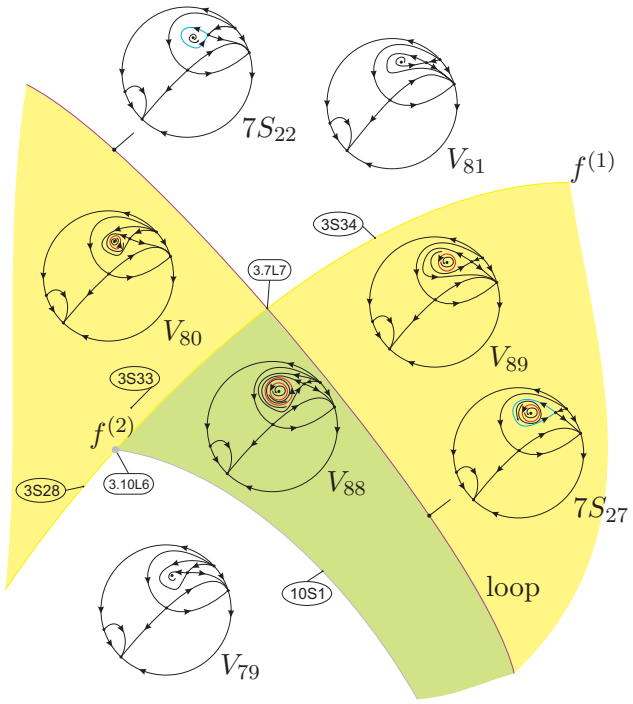

Fig. 59. Neighborhood in the parameter space of the point $3.10L_6$ with the corresponding phase portraits: the existence of double limit cycle through a $f^{(2)}$

between yellow and purple curves $(3.7L_6)$, which cannot be precisely determined, and crosses it. This movement does not imply topological changes in the phase portraits since $3.10L_5$ corresponds to a weak saddle of order two. We show the movement just described in Figs. 60 and 61, and in Table 20.

Table 20. Transition from slice $n = 8/3 - \varepsilon_8$ to $n = 8/3 - \varepsilon_9$

Dead parts	Parts in sing. slice	Born parts
$3S_{27}$	P_{14}	$3S_{36}$

Considering the next singular slice, we analyze the case when $n = 9/4$. According to Lemma 6.4, in this value of n, surface $(\mathcal{S}_3)$ has a line of singularities of degree of degeneration at least three; in fact, when $n = 9/4$, a branch of this surface becomes a cusp after the collision of the point $2.3L_4$ (which is also a common point of surfaces $(\mathcal{S}_2)$, $(\mathcal{S}_6)$ and $(\mathcal{S}_7)$; see Fig. 61) with $3S_{20}$ (a projective line or a single point in each slice) which corresponds to two complex singular points with null trace. In addition

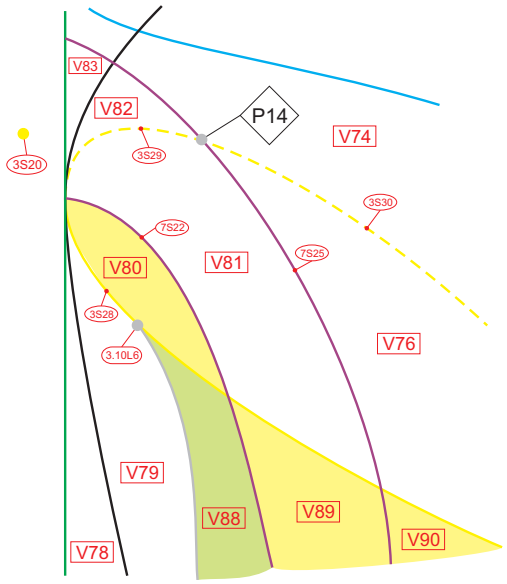

Fig. 60. Slice of parameter space when $n = 8/3 - \varepsilon_8^*$ (see Fig. 58)

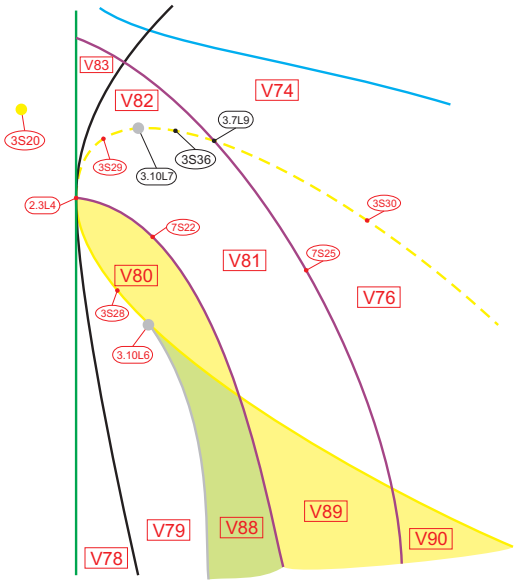

Fig. 61. Slice of parameter space when $n = 8/3 - \varepsilon_9$ (see Fig. 60)

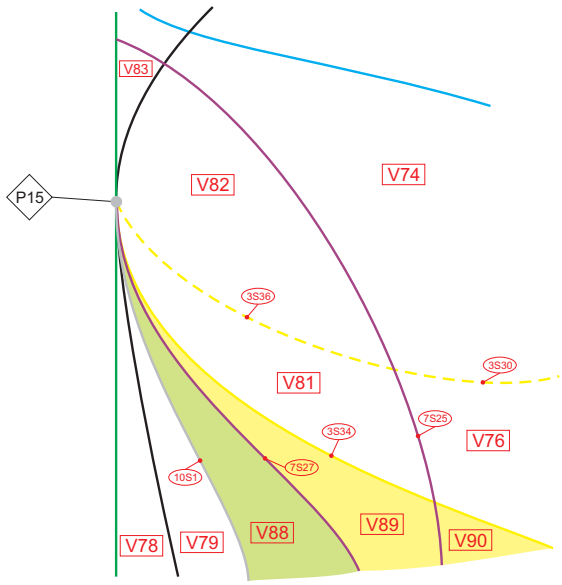

Fig. 62. Slice of parameter space when $n = 9/4$ (see Fig. 61)

to this collision, the points $3.10L_6$ and $3.10L_7$ also collapse and make part of this cusp point of surface $(\mathcal{S}_3)$, as we can see in Fig. 62. It is worth mentioning that the corresponding phase portrait of this cusp point, P_{15}, possesses a singularity (a nilpotent cusp) that grasps simultaneously the properties of a weak saddle of order two and a weak focus of order two; besides, this focus is in the edge of turning into a node. We also note that the part with two limit cycles has remained at this level and it will "survive a bit longer".

The next phenomenon is that the same branch of yellow curve produces itself a loop for values of $n < 9/4$, but close to it, and we arrive at the Fig. 63. We have verified that the purple curves behaves as represented in Fig. 63 and that the part of two limit cycles still persists. However, the elements characterized by possessing a weak point of order two do not persist, since their expression has no image for values of $n \in (-2, 9/4)$.

So, there may arise a question. If there exists no element implying the presence of a weak focus of order two, where does the bifurcation surface of double limit cycle start from? This starts from a weak saddle of order one which produces a loop itself (as suggested in the description of surface $(\mathcal{S}_3)$ on page 22). In the case of planar differential systems, we know that the stability of a homoclinic

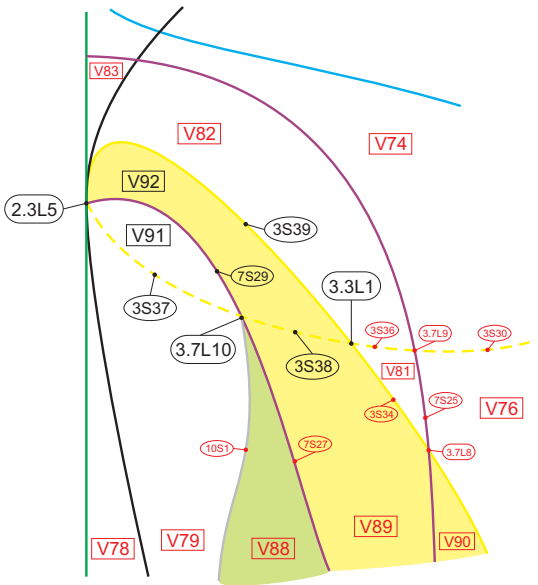

Fig. 63. Slice of parameter space when $n = 11/5$ (see Fig. 62)

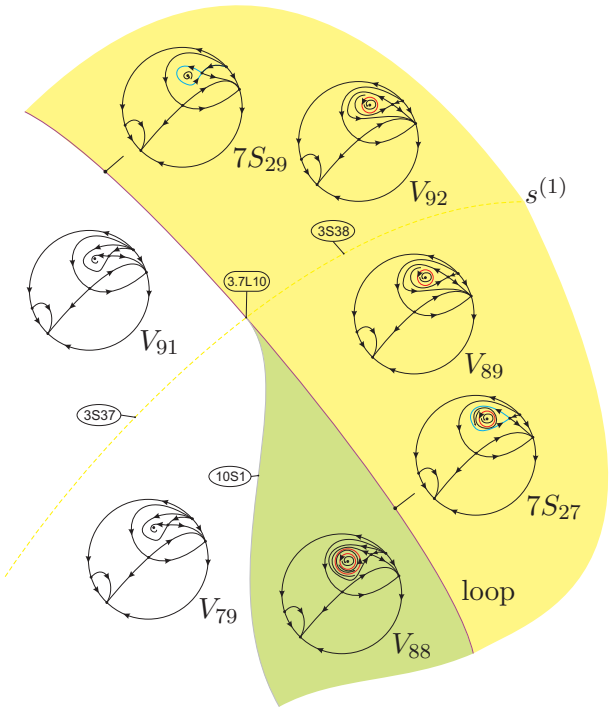

Fig. 64. Neighborhood in the parameter space of the point $3.10L_6$ with the corresponding phase portraits: the existence of double limit cycle through a $s^{(1)}$ one.

loop through a saddle is determined in first approximation by the trace of the saddle. If the trace is nonzero, a loop bifurcation leads to the birth (or death) of a unique limit cycle when the two separatrices of the saddle cross each other, and we strongly use this fact in the results of this thesis. However, according to Joyal and Rousseau [**?**], when the trace of the saddle point vanishes, we can have several limit cycles rising in a loop bifurcation (the authors prove this phenomenon using the Poincar return map in the neighborhood of the loop).

In simple words, when an elementary saddle forms a loop, the interior stability of the loop is ruled by the trace of the saddle. It is unstable, if the trace is positive, and it is stable, if the trace is negative. Thus, if along a set of parameters while the loop persists the trace changes its sign, a limit cycle must bifurcate.

The most interesting phenomenon that happens in the family $\overline{\mathbf{QsnSN(C)}}$ is the fact that we can pass from a (generalized) Hopf bifurcation to a (generalized) loop bifurcation continuously as we can see in Figs. 61 to 63.

Remark 6.37. The terms "generalized" used twice above refer respectively to a Hopf bifurcation associated with a weak focus of order two and a loop bifurcation associated with a weak saddle of order

We show in Fig. 64 an ampliation of the neighborhood in the parameter space of the point $3.7L_{10}$ with the corresponding phase portraits. Table 21 shows the "dead" and "born" parts when we go from slice $n = 8/3 - \varepsilon_9$ to $n = 11/5$.

Table 21. Transition from slice $n = 8/3 - \varepsilon_9$ to $n = 11/5$

Dead parts	Parts in sing. slice	Born parts
V_{80}	P_{15}	V_{91}, V_{92}

In what follows, the point $3.7L_9$ moves towards the point $3.3L_1$, they intersect and new parts are created as can be visualized in Figs. 65 and 66. Table 22 shows the "dead" and "born" parts when we go from slice $n = 11/5$ to $n = 11/5 - \varepsilon_{10}$.

In Figs. 67 to 70, we show the movement of the curves in yellow and purple when we decrease n from $n_{41} = 3(102 - 7\sqrt{21})/100$ (including this value) to $n_{45} = 2$, creating contact points with other curves and after intersecting them transver-

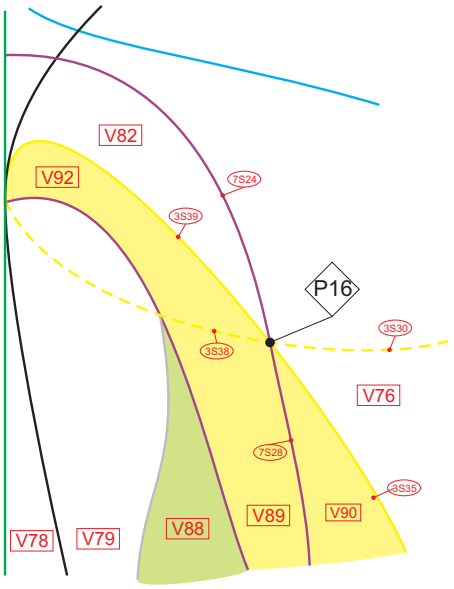

Fig. 65. Slice of parameter space when $n = 11/5 - \varepsilon_9^*$ (see Fig. 63)

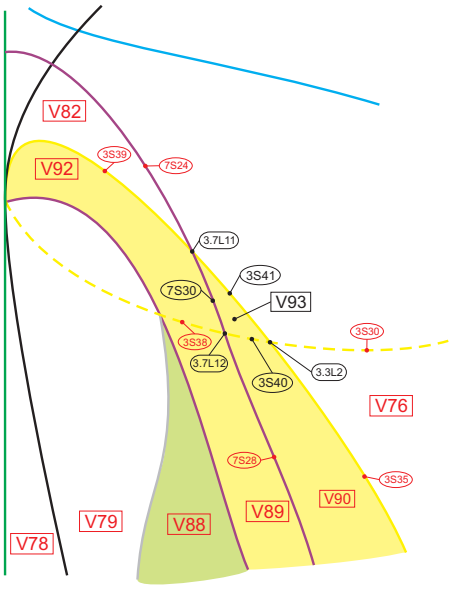

Fig. 66. Slice of parameter space when $n = 11/5 - \varepsilon_{10}$ (see Fig. 65)

Table 22. Transition from slice $n = 11/5$ to $n = 11/5 - \varepsilon_{10}$

Dead parts	Parts in sing. slice	Born parts
V_{81}	P_{16}	V_{93}

sally in two points. Tables 23 and 24 indicate the "dead" and "born" parts during this transition.

Table 23. Transition from slice $n = 11/5 - \varepsilon_{10}$ to $n = 3(102 - 7\sqrt{21})/100 - \varepsilon_{11}$. The symbol '$\emptyset$' means that no part was "dead"

Dead parts	Parts in sing. slice	Born parts
$\emptyset$	$3.6L_8$	V_{94}

Table 24. Transition from slice $n = 3(102 - 7\sqrt{21})/100 - \varepsilon_{11}$ to $n = 2 + \varepsilon_{12}$. The symbol '$\emptyset$' means that no part was "dead"

Dead parts	Parts in sing. slice	Born parts
$\emptyset$	$5.7L_5$	V_{95}

We recall that surface $(\mathcal{S}_3)$ is the union of a plane and a cubic, and the proof of Lemma 6.4 assures that, if $n = 2$, this cubic can be factorized in a line plus a conic: $-4(2h-1)(2+2\ell+2h\ell+\ell^2)$. It is to say that this surface changes its behavior when we move to $n = 2$ and some parts in the bifurcation diagram die and others are created. See Fig. 71 which illustrates the slice when $n = 2$ (we only show the first and fourth quadrants) and Table 25 which indicates the "dead" and "born" parts when we cross slice $n = 2$.

If we consider the next slice when $n = 19/10$, the factorization is not possible and we obtain the slice shown in Fig. 72. We note that in the lower part of this slice the elements of surfaces $(\mathcal{S}_7)$ and $(\mathcal{S}_{10})$ intersect with an element of surface $(\mathcal{S}_4)$. This fact was verified by "walking" along two segments parallel to an element of surface $(\mathcal{S}_4)$ containing $4S_{27}$ in this slice both left and right sides. On the right side (upper part), starting from part V_{101}, the phase portrait possesses a limit cycle and the separatrix which enrolls around it comes from the fi-

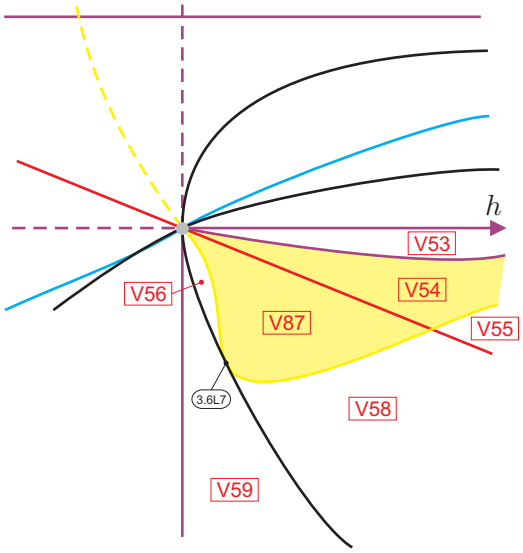

Fig. 67. Slice of parameter space when $n = 3(102 - 7\sqrt{21})/100$ (see Fig. 57)

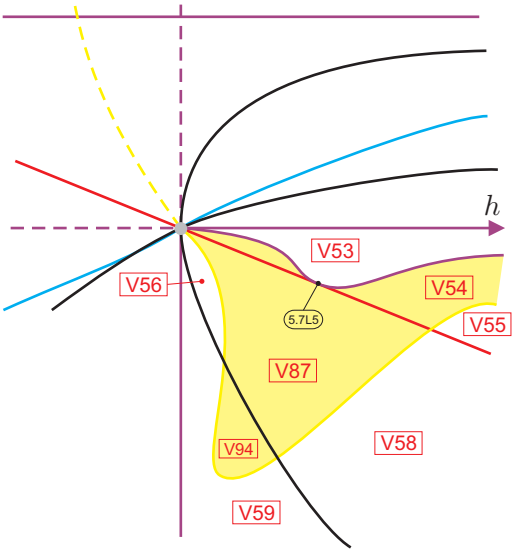

Fig. 69. Slice of parameter space when $n = 2 + \varepsilon_{12}^*$ (see Fig. 68)

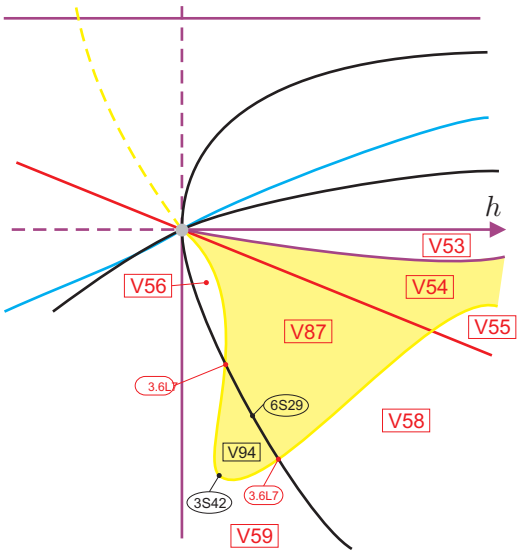

Fig. 68. Slice of parameter space when $n = 3(102 - 7\sqrt{21})/100 - \varepsilon_{11}$ (see Fig. 67)

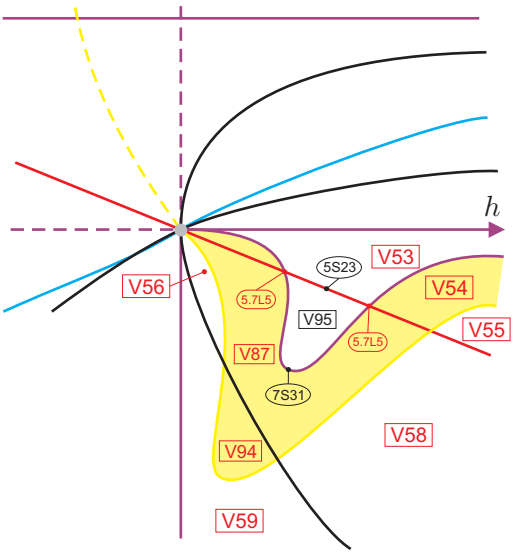

Fig. 70. Slice of parameter space when $n = 2 + \varepsilon_{12}$ (see Fig. 69)

Table 25. Transition from slice $n = 2 + \varepsilon_{12}$ to $n = 19/10$. The notation V_{56}^* means that only one of the two apparently disconnected parts of V_{56} in Fig. 70 has died

Dead parts	Parts in sing. slice	Born parts
V_{44}	$3.4L_6$	V_{96}
V_{48}	$3.4L_7$	V_{97}, V_{98}
V_{56}^*	$3.4L_8$	V_{99}
V_{65}	P_{64}	V_{101}, V_{102}, V_{103}, V_{104}
V_{76}	$3.4L_9$	V_{100}

nite saddle–node. However, after "walking down" a little more, we observed that the limit cycle died and the separatrix which goes towards the focus comes from the finite saddle, implying that we have crossed a loop bifurcation. A little below, a heteroclinic bifurcation between finite singularities also happens.

On the other hand, on the left side, starting from part V_{90} and going down, we first cross the heteroclinic connection and, after, the loop connection, but in this case, instead of meaning the death of the limit cycle, it means the birth of a second one. A little below, these two limit cycles die in a double–limit–cycle bifurcation. A bit further down, we cross surface $(\mathcal{S}_6)$, so the focus becomes a node and no limit cycles are possible anymore. Also, surface $(\mathcal{S}_4)$ crosses surface $(\mathcal{S}_6)$ forcing part V_{88} to be bounded now. Then, the only point where surface $(\mathcal{S}_{10})$ may end is $4.7L_1$, in which we have two heteroclinic connections between the finite saddle and the finite saddle–node. As it is shown in the paper of Dumortier, Roussarie and Rousseau [Dumortier *et al.*, 1994], the graphic in $4.7L_1$ has cyclicity two which is compatible with the fact that this part borders a part with two limit cycles around the same focus and a part with double limit cycle. Fig. 73 shows an ampliation of the neighborhood in the parameter space of the point $4.7L_1$ with the corresponding phase portraits.

In what follows, this point $4.7L_1$ "goes up" in the sense of increasing ℓ along the segment of surface $(\mathcal{S}_4)$. The next singular slice to be considered is when it crosses the intersection $3.4L_{12}$ between yellow and purple curves (see Fig. 74). In addition, the point $3.7L_{10}$ tends towards $4.7L_1$ and, after the bifurcation, all the parts of surface $(\mathcal{S}_3)$ close to the new part $4.7L_2$ will be below it. So, there is no more intersection between the weak–saddle phenomenon and the loop phenomenon on the left side of vertical purple. This avoids the existence of part V_{88}. Then, part V_{88} must have shrunk as n tends to $19/10 - \varepsilon_{13}^*$ and disappeared in P_{21}. On the right side of the vertical purple it still exists an intersection between weak–saddle and loop bifurcations $(3.7L_{13})$, but the loop takes place with the separatrices of the finite saddle–node and, thus, the weak saddle is not related to any limit cycle (see Fig. 75). Table 26 indicates the "dead" and "born" parts in this transition.

Table 26. Transition from slice $n = 19/10$ to $n = 17/10$

Dead parts	Parts in sing. slice	Born parts
V_{88}, V_{89}, V_{90}	P_{21}	V_{105}, V_{106}

Now, it is the turn of the purple curve $7S_{31}$ (see Fig. 72) to "go down" in the parameter space, as shown in Figs. 76 to 81. Firstly, part of it becomes tangent to the red curve $5S_{22}$ at the point $1.3L_5$ making disappear a portion of part V_{54}; then, the tangency is lost and it continues to move down contacting and intersecting the black and the blue curves yielding the curves $6.7L_6$ and $1.7L_2$, respectively. The first crossing produces new part V_{107}, but the second crossing (see Fig. 81) does no produce a new part as we will see in the next step. Tables 27, 28 and 29 indicate the "dead" and "born" parts in the transition from slice $n = 17/10$ to $n = 8/5$.

Table 27. Transition from slice $n = 17/10$ to $n = 17/10 - \varepsilon_{14}$. The notation V_{54}^* means that only one of the two apparently disconnected parts of V_{54} in Fig. 70 has died. The symbol '$\emptyset$' means that no part was created

Dead parts	Parts in sing. slice	Born parts
V_{54}^*	$1.3L_5$	$\emptyset$

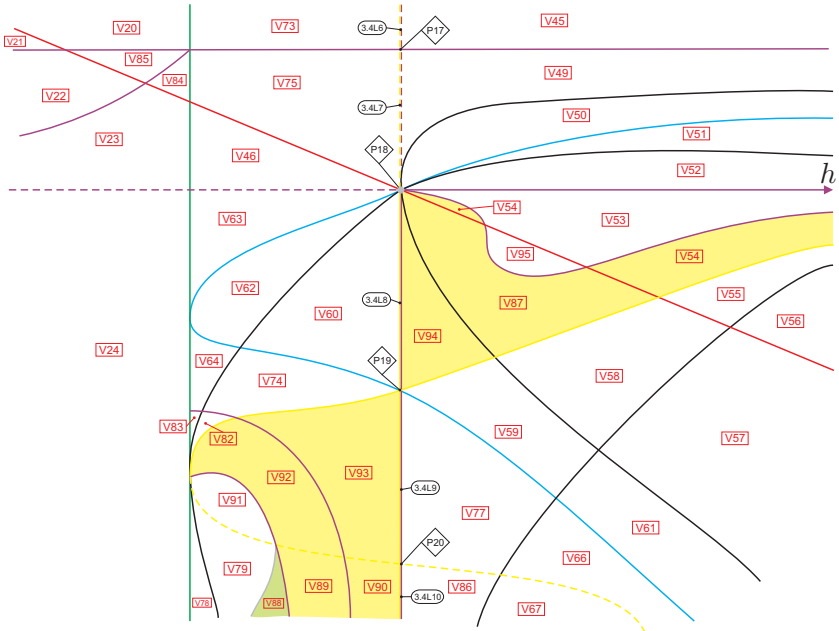

Fig. 71. Slice of parameter space when $n = 2$ (see Figs. 50, 66 and 70)

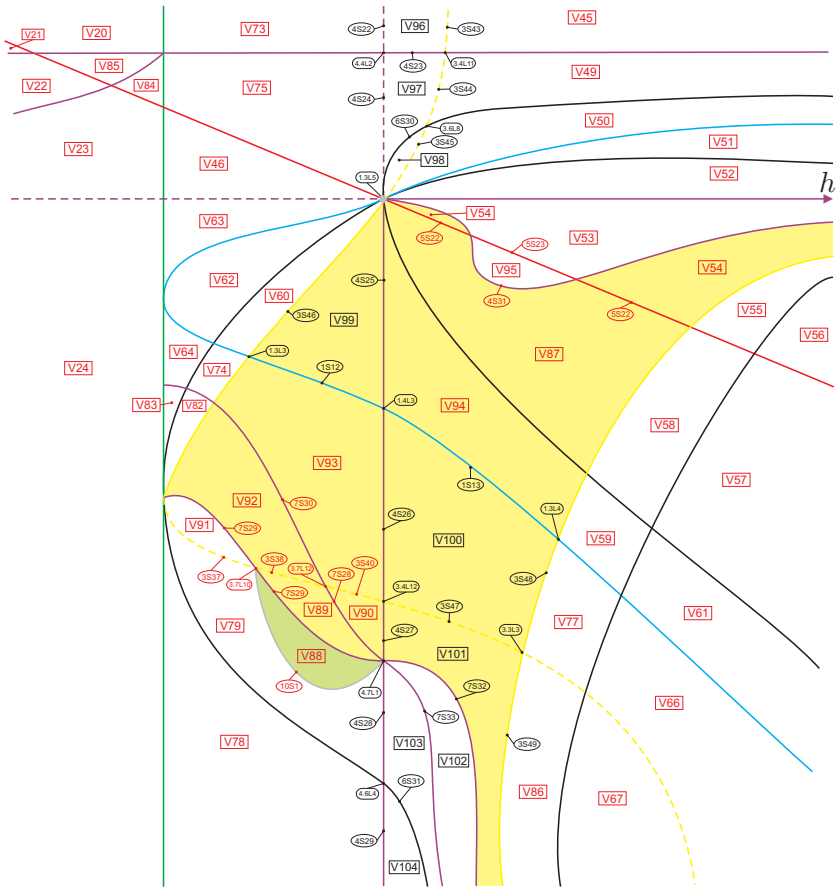

Fig. 72. Slice of parameter space when $n = 19/10$ (see Fig. 71)

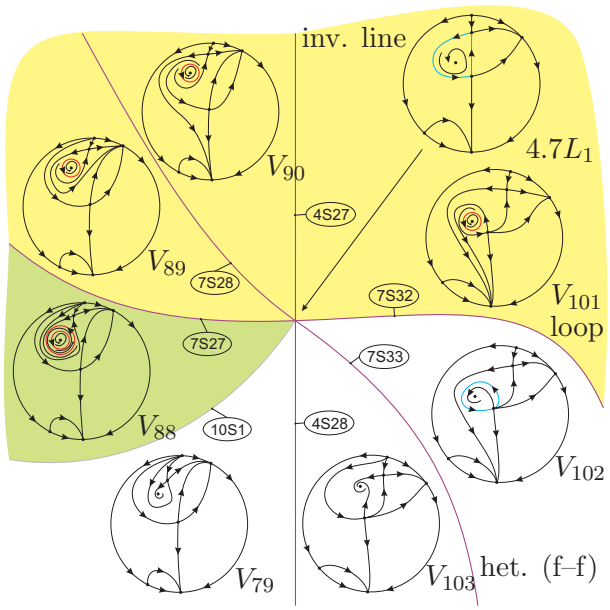

Fig. 73. Neighborhood in the parameter space of the point $4.7L_1$ with the corresponding phase portraits: the existence of double limit cycle through a finite–to–finite heteroclinic and a loop bifurcations

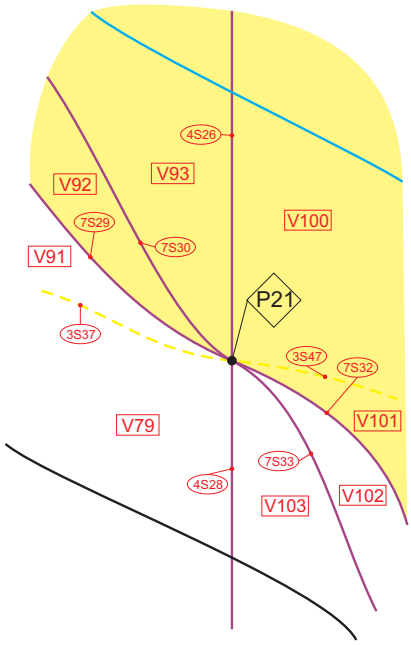

Fig. 74. Slice of parameter space when $n = 19/10 - \varepsilon_{13}^*$ (see Fig. 72)

Table 28. Transition from slice $n = 17/10 - \varepsilon_{14}$ to $n = 41/25$. The symbol '$\emptyset$' means that no part was "dead"

Dead parts	Parts in sing. slice	Born parts
$\emptyset$	$6.7L_6$	V_{107}

Table 29. Transition from slice $n = 41/25$ to $n = 8/5$. The symbol '$\emptyset$' means that no part was "dead". The "born" part V_{105}^* is not new since it will join later with V_{105} (see Fig. 83)

Dead parts	Parts in sing. slice	Born parts
$\emptyset$	$1.7L_2$	V_{105}^*

When we reach the value $n = 1$, some considerable changes happen to the behavior of the curves. The purple vertical line and one component of the green lines collide (since their expressions have the common factor h) and all the elements which were in between of them have collapsed in some parts of this vertical line. See Fig. 82. However, they separate again for $n < 1$ and many new parts ap-

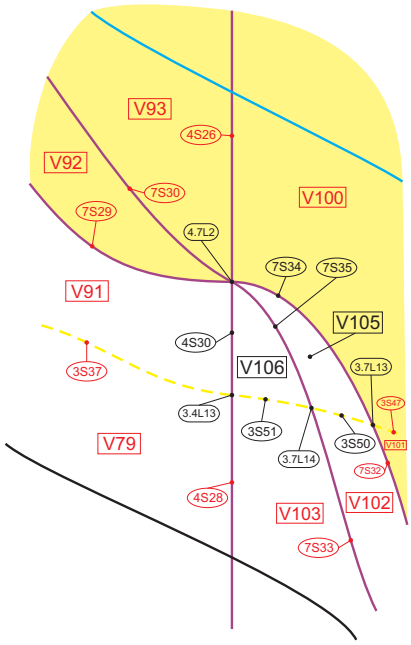

Fig. 75. Slice of parameter space when $n = 17/10$ (see Fig. 74)

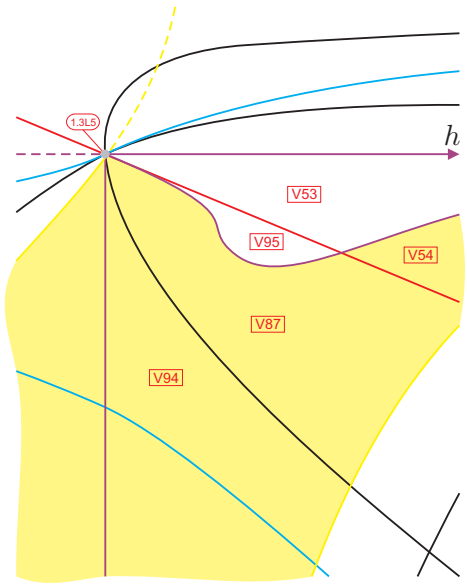

Fig. 76. Slice of parameter space when $n = 17/10 - \varepsilon_{14}^*$ (see Fig. 72)

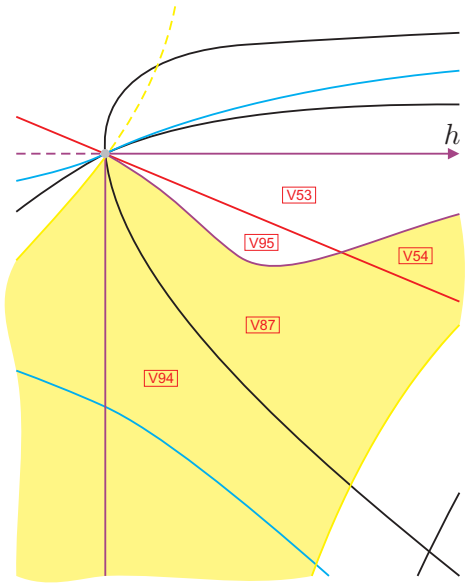

Fig. 77. Slice of parameter space when $n = 17/10 - \varepsilon_{14}$ (see Fig. 76)

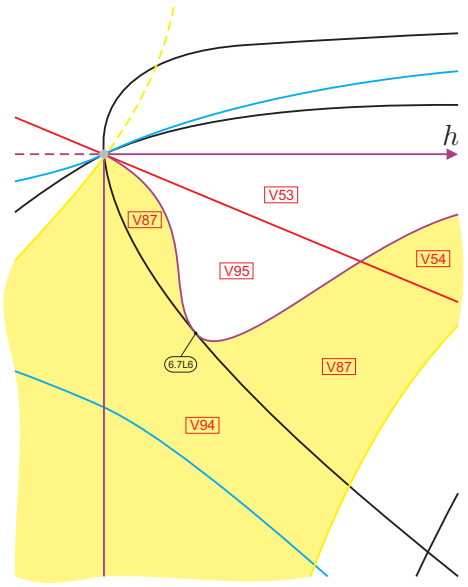

Fig. 78. Slice of parameter space when $n = 41/25 + \varepsilon_{15}^*$ (see Fig. 77)

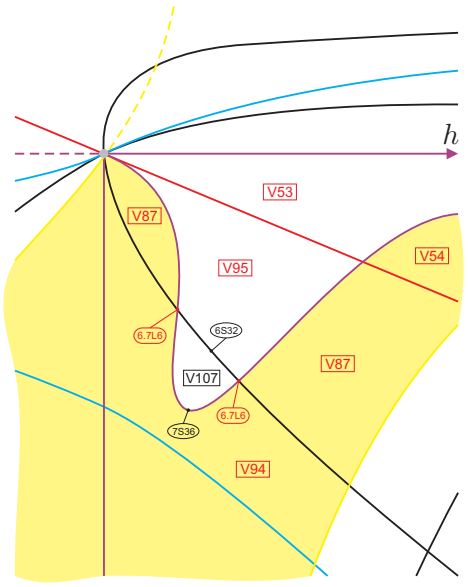

Fig. 79. Slice of parameter space when $n = 41/25$ (see Fig. 78)

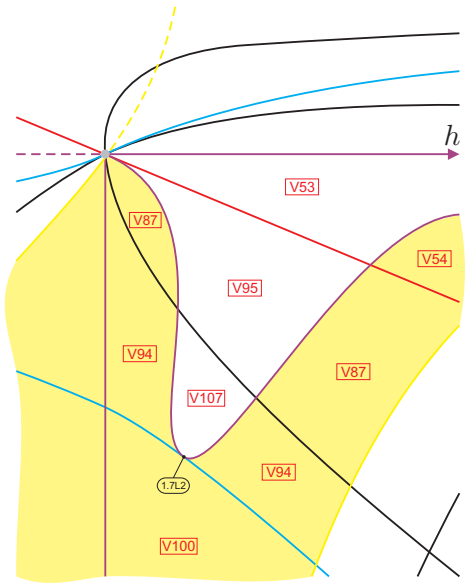

Fig. 80. Slice of parameter space when $n = 8/5 + \varepsilon_{16}^*$ (see Fig. 79)

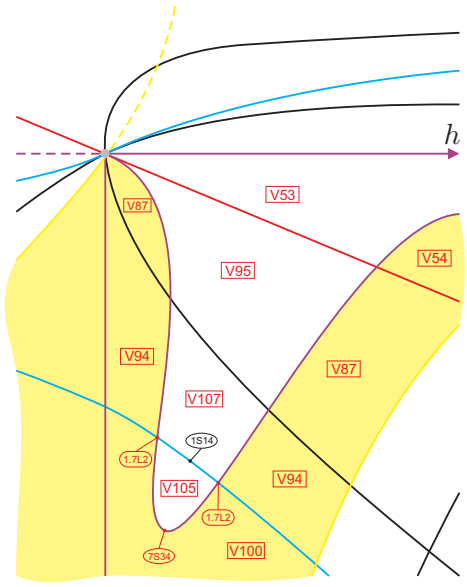

Fig. 81. Slice of parameter space when $n = 8/5$ (see Fig. 80)

pear between them, as shown in Fig. 83. All these "dead" and "born" parts are indicated in Table 30.

Table 30. Transition from slice $n = 8/5$ to $n = 81/100$. Compare Figs. 72 and 83: all parts between the two vertical lines collapse. The lines split again and generate new parts. Parts V_{88}, V_{89} and V_{90} had already disappeared some slices above

Dead parts	Parts in sing. slice	Born parts
V_{46}, V_{60}, V_{62}, V_{63}, V_{64}, V_{73}, V_{74}, V_{75}, V_{78}, V_{82}, V_{83}, V_{91}, V_{92}, V_{93}, V_{99}	$2.4L_6$, $2.4L_7$, $2.4L_8$	from V_{108} to V_{125}

We note that most of the new parts in slice $n = 81/100$ are concentred in the rectangle bounded by green, vertical purple and two horizontal purple curves (we call it *Region 1*), including elements of nonalgebraic surfaces whose existence are necessary for the coherence of that part of the bifurcation diagram. Moreover, we remark that the rest of the changes will occur in the portion of the parameter space in the right side of the vertical purple line (we call it *Region 2*).

In *Region 1*, the three intersection points among green, black and yellow curves ($2.3L_6$), green and blue curves ($1.2L_3$), and green and red curves ($2.5L_7$) are the continuation of the intersections $2.3L_5$, $1.2L_2$ and $2.5L_6$, respectively, but with a different ordering they were before. Moreover, the purple segment $7S_{26}$ which separated parts V_{84} and V_{85} (see Fig. 82) and which started from an intersection of green and horizontal purple curves (P_{22}), now it is called $7S_{38}$ and starts from an intersection of horizontal purple and vertical purple curves ($4.4L_3$, in the right top of *Region 1*), splitting parts V_{109} and V_{110}. In addition, more elements of surface ($\mathcal{S}_7$) were necessary for the coherence and their existence and shape was verified numerically; four of them refer to heteroclinic bifurcations ($7S_{39}$, $7S_{40}$, $7S_{41}$ and $7S_{43}$) and one of them corresponds to loop bifurcation ($7S_{42}$).

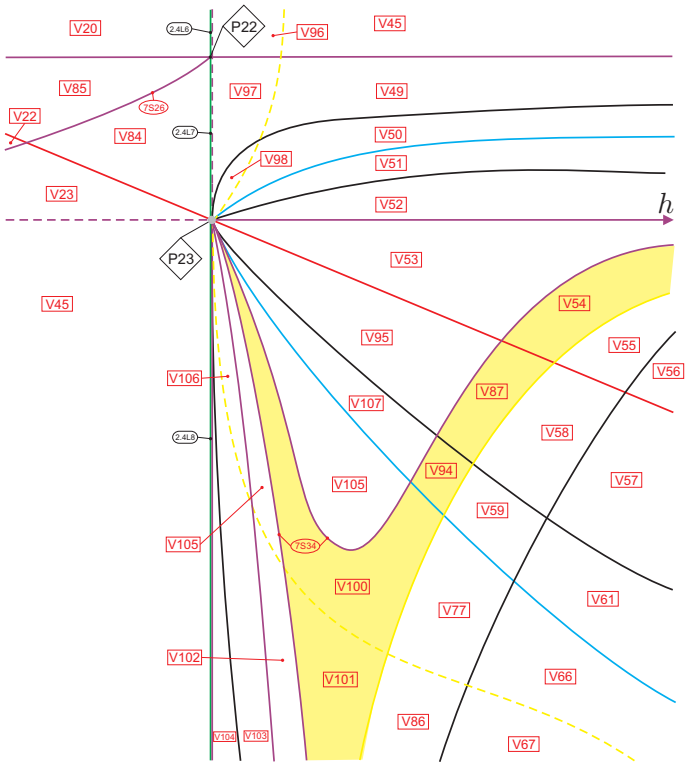

Fig. 82. Slice of parameter space when $n = 1$ (see Figs. 72, 75 and 81)

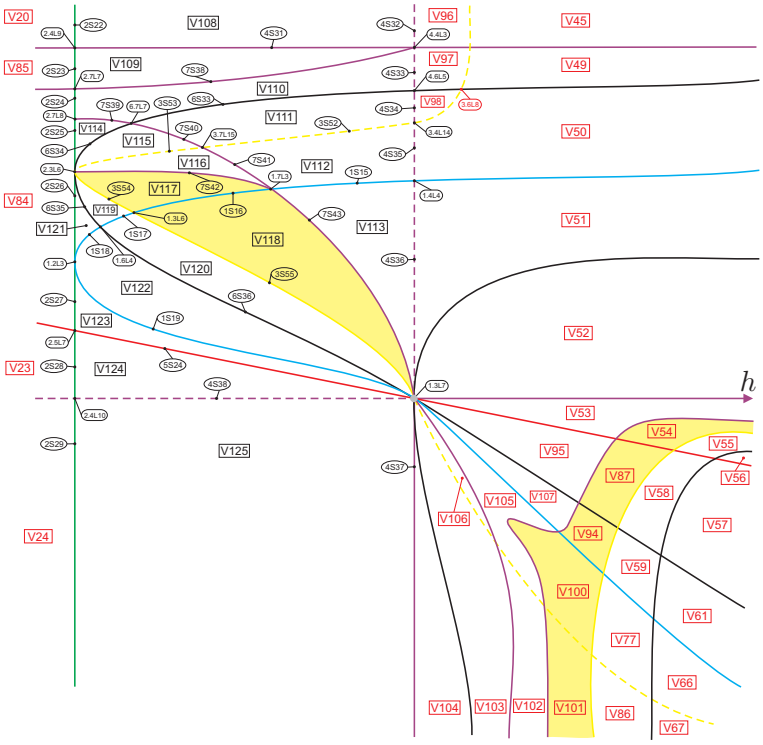

Fig. 83. Slice of parameter space when $n = 81/100$ (see Fig. 82)

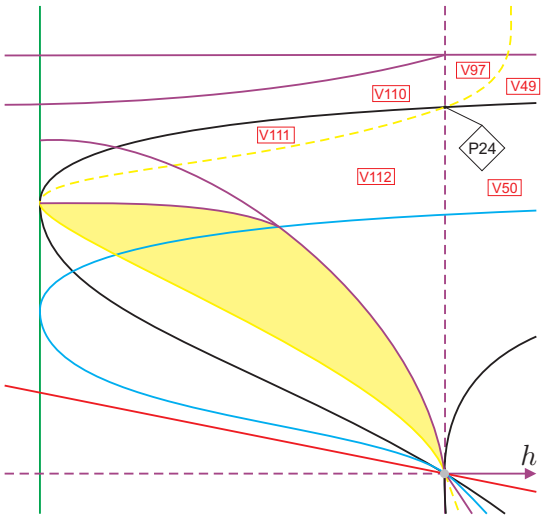

Fig. 84. Slice of parameter space when $n = 2 - \sqrt{2}$ (see Fig. 83)

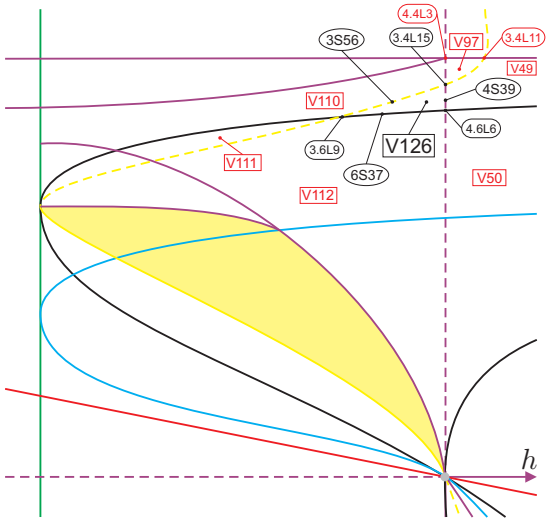

Fig. 85. Slice of parameter space when $n = 9/16$ (see Fig. 84)

In *Region 2*, at the level $n = 81/100$ all the algebraic curves remain and intersect at a single point $1.3L_7$ together with an element of a heteroclinic bifurcation. But the two disjoint elements of loop bifurcation $7S_{34}$ in Figs. 75 and 81 which border two temporary disjoint parts of part V_{105} will have a common point at P_{23} in Fig. 82 and will remain joined and unlinked from any other bifurcation surface. Segment $7S_{34}$ was purposely drawn in Fig. 83 with a beak to show its movement of separation from $1.3L_7$.

In Figs. 84 to 87 we sketch the movement of the intersection between yellow and purple $3.4L_{14}$ along the vertical purple curve $(\mathcal{S}_4)$ as it crosses surface $(\mathcal{S}_6)$ and another component of $(\mathcal{S}_4)$. We note that the intersection shown in Fig. 86 shows it having a tangency between $3S_{56}$ and $7S_{38}$. However, this could not be the case and we could have this transition needing some more steps as a different crossing between $3S_{56}$ and $7S_{38}$ can happen. This intersection cannot be detected algebraically. Anyway, since surface $(\mathcal{S}_3)$ in this surroundings only means the presence of a weak saddle and there is no possible loop, this has no effects in the number of topologically different phase portraits. Tables 31 and 32 indicate the "dead" and "born" parts in the transition from slice $n = 81/100$ to $n = 9/25$.

For the next slices, the intersection between purple and green $2.7L_7$, which is located in the left top of *Region 1*, will "sweep" the segments from

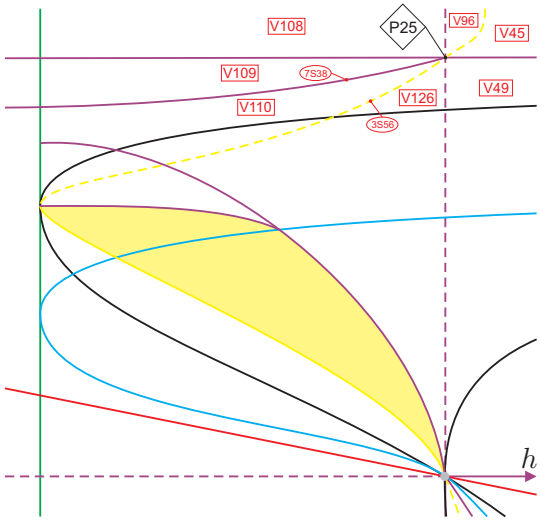

Fig. 86. Slice of parameter space when $n = 1/2$ (see Fig. 85)

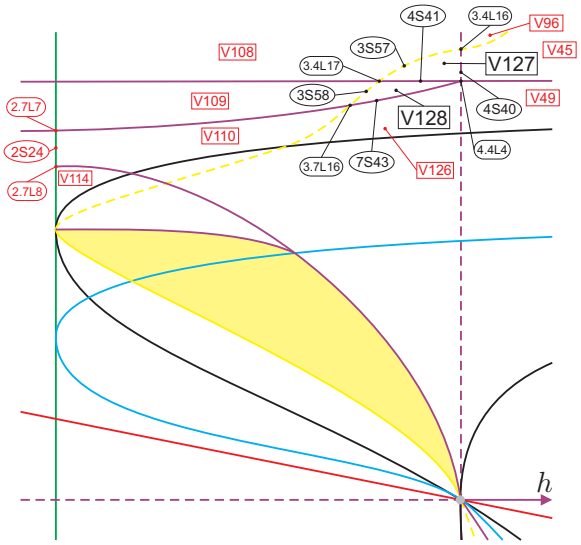

Fig. 87. Slice of parameter space when $n = 9/25$ (see Fig. 86)

Table 31. Transition from slice $n = 81/100$ to $n = 9/16$

Dead parts	Parts in sing. slice	Born parts
V_{98}	P_{24}	V_{126}

Table 32. Transition from slice $n = 9/16$ to $n = 9/25$

Dead parts	Parts in sing. slice	Born parts
V_{97}	P_{25}	V_{127}, V_{128}

$2S_{24}$ up to $2S_{28}$. Consequently, surface $7S_{38}$ will also "sweep" most of the parts in *Region 1*, producing new phase portraits. Due to its nature of being nonalgebraic, we cannot precise the order of the intersection and contact points with the other curves, but any other order different from the one we present in Figs. 88 to 109 will not bring about new phase portraits rather than the ones which have been created. Moreover, Tables 33 to 43 present the "dead" and "born" parts in the transition from slice $n = 9/25$ to $n = 1/25$.

We now consider the slice when $n = 0$. At this level almost all the invariant polynomials we use to describe the bifurcation diagram vanish and, hence, we need to consider other ones which will play a similar role. For this value of n, systems (5)

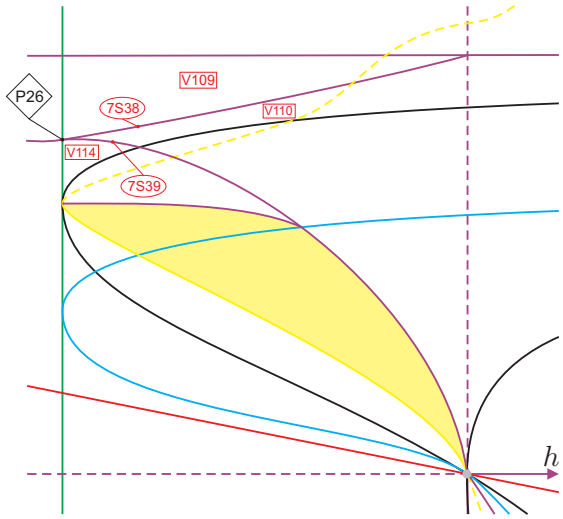

Fig. 88. Slice of parameter space when $n = 9/25 - \varepsilon_{17}^{*}$ (see Fig. 87)

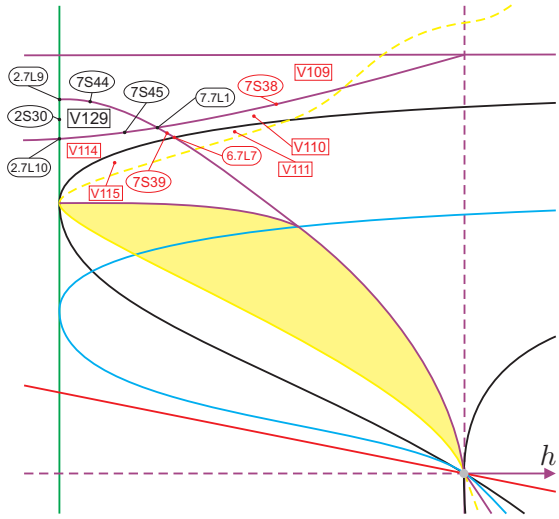

Fig. 89. Slice of parameter space when $n = 81/40$ (see Fig. 88)

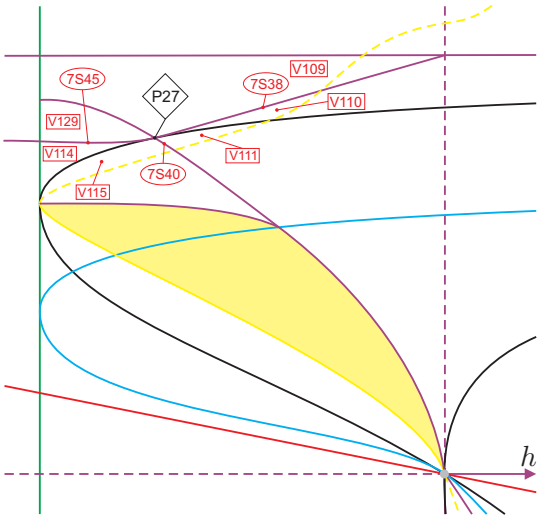

Fig. 90. Slice of parameter space when $n = 81/40 - \varepsilon_{18}^*$ (see Fig. 89)

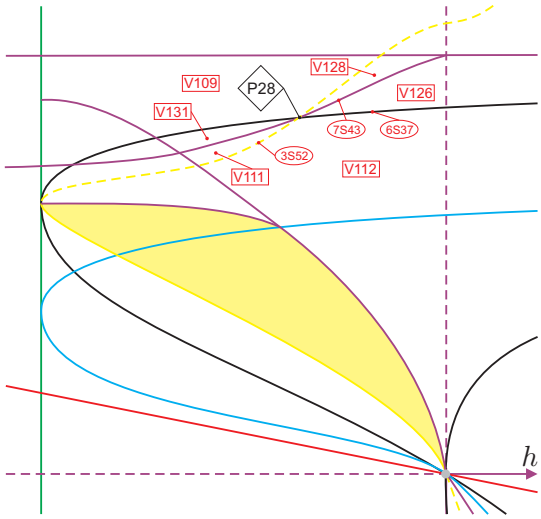

Fig. 92. Slice of parameter space when $n = 81/40 - \varepsilon_{19}^*$ (see Fig. 91)

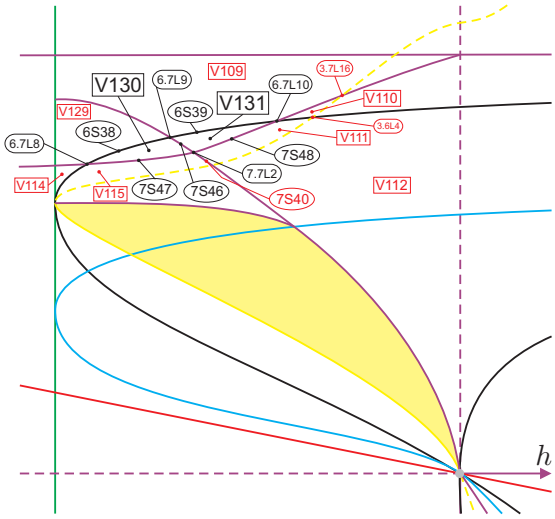

Fig. 91. Slice of parameter space when $n = 81/40 - \varepsilon_{18}$ (see Fig. 90)

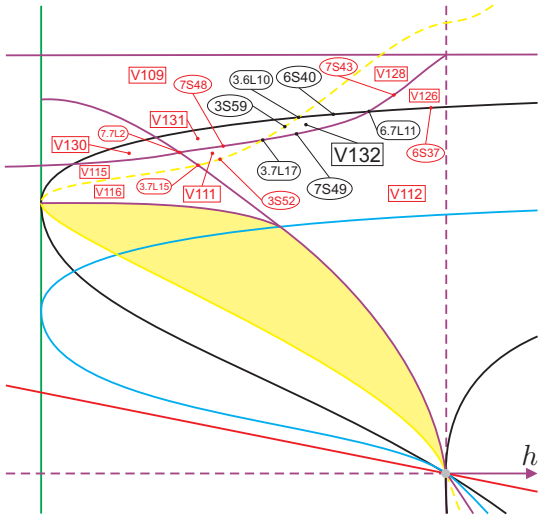

Fig. 93. Slice of parameter space when $n = 81/40 - \varepsilon_{19}$ (see Fig. 92)

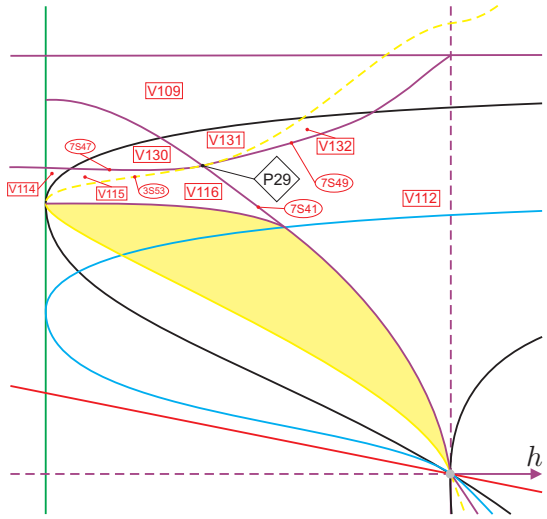

Fig. 94. Slice of parameter space when $n = 81/40 - \varepsilon^*_{20}$ (see Fig. 93)

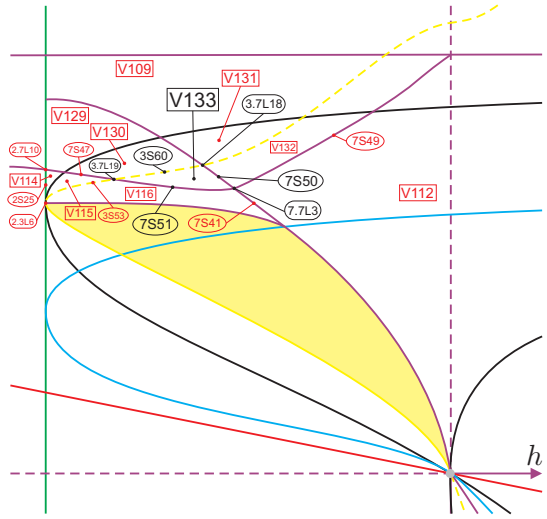

Fig. 95. Slice of parameter space when $n = 81/40 - \varepsilon_{20}$ (see Fig. 94)

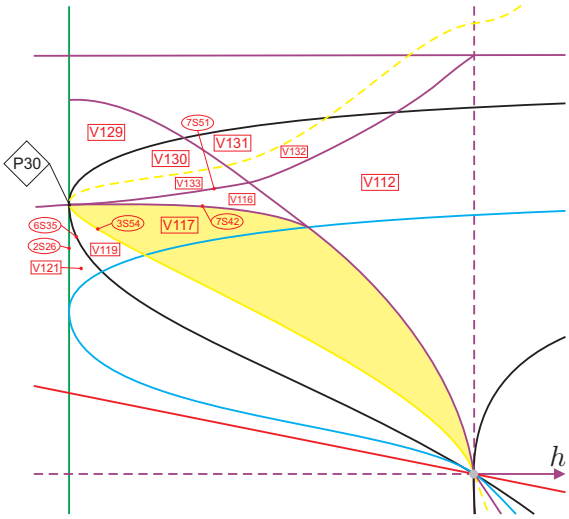

Fig. 96. Slice of parameter space when $n = 81/40 - \varepsilon^*_{21}$ (see Fig. 95)

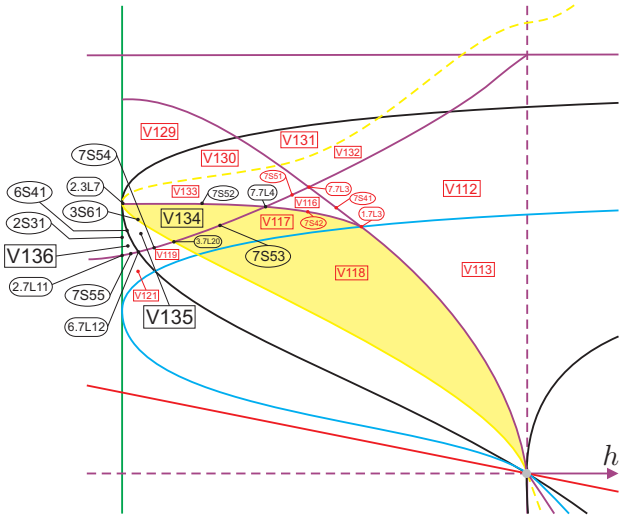

Fig. 97. Slice of parameter space when $n = 4/25$ (see Fig. 96)

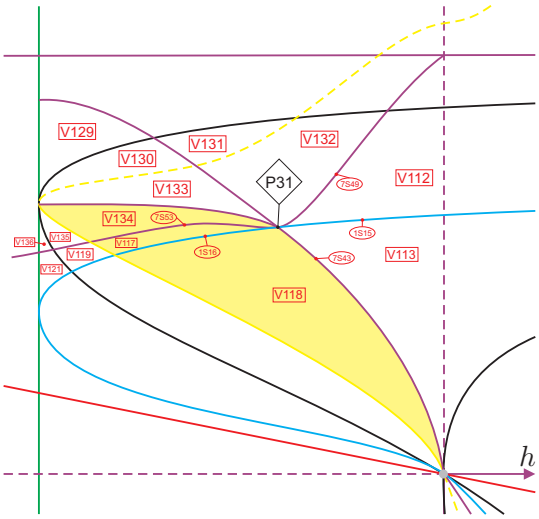

Fig. 98. Slice of parameter space when $n = 4/25 - \varepsilon_{22}^*$ (see Fig. 97)

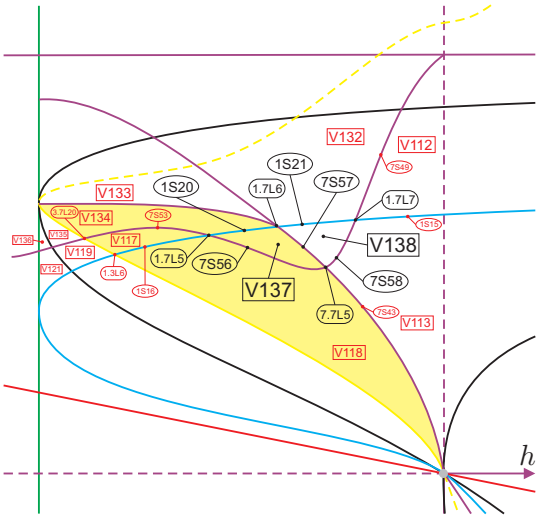

Fig. 99. Slice of parameter space when $n = 4/25 - \varepsilon_{22}$ (see Fig. 98)

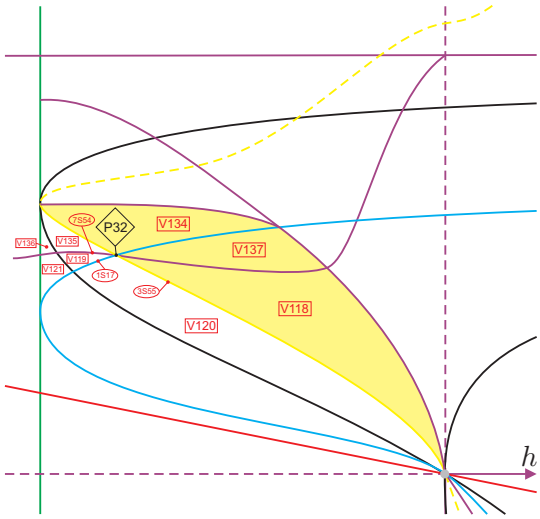

Fig. 100. Slice of parameter space when $n = 4/25 - \varepsilon_{23}^*$ (see Fig. 99)

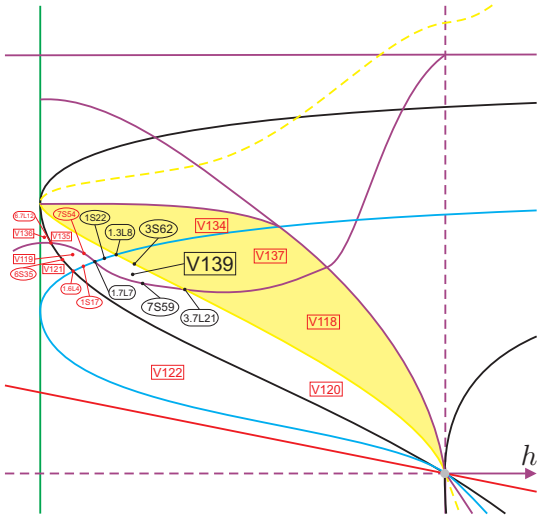

Fig. 101. Slice of parameter space when $n = 4/25 - \varepsilon_{23}$ (see Fig. 100)

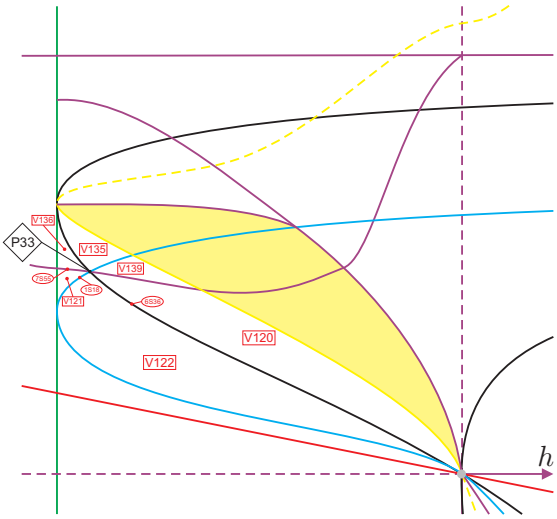

Fig. 102. Slice of parameter space when $n = 4/25 - \varepsilon_{24}^*$ (see Fig. 101)

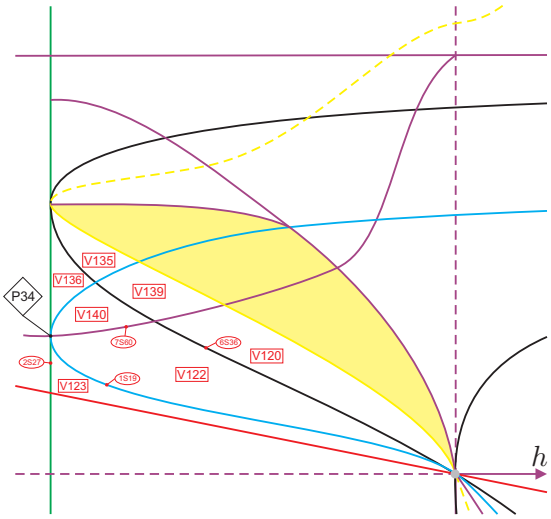

Fig. 104. Slice of parameter space when $n = 4/25 - \varepsilon_{25}^*$ (see Fig. 103)

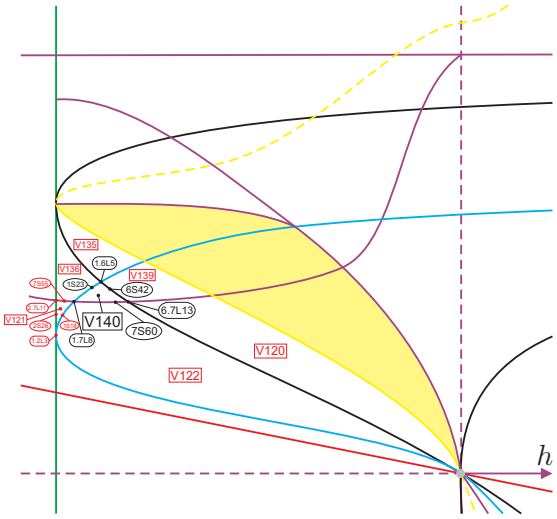

Fig. 103. Slice of parameter space when $n = 4/25 - \varepsilon_{24}$ (see Fig. 102)

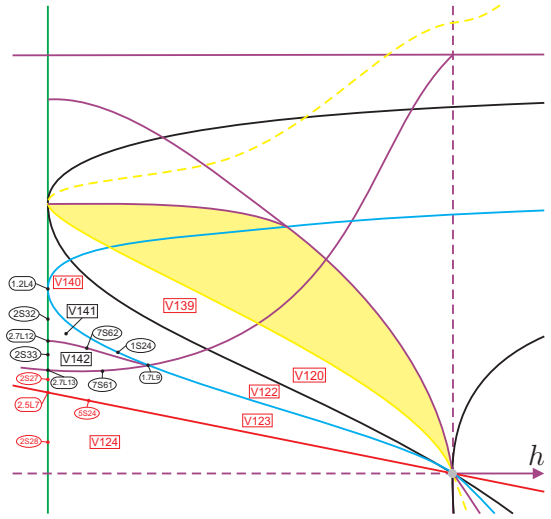

Fig. 105. Slice of parameter space when $n = 9/100$ (see Fig. 104)

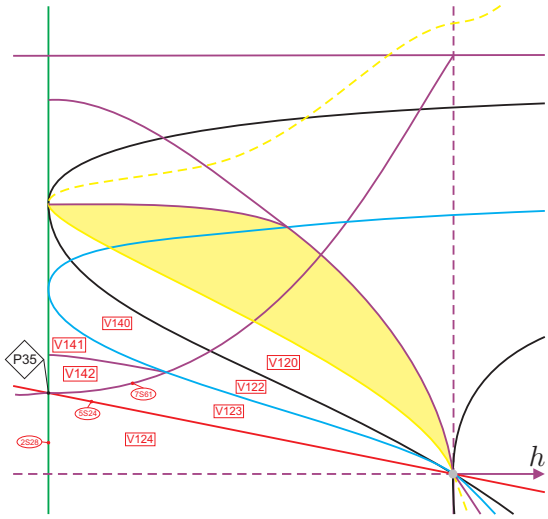

Fig. 106. Slice of parameter space when $n = 9/100 - \varepsilon_{26}^*$ (see Fig. 105)

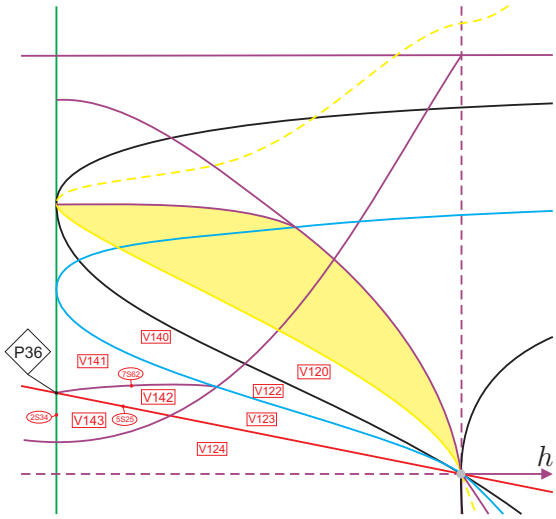

Fig. 108. Slice of parameter space when $n = 9/100 - \varepsilon_{27}^*$ (see Fig. 107)

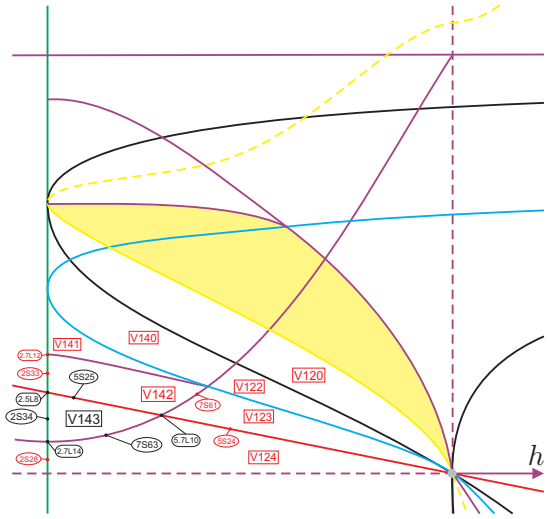

Fig. 107. Slice of parameter space when $n = 9/100 - \varepsilon_{26}$ (see Fig. 106)

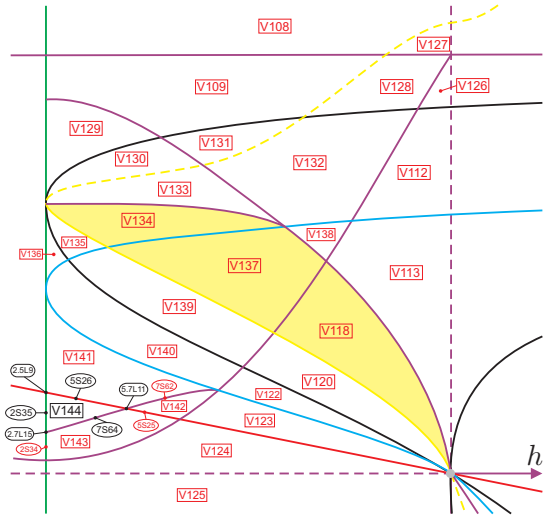

Fig. 109. Slice of parameter space when $n = 1/25$ (see Fig. 108)

Table 33. Transition from slice $n = 9/25$ to $n = 81/40$

Dead parts	Parts in sing. slice	Born parts
$2S_{24}$	P_{26}	V_{129}

Table 34. Transition from slice $n = 81/40$ to $n = 81/40 - \varepsilon_{18}$

Dead parts	Parts in sing. slice	Born parts
$7S_{39}$	P_{27}	V_{130}, V_{131}

Table 35. Transition from slice $n = 81/40 - \varepsilon_{18}$ to $n = 81/40 - \varepsilon_{19}$

Dead parts	Parts in sing. slice	Born parts
V_{110}	P_{28}	V_{132}

Table 36. Transition from slice $n = 81/40 - \varepsilon_{19}$ to $n = 81/40 - \varepsilon_{20}$

Dead parts	Parts in sing. slice	Born parts
V_{111}	P_{29}	V_{133}

Table 37. Transition from slice $n = 81/40 - \varepsilon_{20}$ to $n = 4/25$

Dead parts	Parts in sing. slice	Born parts
V_{114}, V_{115}	P_{30}	V_{134}, V_{135}, V_{136}

Table 38. Transition from slice $n = 4/25$ to $n = 4/25 - \varepsilon_{22}$

Dead parts	Parts in sing. slice	Born parts
V_{116}	P_{31}	V_{137}, V_{138}

get the form:

$$\begin{aligned}\dot{x} &= gx^2 + 2hxy - (g+2h)y^2,\\ \dot{y} &= y + \ell x^2 + (2g+2h-2\ell)xy\\ &\quad + (2h+\ell-2(g+2h))y^2,\end{aligned} \tag{18}$$

Table 39. Transition from slice $n = 4/25 - \varepsilon_{22}$ to $n = 4/25 - \varepsilon_{23}$

Dead parts	Parts in sing. slice	Born parts
V_{117}	P_{32}	V_{139}

Table 40. Transition from slice $n = 4/25 - \varepsilon_{23}$ to $n = 4/25 - \varepsilon_{24}$

Dead parts	Parts in sing. slice	Born parts
V_{119}	P_{33}	V_{140}

Table 41. Transition from slice $n = 4/25 - \varepsilon_{24}$ to $n = 9/100$

Dead parts	Parts in sing. slice	Born parts
V_{121}	P_{34}	V_{141}, V_{142}

Table 42. Transition from slice $n = 9/100$ to $n = 9/100 - \varepsilon_{26}$

Dead parts	Parts in sing. slice	Born parts
$2S_{27}$	P_{35}	V_{143}

Table 43. Transition from slice $n = 9/100 - \varepsilon_{26}$ to $n = 1/25$

Dead parts	Parts in sing. slice	Born parts
$2S_{33}$	P_{36}	V_{144}

and for systems (18), we calculate

$$\begin{aligned}&\mu = \mathcal{T}_4 = W_4 \equiv 0, \quad \mathbb{T} = -48(h+1)^4(\ell-1)^2,\\ &\mathrm{Inv} = \ell(1+2h)(1-\ell), \quad \widetilde{M} = (1+2h+\ell)^2.\end{aligned} \tag{19}$$

Then, we need new comitants which indicate: (i) when a second finite singular point collides with an infinite singular point, (ii) when a second finite singular point becomes weak and (iii) when a second node turns into a focus. The next invariant polynomials we need are, respectively:

(i) $\mu_1 = -4(g+h)^2(g-\ell)$ (drawn in blue);

(ii) $\mathcal{B}_1 = 2g^2 + 2h\ell$ (drawn in yellow);

(*iii*) $W_7 = -12(g+h)^4(g^4+2g^3h-2g^3\ell-4g^2h\ell-h^2\ell^2)$ (drawn in black).

Moreover, by the time we were analyzing this slice, we verified that there exist some parts in the bifurcation diagram corresponding to the presence of invariant parabolas passing through the origin in the phase portraits. Lemma 6.38 assures the existence of two straight lines in the bifurcation diagram with such a characteristic.

Lemma 6.38. *For $g \neq 0$ and $n = 0$, phase portraits possess invariant parabolas passing through the origin if either $h = 0$ or $\ell = 1/2$.*

Proof. We fix $g = 1$ and $n = 0$. First, we suppose $h = 0$. Then, systems (18) become

$$\begin{aligned} \dot{x} &= x^2 - y^2, \\ \dot{y} &= y + \ell x^2 + (2-2\ell)xy + (\ell-2)y^2. \end{aligned} \tag{20}$$

We look for invariant parabolas of the form

$$\mathcal{P} = Ax^2 + By^2 + Cxy + Dx + Ey + F = 0,$$

but as it passes through the origin we set $F = 0$.

If $\mathcal{C} = Ux + Vy + W$ is a cofactor of $\mathcal{P}$, then

$$\frac{\partial \mathcal{P}}{\partial x}\dot{x} + \frac{\partial \mathcal{P}}{\partial y}\dot{y} = \mathcal{C}\,\mathcal{P},$$

which is equivalent to a system of nine equations in the variables A, B, C, D, E, U, V and W, whose solution is

$$\begin{gathered} A = -C/2,\ B = -C/2,\ D = 0,\ E = -C/(2\ell), \\ U = 2(\ell-1),\ V = 2(\ell-1),\ W = 1, \end{gathered}$$

and, hence,

$$\begin{aligned} \mathcal{P} &= -\frac{C(\ell(x-y)^2+y)}{2\ell} = 0, \\ \mathcal{C} &= 1 - 2(\ell-1)x + 2(\ell-1)y. \end{aligned}$$

Applying the change of coordinates $x = X + Y$, $y = Y$, renaming X, Y by x, y and setting $C = 2$, we see that $\mathcal{P}$ can be brought to the parabola

$$\mathcal{P} = -\frac{\ell x^2 + y}{\ell} = 0.$$

An analogous construction can be applied for the case $\ell = 1/2$ and we obtain the invariant parabola

$$\mathcal{P} = -\frac{2x + (1+2h)x^2 + 2y}{1+2h} = 0.$$

■

Remark 6.39. By Lemma 6.38, the straight lines $\{h = 0\} \cup \{\ell = 1/2\}$ in the bifurcation diagram correspond to the presence of invariant parabolas passing through the origin in the phase portraits, and they will be part of surface $(\mathcal{S}_7)$ and colored in purple. Sometimes this invariant parabola will not coincide with connection of separatrices, so these respective parts are drawn in dashed lines in Fig. 110, otherwise they are drawn in a continuous line.

Remark 6.40. For $g \neq 0$ and $n = 0$, the corresponding phase portraits on the line $\{h+\ell = 0\}$ in the bifurcation diagram possess an infinite singular point of type $\widehat{\binom{1}{2}}E-H$, which is a bifurcation between the types $\widehat{\binom{1}{2}}PEP-H$ and $\widehat{\binom{1}{2}}E-PHP$. Such a straight line is needed for the coherence of the bifurcation diagram.

We observe that, since $\mu \equiv 0$ for $g \neq 0$ and $n = 0$ (i.e. this slice is entirely contained in surface $(\mathcal{S}_1)$), all the "generic" parts on this slice are labeled as $1S_j$, the lines are labeled as $1.iL_j$ and the points as points. We could have also used surfaces $(\mathcal{S}_3)$ or $(\mathcal{S}_6)$ for the same reason, but we have used $(\mathcal{S}_1)$ for its higher relevance on singularities. In Fig. 110, we present the slice when $n = 0$ with each part properly labeled.

In Table 44 we indicate the death of all volumetric parts from slice $n = 1/25$ to $n = 0$ and in Table 45, the birth of new parts at $n = -1$ from slice $n = 0$.

Since there exists no symmetry in the parameter n of foliation of the parameter space as this happened to systems in $\mathbf{QT\overline{N}}$ [Artés *et al.*, 2013b], in $\overline{\mathbf{QsnSN(A)}}$ and in $\overline{\mathbf{QsnSN(B)}}$ [Artés *et al.*, 2014], for systems (5) we need to consider negative values for the parameter n according to (17). So, we consider the next generic slice when $n = -1$. In Fig. 111 we present this slice, but we note that the portion bordered by $4S_{51}$ and $4S_{52}$ (the fourth quadrant) is presented only with the volume parts labeled. We show a zoom of this part in Fig. 112. In addition, the dashed vertical line in black represents the $\ell-$axis and we draw it only for reference.

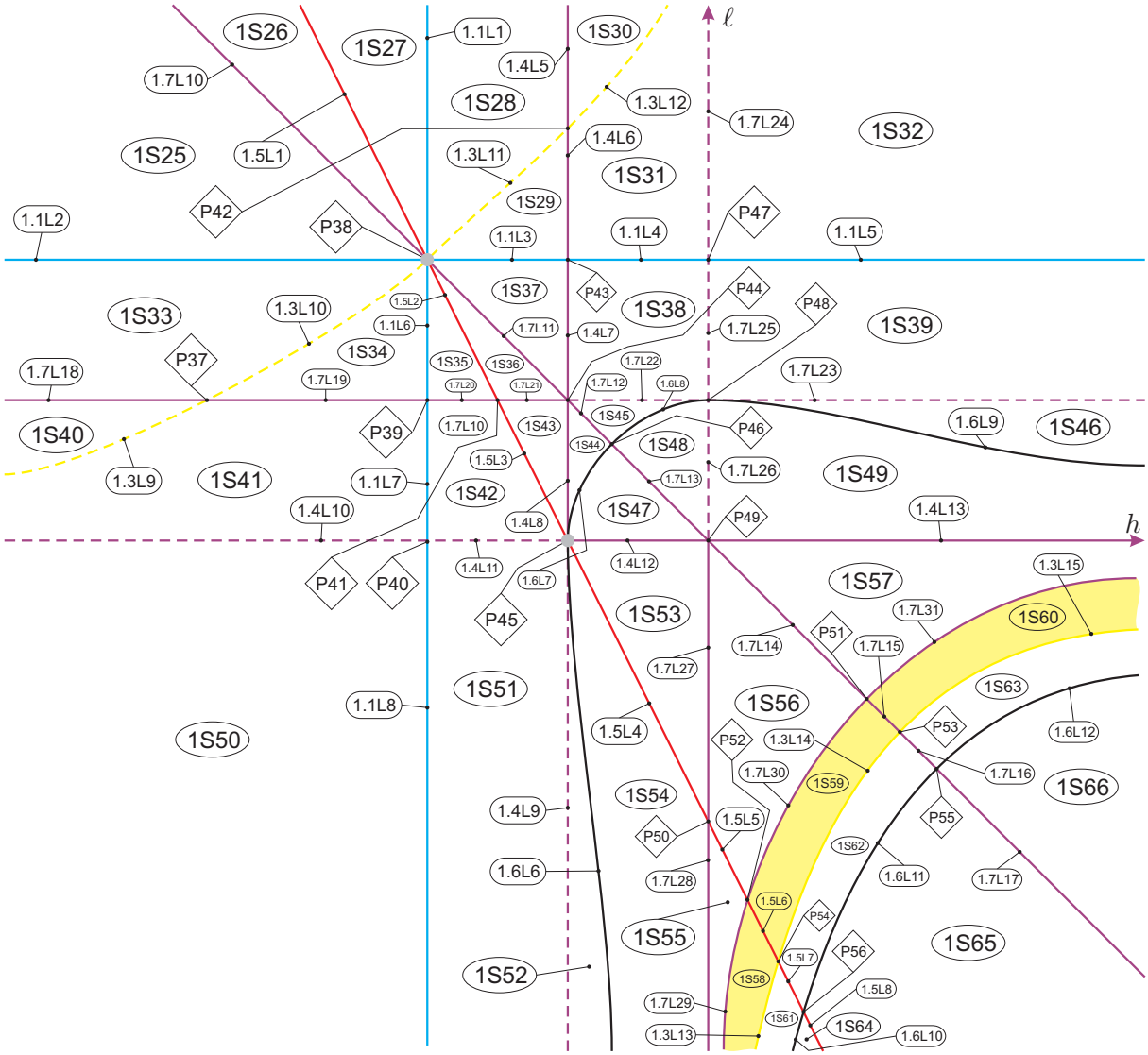

Fig. 110. Slice of parameter space when $n = 0$ (see Figs. 83 and 109)

Table 44. Transition from slice $n = 1/25$ to $n = 0$

Dead parts	Parts in slice $n = 0$	Dead parts	Parts in slice $n = 0$	Dead parts	Parts in slice $n = 0$
V_1	$1S_{27}$	V_{52}	$1S_{47}$, $1S_{48}$, $1S_{49}$	V_{109}	$1.1L_3$
V_2	$1.5L_1$	V_{53}	$1S_{53}$, $1S_{56}$, $1S_{57}$	V_{112}	P_{43}
V_3	$1S_{26}$	V_{54}	$1S_{59}$, $1S_{60}$	V_{113}	$1.4L_7$
V_4	$1.7L_{10}$	V_{55}	$1S_{62}$, $1S_{63}$	V_{118}	$1S_{43}$
V_5	$1.7L_{10}$	V_{56}	$1S_{65}$, $1S_{66}$	V_{120}	$1.5L_3$
V_6	$1S_{25}$	V_{57}	$1.5L_8$	V_{122}	$1.5L_3$
V_7	P_{38}	V_{58}	$1.5L_7$	V_{123}	$1.5L_3$
V_8	$1.1L_2$	V_{59}	$1.5L_7$	V_{124}	$1S_{42}$
V_9	$1.1L_2$	V_{61}	$1.5L_8$	V_{125}	$1S_{51}$
V_{10}	$1S_{33}$	V_{66}	$1.5L_8$	V_{126}	P_{43}
V_{11}	$1S_{40}$	V_{67}	$1S_{64}$	V_{127}	$1S_{29}$
V_{12}	$1S_{34}$	V_{77}	$1.5L_7$	V_{128}	$1.1L_3$
V_{13}	$1S_{41}$	V_{84}	P_{38}	V_{129}	P_{38}
V_{14}	$1S_{50}$	V_{85}	P_{38}	V_{130}	P_{38}
V_{15}	P_{38}	V_{86}	$1S_{61}$	V_{131}	$1.1L_3$
V_{16}	P_{38}	V_{87}	$1.5L_6$	V_{132}	$1.1L_3$
V_{17}	P_{38}	V_{94}	$1.5L_6$	V_{133}	P_{38}
V_{18}	P_{38}	V_{95}	$1.5L_5$	V_{134}	P_{38}
V_{19}	P_{38}	V_{96}	$1S_{30}$	V_{135}	P_{38}
V_{20}	$1.1L_1$	V_{100}	$1.5L_6$	V_{136}	P_{38}
V_{21}	P_{38}	V_{101}	$1S_{58}$	V_{137}	$1S_{36}$
V_{22}	$1.1L_6$	V_{102}	$1S_{55}$	V_{138}	$1S_{37}$
V_{23}	$1.1L_7$	V_{103}	$1S_{54}$	V_{139}	$1.5L_2$
V_{24}	$1.1L_8$	V_{104}	$1S_{52}$	V_{140}	$1.5L_2$
V_{45}	$1S_{31}$, $1S_{32}$	V_{105}	$1.5L_5$	V_{141}	$1.5L_2$
V_{49}	$1.1L_4$, $1.1L_5$	V_{106}	$1.5L_4$	V_{142}	$1.5L_2$
V_{50}	$1.1L_4$, $1.1L_5$	V_{107}	$1.5L_5$	V_{143}	$1.7L_{20}$
V_{51}	$1S_{38}$, $1S_{39}$, $1S_{44}$, $1S_{45}$, $1S_{46}$	V_{108}	$1S_{28}$	V_{144}	$1S_{35}$

Table 45. Transition from slice $n = -1$ to $n = 0$

Dead parts	Parts in slice $n = 0$	Dead parts	Parts in slice $n = 0$
V_{145}	$1S_{30}$	V_{172}	$1S_{55}$
V_{146}	$1S_{29}$, $1S_{31}$, $1S_{32}$	V_{173}	$1.5L_5$
V_{147}	$1S_{27}$, $1S_{28}$	V_{174}	$1.5L_5$
V_{148}	$1.5L_1$	V_{175}	$1.5L_5$
V_{149}	$1.5L_1$	V_{176}	$1S_{56}$
V_{150}	$1.1L_3$, $1.1L_4$, $1.1L_5$	V_{177}	$1S_{57}$
V_{151}	$1.5L_1$	V_{178}	$1S_{58}$
V_{152}	$1S_{25}$, $1S_{26}$	V_{179}	$1.5L_6$
V_{153}	$1.1L_2$	V_{180}	$1.5L_6$
V_{154}	$1S_{33}$	V_{181}	$1.5L_6$
V_{155}	$1S_{40}$	V_{182}	$1S_{59}$
V_{156}	$1S_{41}$, $1S_{42}$	V_{183}	$1S_{60}$
V_{157}	$1S_{34}$, $1S_{35}$	V_{184}	$1S_{61}$
V_{158}	$1.5L_2$	V_{185}	$1.5L_7$
V_{159}	$1S_{36}$, $1S_{37}$, $1S_{43}$	V_{186}	$1.5L_7$
V_{160}	$1S_{38}$, $1S_{39}$, $1S_{44}$, $1S_{45}$, $1S_{46}$	V_{187}	$1.5L_7$
V_{161}	$1S_{47}$, $1S_{48}$, $1S_{49}$	V_{188}	$1S_{62}$
V_{162}	$1S_{50}$, $1S_{51}$	V_{189}	$1S_{63}$
V_{163}	$1S_{52}$	V_{190}	$1S_{64}$
V_{164}	$1S_{54}$	V_{191}	$1.5L_8$
V_{165}	P_{50}	V_{192}	$1.5L_8$
V_{166}	$1.5L_4$	V_{193}	$1.5L_8$
V_{167}	$1.5L_4$	V_{194}	$1S_{65}$
V_{168}	$1S_{53}$	V_{195}	$1S_{66}$
V_{169}	$1.4L_{13}$	V_{196}	$1.1L_2$
V_{170}	$1.7L_{28}$	V_{197}	$1.1L_3$
V_{171}	$1.7L_{27}$	V_{198}	$1.1L_4$, $1.1L_5$

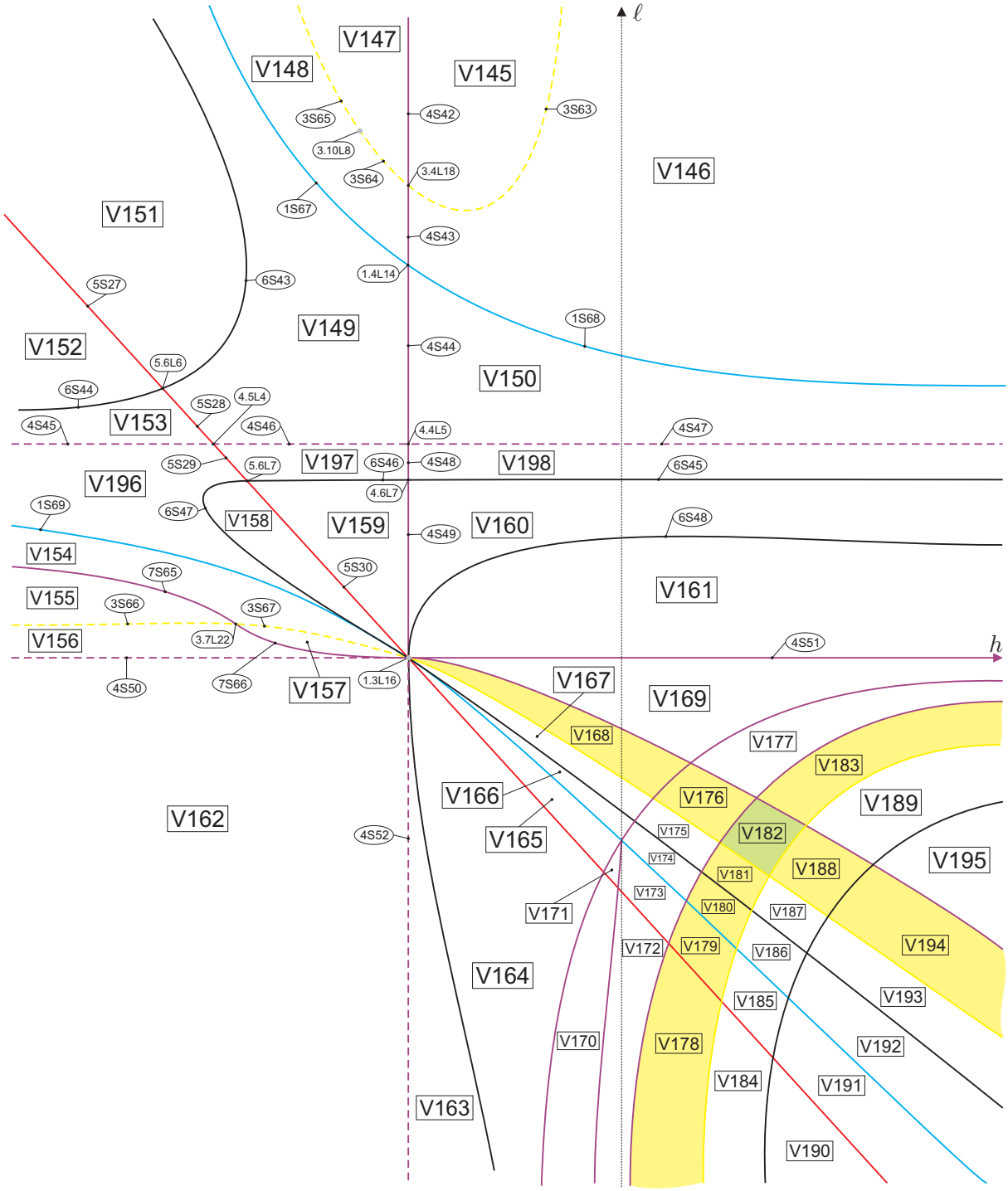

Fig. 111. Slice of parameter space when $n = -1$ (see Fig. 110)

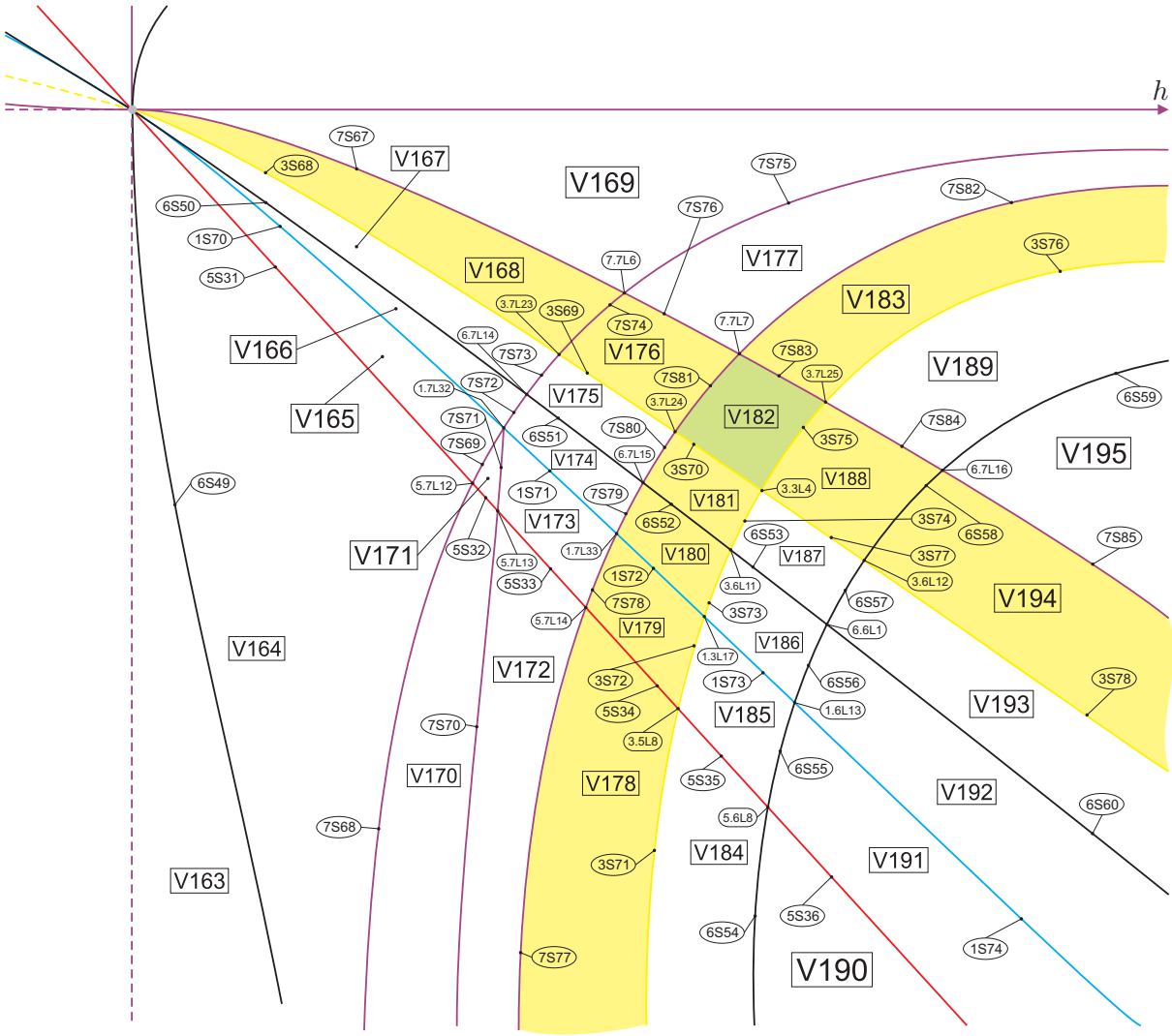

Fig. 112. Slice of parameter space when $n = -1$ (zoom) (see Fig. 111)

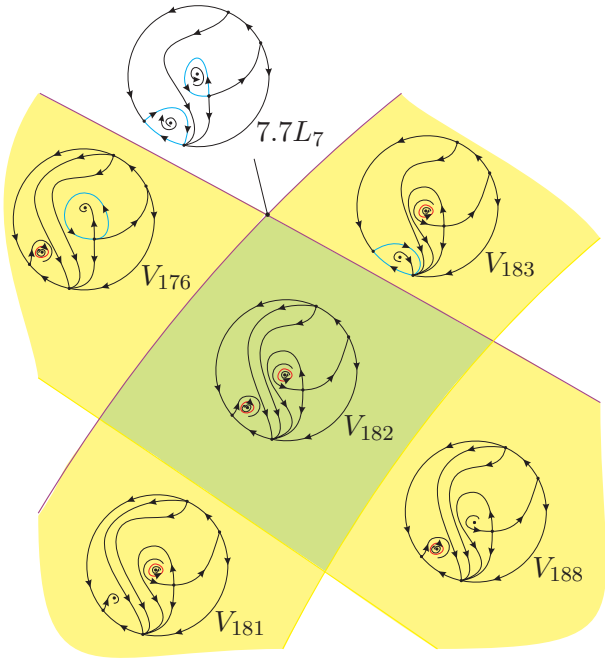

Fig. 113. Phase portraits in a neighborhood of V_{182}

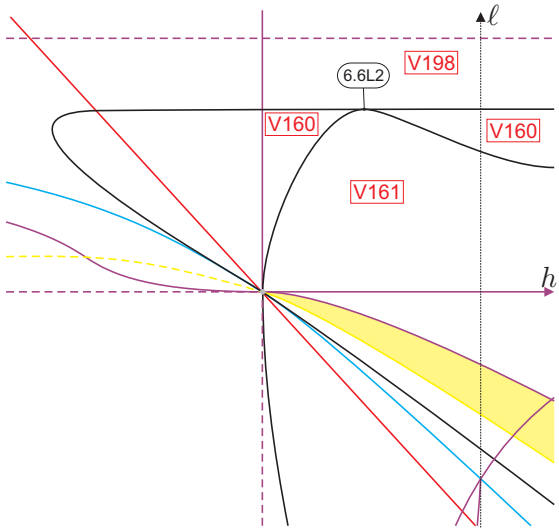

Fig. 114. Slice of parameter space when $n \approx -3'4013\ldots$ (see Fig. 111)

We highlight that in part V_{182} there exist two limit cycles in the phase portrait, but each one around different foci. Each one of the limit cycles can be created (or lost) either by Hopf bifurcation on $3S_{70}$ or $3S_{75}$, or by loop bifurcation on $7S_{81}$ or $7S_{83}$. There also exists the possibility of both limit cycles being created (or lost) at the same time either by Hopf bifurcation on $3.3L_4$, or by loop bifurcation on $7.7L_7$. We present in Fig. 113 the phase portraits in a neighborhood of V_{182}.

In Figs. 114 and 115 we present the movement of a branch of surface $(\mathcal{S}_6)$ which contacts another branch of the same surface and, then, they intersect transversally in two points. Table 46 indicates the "dead" and "born" parts in this transition.

Table 46. Transition from slice $n = -1$ to $n = -4$. The symbol '$\emptyset$' means that no part was "dead"

Dead parts	Parts in sing. slice	Born parts
$\emptyset$	$6.6L_2$	V_{199}

Following the values of n in (17), the last slice we need to described is when $n = -\infty$. However, on page 41 we have already discussed about the behavior of the surfaces as $n \to \infty$. Due to the

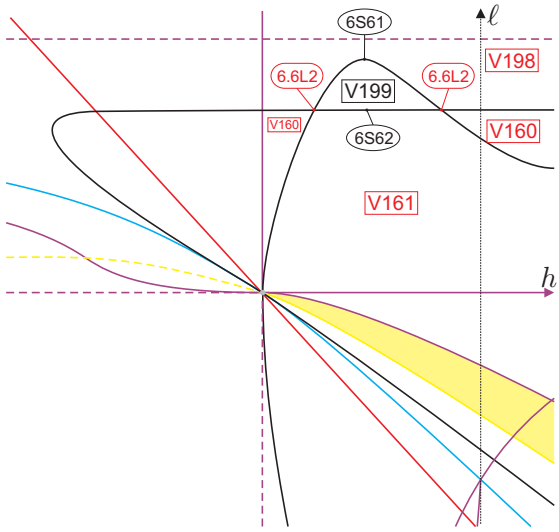

Fig. 115. Slice of parameter space when $n = -4$ (see Fig. 114)

symmetry in g (see page 18), the slices $n = -\infty$ and $n = \infty$ are symmetrical. These slices correspond to $g = 0$ and $n \neq 0$. Setting $g = 0$ and $n = -1$, systems (5) become

$$\begin{aligned} \dot{x} &= 2hxy - (1+2h)y^2, \\ \dot{y} &= y + \ell x^2 + (1+2h-2\ell)xy \\ &\quad + (2h+\ell-2(1+2h))y^2, \end{aligned} \tag{21}$$

for which we calculate

$$\begin{aligned} &\mu = \ell(2h+\ell), \quad \mathbb{T} \equiv 0, \quad \mathcal{T}_4 = \ell(8h^2+\ell+4h\ell), \\ &\text{Inv} = -\ell^2(1+2h), \quad \widetilde{M} = (2h+\ell+1)^2, \\ &W_4 = \ell^3(16h^2+32h^3+\ell+8h\ell+16h^2\ell). \end{aligned} \tag{22}$$

As $\mathbb{T}$ vanishes as $n \to -\infty$, we need to consider the next comitant which is responsible for the multiplicity of finite singular points. This next comitant is $\mathbb{R} = h^2\ell^2$, whose set of zeroes will be called surface ($\mathcal{S}_{11}$) and colored in green. In Fig. 116 we present the slice when $n = -\infty$ properly labeled.

In Table 47 we indicate the death of all volumetric parts from slice $n = -4$ to $n = -\infty$ and in Table 48, the birth of new parts at $n = 10$ from slice $n = \infty$ (see Fig. 25 where nonalgebraic bifurcations and labels must be considered from Fig. 116 with proper symmetry).

Since there is coherence between the generic slices bordering the most singular slices $n = 1$, $n = 0$ and $n = -\infty$ with their respective generic side slices, no more slices are needed for the complete coherence of the bifurcation diagram. So, all the values of n in (17) are sufficient for the coherence of the bifurcation diagram. Thus, we can affirm that we have described a complete bifurcation diagram for family $\overline{\mathbf{QsnSN(C)}}$ modulo islands, as discussed in Sec. 7.

7. Other relevant facts about the bifurcation diagrams

The bifurcation diagram we have obtained for the family $\overline{\mathbf{QsnSN(C)}}$ is completely coherent, i.e. in each family, by taking any two points in the parameter space and joining them by a continuous curve, along this curve the changes in phase portraits that occur when crossing the different bifurcation surfaces we mention can be completely explained.

Nevertheless, we cannot be sure that these bifurcation diagrams are the complete bifurcation diagrams for $\overline{\mathbf{QsnSN(C)}}$ due to the possibility of "islands" inside the parts bordered by unmentioned bifurcation surfaces. In case they exist, these "islands" would not mean any modification of the nature of the singular points. So, on the border of these "islands" we could only have bifurcations due to saddle connections or multiple limit cycles.

In case there were more bifurcation surfaces, we should still be able to join two representatives of any two parts of the 1034 parts of $\overline{\mathbf{QsnSN(C)}}$ found until now with a continuous curve either without crossing such bifurcation surface or, in case the curve crosses it, it must do it an even number of times without tangencies, otherwise one must take into account the multiplicity of the tangency, so the total number must be even. This is why we call these potential bifurcation surfaces "*islands*".

However, we have not found a different phase portrait which could fit in such an island. A potential "island" would be the set of parameters for which the phase portraits possesses a double limit cycle and this "island" would be inside the parts where $W_4 < 0$ since we have the presence of a focus (recall the item (iii) of Sec. 4).

8. Completion of the proof of the main theorem

In the bifurcation diagram we may have topologically equivalent phase portraits belonging to distinct parts of the parameter space. As here we have 1034 distinct parts of the parameter space, to help us identify or to distinguish phase portraits, we need to introduce some invariants and we actually choose integer–valued, character and symbol invariants. Some of them were already used in [Artés *et al.*, 2013b] and [Artés *et al.*, 2014], but we recall them and introduce some needed ones. These invariants yield a classification which is easier to grasp.

Definition 8.1. We denote by $I_1(S)$ the number of the real finite singular points. We note that this number can also be infinity, which is represented by ∞.

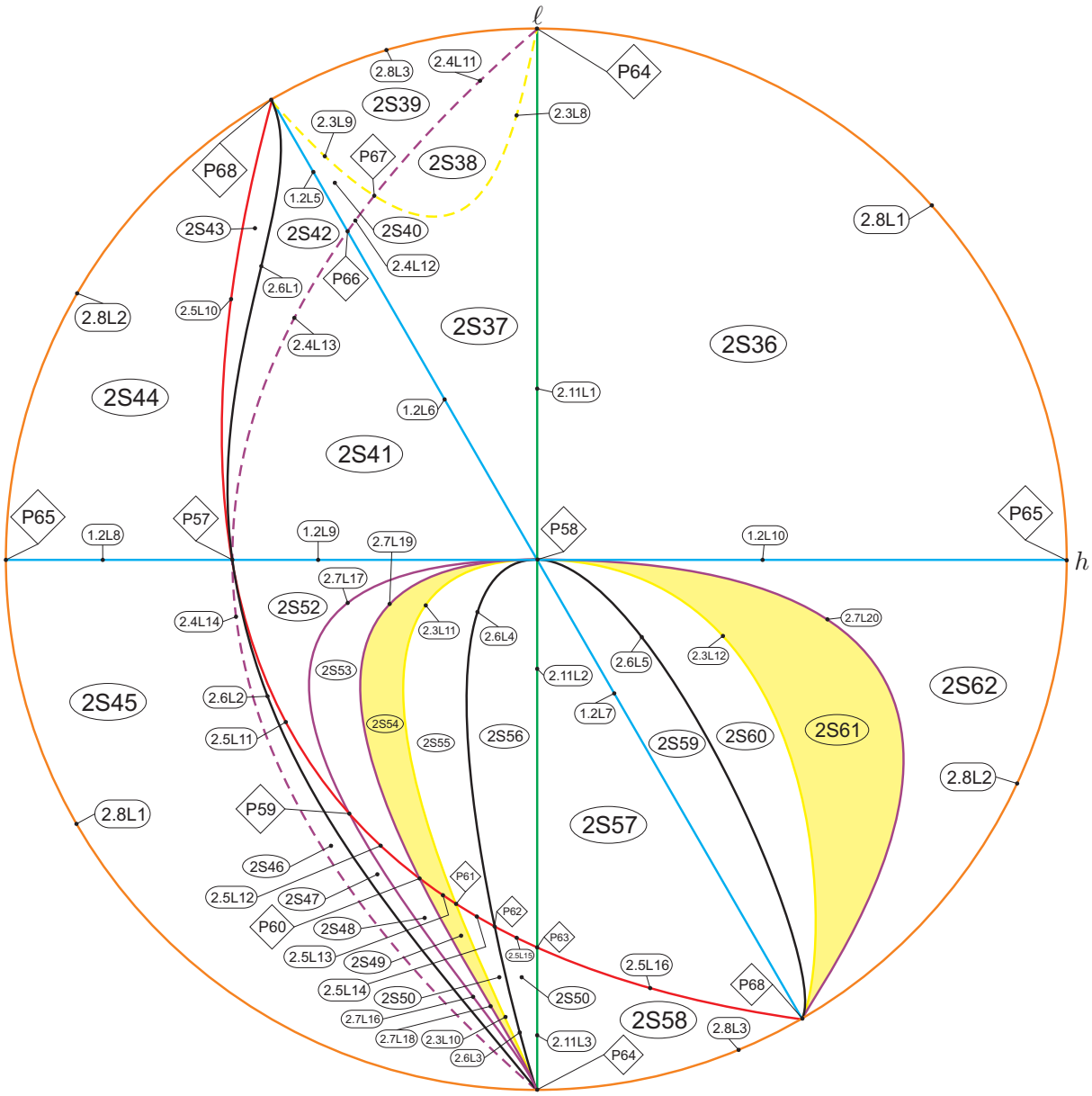

Fig. 116. Slice of parameter space when $n = -\infty$

Table 47. Transition from slice $n = -4$ to $n = -\infty$

Dead parts	Parts in slice $n = -\infty$	Dead parts	Parts in slice $n = -\infty$
V_{145}	$2S_{38}$	V_{173}	$2S_{53}$
V_{146}	$2S_{36}$, $2S_{37}$	V_{174}	P_{58}
V_{147}	$2S_{39}$	V_{175}	P_{58}
V_{148}	$2S_{40}$	V_{176}	P_{58}
V_{149}	$2S_{42}$	V_{177}	$1.2L_{10}$
V_{150}	$2S_{41}$, $1.2L_{10}$	V_{178}	$2S_{49}$
V_{151}	$2S_{43}$	V_{179}	$2S_{54}$
V_{152}	$2S_{44}$	V_{180}	P_{58}
V_{153}	$1.2L_8$	V_{181}	P_{58}
V_{154}	$1.2L_8$	V_{182}	P_{58}
V_{155}	$1.2L_8$	V_{183}	$1.2L_{10}$
V_{156}	$1.2L_8$	V_{184}	$2S_{50}$
V_{157}	$1.2L_8$	V_{185}	$2S_{55}$
V_{158}	P_{57}	V_{186}	P_{58}
V_{159}	P_{57}	V_{187}	P_{58}
V_{160}	$1.2L_9$, $1.2L_{10}$	V_{188}	P_{58}
V_{161}	$1.2L_9$, $1.2L_{10}$	V_{189}	$1.2L_{10}$
V_{162}	$2S_{45}$	V_{190}	$2S_{51}$, $2S_{58}$
V_{163}	$2S_{46}$	V_{191}	$2S_{56}$, $2S_{57}$
V_{164}	$2S_{47}$	V_{192}	$2S_{59}$
V_{165}	$2S_{52}$	V_{193}	$2S_{60}$
V_{166}	P_{58}	V_{194}	$2S_{61}$
V_{167}	P_{58}	V_{195}	$2S_{62}$
V_{168}	P_{58}	V_{196}	$1.2L_8$
V_{169}	$1.2L_{10}$	V_{197}	P_{57}
V_{170}	$2.7L_{16}$	V_{198}	$1.2L_9$, $1.2L_{10}$
V_{171}	$2.7L_{17}$	V_{199}	$1.2L_9$
V_{172}	$2S_{48}$		

Table 48. Transition from slice $n = 10$ to $n = \infty$

Dead parts	Parts in slice $n = -\infty$	Dead parts	Parts in slice $n = -\infty$
V_1	$2S_{58}$	V_{35}	$2S_{53}$
V_2	$2S_{57}$	V_{36}	$2S_{52}$
V_3	$2S_{59}$	V_{37}	P_{57}
V_4	$2S_{60}$	V_{38}	P_{58}
V_5	$2S_{61}$	V_{39}	P_{58}
V_6	$2S_{62}$	V_{40}	$1.2L_9$
V_7	P_{58}	V_{41}	P_{58}
V_8	$1.2L_{10}$	V_{42}	P_{58}
V_9	$1.2L_{10}$	V_{43}	$1.2L_9$
V_{10}	$1.2L_{10}$	V_{44}	$2S_{46}$
V_{11}	$1.2L_{10}$	V_{45}	$2S_{45}$
V_{12}	$1.2L_{10}$	V_{46}	$1.2L_9$
V_{13}	$1.2L_{10}$	V_{47}	$1.2L_9$
V_{14}	$2S_{36}$	V_{48}	P_{57}
V_{15}	P_{58}	V_{49}	$1.2L_8$
V_{16}	P_{58}	V_{50}	$1.2L_8$
V_{17}	P_{58}	V_{51}	$1.2L_8$
V_{18}	P_{58}	V_{52}	$1.2L_8$
V_{19}	P_{58}	V_{53}	$1.2L_8$
V_{20}	$2.11L_3$	V_{54}	$1.2L_8$
V_{21}	$2.11L_2$	V_{55}	$1.2L_8$
V_{22}	P_{58}	V_{56}	$2S_{44}$
V_{23}	P_{58}	V_{57}	$2S_{43}$
V_{24}	$2.11L_1$	V_{58}	P_{57}
V_{25}	$2S_{51}$	V_{59}	P_{57}
V_{26}	$2S_{50}$	V_{60}	P_{57}
V_{27}	$2S_{49}$	V_{61}	$2S_{42}$,
V_{28}	$2.7L_{18}$	V_{62}	$2S_{41}$
V_{29}	$2S_{48}$	V_{63}	$1.2L_9$
V_{30}	$2S_{47}$	V_{64}	$2S_{37}$
V_{31}	$2S_{56}$	V_{65}	$2S_{38}$
V_{32}	$2S_{55}$	V_{66}	$2S_{40}$
V_{33}	$2S_{54}$	V_{67}	$2S_{39}$
V_{34}	$2.7L_{19}$		

Definition 8.2. We denote by $I_2(S)$ the sum of the indices of the isolated real finite singular points.

Definition 8.3. We denote by $I_3(S)$ the number of the real infinite singular points.

Definition 8.4. For a given infinite singularity s of a system S, let ℓ_s be the number of global or local separatrices beginning or ending at s and which do not lie on the line at infinity. We have $0 \leq \ell_s \leq 4$. We denote by $I_4(S)$ the sequence of all such ℓ_s when s moves in the set of infinite singular points of the system S. We start the sequence at the infinite singular point which receives (or sends) the greatest number of separatrices and take the direction which yields the greatest absolute value, e.g. the values 2110 and 2011 for this invariant are symmetrical (and, therefore, they are the same), so we consider 2110.

Definition 8.5. We denote by $I_5(S)$ the sequence of digits between parenthesis and separated by commas, if there is more than one digit, denoting the number of limit cycles around foci.

Definition 8.6. We denote by $I_6(S)$ the sequence of digits (ranging from 0 to 5) between parenthesis and separated by commas, if there is more than one digit, meaning the existence or the nonexistence of separatrices connection, where "0" means no separatrices connection, "1" means a loop–type connection, "2" means a connection of separatrices from two finite singular points, "3" means a connection of separatrices from one finite singular point to an infinite one, "4" means a connection of separatrices from nonadjacent infinite singular points, and "5" means a connection of separatrices from adjacent infinite singular points.

Definition 8.7. We denote by $I_7(S)$ the sequence of digits (ranging from 0 to 4) between parenthesis and separated by commas which describes the number of local or global separatrices starting or ending at the nodal sector of the finite saddle–node and at each finite antisaddle or each limit cycle.

Definition 8.8. We denote by $I_8(S)$ the sequence of two digits (each one ranging from 0 to 2) between parenthesis and separated by commas which describes the total number of local or global separatrices linking the finite multiple singular points to the infinite multiple singular points in each local chart. For example, "$(1,0)$" means that there exist only one separatrix linking the finite multiple singular point to the infinite multiple singular point in the local chart U_1 whereas there exists no linking separatrix going to the local chart U_2.

Definition 8.9. We denote by $I_9(S)$ a character from the set $\{f, \infty\}$ describing the origin of the orbits that arrive to a finite antisaddle, where "f" means that all the separatrices arrive from finite singular points and "∞" means that at least one separatrix arrives from an infinite singular point. We observe that this invariant makes sense only in the case of the existence of only one antisaddle.

Definition 8.10. We denote by $I_{10}(S)$ a digit (ranging from 0 to 2) describing the connection of separatrices involving the separatrices of finite saddle–nodes, where "0" means that the connection is produced by separatrices associated with nonzero eigenvalues, "1" means that one of the separatrices in the connection is associated with a zero eigenvalue and "2" means that both of the separatrices are associated with zero eigenvalues.

Definition 8.11. We denote by $I_{11}(S)$ an element from the set $\{a, N, SN\}$ which describes the singular point which would receive one or two separatrices of the finite elemental saddle, if the finite saddle–node disappears. Here, "a" means an antisaddle, "N" means an infinite node and "SN" means $\binom{0}{2}SN$.

Definition 8.12. We denote by $I_{12}(S)$ an element from the set $\{s, d\}$ describing if the stability of the focus inside a graphic is the **s**ame as or **d**ifferent from the nodal part of the finite saddle–node.

Definition 8.13. We denote by $I_{13}(S)$ an element from the set $\{S, SN\}$ describing the origin of the middle separatrix (of three) received by the nodal sector of the finite saddle–node. Here, "S" means an infinite saddle and "SN" means $\binom{0}{2}SN$.

Definition 8.14. We denote by $I_{14}(S)$ a character from the set $\{f, \infty\}$ describing the nature of the singular point which sends or receives a separatrix

to or from a limit cycle.

Definition 8.15. We denote by $I_{15}(S)$ the sum of the indices of the isolated infinite multiple singular points (considered in only one local chart).

Definition 8.16. We denote by $I_{16}(S)$ a character from the set $\{H, P\}$, where H determines that a finite antisaddle sends (or receives) orbits to (from) a parabolic sector of a multiple infinite singular point situated in the local chart where the parabolic sector is accompanied by other hyperbolic sectors, and P denotes that the parabolic sector is the only sector of the infinite singular point in that local chart. This invariant is needed to distinguish $1.5L_3$ from $1.5L_4$.

Definition 8.17. We denote by $I_{17}(S)$ a symbol to represent the configuration of the curves of singularities. The symbols are: "$-$" to represent a straight line and "$\cup$" to represent a parabola.

Definition 8.18. We denote by $I_{18}(S)$ a character from the set $\{n, y\}$ describing the nonexistence ("n") or the existence ("y") of graphics.

Definition 8.19. We denote by $I_{19}(S)$ a character from the set $\{c, s\}$ describing the position of the separatrix of the finite saddle–node associated with the eigenvector with zero eigenvalue which arrives to (or leaves from) $\overline{\binom{0}{2}}SN$ when this point receives 3 separatrices. We use "c" for the central position and "s" for the lateral (side) position.

Definition 8.20. We denote by $I_{20}(S)$ a character from the set $\{s, d\}$ describing if each point of the pair of infinite saddle–nodes sends (or receives) two separatrices to/from the **s**ame or **d**ifferent finite saddle–nodes. This invariant only makes sense in case of existence of two finite saddle–nodes.

As we have noted previously in Remark 6.31, we do not distinguish between phase portraits whose only difference is that in one we have a finite node and in the other a focus. Both phase portraits are topologically equivalent and they can only be distinguished within the C^1 class. In case we may want to distinguish between them, a new invariant may easily be introduced.

Theorem 8.21. *Consider the family* $\overline{\mathbf{QsnSN(C)}}$ *and all the phase portraits that we have obtained for this family. The values of the affine invariant* $\mathcal{I} = (I_1, I_2, I_3, I_4, I_5, I_6, I_7, I_8, I_9, I_{10}, I_{11}, I_{12}, I_{13}, I_{14}, I_{15}, I_{16}, I_{17}, I_{18}, I_{19}, I_{20})$ *given in the following diagram yield a partition of these phase portraits of the family* $\overline{\mathbf{QsnSN(C)}}$.

Furthermore, for each value of $\mathcal{I}$ *in this diagram there corresponds a single phase portrait; i.e.* S *and* S' *are such that* $I(S) = I(S')$, *if and only if* S *and* S' *are topologically equivalent.*

The bifurcation diagram for $\overline{\mathbf{QsnSN(C)}}$ has 1034 parts which produce 371 topologically different phase portraits as described in Tables 50 to 59. The remaining 663 parts do not produce any new phase portrait which was not included in the 371 previous ones. The difference is basically the presence of a strong focus instead of a node and vice versa and weak points.

The phase portraits having neither limit cycle nor graphic have been denoted surrounded by parenthesis, for example $(5S_2)$; the phase portraits having one or two limit cycles have been denoted surrounded by brackets, for example $[V_{80}]$, possessing one limit cycle, and $[[V_{88}]]$, possessing two limit cycles; the phase portraits having one or two graphics have been denoted surrounded by $\{*\}$ or $\{\{*\}\}$, for example $\{1S_{28}\}$ and $\{\{1S_{57}\}\}$; the phase portraits having one limit cycle and one graphic have been denoted surrounded by $[\{*\}]$, for example $[\{1S_{60}\}]$.

Proof of Theorem 8.21. The above result follows from the results in the previous sections and a careful analysis of the bifurcation diagrams given in Sec. 6, in Figs. 23 to 116, the definition of the invariants I_j and their explicit values for the corresponding phase portraits. ■

We recall some observations regarding the equivalence relations used in this study: the affine and time rescaling, C^1 and topological equivalences.

The coarsest one among these three is the topological equivalence and the finest is the affine equivalence. We can have two systems which are topologically equivalent but not C^1-equivalent. For example, we could have a system with a finite antisaddle which is a structurally stable node and in another system with a focus, the two systems being

topologically equivalent but belonging to distinct C^1-equivalence classes, separated by the surface $(\mathcal{S}_6)$ on which the node turns into a focus.

In Tables 60 to 73 we listed in the first column 371 parts with all the distinct phase portraits of Figs. 1 to 11. Corresponding to each part listed in column 1 we have in its horizontal block, all parts whose phase portraits are topologically equivalent to the phase portrait appearing in column 1 of the same horizontal block.

In the second column we have put all the parts whose systems yield topologically equivalent phase portraits to those in the first column, but which may have some algebro–geometric features related to the position of the orbits. In the third column we have presented all the parts which are topologically equivalent to the ones from the first column having a focus instead of a node.

In the fourth (respectively, fifth; sixth; seventh; and eightieth) column we have listed all parts whose phase portraits have a node which is at a bifurcation point producing foci close to the node in perturbations, a node–focus to shorten (respectively, a finite weak singular point; belong to disconnected parts; possess an invariant curve not yielding a connection of separatrices; and have symmetry).

The last column refers to other reasons associated to different geometrical aspects and they are described as follows:

(1) it possesses a $\overline{sn}_{(4)}$ as a finite singular point;
(2) it possesses a $\binom{\overline{2}}{1}N$ at infinity;
(3) $3S_{20}$ is the singularity of the surface $(\mathcal{S}_3)$, i.e. of the invariant polinomial $\mathcal{T}_4$, where the two finite complex singularities are weak;
(4) it possesses a $\binom{\widehat{1}}{2}E - H$ at infinity;
(5) the antisaddle is triple;
(6) it possesses a $\binom{\widehat{2}}{3}N$ at infinity;

Whenever phase portraits appear on a horizontal block in a specific column, the listing is done according to the decreasing dimension of the parts where they appear, always placing the lower dimensions on lower lines.

8.1. Proof of the main theorem

The bifurcation diagram described in Sec. 6, plus Tables 50 to 59 of the geometrical invariants distinguishing the 371 phase portraits, plus Tables 60 to 79 giving the equivalences with the remaining phase portraits lead to the proof of the main statement of Theorem 1.1.

Moreover, the phase portraits P_3 from family $\overline{\mathbf{QsnSN}(\mathbf{A})}$, P_2 from family $\overline{\mathbf{QsnSN}(\mathbf{B})}$ and P_{57} from family $\overline{\mathbf{QsnSN}(\mathbf{C})}$ are topologically equivalent since there exists no geometrical invariant that distinguishes them. It has been needed to have the curve at infinity filled up with an infinite number of singularities to have a common element in the three families. The same argument is applied to prove the equivalence of the two other triplets. Also, there are 10 more cases of coincidences between phase portraits of family $\overline{\mathbf{QsnSN}(\mathbf{C})}$ and one of either $\overline{\mathbf{QsnSN}(\mathbf{A})}$ or $\overline{\mathbf{QsnSN}(\mathbf{B})}$ and we have discovered another equivalence between $5S_2$ from $\overline{\mathbf{QsnSN}(\mathbf{A})}$ and $5S_3$ from $\overline{\mathbf{QsnSN}(\mathbf{B})}$ which have no equivalence in $\overline{\mathbf{QsnSN}(\mathbf{C})}$. This proves Corollary 1.2.

Now, summing all the topologically distinct phase portraits from families $\overline{\mathbf{QsnSN}(\mathbf{A})}$, $\overline{\mathbf{QsnSN}(\mathbf{B})}$ and $\overline{\mathbf{QsnSN}(\mathbf{C})}$ and subtracting the intersections among them, according to Corollary 1.2, we obtain $38 + 25 + 371 - 17 = 417$ topologically distinct phase portraits in $\overline{\mathbf{QsnSN}}$, and we prove Corollary 1.3.

In the family $\overline{\mathbf{QsnSN}(\mathbf{C})}$, all the phase portraits corresponding to parts of volume yield all the topologically possible phase portraits of codimension one from group (A) (see page **??** for the description of this group). Many of them had already been discovered being realizable, and others which realization was missing have been found within the perturbations of family $\overline{\mathbf{QsnSN}(\mathbf{C})}$. In the next example we perturbe one phase portrait from family $\overline{\mathbf{QsnSN}(\mathbf{C})}$ and obtain one phase portrait of codimension one which was missing. Also three new phase portraits of group (B) can be found from perturbations of family $\overline{\mathbf{QsnSN}(\mathbf{C})}$.

Example 8.22. Phase portrait V_{177} yields an example of the "wanted" case A_{66} of codimension one. Indeed, by adding the small perturbation $x^2/100$ in a representative of the part V_{177} we obtain the following system:

$$\begin{aligned} \dot{x} &= x^2 + 12xy/5 - 22y^2/5 + x^2/100, \\ \dot{y} &= y - x^2/10 + 28xy/5 - 13y^2/2, \end{aligned} \tag{23}$$

and, hence, the infinite saddle–node $\binom{\overline{0}}{2}SN$ splits into a saddle and a node, and we obtain the

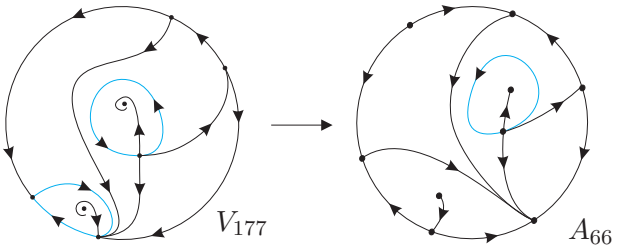

Fig. 117. The perturbation of phase portrait V_{177} yielding the structurally unstable phase portrait A_{66}

phase portrait A_{66} of codimension one, as shown in Fig. 117.

By applying perturbations to the phase portraits of family $\overline{\mathbf{QsnSN(C)}}$ we obtain the "wanted" new phase portraits of codimension one in Table 49. Then, Corollary 1.4 is proved.

Table 49. New codimension–one phase portraits obtained after perturbations

Phase portrait from $\overline{\mathbf{QsnSN(C)}}$	Splitting $\overline{\binom{0}{2}}SN$	Splitting $\overline{sn}_{(2)}$
V_{29}	A_{49}	B_{33}
V_{35}	—	B_{34}
V_{36}	—	B_{36}
V_{102}	A_{44}	—
V_{170}	A_{50}	—
V_{172}	A_{37}	—
V_{174}	A_{73}	—
V_{177}	A_{66}	—
$2S_{34}$	A_{51}	—

Table 50. Geometric classification for the family **QsnSN**(**C**)

$$
I_1 = \begin{cases}
1 \;\&\; I_2 = \begin{cases}
-1\ \{2.8L_1\}, \\
0 \;\&\; I_3 = \begin{cases}
1\ (5S_2), \\
2 \;\&\; I_4 = \begin{cases}
1110\ \{P_{43}\}, \\
2100\ (P_{39}), \\
2101 \;\&\; I_{18} = \begin{cases} y\ (1.1L_4), \\ n\ (1.1L_7), \end{cases} \\
2111\ (7S_6), \\
2120\ (7S_{26}), \\
2210 \;\&\; I_{18} = \begin{cases} y\ (1.1L_3), \\ n\ (4S_{20}), \end{cases} \\
2211\ (V_{23}), \\
3101\ \{1.1L_2\}, \\
3110\ (4S_3), \\
3120\ (V_{84}), \\
3200 \;\&\; I_8 = \begin{cases} (1,0)\ (1.1L_1), \\ (0,2)\ (1.1L_6), \end{cases} \\
3211 \;\&\; I_8 = \begin{cases} (1,0)\ (V_{20}), \\ (0,2)\ (V_{22}), \end{cases} \\
3220\ (V_{85}), \\
4120\ (V_{21}), \\
5211\ (V_1),
\end{cases} \\
\infty\ \{P_{23}\},
\end{cases} \\
1 \;\&\; I_3 = \begin{cases}
1\ (P_{68}), \\
2 \;\&\; I_4 = \begin{cases}
1110\ \{2.8L_2\}, \\
1111\ (1.2L_5), \\
2100\ (2.8L_3), \\
2120\ (1.2L_7),
\end{cases}
\end{cases}
\end{cases} \\
2 \;\&\; I_2 = \begin{cases}
-1 \;\&\; I_4 = \begin{cases}
2210\ \{1.4L_5\}, \\
3101\ \{1.7L_{18}\}, \\
3201 \;\&\; I_8 = \begin{cases} (1,0)\ \{1S_{40}\}, \\ (1,2)\ \{1S_{30}\}, \end{cases} \\
3310\ \{1S_{28}\}, \\
4201\ \{1S_{33}\},
\end{cases} \\
0 \;\&\; I_3 = \mathcal{A}_1\ \textit{(next page)} \\
1 \;\&\; I_3 = \mathcal{A}_2\ \textit{(next page)} \\
2 \;\&\; I_3 = \mathcal{A}_3\ \textit{(next page)}
\end{cases} \\
3 \;\&\; I_2 = \mathcal{A}_4\ \textit{(next page)} \\
\infty \;\&\; I_2 = \mathcal{A}_5\ \textit{(next page)}
\end{cases}
$$

Table 51. Geometric classification for the family **QsnSN(C)** *(cont.)*

$$
I_1=\begin{cases}
\begin{matrix}\mathcal{A}_1\\ [I_1=2,\\ I_2=0]\end{matrix}\ \&\ I_3=\begin{cases}
1\ \&\ I_4=\begin{cases}
11\ \{P_{60}\},\\
21\ \&\ I_5=\begin{cases}(0)\ \&\ I_6=\begin{cases}(0)\ (2.5L_{11}),\\ (2)\ (P_4),\end{cases}\\ (1)\ [2.5L_{13}],\end{cases}\\
22\ (2.5L_4),\\
31\ \&\ I_7=\begin{cases}(0,2)\ (2.5L_3),\\ (1)\ (P_1),\end{cases}\\
41\ (2.5L_1),
\end{cases}\\
2\ \&\ I_4=\begin{cases}
2111\ \&\ I_6=\begin{cases}(3)\ \&\ I_7=\begin{cases}(1)\ (2.7L_{16}),\\ (1,2)\ (2.4L_5),\end{cases}\\ (2,3)\ (P_{22}),\end{cases}\\
2120\ \&\ I_7=\begin{cases}(1)\ (2.7L_{17}),\\ (1,2)\ (2.4L_3),\end{cases}\\
2121\ \&\ I_6=\begin{cases}(0)\ \&\ I_{20}=\begin{cases}s\ (2S_{13}),\\ d\ (2S_{21}),\end{cases}\\ (2)\ (2.4L_7),\\ (3,3)\ (P_{26}),\end{cases}\\
2211\ \&\ I_6=\begin{cases}(0)\ (2S_{45}),\\ (1)\ \{2.7L_{18}\},\\ (3)\ (2.7L_5),\end{cases}\\
2221\ \&\ I_6=\begin{cases}(0)\ (2S_{18}),\\ (2)\ (2.4L_6),\end{cases}\\
3120\ \&\ I_6=\begin{cases}(0)\ (2S_{52}),\\ (1)\ \{2.7L_{19}\},\\ (3)\ (2.7L_3),\end{cases}\\
3121\ \&\ I_7=\begin{cases}(1,0)\ (2.7L_7),\\ (0)\ (P_{30}),\end{cases}\\
3130\ (2S_{12}),\\
3131\ (2S_{24}),\\
3211\ \&\ I_5=\begin{cases}(0)\ \&\ I_6=\begin{cases}(0)\ \&\ I_7=\begin{cases}(1,0)\ (2S_{51}),\\ (2,0)\ (2S_{48}),\end{cases}\\ (2)\ \&\ I_7=\begin{cases}(1,0)\ (2.7L_4),\\ (3,0)\ (2.7L_1),\end{cases}\\ (3)\ (2.4L_9),\end{cases}\\ (1)\ [2S_{49}],\end{cases}\\
\mathcal{A}_6\ \textit{(next page)}
\end{cases}\\
2\ \&\ I_2=\begin{cases}1\ \&\ I_3=\mathcal{A}_2\ \textit{(next page)}\\ 2\ \&\ I_3=\mathcal{A}_3\ \textit{(next page)}\end{cases}\\
3\ \&\ I_2=\mathcal{A}_4\ \textit{(next page)}\\
\infty\ \&\ I_2=\mathcal{A}_5\ \textit{(next page)}
\end{cases}
$$

Table 52. Geometric classification for the family **QsnSN**(**C**) *(cont.)*

$$
I_1 = \begin{cases}
\begin{matrix}\mathcal{A}_6\\ \begin{bmatrix} I_1=2,\\ I_2=0,\\ I_3=2\end{bmatrix}\end{matrix} \ \&\ I_4 = \begin{cases}
3212\ (2.3L_4),\\
3220\ (2S_{53}),\\
3221\ (2.7L_9),\\
3231\ (2.3L_7),\\
3232\ (2S_{30}),\\
3311\ \&\ I_8 = \begin{cases}(2,0)\ (2S_{17}),\\ (3,0)\ (2S_6),\end{cases}\\
3321\ (2S_{19}),\\
4111\ (2.4L_1),\\
4120\ \&\ I_5 = \begin{cases}(0)\ \&\ I_6 = \begin{cases}(0)\ (2S_{56}),\\ (2)\ (2.7L_2),\end{cases}\\ (1)\ [2S_{54}],\end{cases}\\
4121\ \&\ I_6 = \begin{cases}(0)\ (2.3L_6),\\ (3)\ (2.7L_{11}),\end{cases}\\
4131\ (2.3L_1),\\
4141\ (2S_3),\\
4211\ \&\ I_7 = \begin{cases}(0,2)\ (2S_{16}),\\ (1)\ (2.3L_3),\end{cases}\\
4212\ (2S_5),\\
4220\ (2S_{11}),\\
4221\ (2S_{23}),\\
4231\ (2S_{31}),\\
5120\ \&\ I_7 = \begin{cases}(1,2)\ (2.3L_2),\\ (0,2)\ (2S_{10}),\end{cases}\\
5121\ (2S_4),\\
5211\ (2S_1),\\
6120\ (2S_2),
\end{cases}\\
2\ \&\ I_2 = \begin{cases}
\begin{matrix}\mathcal{A}_2\\ \begin{bmatrix} I_1=2,\\ I_2=1\end{bmatrix}\end{matrix} \ \&\ I_3 = \begin{cases}
1\ \&\ I_4 = \begin{cases}
21\ \&\ I_7 = \begin{cases}(0,2)\ (P_{41}),\\ (1,1)\ \{P_{50}\},\end{cases}\\
22\ \&\ I_6 = \begin{cases}(0)\ \&\ I_7 = \begin{cases}(0,3)\ (1.5L_2),\\ (2,1)\ \{1.5L_5\},\end{cases}\\ (1)\ \{P_{52}\},\end{cases}\\
31\ \&\ I_{16} = \begin{cases}H\ \{1.5L_4\},\\ P\ (1.5L_3),\end{cases}\\
32\ \&\ I_5 = \begin{cases}(0)\ \&\ I_7 = \begin{cases}(0,2)\ (1.5L_1),\\ (1,1)\ (1.5L_7),\end{cases}\\ (1)\ [1.5L_6],\end{cases}
\end{cases}\\
\mathcal{A}_2'\ \textit{(next page)}
\end{cases}\\
2\ \&\ I_3 = \mathcal{A}_3\ \textit{(next page)}
\end{cases}\\
3\ \&\ I_2 = \mathcal{A}_4\ \textit{(next page)}\\
\infty\ \&\ I_2 = \mathcal{A}_5\ \textit{(next page)}
\end{cases}
$$

Table 53. Geometric classification for the family **QsnSN(C)** *(cont.)*

$$
I_1=\left\{\begin{array}{l}
\mathcal{A}_2'\\
\begin{bmatrix} I_1=2,\\ I_2=1\end{bmatrix}\ \&\ I_3=\left\{\begin{array}{l}
2\ \&\ I_4=\left\{\begin{array}{l}
1110\ \&\ I_7=\left\{\begin{array}{l}(0,2)\ \{1.4L_7\},\\(1,1)\ \{1.4L_{13}\},\end{array}\right.\\
2100\ \&\ I_7=\left\{\begin{array}{l}(0,2)\ (1.7L_{20}),\\(1,1)\ \{1.7L_{28}\},\end{array}\right.\\
2101\ \&\ I_7=\left\{\begin{array}{l}(0,3)\ \{1S_{37}\},\\(1,0)\ \{\{1.7L_{31}\}\},\\(1,2)\ \&\ I_8=\left\{\begin{array}{l}(1,0)\ (1S_{52}),\\(2,0)\ \{1S_{45}\},\end{array}\right.\\(2,1)\ \{\{1S_{57}\}\},\end{array}\right.\\
2111\ \&\ I_5=\left\{\begin{array}{l}(0)\ \&\ I_6=\left\{\begin{array}{l}(0)\ \&\ I_7=\left\{\begin{array}{l}(0,4)\ (1S_{69}),\\(1,3)\ (1S_7),\\(2,2)\ (1S_6),\\(3,1)\ \{1S_{14}\},\end{array}\right.\\(1)\ \{1.7L_2\},\\(3)\ \&\ I_7=\left\{\begin{array}{l}(0,2)\ (1.4L_{14}),\\(1,1)\ \&\ I_9=\left\{\begin{array}{l}f\ (1.4L_1),\\\infty\ (1.4L_4),\end{array}\right.\\(1,3)\ \{1.4L_8\},\\(2,2)\ \{1.4L_{12}\},\end{array}\right.\\(3,5)\ \{\{P_{31}\}\},\end{array}\right.\\(1)\ [1.4L_3],\end{array}\right.\\
2120\ \&\ I_7=\left\{\begin{array}{l}(0,2)\ (1.7L_9),\\(1,1)\ (1.7L_{32}),\end{array}\right.\\
2121\ \&\ I_5=\left\{\begin{array}{l}(0)\ \&\ I_6=\left\{\begin{array}{l}(0)\ \{1S_{44}\},\\(3)\ \&\ I_7=\left\{\begin{array}{l}(0,1)\ (1.7L_7),\\(0,3)\ \{1.7L_{21}\},\\(1,2)\ \{\{1.7L_{27}\}\},\end{array}\right.\\(5)\ \{1.7L_3\},\end{array}\right.\\(1)\ [1.7L_4],\end{array}\right.\\
2200\ \&\ I_6=\left\{\begin{array}{l}(0)\ \&\ I_7=\left\{\begin{array}{l}(0,3)\ (1S_{35}),\\(2,1)\ \{1S_{55}\},\end{array}\right.\\(1)\ \{1.7L_{29}\},\end{array}\right.\\
\mathcal{A}_7\ \textit{(next page)}
\end{array}\right.\\
\infty\ \{1.3L_2\},
\end{array}\right.\\
2\ \&\ I_2=2\ \&\ I_3=\mathcal{A}_3\ \textit{(next page)}\\
3\ \&\ I_2=\mathcal{A}_4\ \textit{(next page)}\\
\infty\ \&\ I_2=\mathcal{A}_5\ \textit{(next page)}
\end{array}\right.
$$

Table 54. Geometric classification for the family **QsnSN**(**C**) *(cont.)*

$$
I_1 = \left\{ \begin{array}{l}
\begin{matrix}\mathcal{A}_7 \\ \begin{bmatrix} I_1=2, \\ I_2=1, \\ I_3=2 \end{bmatrix}\end{matrix} \ \&\ I_4 = \left\{ \begin{array}{l}
2211\ \&\ I_5 = \left\{ \begin{array}{l} (0)\ \&\ I_8 = \left\{ \begin{array}{l} (1,1)\ (1S_{68}), \\ (2,0)\ (1S_8), \end{array} \right. \\ (1)\ [1S_{12}], \end{array} \right. \\
3101\ \&\ I_5 = \left\{ \begin{array}{l} (0)\ \&\ I_8 = \left\{ \begin{array}{l} (0,2)\ \{1S_{25}\}, \\ (1,1)\ \{1S_{66}\}, \end{array} \right. \\ (1)\ [\{1S_{60}\}], \end{array} \right. \\
3111\ \&\ I_5 = \left\{ \begin{array}{l} (0)\ \&\ I_6 = \left\{ \begin{array}{l} (0)\ \&\ I_7 = \left\{ \begin{array}{l} (0,3)\ (1S_{67}), \\ (2,1)\ (1S_9), \end{array} \right. \\ (3)\ \{1.7L_6\}, \end{array} \right. \\ (1)\ [1S_{13}], \end{array} \right. \\
3120\ \&\ I_6 = \left\{ \begin{array}{l} (0)\ \&\ I_7 = \left\{ \begin{array}{l} (0,3)\ (1S_{24}), \\ (1,2)\ (1S_{19}), \\ (2,1)\ \{1S_{71}\}, \end{array} \right. \\ (1)\ \{1.7L_{33}\}, \end{array} \right. \\
3121\ \&\ I_5 = \left\{ \begin{array}{l} (0)\ \&\ I_6 = \left\{ \begin{array}{l} (0)\ \&\ I_7 = \left\{ \begin{array}{l} (1,1)\ \&\ I_{18} = \left\{ \begin{array}{l} y\ \{1S_{15}\}, \\ n\ (1S_{18}), \end{array} \right. \\ (1,3)\ \{\{1S_{56}\}\}, \\ (2,2)\ \{\{1S_{53}\}\}, \\ (3,1)\ \{1S_{43}\}, \\ (4,0)\ \{1S_{36}\}, \end{array} \right. \\ (1)\ \{\{1.7L_{30}\}\}, \end{array} \right. \\ (1)\ [1S_{16}], \end{array} \right. \\
3200\ \&\ I_5 = \left\{ \begin{array}{l} (0)\ \&\ I_7 = \left\{ \begin{array}{l} (0,2)\ (1S_{27}), \\ (1,1)\ (1S_{64}), \end{array} \right. \\ (1)\ [1S_{58}], \end{array} \right. \\
3211\ \{1.7L_5\}, \\
3221\ \&\ I_5 = \left\{ \begin{array}{l} (0)\ (1S_{23}), \\ (1)\ [1S_{20}], \end{array} \right. \\
4111\ \{1.7L_1\}, \\
4120\ \&\ I_5 = \left\{ \begin{array}{l} (0)\ \&\ I_7 = \left\{ \begin{array}{l} (0,2)\ (1S_1), \\ (1,1)\ (1S_{74}), \end{array} \right. \\ (1)\ [1S_{72}], \end{array} \right. \\
4121\ \&\ I_5 = \left\{ \begin{array}{l} (0)\ \&\ I_7 = \left\{ \begin{array}{l} (0,1)\ (1S_2), \\ (0,3)\ \{1S_{26}\}, \\ (2,1)\ \{1S_{65}\}, \end{array} \right. \\ (1)\ \&\ I_{18} = \left\{ \begin{array}{l} y\ [\{1S_{59}\}], \\ n\ [1S_4], \end{array} \right. \end{array} \right. \\
4211\ \{1S_{21}\}, \\
5111\ \{1S_5\}, \end{array} \right. \\
2\ \&\ I_2=2\ \&\ I_3=\mathcal{A}_3\ \textit{(next page)} \\
3\ \&\ I_2=\mathcal{A}_4\ \textit{(next page)} \\
\infty\ \&\ I_2=\mathcal{A}_5\ \textit{(next page)}
\end{array} \right.
$$

Table 55. Geometric classification for the family **QsnSN(C)** *(cont.)*

$$
I_1=\left\{\begin{array}{l}
\mathcal{A}_3\ \left[\begin{array}{l}I_1=2,\\ I_2=2\end{array}\right]\ \&\ I_3=\left\{\begin{array}{l}
1\ (2.5L_{10}),\\
2\ \&\ I_4=\left\{\begin{array}{l}
1111\ (2S_{41}),\\
2111\ \{2.7L_{20}\},\\
2121\ \&\ I_5=\left\{\begin{array}{l}(0)\ (2S_{59}),\\(1)\ [2S_{61}],\end{array}\right.\\
3111\ \{2S_{62}\},
\end{array}\right.
\end{array}\right.\\
\mathcal{A}_4\ [I_1=3]\ \&\ I_2=\left\{\begin{array}{l}
0\ \&\ I_3=\left\{\begin{array}{l}
1\ \&\ I_4=\left\{\begin{array}{l}
21\ \&\ I_7=\left\{\begin{array}{l}(0,2)\ (5.7L_{11}),\\(1,1)\ (5.7L_2),\end{array}\right.\\
22\ (5S_9),\\
31\ \&\ I_6=\left\{\begin{array}{l}
(0)\ \&\ I_7=\left\{\begin{array}{l}(0,3)\ (5S_{26}),\\(2,1)\ \&\ I_{18}=\left\{\begin{array}{l}y\ \{5S_{33}\},\\n\ (5S_{13}),\end{array}\right.\end{array}\right.\\
(1)\ \{5.7L_1\},\\
(2)\ \{5.7L_{14}\},
\end{array}\right.\\
41\ \&\ I_5=\left\{\begin{array}{l}
(0)\ \&\ I_7=\left\{\begin{array}{l}(0,2)\ (5S_1),\\(1,1)\ (5S_3),\\(2,1)\ (5S_{36}),\end{array}\right.\\
(1)\ [5S_5],
\end{array}\right.
\end{array}\right.\\
2\ \&\ I_4=\left\{\begin{array}{l}
2111\ \&\ I_6=\left\{\begin{array}{l}(3)\ (4S_8),\\(1,5)\ \{7.7L_4\},\\(2,3)\ (4.4L_3),\end{array}\right.\\
2120\ (4S_6),\\
2121\ \&\ I_6=\left\{\begin{array}{l}
(0)\ \&\ I_8=\left\{\begin{array}{l}(1,1)\ (V_{49}),\\(2,0)\ (V_{46}),\end{array}\right.\\
(2)\ (4S_{33}),\\
(3,3)\ (7.7L_1),
\end{array}\right.\\
2211\ \&\ I_6=\left\{\begin{array}{l}
(2)\ \&\ I_7=\left\{\begin{array}{l}(0,3)\ (7S_{65}),\\(2,1)\ (7S_{33}),\end{array}\right.\\
(3)\ \&\ I_{10}=\left\{\begin{array}{l}0\ \&\ I_{11}=\left\{\begin{array}{l}N\ (7S_{63}),\\SN\ (7S_9),\end{array}\right.\\1\ (7S_{68}),\end{array}\right.\\
(2,2)\ \{4.7L_1\},\\
(2,3)\ (4.4L_1),
\end{array}\right.\\
2221\ \&\ I_6=\left\{\begin{array}{l}
(0)\ \&\ I_7=\left\{\begin{array}{l}(1,3)\ \&\ I_{11}=\left\{\begin{array}{l}N\ (V_{155}),\\SN\ (V_{44}),\end{array}\right.\\(2,2)\ (V_{104}),\end{array}\right.\\
(2)\ \&\ I_7=\left\{\begin{array}{l}(0,2)\ (4S_{32}),\\(1,1)\ (4S_{29}),\end{array}\right.
\end{array}\right.\\
3120\ \&\ I_{10}=\left\{\begin{array}{l}0\ (7S_{69}),\\1\ \&\ I_{11}=\left\{\begin{array}{l}N\ (7S_{16}),\\SN\ (7S_{61}),\end{array}\right.\end{array}\right.\\
\mathcal{A}_8\ \textit{(next page)}
\end{array}\right.
\end{array}\right.\\
2\ \&\ I_3=\mathcal{A}_9\ \textit{(next page)}
\end{array}\right.\\
\infty\ \&\ I_2=\mathcal{A}_5\ \textit{(next page)}
\end{array}\right.
$$

Table 56. Geometric classification for the family **QsnSN**(**C**) *(cont.)*

$$
I_1=\left\{\begin{array}{l}
\mathcal{A}_8\\
\begin{bmatrix} I_1=3,\\ I_2=0,\\ I_3=2\end{bmatrix}\ \&\ I_4=\left\{\begin{array}{l}
3121\ \&\ I_5=\left\{\begin{array}{l}
(0)\ \&\ I_6=\left\{\begin{array}{l} (0)\ (V_{122}),\\ (3)\ \&\ I_7=\left\{\begin{array}{l} (0,2)\ (7S_{37}),\\ (1,1)\ (7S_{38}),\end{array}\right.\end{array}\right.\\
(1)\ [V_{118}],
\end{array}\right.\\
3130\ \&\ I_7=\left\{\begin{array}{l}
(1,3)\ \&\ I_{11}=\left\{\begin{array}{l} N\ (V_{37}),\\ SN\ (V_{165}),\end{array}\right.\\
(2,2)\ (V_{123}),
\end{array}\right.\\
3131\ (V_{110}),\\
3211\ \&\ I_5=\left\{\begin{array}{l}
(0)\ \&\ I_6=\left\{\begin{array}{l}
(0)\ \&\ I_7=\left\{\begin{array}{l} (0,4)\ (V_{154}),\\ (3,1)\ (V_{102}),\end{array}\right.\\
(1)\ \{7S_{32}\},\\
(2)\ \&\ I_7=\left\{\begin{array}{l}
(0,2)\ \&\ I_8=\left\{\begin{array}{l} (0,0)\ \&\ I_{11}=\left\{\begin{array}{l} a\ (4S_{42}),\\ N\ (7S_{64}),\end{array}\right.\\ (1,0)\ (7S_4),\end{array}\right.\\
(1,1)\ \&\ I_8=\left\{\begin{array}{l} (0,0)\ (7S_{70}),\\ (1,0)\ \&\ I_{10}=\left\{\begin{array}{l} 0\ \&\ I_{11}=\left\{\begin{array}{l} a\ (4S_{16}),\\ SN\ (7S_8),\end{array}\right.\\ 1\ (7S_{71}),\end{array}\right.\\ (2,0)\ (7S_{23}),\end{array}\right.
\end{array}\right.\\
(3)\ (4S_{31}),
\end{array}\right.\\
(1)\ \&\ I_{10}=\left\{\begin{array}{l} 0\ [4S_{26}],\\ 1\ [7S_{28}],\end{array}\right.
\end{array}\right.\\
3212\ \&\ I_5=\left\{\begin{array}{l}
(0)\ \&\ I_{12}=\left\{\begin{array}{l} s\ \{7S_{22}\},\\ d\ \{7S_{29}\},\end{array}\right.\\
(1)\ [\{7S_{27}\}],
\end{array}\right.\\
3221\ \&\ I_7=\left\{\begin{array}{l}
(0,1)\ \&\ I_8=\left\{\begin{array}{l} (0,1)\ (7S_{44}),\\ (1,1)\ (7S_{45}),\end{array}\right.\\
(1,4)\ (4S_9),
\end{array}\right.\\
3231\ \{7S_{52}\},\\
3232\ (V_{129}),\\
3311\ \&\ I_5=\left\{\begin{array}{l}
(0)\ \&\ I_8=\left\{\begin{array}{l}
(1,0)\ \&\ I_9=\left\{\begin{array}{l}
f\ \&\ I_{11}=\left\{\begin{array}{l} N\ (V_{143}),\\ SN\ \&\ I_{19}=\left\{\begin{array}{l} c\ (V_{170}),\\ s\ (V_{71}),\end{array}\right.\end{array}\right.\\
\infty\ \&\ I_{11}=\left\{\begin{array}{l} a\ (V_{145}),\\ N\ (V_{13}),\end{array}\right.
\end{array}\right.\\
(2,0)\ (V_{64}),
\end{array}\right.\\
(1)\ [V_{90}],
\end{array}\right.\\
3321\ \&\ I_5=\left\{\begin{array}{l}
(0)\ \&\ I_7=\left\{\begin{array}{l} (0,2)\ (V_{108}),\\ (1,1)\ (V_{78}),\end{array}\right.\\
(1)\ \&\ I_{12}=\left\{\begin{array}{l} s\ [V_{80}],\\ d\ [10S_1],\end{array}\right.\\
(2)\ [[V_{88}]],
\end{array}\right.\\
\mathcal{A}'_8\ \textit{(next page)}
\end{array}\right.\\
3\ \&\ I_2=2\ \&\ I_3=\mathcal{A}_9\ \textit{(next page)}\\
\infty\ \&\ I_2=\mathcal{A}_5\ \textit{(next page)}
\end{array}\right.
$$

Table 57. Geometric classification for the family **QsnSN(C)** *(cont.)*

$$
I_1=\begin{cases}
\begin{matrix}\mathcal{A}_8'\\ \begin{bmatrix} I_1=3,\\ I_2=0,\\ I_3=2\end{bmatrix}\end{matrix}\ \&\ I_4=\begin{cases}
4111\ (4S_1),\\
4120\ (7S_{62}),\\
4121\ \&\ I_5=\begin{cases}(0)\ \&\ I_6=\begin{cases}(0)\ (V_{66}),\\ (1)\ \{7S_{41}\},\\ (3)\ \&\ I_8=\begin{cases}(1,1)\ (7S_{55}),\\ (2,0)\ (7S_3),\end{cases}\end{cases}\\ (1)\ \&\ I_6=\begin{cases}(0)\ [V_{100}],\\ (3)\ [7S_{53}],\end{cases}\end{cases}\\
4131\ \{7S_2\},\\
4141\ \&\ I_5=\begin{cases}(0)\ (V_{15}),\\ (1)\ [V_{17}],\end{cases}\\
4211\ \&\ I_6=\begin{cases}(0)\ \&\ I_7=\begin{cases}(0,3)\ \&\ I_7=\begin{cases}f\ (V_{144}),\\ \infty\ (V_{147}),\end{cases}\\ (2,1)\ \&\ I_{11}=\begin{cases}a\ \{V_{172}\},\\ SN\ (V_{69}),\end{cases}\end{cases}\\ (1)\ \&\ I_{11}=\begin{cases}a\ \{7S_{77}\},\\ SN\ \{7S_7\},\end{cases}\end{cases}\\
4212\ \&\ I_5=\begin{cases}(0)\ \&\ I_7=\begin{cases}(0,2)\ (V_{10}),\\ (1,1)\ (V_{83}),\end{cases}\\ (1)\ [V_{89}],\end{cases}\\
4220\ \&\ I_{11}=\begin{cases}N\ (V_{42}),\\ SN\ (V_{142}),\end{cases}\\
4221\ \&\ I_7=\begin{cases}(0,2)\ (V_{109}),\\ (1,1)\ (V_{114}),\end{cases}\\
4231\ \&\ I_5=\begin{cases}(0)\ \&\ I_8=\begin{cases}(1,0)\ (V_{136}),\\ (2,0)\ (V_7),\end{cases}\\ (1)\ [V_{134}],\end{cases}\\
5120\ \&\ I_6=\begin{cases}(0)\ \&\ I_7=\begin{cases}(0,3)\ (V_{141}),\\ (2,1)\ \&\ I_{11}=\begin{cases}a\ \{V_{173}\},\\ N\ (V_{41}),\end{cases}\end{cases}\\ (1)\ \&\ I_{11}=\begin{cases}a\ \{7S_{78}\},\\ N\ \{7S_{10}\},\end{cases}\end{cases}\\
5121\ \&\ I_5=\begin{cases}(0)\ \&\ I_7=\begin{cases}(0,2)\ (V_9),\\ (1,1)\ (V_{121}),\end{cases}\\ (1)\ [V_{117}],\end{cases}\\
5211\ \&\ I_5=\begin{cases}(0)\ \&\ I_{11}=\begin{cases}a\ (V_{190}),\\ SN\ (V_{25}),\end{cases}\\ (1)\ \&\ I_{11}=\begin{cases}a\ [V_{178}],\\ SN\ [V_{27}],\end{cases}\end{cases}\\
6120\ \&\ I_5=\begin{cases}(0)\ \&\ I_6=\begin{cases}(0)\ \&\ I_7=\begin{cases}(0,2)\ (V_2),\\ (1,1)\ \&\ I_{11}=\begin{cases}a\ (V_{191}),\\ N\ (V_{31}),\end{cases}\end{cases}\\ (2)\ (7S_{15}),\end{cases}\\ (1)\ \&\ I_{11}=\begin{cases}a\ [V_{179}],\\ N\ [V_{33}],\end{cases}\end{cases}
\end{cases}\\
3\ \&\ I_2=2\ \&\ I_3=\mathcal{A}_9\ \textit{(next page)}\\
\infty\ \&\ I_2=\mathcal{A}_5\ \textit{(next page)}
\end{cases}
$$

Table 58. Geometric classification for the family **QsnSN**(**C**) *(cont.)*

$$
I_1=\left\{\begin{array}{l}
\mathcal{A}_9\\
\begin{bmatrix}I_1=3,\\ I_2=2\end{bmatrix}\ \&\ I_3=\left\{\begin{array}{l}
1\ \&\ I_5=\left\{\begin{array}{l}
(0)\ \&\ I_6=\left\{\begin{array}{l}
(0)\ \&\ I_7=\left\{\begin{array}{l}(0,2,3)\ (5S_{28}),\\ (1,1,3)\ (5S_{12}),\\ (2,1,2)\ \{5S_{23}\},\end{array}\right.\\
(1)\ \{5.7L_9\},
\end{array}\right.\\
(1)\ [5S_{22}],
\end{array}\right.\\
2\ \&\ I_4=\left\{\begin{array}{l}
1111\ \&\ I_5=\left\{\begin{array}{l}
(0)\ \&\ I_6=\left\{\begin{array}{l}
(0)\ \&\ I_7=\left\{\begin{array}{l}(0,3,4)\ (V_{149}),\\ (2,1,4)\ (V_{61}),\\ (3,1,3)\ \&\ I_{13}=\left\{\begin{array}{l}S\ (V_{107}),\\ SN\ \{V_{53}\},\end{array}\right.\end{array}\right.\\
(1)\ \&\ I_{13}=\left\{\begin{array}{l}S\ \{7S_{31}\},\\ SN\ \{7S_{17}\},\end{array}\right.\\
(3)\ \&\ I_7=\left\{\begin{array}{l}(0,2,3)\ (4S_{44}),\\ (1,1,3)\ (4S_{15}),\\ (2,1,2)\ \{4S_{13}\},\end{array}\right.
\end{array}\right.\\
(1)\ \&\ I_6=\left\{\begin{array}{l}
(0)\ \&\ I_{13}=\left\{\begin{array}{l}S\ [V_{94}],\\ SN\ [V_{54}],\end{array}\right.\\
(3)\ [4S_{25}],
\end{array}\right.
\end{array}\right.\\
2111\ \&\ I_5=\left\{\begin{array}{l}
(0)\ \&\ I_6=\left\{\begin{array}{l}
(0)\ \&\ I_7=\left\{\begin{array}{l}(1,2,3)\ \&\ I_8=\left\{\begin{array}{l}(1,0)\ (V_{198}),\\ (2,0)\ (V_{62}),\end{array}\right.\\
(2,2,2)\ (V_{51}),
\end{array}\right.\\
(3)\ \&\ I_8=\left\{\begin{array}{l}(0,1)\ \{4S_{51}\},\\ (1,1)\ (4S_{36}),\end{array}\right.\\
(3,5)\ \&\ I_7=\left\{\begin{array}{l}(0,0,2)\ \{\{7.7L_6\}\},\\ (1,0,1)\ \{7.7L_5\},\end{array}\right.
\end{array}\right.\\
(1)\ [V_{99}],
\end{array}\right.\\
2121\ \&\ I_5=\left\{\begin{array}{l}
(0)\ \&\ I_6=\left\{\begin{array}{l}
(3)\ \&\ I_7=\left\{\begin{array}{l}(0,1,2)\ (7S_{72}),\\ (1,1,1)\ (7S_{60}),\end{array}\right.\\
(5)\ \&\ I_{11}=\left\{\begin{array}{l}s\ \{\{7S_{67}\}\},\\ d\ \{7S_{42}\},\end{array}\right.
\end{array}\right.\\
(1)\ \&\ I_7=\left\{\begin{array}{l}(0,1,2)\ [7S_{56}],\\ (1,1,1)\ [\{7S_{74}\}],\end{array}\right.
\end{array}\right.\\
3111\ \&\ I_6=\left\{\begin{array}{l}
(3)\ \&\ I_7=\left\{\begin{array}{l}(0,1,2)\ \{7S_{58}\},\\ (1,1,1)\ \{\{7S_{75}\}\},\end{array}\right.\\
(5)\ \&\ I_7=\left\{\begin{array}{l}(0,0,3)\ \{7S_{57}\},\\ (2,0,1)\ \{\{7S_{76}\}\},\end{array}\right.\\
(1,5)\ \{\{7.7L_7\}\},
\end{array}\right.\\
3121\ \&\ I_5=\left\{\begin{array}{l}
(0)\ \&\ I_6=\left\{\begin{array}{l}
(0)\ \&\ I_7=\left\{\begin{array}{l}(0,1,3)\ (V_{140}),\\ (1,1,2)\ \&\ I_8=\left\{\begin{array}{l}(1,1)\ \&\ I_{18}=\left\{\begin{array}{l}1\ \{V_{166}\},\\ 2\ \{\{V_{169}\}\},\end{array}\right.\\ (2,1)\ \{V_{113}\},\end{array}\right.\\ (2,1,1)\ \{V_{174}\},\end{array}\right.\\
(1)\ \{7S_{79}\},
\end{array}\right.\\
(1)\ \&\ I_6=\left\{\begin{array}{l}
(0)\ \&\ I_7=\left\{\begin{array}{l}(0,1,3)\ [V_{137}],\\ (1,1,2)\ [\{V_{168}\}],\\ (2,1,1)\ [\{V_{176}\}],\end{array}\right.\\
(1)\ [\{7S_{81}\}],
\end{array}\right.
\end{array}\right.\\
\mathcal{A}_{10}\ \textit{(next page)}
\end{array}\right.
\end{array}\right.\\
\infty\ \&\ I_2=\mathcal{A}_5\ \textit{(next page)}
\end{array}\right.
$$

Table 59. Geometric classification for the family **QsnSN(C)** *(cont.)*

$$
I_1=\begin{cases}
\begin{matrix}\mathcal{A}_{10}\\ \begin{bmatrix} I_1=3,\\ I_2=2,\\ I_3=2\end{bmatrix}\end{matrix}\ \&\ I_4=\begin{cases}
4111\ \&\ I_5=\begin{cases}
(0)\ \&\ I_6=\begin{cases}(0)\ \&\ I_{18}=\begin{cases}1\ \{V_{138}\},\\ 2\ \{\{V_{177}\}\},\end{cases}\\ (1)\ \{\{7S_{82}\}\},\\ (5)\ \&\ I_7=\begin{cases}(0,2,0)\ \{7S_1\},\\ (1,1,0)\ \{7S_{85}\},\end{cases}\end{cases}\\
(1)\ [\{7S_{83}\}],
\end{cases}\\
4121\ \&\ I_5=\begin{cases}
(0)\ \&\ I_7=\begin{cases}(0,2,1)\ (V_3),\\ (1,1,1)\ (V_{192}),\end{cases}\\
(1)\ \&\ I_7=\begin{cases}(0,2,1)\ [V_5],\\ (1,1,1)\ \&\ I_{14}=\begin{cases}f\ [V_{180}],\\ \infty\ [V_{194}],\end{cases}\end{cases}\\
(1,1)\ [[V_{182}]],
\end{cases}\\
5111\ \&\ I_5=\begin{cases}
(0)\ \&\ I_7=\begin{cases}(0,1,2)\ \{V_6\},\\ (1,1,1)\ \{V_{189}\},\end{cases}\\
(1)\ [\{V_{183}\}],
\end{cases}
\end{cases}\\
\begin{matrix}\mathcal{A}_5\\ [I_1=\infty]\end{matrix}\ \&\ I_2=\begin{cases}
0\ \&\ I_{15}=\begin{cases}0\ \{P_{58}\},\\ 1\ \&\ I_{17}=\begin{cases}-\ \{P_{65}\},\\ \cup\ \{P_{64}\},\end{cases}\end{cases}\\
1\ \&\ I_3=\begin{cases}2\ \{1.2L_8\},\\ \infty\ \{P_{57}\}.\end{cases}
\end{cases}
\end{cases}
$$

Table 60. Topological equivalences for the family **QsnSN**(**C**)

Presented phase portrait	Identical under perturbations	Finite antisaddle focus	Finite antisaddle node–focus	Finite weak point	Disconnected parts	Possessing invariant curve (no separatrix)	Symmetry	Other reasons
V_1								
V_2								
V_3		V_4	$6S_1$	$3S_1$				
V_5								
V_6								
V_7								
V_9	V_{19}	V_8, V_{18}	$6S_3$, $6S_4$ $3.6L_1$	$3S_3$, $3S_4$				
V_{10}	V_{12}		$3.10L_1$	$3S_5$, $3S_6$				
V_{13}	V_{11}, V_{14}			$3S_7$		$4S_4$		
V_{15}		V_{16}	$6S_2$	$3S_2$				
V_{17}								
V_{20}								$2.11{L_3}^{(1)}$
V_{21}								${1.2L_1}^{(2)}$, ${2.11L_2}^{(1)}$
V_{22}								
V_{23}	V_{24}					$4S_{15}$		${3S_{20}}^{(3)}$ ${1.2L_2}^{(2)}$, ${2.11L_2}^{(1)}$
V_{25}		V_{26}	$6S_5$	$3S_8$				
V_{27}								

Table 61. Topological equivalences for the family **QsnSN**(**C**) *(cont.)*

Presented phase portrait	Identical under perturbations	Finite antisaddle focus	Finite antisaddle node–focus	Finite weak point	Disconnected parts	Possessing invariant curve (no separatrix)	Symmetry	Other reasons
V_{31}		V_{32}	$6S_6$	$3S_9$				
V_{33}								
V_{37}	V_{43}	V_{36}, V_{40}	$6S_9$, $6S_{10}$ $3.6L_2$	$3S_{12}$, $3S_{13}$				
V_{41}		V_{34}, V_{38}	$6S_7$	$3S_{10}$				
V_{42}		V_{35}, V_{39}	$6S_8$	$3S_{11}$				
V_{44}	V_{45}, V_{73}, V_{96}	V_{30}, V_{72}	$6S_{11}$, $6S_{22}$ $3.6L_3$	$3S_{23}$, $3S_{24}$, $3S_{26}$, $3S_{43}$ $3.10L_4$				
V_{46}	V_{47}, V_{63}			$3S_{14}$, $3S_{15}$ $3.10L_2$		$4S_{11}$		
V_{49}	V_{48}, V_{75}, V_{97}	V_{50}, V_{98}	$6S_{12}$, $6S_{30}$	$3S_{25}$, $3S_{44}$, $3S_{45}$ $3.4L_7$, $3.6L_8$		$4S_{12}$, $4S_{24}$		
V_{51}		V_{52}	$6S_{13}$					
V_{53}								
V_{54}								
V_{61}		V_{55}, V_{56}, V_{57} V_{58}, V_{59}	$6S_{15}$, $6S_{16}$, $6S_{17}$ $6S_{18}$, $6S_{19}$ $3.6L_7$, $6.6L_1$	$3S_{16}$, $3S_{32}$, $3S_{42}$				

Table 62. Topological equivalences for the family **QsnSN**(**C**) *(cont.)*

Presented phase portrait	Identical under perturbations	Finite antisaddle focus	Finite antisaddle node–focus	Finite weak point	Disconnected parts	Possessing invariant curve (no separatrix)	Symmetry	Other reasons
V_{62}		V_{60}	$6S_{14}$	$3S_{46}$				
V_{64}	V_{65}	V_{74}, V_{76}	$6S_{23}$, $6S_{24}$ $3.6L_4$, $3.6L_5$ P_{12}	$3S_{17}$, $3S_{18}$, $3S_{27}$ $3S_{30}$, $3S_{35}$, $3S_{41}$ $3.3L_2$, $3.10L_3$, $3.10L_5$				
V_{66}	V_{67}	V_{77}, V_{86}	$6S_{25}$, $6S_{28}$	$3S_{19}$, $3S_{31}$, $3S_{48}$, $3S_{49}$ $3.3L_3$, $3.6L_6$				
V_{69}		V_{28}, V_{68}	$6S_{20}$	$3S_{21}$				
V_{71}		V_{29}, V_{70}	$6S_{21}$	$3S_{22}$				
V_{78}		V_{79}, V_{91}	$6S_{26}$	$3S_{28}$, $3S_{37}$ $3.10L_6$				
V_{80}				$3S_{33}$				
V_{83}		V_{81}, V_{82}	$6S_{27}$	$3S_{29}$, $3S_{34}$, $3S_{36}$, $3S_{39}$ $3.3L_1$, $3.10L_7$				
V_{84}								$1.2{L_3}^{(2)}$
V_{85}								$1.2{L_4}^{(2)}$
V_{88}								
V_{89}	V_{92}			$3S_{38}$				
V_{90}	V_{93}			$3S_{40}$				

Table 63. Topological equivalences for the family **QsnSN**(**C**) *(cont.)*

Presented phase portrait	Identical under perturbations	Finite antisaddle focus	Finite antisaddle node–focus	Finite weak point	Disconnected parts	Possessing invariant curve (no separatrix)	Symmetry	Other reasons
V_{94}		V_{87}	$6S_{29}$					
V_{99}								
V_{100}	V_{101}			$3S_{47}$				
V_{102}	V_{105}			$3S_{50}$				
V_{104}		V_{103}, V_{106}	$6S_{31}$	$3S_{51}$	V_{125}, V_{126}	$4S_{37}$, $4S_{38}$		
V_{107}		V_{95}	$6S_{32}$					
V_{108}	V_{127}			$3S_{57}$				
V_{109}	V_{128}	V_{131}, V_{132}	$6S_{39}$, $6S_{40}$ $3.6L_{10}$	$3S_{58}$, $3S_{59}$				
V_{110}	V_{126}	V_{111}, V_{112}	$6S_{33}$, $6S_{37}$ $3.6L_{9}$	$3S_{52}$, $3S_{56}$				
V_{113}								
V_{114}		V_{115}, V_{116}	$6S_{34}$	$3S_{53}$				
V_{117}								
V_{118}								
V_{121}		V_{119}	$6S_{35}$	$3S_{54}$				
V_{122}		V_{120}	$6S_{36}$	$3S_{55}$				
V_{123}								

Table 64. Topological equivalences for the family **QsnSN**(**C**) *(cont.)*

Presented phase portrait	Identical under perturbations	Finite antisaddle focus	Finite antisaddle node–focus	Finite weak point	Disconnected parts	Possessing invariant curve (no separatrix)	Symmetry	Other reasons
V_{129}		V_{130}, V_{133}	$6S_{38}$	$3S_{60}$				
V_{134}								
V_{136}		V_{135}	$6S_{41}$	$3S_{61}$				
V_{137}								
V_{138}								
V_{140}		V_{139}	$6S_{42}$	$3S_{62}$				
V_{141}								
V_{142}								
V_{143}								
V_{144}								
V_{145}	V_{144}			$3S_{63}$				
V_{147}	V_{148}			$3S_{64}$, $3S_{56}$ $3.10L_8$				
V_{149}	V_{153}, V_{158} V_{196}, V_{197}	V_{151}, V_{152} V_{159}	$6S_{43}$, $6S_{44}$ $6S_{46}$, $6S_{47}$			$4S_{45}$, $4S_{46}$		
V_{154}	V_{157}			$3S_{67}$				
V_{155}	V_{156}, V_{162}, V_{163}	V_{164}	$6S_{49}$	$3S_{66}$		$4S_{50}$, $4S_{52}$		
V_{165}								
V_{166}		V_{167}	$6S_{50}$	$3S_{68}$				

Table 65. Topological equivalences for the family **QsnSN**(**C**) *(cont.)*

Presented phase portrait	Identical under perturbations	Finite antisaddle focus	Finite antisaddle node–focus	Finite weak point	Disconnected parts	Possessing invariant curve (no separatrix)	Symmetry	Other reasons
V_{168}								
V_{169}								
V_{170}							V_{171}	
V_{172}								
V_{173}								
V_{174}		V_{175}	$6S_{51}$	$3S_{69}$				
V_{176}								
V_{177}								
V_{178}								
V_{179}				$3S_{72}$				
V_{180}		V_{181}	$6S_{52}$	$3S_{70}$				
V_{182}								
V_{183}								
V_{189}		V_{195}	$6S_{59}$	$3S_{76}$				
V_{190}		V_{184}	$6S_{54}$	$3S_{71}$				
V_{191}		V_{185}	$6S_{55}$					
V_{192}	V_{186}, V_{187}, V_{193}		$6S_{53}$, $6S_{56}$ $6S_{57}$, $6S_{60}$ $3.6L_{11}$, $3.6L_{12}$ $6.6L_2$	$3S_{73}$, $3S_{74}$ $3S_{77}$, $3S_{78}$ $3.3L_4$				

Table 66. Topological equivalences for the family **QsnSN**(**C**) *(cont.)*

Presented phase portrait	Identical under perturbations	Finite antisaddle focus	Finite antisaddle node–focus	Finite weak point	Disconnected parts	Possessing invariant curve (no separatrix)	Symmetry	Other reasons
V_{194}		V_{188}	$6S_{59}$	$3S_{76}$				
V_{198}	V_{150}	V_{160}, V_{161}, V_{199}	$6S_{45}$, $6S_{48}$ $6S_{61}$, $6S_{62}$ $6.6L_3$			$4S_{47}$		
$1S_1$								
$1S_2$		$1S_3$	$1.6L_1$	$1.3L_1$				
$1S_4$								
$1S_5$								
$1S_6$								
$1S_7$								
$1S_8$		$1S_{10}$	$1.6L_2$	$1.3L_3$				
$1S_9$		$1S_{11}$	$1.6L_3$	$1.3L_4$				
$1S_{12}$								
$1S_{13}$								
$1S_{14}$								
$1S_{15}$								
$1S_{16}$								
$1S_{18}$		$1S_{17}$	$1.6L_4$	$1.3L_6$				
$1S_{19}$					$1S_{70}$			
$1S_{20}$								
$1S_{21}$								
$1S_{23}$		$1S_{22}$	$1.6L_5$	$1.3L_8$				

Table 67. Topological equivalences for the family **QsnSN**(**C**) *(cont.)*

Presented phase portrait	Identical under perturbations	Finite antisaddle focus	Finite antisaddle node–focus	Finite weak point	Disconnected parts	Possessing invariant curve (no separatrix)	Symmetry	Other reasons
$1S_{24}$								
$1S_{25}$								$1.7L_{10}{}^{(4)}$
$1S_{26}$								
$1S_{27}$								
$1S_{28}$	$1S_{29}$			$1.3L_{11}$				
$1S_{30}$	$1S_{31}$, $1S_{32}$			$1.3L_{12}$		$1.7L_{24}$		
$1S_{33}$	$1S_{34}$			$1.3L_{10}$				
$1S_{35}$								
$1S_{36}$								
$1S_{37}$								$1.7L_{11}{}^{(4)}$
$1S_{40}$	$1S_{41}$, $1S_{50}$			$1.3L_{9}$		$1.4L_{10}$		
$1S_{43}$								
$1S_{44}$		$1S_{47}$	$1.6L_{7}$					
$1S_{45}$	$1S_{38}$, $1S_{39}$ $1S_{46}$	$1S_{48}$, $1S_{49}$	$1.6L_{8}$, $1.6L_{9}$ P_{48}			$1.7L_{22}$, $1.7L_{23}$ $1.7L_{25}$, $1.7L_{26}$		$1.7L_{12}{}^{(4)}$, $1.7L_{13}{}^{(4)}$ $P_{46}{}^{(4)}$
$1S_{52}$	$1S_{42}$, $1S_{51}$	$1S_{54}$	$1.6L_{6}$			$1.4L_{9}$, $1.4L_{11}$		
$1S_{53}$								
$1S_{55}$								
$1S_{56}$								
$1S_{57}$								$1.7L_{14}{}^{(4)}$

Table 68. Topological equivalences for the family **QsnSN**(**C**) *(cont.)*

Presented phase portrait	Identical under perturbations	Finite antisaddle focus	Finite antisaddle node–focus	Finite weak point	Disconnected parts	Possessing invariant curve (no separatrix)	Symmetry	Other reasons
$1S_{58}$								
$1S_{59}$								
$1S_{60}$								$1.7L_{15}{}^{(4)}$
$1S_{64}$		$1S_{61}$	$1.6L_{10}$	$1.3L_{13}$				
$1S_{65}$		$1S_{62}$	$1.6L_{11}$	$1.3L_{14}$				
$1S_{66}$		$1S_{63}$	$1.6L_{12}$	$1.3L_{15}$			$P_{53}{}^{(4)}$, $P_{55}{}^{(4)}$	$1.7L_{16}{}^{(4)}$, $1.7L_{17}{}^{(4)}$
$1S_{67}$								
$1S_{68}$								
$1S_{69}$								
$1S_{71}$								
$1S_{72}$								
$1S_{74}$		$1S_{73}$	$1.6L_{13}$	$1.3L_{17}$				
$2S_1$							$2S_8$	
$2S_2$					$2S_9$			
$2S_3$								
$2S_4$					$2S_{26}$			
$2S_5$					$2S_{20}$			
$2S_6$	$2S_7$				$2S_{15}$	$2.4L_2$		
$2S_{10}$					$2S_{32}$			
$2S_{11}$					$2S_{33}$			
$2S_{12}$					$2S_{27}$			

Table 69. Topological equivalences for the family **QsnSN**(**C**) *(cont.)*

Presented phase portrait	Identical under perturbations	Finite antisaddle focus	Finite antisaddle node–focus	Finite weak point	Disconnected parts	Possessing invariant curve (no separatrix)	Symmetry	Other reasons
$2S_{13}$	$2S_{14}$					$2.4L_4$		
$2S_{16}$					$2S_{35}$			
$2S_{17}$					$2S_{34}$			
$2S_{18}$					$2S_{28}$, $2S_{29}$	$2.4L_{10}$		
$2S_{19}$					$2S_{22}$			
$2S_{21}$								
$2S_{22}$								
$2S_{23}$					$2S_{25}$			
$2S_{24}$								
$2S_{30}$								
$2S_{31}$								
$2S_{41}$	$2S_{42}$, $2S_{44}$	$2S_{43}$	$2.6L_1$			$2.4L_{13}$		
$2S_{45}$	$2S_{36}$, $2S_{46}$	$2S_{47}$	$2.6L_2$	$2.3L_8$, $2.3L_{12}$		$2.4L_{11}$, $2.2L_{12}$, $2.4L_{14}$		${2S_{37}}^{(5)}$, ${2S_{38}}^{(5)}$ ${2S_{39}}^{(5)}$, ${2S_{40}}^{(5)}$ ${P_{67}}^{(5)}$
$2S_{48}$								
$2S_{49}$								
$2S_{51}$		$2S_{50}$	$2.6L_3$	$2.3L_{10}$				${2S_{58}}^{(5)}$
$2S_{52}$								
$2S_{53}$								

Table 70. Topological equivalences for the family **QsnSN**(**C**) *(cont.)*

Presented phase portrait	Identical under perturbations	Finite antisaddle focus	Finite antisaddle node–focus	Finite weak point	Disconnected parts	Possessing invariant curve (no separatrix)	Symmetry	Other reasons
$2S_{54}$								
$2S_{56}$		$2S_{55}$	$2.6L_4$	$2.3L_{11}$				$2S_{57}{}^{(5)}$
$2S_{59}$		$2S_{60}$	$2.6L_5$	$2.3L_{12}$				
$2S_{61}$								
$2S_{62}$								
$4S_1$	$4S_2$			$3.4L_1$				
$4S_3$								
$4S_6$	$4S_7$			$3.4L_2$				
$4S_8$	$4S_{10}$, $4S_{18}$, $4S_{23}$			$3.4L_4$, $3.4L_{11}$				
$4S_9$	$4S_{22}$			$3.4L_6$				
$4S_{13}$								
$4S_{15}$		$4S_{14}$	$4.6L_1$	$3.4L_8$				
$4S_{16}$	$4S_{17}$	$4S_{19}$, $4S_{21}$	$4.6L_2$, $4.6L_3$ P_{13}	$3.4L_3$, $3.4L_5$ $3.4L_9$, $3.4L_{10}$ P_{20}				
$4S_{20}$								
$4S_{25}$								
$4S_{26}$	$4S_{27}$			$3.4L_{12}$				

Table 71. Topological equivalences for the family **QsnSN**(**C**) *(cont.)*

Presented phase portrait	Identical under perturbations	Finite antisaddle focus	Finite antisaddle node–focus	Finite weak point	Disconnected parts	Possessing invariant curve (no separatrix)	Symmetry	Other reasons
$4S_{29}$	$4S_{30}$	$4S_{28}$	$4.6L_4$	$3.4L_{13}$				
$4S_{31}$	$4S_{41}$			$3.4L_{17}$				
$4S_{32}$	$4S_{40}$			$3.4L_{16}$				
$4S_{33}$	$4S_{39}$	$4S_{34}$, $4S_{35}$	$4.6L_5$, $4.6L_6$ P_{24}	$3.4L_{14}$, $3.4L_{15}$				
$4S_{36}$								
$4S_{42}$	$4S_{43}$			$3.4L_{18}$				
$4S_{44}$	$4S_{48}$	$4S_{49}$	$4.6L_7$			$4.4L_5$		
$4S_{51}$								
$5S_1$								
$5S_2$	$5S_{20}$, $5S_{21}$ $5.7L_4$					$4.5L_3$ ${P_{38}}^{(6)}$, ${P_{63}}^{(1)}$		
$5S_3$		$5S_4$	$5.6L_1$	$3.5L_1$				
$5S_5$					$5S_{34}$			
$5S_9$	$5S_8$, $5S_{10}$, $5S_{16}$ $5S_{18}$, $5S_{19}$ $5.7L_{10}$	$5S_7$, $5S_{15}$ $5S_{17}$ $5.7L_3$, $5.7L_6$ $5.7L_7$, $5.7L_{12}$ P_5	$5.6L_4$, $5.6L_5$ P_6, P_8	$3.5L_3$, $3.5L_4$ $3.5L_5$, $3.5L_6$ P_9	$5S_{24}$, $5S_{25}$ $5S_{31}$, $5S_{32}$	$4.5L_1$, $4.5L_2$		

Table 72. Topological equivalences for the family **QsnSN**(**C**) *(cont.)*

Presented phase portrait	Identical under perturbations	Finite antisaddle focus	Finite antisaddle node–focus	Finite weak point	Disconnected parts	Possessing invariant curve (no separatrix)	Symmetry	Other reasons
$5S_{12}$		$5S_{11}$	$5.6L_2$	$3.5L_7$				
$5S_{13}$		$5S_6$, $5S_{14}$	$5.6L_3$	$3.5L_2$				
$5S_{22}$								
$5S_{23}$								
$5S_{26}$								
$5S_{28}$	$5S_{29}$	$5S_{27}$, $5S_{30}$	$5.6L_6$, $5.6L_7$			$4.5L_4$		
$5S_{33}$								
$5S_{36}$		$5S_{35}$	$5.6L_8$	$3.5L_8$				
$7S_1$								
$7S_2$								
$7S_3$								
$7S_4$	$7S_5$			$3.7L_1$				
$7S_6$								
$7S_7$								
$7S_8$	$7S_{18}$	$7S_{19}$	$6.7L_3$	$3.7L_4$				
$7S_9$	$7S_{20}$	$7S_{21}$	$6.7L_4$	$3.7L_5$				
$7S_{10}$								
$7S_{15}$		$7S_{11}$, $7S_{13}$	$6.7L_1$	$3.7L_2$				
$7S_{16}$		$7S_{12}$, $7S_{14}$	$6.7L_2$	$3.7L_3$				

Table 73. Topological equivalences for the family **QsnSN**(**C**) *(cont.)*

Presented phase portrait	Identical under perturbations	Finite antisaddle focus	Finite antisaddle node–focus	Finite weak point	Disconnected parts	Possessing invariant curve (no separatrix)	Symmetry	Other reasons
$7S_{17}$								
$7S_{22}$				$3.7L_7$				
$7S_{23}$		$7S_{24}$, $7S_{25}$ $3.7L_6$	$6.7L_5$	$3.7L_8$, $3.7L_9$, $3.7L_{11}$ P_{14}, P_{16}				
$7S_{26}$								
$7S_{27}$								
$7S_{28}$	$7S_{30}$			$3.7L_{12}$				
$7S_{29}$				$3.7L_{10}$				
$7S_{31}$		$7S_{36}$		$3.7L_{12}$				
$7S_{32}$	$7S_{34}$			$3.7L_{13}$				
$7S_{33}$	$7S_{35}$			$3.7L_{14}$				
$7S_{37}$	$7S_{43}$	$7S_{48}$, $7S_{49}$	$6.7L_{10}$, $6.7L_{11}$ P_{28}	$3.7L_{16}$, $3.7L_{17}$				
$7S_{38}$		$7S_{39}$, $7S_{40}$	$6.7L_7$	$3.7L_{15}$				
$7S_{41}$								
$7S_{42}$								
$7S_{44}$		$7S_{46}$, $7S_{50}$	$6.7L_9$	$3.7L_{18}$				
$7S_{45}$		$7S_{47}$, $7S_{51}$	$6.7L_8$	$3.7L_{19}$				

Table 74. Topological equivalences for the family **QsnSN**(**C**) *(cont.)*

Presented phase portrait	Identical under perturbations	Finite antisaddle focus	Finite antisaddle node–focus	Finite weak point	Disconnected parts	Possessing invariant curve (no separatrix)	Symmetry	Other reasons
$7S_{52}$								
$7S_{53}$								
$7S_{55}$		$7S_{54}$	$6.7L_{12}$	$3.7L_{20}$				
$7S_{56}$								
$7S_{57}$								
$7S_{58}$								
$7S_{60}$		$7S_{59}$	$6.7L_{13}$	$3.7L_{21}$				
$7S_{61}$								
$7S_{62}$								
$7S_{63}$								
$7S_{64}$								
$7S_{65}$		$7S_{66}$		$3.7L_{22}$				
$7S_{67}$								
$7S_{68}$								
$7S_{69}$								
$7S_{70}$								
$7S_{71}$								
$7S_{72}$		$7S_{73}$	$6.7L_{14}$	$3.7L_{23}$				
$7S_{74}$								
$7S_{75}$								
$7S_{76}$								
$7S_{77}$								

Table 75. Topological equivalences for the family **QsnSN**(**C**) *(cont.)*

Presented phase portrait	Identical under perturbations	Finite antisaddle focus	Finite antisaddle node–focus	Finite weak point	Disconnected parts	Possessing invariant curve (no separatrix)	Symmetry	Other reasons
$7S_{78}$								
$7S_{79}$		$7S_{80}$	$6.7L_{15}$	$3.7L_{24}$				
$7S_{81}$								
$7S_{82}$								
$7S_{83}$								
$7S_{85}$		$7S_{84}$	$6.7L_{16}$	$3.7L_{25}$				
$10S_1$								
$1.1L_1$								
$1.1L_2$								
$1.1L_3$								
$1.1L_4$	$1.1L_5$					P_{47}		
$1.1L_6$								
$1.1L_7$	$1.1L_8$					P_{40}		
$1.2L_5$	$1.2L_6$					P_{66}		
$1.2L_7$								
$1.2L_8$	$1.2L_9$, $1.2L_{10}$							
$1.3L_2$					$1.3L_5$, $1.3L_7$, $1.3L_{16}$ P_{18}, P_{45}			
$1.4L_1$		$1.4L_2$		P_{19}		P_{10}		
$1.4L_3$								

Table 76. Topological equivalences for the family **QsnSN**(**C**) *(cont.)*

Presented phase portrait	Identical under perturbations	Finite antisaddle focus	Finite antisaddle node–focus	Finite weak point	Disconnected parts	Possessing invariant curve (no separatrix)	Symmetry	Other reasons
$1.4L_4$								
$1.4L_5$								
$1.4L_7$								$P_{44}{}^{(4)}$
$1.4L_8$								
$1.4L_{12}$								
$1.4L_{13}$								$P_{49}{}^{(4)}$
$1.4L_{14}$								
$1.5L_1$								
$1.5L_2$								
$1.5L_3$								
$1.5L_4$								
$1.5L_5$								
$1.5L_6$								
$1.5L_7$		$1.5L_8$	P_{56}	P_{54}				
$1.7L_1$								
$1.7L_2$								
$1.7L_3$								
$1.7L_4$								
$1.7L_5$								
$1.7L_6$								
$1.7L_7$		$1.7L_8$	P_{32}	P_{33}				
$1.7L_9$								
$1.7L_{18}$	$1.7L_{19}$			P_{37}				
$1.7L_{20}$								

Table 77. Topological equivalences for the family **QsnSN(C)** *(cont.)*

Presented phase portrait	Identical under perturbations	Finite antisaddle focus	Finite antisaddle node–focus	Finite weak point	Disconnected parts	Possessing invariant curve (no separatrix)	Symmetry	Other reasons
$1.7L_{21}$								
$1.7L_{27}$								
$1.7L_{28}$								
$1.7L_{29}$								
$1.7L_{30}$								
$1.7L_{31}$								$P_{51}{}^{(4)}$
$1.7L_{32}$								
$1.7L_{33}$								
$2.3L_1$								
$2.3L_2$								
$2.3L_3$								
$2.3L_4$	$2.3L_5$			P_{15}				
$2.3L_6$								
$2.3L_7$								
$2.4L_1$								
$2.4L_3$								
$2.4L_5$								
$2.4L_6$					$2.4L_8$			
$2.4L_7$								
$2.4L_9$								
$2.5L_1$							$2.5L_2$	
$2.5L_3$					$2.5L_9$			
$2.5L_4$					$2.5L_5$, $2.5L_6$ $2.5L_7$, $2.5L_8$ P_7, P_{35}	P_{11}		
$2.5L_{10}$								

Table 78. Topological equivalences for the family **QsnSN**(**C**) *(cont.)*

Presented phase portrait	Identical under perturbations	Finite antisaddle focus	Finite antisaddle node–focus	Finite weak point	Disconnected parts	Possessing invariant curve (no separatrix)	Symmetry	Other reasons
$2.5L_{11}$	$2.5L_{12}$, $2.5L_{14}$ P_{59}	$2.5L_{15}$	P_{62}	P_{61}				$2.5L_{16}{}^{(5)}$
$2.5L_{13}$								
$2.7L_1$					$2.7L_6$			
$2.7L_2$					$2.7L_{12}$			
$2.7L_3$					$2.7L_{13}$			
$2.7L_4$					$2.7L_{15}$			
$2.7L_5$					$2.7L_{14}$			
$2.7L_7$					$2.7L_8$			
$2.7L_9$					$2.7L_{10}$			
$2.7L_{11}$								
$2.7L_{16}$								
$2.7L_{17}$								
$2.7L_{18}$								
$2.7L_{19}$								
$2.7L_{20}$								
$2.8L_1$								
$2.8L_2$								
$2.8L_3$								
$4.4L_1$	$4.4L_2$			P_{17}				
$4.4L_3$	$4.4L_4$			P_{25}				
$4.7L_1$	$4.7L_2$			P_{21}				
$5.7L_2$	$5.7L_4$	$5.7L_5$	P_3	P_2	$5.7L_{13}$			
$5.7L_9$								

Table 79. Topological equivalences for the family **QsnSN**(**C**) *(cont.)*

Presented phase portrait	Identical under perturbations	Finite antisaddle focus	Finite antisaddle node–focus	Finite weak point	Disconnected parts	Possessing invariant curve (no separatrix)	Symmetry	Other reasons
$5.7L_{11}$								
$5.7L_{14}$								
$7.7L_1$	$7.7L_3$	$7.7L_2$	P_{27}	P_{29}	$5.7L_{13}$			
$7.7L_4$								
$7.7L_5$								
$7.7L_6$								
$7.7L_7$								
P_1								
P_4					P_{36}			
P_{22}								
P_{23}								
P_{26}								
P_{30}								
P_{31}								
P_{39}								
P_{41}								
P_{43}								
P_{50}								
P_{52}								
P_{57}								
P_{58}								
P_{60}								
P_{64}								
P_{65}								
P_{68}								

Acknowledgements. The first author is partially supported by a MEC/FEDER grant number MTM 2013–40998–P and by a CICYT grant number 2014SGR 00568. The second author is supported by CAPES/DGU grant number BEX 9439/12–9 and CAPES/CSF–PVE's 88887.068602/2014–00. The last author is partially supported by FP7–PEOPLE–2012–IRSES–316338, CAPES/CSF–PVE's 88881.030454/2013-01 and CNPq grant "Projeto Universal 472796/2013-5".

References

Andronov, A.A., Leontovich, E.A., Gordon, I.I. & Maier, A.G. [1973] "Qualitative theory of second–order dynamic systems." *Israel Program for Scientific Translations* (Halsted Press, A division of John Wiley & Sons, NY-Toronto, Ontario).

Artés, J.C., Dumortier, F., Herssens, C., Llibre, J. & de Maesschalck, P. [2005] "Computer program P4 to study phase portraits of planar polynomial differential equations," Available at: <http://mat.uab.es/∼artes/p4/p4.htm>.

Artés, J.C., Kooij, R. & Llibre, J. [1998] "Structurally stable quadratic vector fields," Memoires Amer. Math. Soc., **134 (639)**.

Artés, J.C. & Llibre, J. [2014] "Structurally unstable quadratic systems of codimension 1", *Work in progress.*

Artés, J.C., Llibre, J. & Schlomiuk, D. [2006] "The geometry of quadratic differential systems with a weak focus of second order," *Internat. J. Bifur. Chaos Appl. Sci. Engrg.* **16**, 3127–3194.

Artés, J.C., Llibre, J. & Vulpe, N. [2008] "Singular points of quadratic systems: a complete classification in the coefficient space $\mathbb{R}^{12}$," *Internat. J. Bifur. Chaos Appl. Sci. Engrg.* **18**, 313–362.

Artés, J.C., Llibre, J., Schlomiuk, D. & Vulpe, N. [2013a] "Geometric configurations of singularities for quadratic differential systems with total finite multiplicity lower than 2," *Bul. Acad. Ştiinţe Repub. Mold. Mat.* **71**, 72–124.

Artés, J.C., Rezende, A.C. & Oliveira, R.D.S. [2013b] "Global phase portraits of quadratic polynomial differential systems with a semi–elemental triple node," *Internat. J. Bifur. Chaos Appl. Sci. Engrg.* **23**, 21pp.

Artés, J.C., Rezende, A.C. & Oliveira, R.D.S. [2014] "The geometry of quadratic polynomial differential systems with a finite and an infinite saddle–node (A, B)," *Internat. J. Bifur. Chaos Appl. Sci. Engrg.* **24**, 30pp.

Bautin, N.N. [1954] "On periodic solutions of a system of differential equations," *Prikl. Mat. Meh.* **18**, 128.

Coll, B. & Llibre, J. [1988] "Limit cycles for a quadratic system with an invariant straight line and some evolution of phase portraits," *Qualitative Theory of Differential Equations, Colloq. Math. Soc. János Bolyai, Bolyai Institut, Szeged, Hungria* **53**, 111–123.

Coppel, W.A. [1966] "A survey of quadratic systems," *J. Differential Equations* **2**, 293–304.

Dumortier, F., Llibre, J. & Artés, J.C. [2006] "Qualitative Theory of Planar Differential Systems," *Universitext, Springer–Verlag, New York–Berlin.*

Dumortier, F., Roussarie, R. & Rousseau, C. [1994] "Hilbert's 16th problem for quadratic vector fields," *J. Differential Equations* **110**, 66–133.

Fulton, W. [1969] "Algebraic curves. An introduction to Algebraic Geometry," *W.A. Benjamin, Inc.*, New York.

González, E.A. [1969] "Generic properties of polynomial vector fields at infinity," *Trans. Amer. Math. Soc.* **143**, 201–222.

Hartshorne, R. [1977] "Algebraic geometry," *Graduate Texts in Math.* **52**, Springer.

Hilbert, D. [1900] "Mathematische probleme", *In Nachr. Ges. Wiss., editor Second Internat. Congress Math. Paris, 1900*, 253–297. Göttingen Math.–Phys. Kl.

Hilbert, D. [1902] "Mathematical problems," *Bull. Amer. Math. Soc.* **8**, 437–479.

Llibre, J. & Schlomiuk, D. [2004] "The geometry of quadratic differential systems with a weak focus of third order," *Canad. J. Math.* **56**, 310–343.

Rezende, A.C. [2014] "The geometry of some tridimensional families of planar quadratic differential systems," (Doctoral dissertation) – Universidade de São Paulo (ICMC), São Carlos.

Schlomiuk, D. & Pal, J. [2001] "On the geometry in the neighborhood of infinity of quadratic differential systems with a weak focus," *Qual. Theory Dyn. Syst.* **2**, 1–43.

Schlomiuk, D. & Vulpe, N.I. [2005] "Geometry of quadratic differential systems in the neighborhood of the infinity," *J. Differential Equations* **215**, 357–400.

Vulpe, N.I. [2011] "Characterization of the finite weak singularities of quadratic systems via invariant theory," *Nonlinear Anal.* **74**, 6553–6582.

Ye, Y.Q. *et al.* [1986] "Theory of limit cycles," *Trans. of Mathematical Monographs*, **66**. Amer. Math. Soc., Providence, RI, 2 edition.